NASA Contractor Report 172419

(NASA-CR-172419) DESIGN OF A DIGITAL RIDE QUALITY AUGMENTATION SYSTEM FOR COMMUTER AIRCRAFT Final Report (Kansas Univ. Center for Research, Inc.) 366 p HC A16/MF A01 CSCL 01C G3/05

N85-10037

Unclas 24212

DESIGN OF A DIGITAL RIDE QUALITY AUGMENTATION SYSTEM FOR COMMUTER AIRCRAFT

Terry A. Hammond, Shailesh P. Amin,
James D. Paduano, and David R. Downing

THE UNIVERSITY OF KANSAS CENTER FOR RESEARCH, INC.
Flight Research Laboratory
Lawrence, Kansas

Grant NAG1-345
October 1984

National Aeronautics and
Space Administration

Langley Research Center
Hampton, Virginia 23665

DESIGN OF A DIGITAL RIDE QUALITY AUGMENTATION SYSTEM FOR COMMUTER AIRCRAFT

ABSTRACT

Commuter aircraft typically have low wing loadings, and fly at low altitudes, and so they are susceptible to undesirable accelerations caused by random atmospheric turbulence. Larger commercial aircraft typically have higher wing loadings and fly at altitudes where the turbulence level is lower, and so they provide smoother rides. This project was initiated based on the goal of making the ride of the commuter aircraft as smooth as the ride experienced on the major commercial airliners. The objectives of this project were to design a digital, longitudinal mode ride quality augmentation system (RQAS) for a commuter aircraft, and to investigate the effect of selected parameters on those designs.

The initial stage of this research was the development of an interactive control augmentation design (ICAD) program for use in the design and evaluation of the candidate RQASs. This computer aided design program included both optimal and classical design approaches for either continuous or digital systems, and provided data for analyses in both the time and frequency domains.

Both optimal and classical RQAS designs were generated for the five flight conditions selected as representative of a typical commuter mission, using a Cessna 402B. These RQASs used direct lift flaps and the elevator for control of the longitudinal accelerations. The design parameters selected include the sample time (Ts), computation delay time (Td), servo

bandwidth, and the flap and elevator control power. Optimal and classical point designs, based on the nominal design parameters, are presented for all five flight conditions. Parametric analyses for all five flight condition for both the optimal and classical designs are also presented.

Each of the nominal designs was tested on the KU-FRL hybrid simulator using the digital prototype controller developed during this project. Both time and frequency domain analyses are again presented for each point design. This simulation served to validate the RQAS designs on a system where the aircraft was modeled continuously on an analog computer, and the RQAS function was provided by the prototype controller.

The final phase of this project was another validation of the RQAS designs, again using the prototype controller, this time on the full 6 degree-of-freedom (DOF) NASA moving-base Cessna 402B simulator. Piloted simulations to evaluate the handling qualities were done as a part of this simulation, in addition to the unpiloted tests similar to the ones done on the hybrid and digital simulations.

The results of this study indicated that either optimal or classical, longitudinal mode, digital RQASs can provide 15-50% reductions in RMS acceleration for various combinations of design parameters in three different simulations. The next step should be a detailed hardware and structural design program, leading to a flight test of a digital RQAS on the Cessna 402B.

TABLE OF CONTENTS

TABLE OF CONTENTS (CONTINUED)

TABLE OF CONTENTS (CONTINUED)

TABLE OF CONTENTS (CONCLUDED)

LIST OF FIGURES

LIST OF FIGURES (CONTINUED)

LIST OF FIGURES (CONTINUED)

LIST OF FIGURES (CONCLUDED)

LIST OF TABLES

LIST OF TABLES (CONTINUED)

LIST OF ABBREVIATIONS AND SYMBOLS

ABBREVIATIONS

ADC	Analog-to-Digital Converter
AGL	Above Ground Level
AR	Aspect Ratio
BW	Bandwidth
C-402B	Cessna Model 402B
CAS	Control Augmentation System
CONTROL	NASA Classical Design Program
CRT	Cathode Ray Tube
CRW	Control Rate Weighting
DAC	Digital-to-Analog Converter
DC	Direct Current
DOF	Degrees Of Freedom
EMA	Electromechanical Actuator
exp	Exponential Function
FFT	Fast Fourier Transform
GA	General aviation
GAIN1	Feedback Gain to the Elevator
GAIN2	Feedback Gain to the Direct Lift Flaps
GPAS	General Purpose Airborne Simulator
Hz	Hertz
ICAD	Interactive Control Augmentation Design
J	Quadratic Cost Functional

KU-FRL	University Of Kansas-Flight Research Laboratory
LaRC	Langley Research Center
LQG	Linear Quadratic Gaussian
LUN	Logical Unit Number
MST	Medium STOL Transport
m.u.	Machine Unit
NASA	National Aeronautics And Space Administration
ORACLS	Optimal Regulator Algorithm for the Control of Linear Systems
PDN	Physical Device Number
PP	Performance penalty
PSD	Power Spectral Density
RMS	Root Mean Square
RQAS	Ride Quality Augmentation System
RQI	Ride Quality Index
SAS	Stability Augmentation System
sbw	Servo Bandwidth
SL	Sea Level
STOL	Short Takeoff and Landing
TAS	True Airspeed
T/O	Takeoff

SYMBOLS

a_{ij}	State A Matrix Coefficient
Ay	Acceleration in the Lateral Direction, ft/sec^2
Az	Acceleration in the Vertical Direction, ft/sec^2
b	Wing Span
b_{ij}	State B Matrix Coefficient
C_L	Aircraft Lift Coefficient
$C_{L\alpha}$	Lift Curve Slope, rad^{-1}
$C_{Y\beta}$	Side Force Due to Sideslip Angle, rad^{-1}
D(z)	Transfer Function of the Digital Controller
e_i	Error Signal
e_{i-1}	Error Signal of the Previous Sample
g	Acceleration of Gravity, ft/sec^2
$G(j\omega)$	Frequency Response Magnitude at ω
K	Gain Constant
L	Scale Length, ft
L_w	Scale of Turbulence for a Vertical Gust, ft
m	Number of Controls
M_α	Dimensional Variation of Pitching Moment with Angle of Attack, sec^{-2}
n	Steady State Normal Acceleration, g's
n	Number of States
$P_i(\omega)$	Input Power Spectral Density
$P_o(\omega)$	Output Power Spectral Density
q	Aircraft Angular Velocity in Pitch, rad/sec

q_g	Variation of Aircraft Angular Velocity in Pitch due to a Gust, rad/sec
r	Aircraft Angular Velocity in Yaw, rad/sec
s	Laplace Variable, sec^{-1}
t,T	Time, sec
Td	Computational Delay Time, sec
t_f	Final Time, sec
t_o	Initial Time, sec
Ts	Sample Time, sec
u	Forward Perturbed Velocity, ft/sec
U	Control Command to Servo
u_i	ith Control Variable
u_{i-1}	Control Command of the Previous Sample
v	True Air Speed, ft/sec
w'	w' Transform Variable
W/S	Wing Loading, lbs/ft^2
x_i	ith State Variable
y_i	ith Output Variable
z	z Transform Variable
Z_α	Dimensional Variation of Vertical Force With Angle of Attack, ft/sec^2

GREEK SYMBOLS

α	Angle of Attack, deg, rad
α_g	Gust Perturbation of the Angle of Attack, deg, rad
α^*_g	Dummy Gust Perturbation, deg, rad
α_T	Total Angle of Attack, deg, rad
β	Sideslip Angle, deg, rad
δ_e	Elevator Angle, deg, rad
δ_f	Flap Angle, deg, rad
Δt	Incremental Time, sec
ρ	Air Density, slug/ft^3
σ_v	Lateral Gust Intensity, ft/sec
σ_w	Vertical Gust Intensity, ft/sec
θ	Pitch Attitude Angle, deg, rad
ω	Frequency, rad/sec

MATRICES

1. All matrices are in upper case bold face print.
2. All vectors are in lower case bold face print.
3. Matrix and vector transposition is denoted by a (') , e.g. the transpose of A is A'.

A	Continuous State Matrix
AC	Continuous Servo Augmented State Matrix
ACD	Discrete Servo Augmented State Matrix
ACDT	Time History Discrete Servo Augmented State Matrix
ACL	Continuous Closed Loop State Matrix
ACLD	Discrete Closed Loop State Matrix
AD	Discrete State Matrix
AP	Continuous Control Rate Augmented State Matrix
APD	Discrete Control Rate Augmented State Matrix
A_s	Scaled State Matrix
B	Continuous Control Matrix
BC	Continuous Servo Augmented Control Matrix
BCD	Discrete Servo Augmented Control Matrix
BCDT	Time History Discrete Servo Augmented Control Matrix
BD	Discrete Control Matrix
BP	Continuous Control Rate Augmented Control Matrix
BPD	Discrete Control Rate Augmented Control Matrix
B_s	Scaled Control Matrix
D	Continuous Disturbance Matrix
DC	Continuous Augmented Disturbance Matrix
DCD	Discrete Augmented Disturbance Matrix
DCDT	Time History Discrete Augmented Disturbance Matrix

F	Feedback Gain Matrix
FU	Output Controls Matrix
FUC	Augmented Output Controls Matrix
FU1	Output Controls Matrix Input to ICAD
G	Output State Derivatives Matrix
G1	Output State Derivatives Matrix Input to ICAD
GD	Output Disturbance Matrix
GDC	Augmented Output Disturbance Matrix
H	Output State Matrix
H1	Output State Matrix Input to ICAD
HC	Output Continuous Servo Augmented State Matrix
HCL	Closed Loop Output Matrix
H_s	Scaled Output State Matrix
Q	Output Weighting Matrix
R	Control Weighting Matrix
S_u	Control Scale Factor Matrix
S_x	State Scale Factor Matrix
S_y	Output Scale Factor Matrix
u	Control Vector
uc	Servo Augmented Control Vector
ucom	Pilot Comanded Control Vector
u_s	Scaled Control Vector
w	Disturbance Vector
x	State Vector
xc	Servo Augmented State Vector

x_s	Scaled State Vector
y	Output Vector
y_s	Scaled Output Vector

1. INTRODUCTION

1.1 BACKGROUND

The commuter airline industry has expanded rapidly in both numbers of carriers and numbers of flights over the past several years, due primarily to the federal deregulation of the major air carriers in 1978. Following deregulation, the major airlines showed an understandable preference for continuing their longer, more profitable routes, while divesting themselves of the shorter, less populated routes previously forced on them by the Civil Aeronautics Board. Commuter airlines have picked up most of the routes dropped. For example, in 1980 the number of commuter passengers increased by 6% while the number of major airline passengers decreased. The number of commuter passengers has continued to increase by about 15% per year from 1981 through 1983, and that rate is expected to continue at least through 1985 [1]. The result of this growth is that more of the general public is now riding on smaller and generally less sophisticated commuter aircraft.

To accommodate this increased market, there has been a renewed interest in small (15-50 passenger), short-haul, propeller driven commuter aircraft. Advances in aerodynamic and powerplant efficiencies, propeller design, and noise abatement are now being applied to commuter aircraft. New designs incorporating these advances are currently being generated by major domestic and foreign airframe and engine manufacturers, and by leading educational institutions. In addition, human factors engineering has improved seating comfort, reduced internal noise levels, and increased

carry-on luggage space - three commonly voiced criticisms of commuter aircraft. In summary, much effort is being expended toward making commuter aircraft as efficient and as comfortable as the larger aircraft that they are replacing.

However, one important area that has received little recent attention is ride quality or ride smoothness. Ride quality is basically a function of the aircraft aerodynamics and mission profile. The commuter aircraft, because of its characteristic aerodynamic design and typical mission profile, is a good candidate for an active Ride Quality Augmentation System (RQAS). This is particularly true because an increasing number of new commuter passengers have had previous flight experience only on large, smooth-flying aircraft, and thus expect the commuter aircraft to have a comparable ride. This research project was initiated with the overall goal of providing a ride quality on the commuter aircraft which was comparable to the ride currently experienced on the larger commercial aircraft. The initial phase of this project consisted of a literature search and feasibility study [2] to determine the best approach to follow for the detailed design of an active control RQAS. The results of that feasibility study suggested that the requirement and technology now exist to make implementation of a RQAS on commuter aircraft both technically and economically attractive. Based on that finding, this project was initiated to provide detailed design and parameter studies for a RQAS for the Cessna 402B. The rest of this chapter describes the basic concepts, past research, and the proposed configuration for which the detailed design work was done.

1.2 BASIC DEFINITIONS AND CONCEPTS

A poor ride is one with enough motion perturbations of significant magnitude to be uncomfortable to the passengers. These motion perturbations, or bumps, are primarily vertical and lateral accelerations. For an unaugmented aircraft these accelerations are a function of the vertical gust intensity (σ_W), wing loading (W/S), and lift curve slope (C_{L_α}) in the vertical mode; and lateral gust intensity (σ_V), W/S, and side force due to sideslip angle (C_{Y_β}) in the lateral mode. A first level approximation of the acceleration response to these parameters is shown below.

$$A_z = \frac{\rho U}{2} (C_{L_\alpha}) \left(\frac{1}{W/S}\right) (\sigma_W), \qquad (1.1)$$

and $$A_y = \frac{\rho U}{2} (C_{Y_\beta}) \left(\frac{1}{W/S}\right) (\sigma_V).$$

From an inspection of Eqn (1.1), the parameters that cause poor rides are high gust intensity, low W/S, and a high C_{L_α} or high C_{Y_β}. The commuter aircraft is typically adversely affected by all three of these parameters plus one additional factor that does not show up in the first order approximation. Table 1.1 lists the characteristics of many current and future commuter aircraft, and compares them to those of three Boeing 700 series aircraft.

Before going into a specific discussion of commuter characteristics, a mention of the relative importance of the two accelerations is appropriate. It is not obvious from Eqn (1.1) which of the accelerations is the most important, the lateral or the vertical. The principle difference in the

Table 1.1 Current and Future Commuter Characteristics

Aircraft	Cruise Vel (mph)	Cruise Alt (ft)	Number of Pass.	Max T/O Weight (lb)	W/S	AR
Aerospatiale (Nord)						
262	233		26-29	23369	39.5	8.7
ATR-42	319	20000	49	32450	57.5	12.4
Ahrens AR404	195	5000	30	17500	41.5	10.3
Antonov An-26	266	19700	39 (Mil)	52950	65.6	11.4
Beech Aircraft Co.						
C-99	288	10000	15	11300	40.4	7.6
1900	304	10000	19	15245	50.3	9.8
British Aerospace						
Jetstream 31	304	15000	18-19	14100	52.3	12.0
CASA C-212-200	240	10000	26	16093	37.4	9.0
DeHavilland						
DHC-6 (Twin Otter)	210	10000	13-18	12500	29.8	10.1
DHC-7 (Dash 7)	266	10000	50	44000	51.2	10.1
DHC-8 (Dash 8)	300		32			
Dornier Commuter LTA	250	9850	24	15102	41.4	9.4
Embraer EMB-120	291	20000	30	21164	51.7	10.3
Fokker F.27-200	298	20000	52	44996	59.7	12.0
F.27-500	300	20000	60	45000	59.7	12.0
F.27-600	300	20000	44	45000	59.7	12.0
Gulfstream American G1-C	291	25000	37	36000	59.0	10.1
Saab-Fairchild SF-340	313	15000	34	25000	55.5	11.0
Shorts						
330	220	10000	30	22688	49.9	12.3
360	243	10000	36	25700	56.7	12.3
Swearingen Metro II	294	10000	20	12500	45.0	7.7
Cessna 402B	240		6	6300	32.2	
Boeing						
727-200	614	25000	189	209500	127.0	7.1
737-200	568	25000	130	117000	119.4	8.8
757-200	494	29000	196	230000	115.3	7.8

accelerations is due to the C_{L_α} and C_{Y_β} terms. Normally, at altitudes greater than 500 ft, turbulence is isotropic so that the vertical and lateral gusts will be of approximately the same magnitude. However, C_{L_α} is always larger than C_{Y_β}, often by a factor of 4-10 times. Thus, the vertical accelerations are by far the dominant influence on the ride quality, and most efforts in the past have been dedicated to smoothing the longitudinal mode.

The commuter aircraft has poor ride characteristics due to four specific factors. First, as shown in Figure 1.1, gust intensity is basically a function of altitude. The Root Mean Square (RMS) gust velocity reaches a peak between 1000 and 8000 feet AGL, and then gradually decreases with altitude. Commuter aircraft tend to fly at altitudes ranging from 5000 to 20000 feet while major airliners typically fly at altitudes well above 20000 feet. Second, commuter aircraft have low W/S for short takeoff and landing distances and because they typically cruise at low speeds. Third, commuter aircraft tend to have high aspect ratio, unswept wings, factors that contribute to a high C_{L_α}. And finally, the factor that doesn't show up in equation (1.1), commuters are basically rigid aircraft; so very little of the turbulence encountered is absorbed by the aircraft structure. The clear differences between the Boeing aircraft and the typical commuter aircraft create a fundamental ride disadvantage which cannot be cured solely by aerodynamic design changes. This is mainly because W/S must be kept reasonably low to maintain the short field length requirements associated with commuter aircraft. Therefore, an active control augmentation system was selected as the best way to alleviate a poor ride.

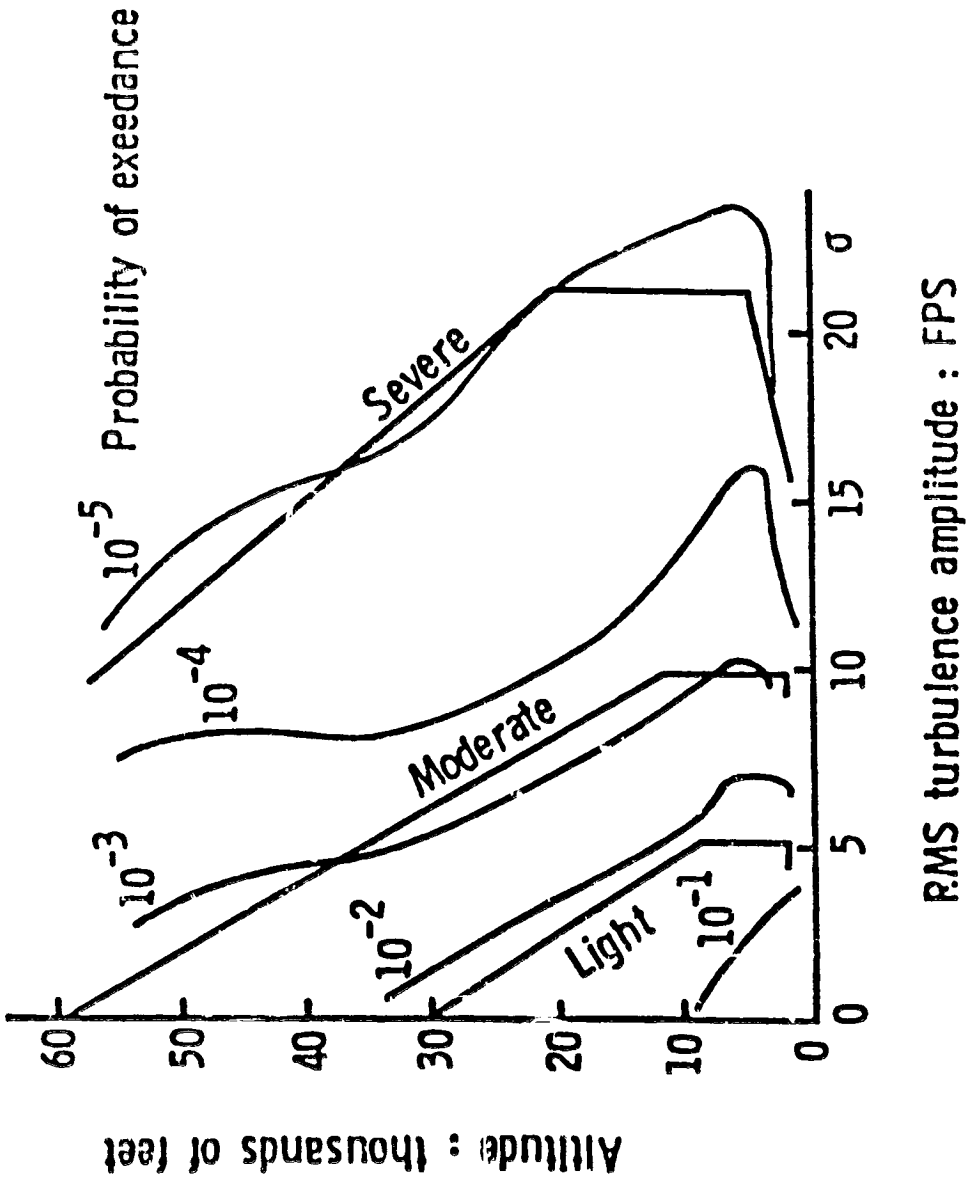

FIGURE 1.1 Variation of Turbulence Gust Intensity with Altitude [from MIL-F-8785C]

1.3 REVIEW OF RIDE QUALITY AUGMENTATION RESEARCH

A comprehensive review of past ride quality research is provided in reference [2]. The two basic approaches, commonly refered to as open- and closed-loop systems, have been used for ride smoothing systems in the past, and block diagrams for each are shown in Figure 1.2.

An open-loop system senses gusts with an angle of attack sensor on a nose boom, and uses the gust magnitude to calculate control surface deflections that cancel out the effect of the gust. This type of system has the distinct disadvantage typical of any open-loop system; i.e. it requires a very accurate system model and very accurate sensing of the disturbance. Several systems have been designed as open-loop controllers, both in the United States and in Europe [3,4,5,6], and flight test programs have been performed with varying degrees of success [3,4].

The closed loop system senses one or more motion variable(s), such as the acceleration and/or the angle of attack, rather than the gust itself. The sensed variable(s) are then used to calculate a control signal that is used to cancel out the motion sensed. Feedback control systems like these tend to be less sensitive to model or sensor errors than open-loop systems. Several designs of this type of system have also been made [7,8,9] using classical design methods and analog control system implementation.

Normally, whether the systems were open- or closed-loop systems, direct lift flaps, often in coordination with the elevators, were used as control surfaces for the vertical mode. Rudders, ailerons, and direct side-force generators (when they were available), were typically used for lateral control.

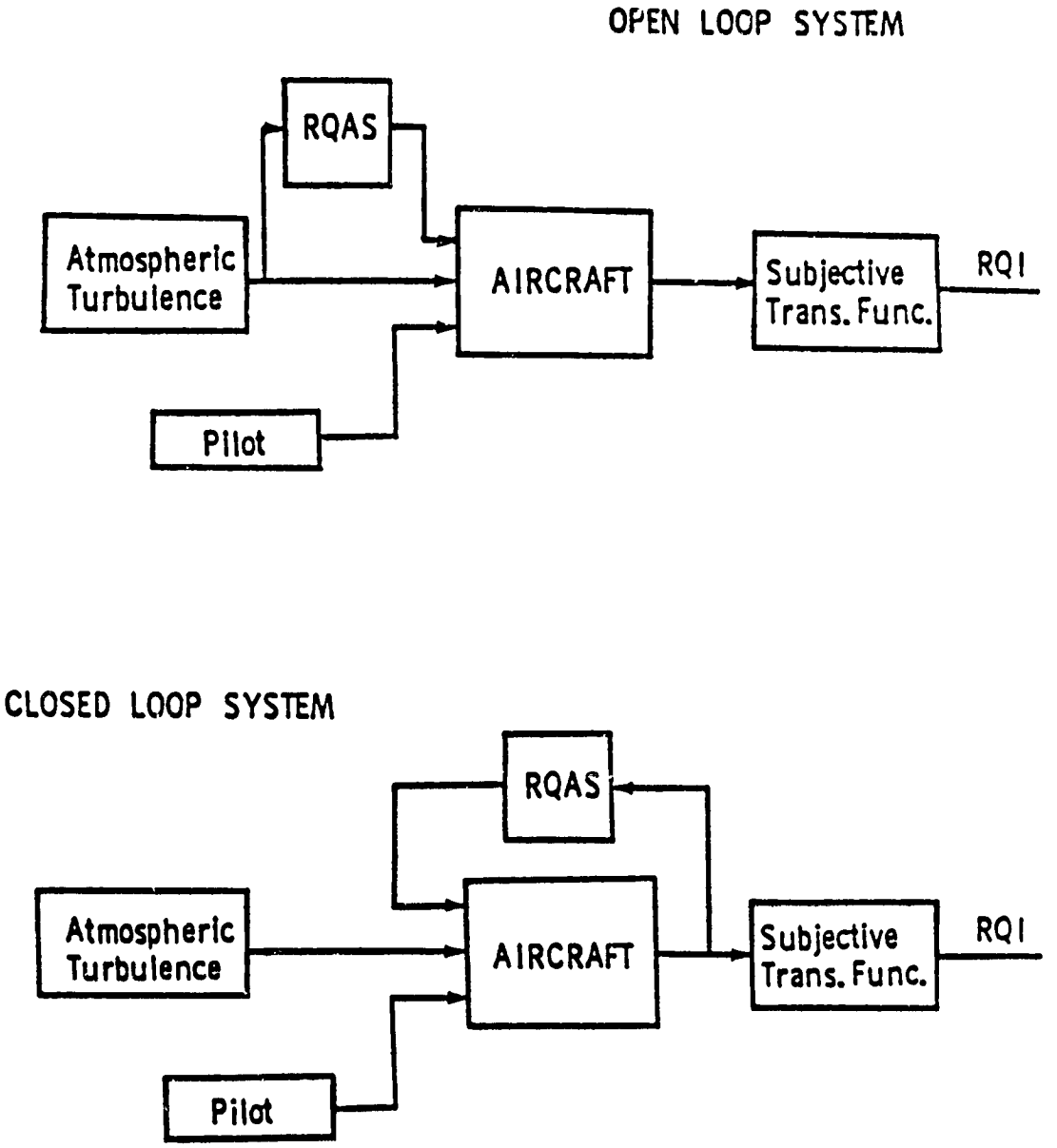

FIGURE 1.2 Fundamental Ride Quality System Approaches

One ROAS design was generated by the Boeing Co. for a Medium STOL Transport (MST) candidate design for the military in the early 1970's [10]. This ROAS design was an analytic study on an aircraft with a W/S of 50 psf, using landing flaps for direct lift, and rudder for lateral control. These designs were generated using classical techniques, and were simulated using high-bandwidth, high-rate actuators with analog control laws. Simulations of these ROASs demonstrated reductions in RMS acceleration to less than the 0.11 g threshold for cruise, descent, and approach configurations.

The civilian system most recently flight tested [11] was flown only on a specially equipped Lockheed Jetstar research aircraft, the NASA General Purpose Airborne Simulator (GPAS). The GPAS has direct lift flaps and direct side-force generators with high-bandwidth, high-rate actuators, and an onboard analog computer for control system implementation. This ROAS was designed using classical control design techniques and was implemented as an analog system using the onboard analog computer. This system reduced RMS accelerations by about 50% in simulations and flight tests, but it was never implemented on a production aircraft.

Many other systems were reviewed. However, none was ever implemented on a production aircraft due to handling quality problems, difficulty in providing good performance over an entire flight profile, and concerns about the cost. Nevertheless, the conclusion of this feasibility study was that the state-of-the-art had advanced to the point that ROASs are now more technically and economically feasible than in the past.

1.4 PROPOSED ROAS CONFIGURATION AND DESIGN PARAMETERS

The conclusion of the preliminary research and feasibility study was that a ROAS should be designed for a commuter aircraft. The detailed review of past ROAS, in conjunction with a review of the technology of current sensors, actuators, digital processors, and a review of control design techniques suggested that the ROAS configuration in Table 1.2 was the most appropriate one for a detailed design.

TABLE 1.2 INITIAL DESIGN CONFIGURATION

Longitudinal Mode System
Closed-Loop Feedback System
Separate Surface Dedicated Controls
Digital System Implementation
Rigid Body Dynamics

The longitudinal mode was chosen for emphasis because the vertical accelerations are typically 2 to 5 times larger than lateral accelerations. Also in a practical sense, flaps can normally be used for direct force generation in the vertical direction, but no such control exists for direct force in the lateral direction.

The closed-loop system was chosen because of its greater insensitivity to model errors and a much larger base of design information. An additional consideration was that sensors for accelerations, angles, and angular rates are commonly available at reasonable cost for commuter systems.

The selection of dedicated control surfaces was predicated on the desire to create a system that would not be flight-critical, and thus would be easier to certify and accept by the commuter manufacturers and users. In addition, a separate surface was desired so that there would be no feedback to the pilot through the reversible controls typically used in the commuter class of aircraft.

The selection of a digital implementation, instead of a more conventional analog control system, was based on three factors.

1. The desire to provide extra flexibility in the implementation of the control laws. Two possible uses for this expanded flexibility are gain scheduling (a need cited in past research [11]) and modification of the control laws to restore degraded handling qualities.

2. The fact that the advanced state-of-the-art and reduced cost of microprocessors now make it technically and economically attractive to introduce digital fly-by-wire technology in commuter class aircraft.

3. The digital microprocessor, after introduction into the commuter class aircraft for this specific task, will also be available for other functions, such as navigation and guidance.

An additional recommendation from the feasibility study was that a prototype controller should be built so the digital nature of the system, e.g. the effects of sample (Ts) and delay time (Td) on the system performance, could be tested on both hybrid and moving-base simulators. A hybrid simulation was selected as an appropriate research tool to provide a continuous model of both the aircraft and the gust field for the development of the digital controller, and to evaluate the RQAS designs on a true sampled data system. The objectives of the moving-base simulation were to evaluate the RQAS designs generated for a 3 degree of freedom (DOF) linear

model on a full 6 DOF, nonlinear system; and to perform "pilot in the loop" simulations for handling qualities evaluations.

1.4.1 SELECTION OF OUTPUT VARIABLES

The selection of the output variables for evaluation must be based on the specifics of the problem. For the RQAS design problem, elimination of vertical acceleration is the primary objective. Therefore vertical acceleration was selected as one of the outputs to be used in RQAS evaluations. The output vector, Table 1.3, also incuded the angle of attack and the pitch rate, because of their direct contribution to acceleration; the pitch attitude, because a passenger actually sees variations in this variable; and the control surface deflections.

TABLE 1.3 OUTPUT VECTOR ELEMENTS

Vertical Acceleration
Angle of Attack
Pitch Rate
Pitch Attitude
Elevator Deflection
Flap Deflection

The acceleration is computed for an inertial reference frame, including contributions from both the linear and rotational components of the body-axis system. The equation used for the vertical acceleration is

$$Az = \dot{w} - U_0 q + g \sin \theta_0 \theta. \qquad (1.2)$$

1.4.2 DESIGN PARAMETERS

Four design parameters were selected for examination in this project. The sample time (Ts), and computational delay time (Td) were selected to provide additional design information on the digital nature of the ROAS designs. The servo bandwidth (BW) and control power parameters were selected to provide a basis for the actual design and implementation of the modified direct-lift flap system. Nominal values for each of these parameters were selected at the beginning of the project and are presented in Table 1.4.

TABLE 1.4 VARIABLES SELECTED FOR PARAMETRIC ANALYSES

Parameter	Nominal Value
Sample Time	Ts = .1 sec
Computational Delay Time	Td = .1 sec (Optimal) Td = .01 sec (Classical)
Servo Bandwidth	10 rad/sec
Control Power	Half Flap Control Power (Optimal & Classical) Full Flap Control Power (Optimal)

1.5 REPORT OVERVIEW

The remainder of this report is divided into seven chapters and four appendices. Chapter 2 defines the research tasks, discusses the formulation of the basic equations of motion and the aircraft mathematical models (Appendix A), and provides an overview of the design approach and parameters. Chapter 3 is a detailed description of the interactive design and evaluation program which was the design tool used to generate the point designs and parameter studies (Appendix B is a user's manual for that program). Chapters 4 and 5 are in-depth discussions of the point designs, and parameter studies for the optimal and classical approaches, respectively. Chapter 6 describes the development of the prototype digital controller, and the control system validation efforts on the University of Kansas Flight Research Laboratory (KU-FRL) hybrid, and the NASA Langley Research Center (LaRC) nonlinear moving-base simulators (Appendix C is a brief description and discussion of the KU-FRL analog simulation of the aircraft and gust field). Chapter 7 is a discussion of the system implementation considerations, ranging from hardware requirements for sensors and actuators, to handling quality considerations. Chapter 8 concludes the technical portion of the paper with a summary, and a discussion of conclusions and recommended follow-on research.

2. EQUATIONS OF MOTION

The fundamental assumption in the design and evaluation of the candidate ROASs is that the motion of the aircraft can be described by a set of standard, linear, small-perturbation equations of motion in a state-matrix format, as shown in the equation below.

$$\dot{x} = A\,x + B\,u, \tag{2.1}$$

where

$x' = \{\alpha, \iota, q, \theta\}$, and

$u' = \{\delta_e, \delta_f\}$.

Standard derivations of the perturbation differential equations can be found in most texts on aircraft flight mechanics [12], usually in the stability-axis coordinate system. These basic equations can easily be transformed into any reference system for application to a specific problem.

The linear, small-perturbation mathematical models of the Cessna 402B used for this study were furnished by NASA LaRC. These mathematical models were derived from a nonlinear simulation model using a standard NASA LaRC technique [13]. The model was furnished in state-matrix form, as shown in equation (2.1), in the body-axis system. The body-axis system was used throughout this project to simplify formulating the feedback variables from the aircraft sensors. An example of the data furnished is provided in Appendix A for the takeoff configuration.

The validity of these state-matrix formulations of the small-perturbation equations of motion are subject to the following assumptions:

1. the earth is an inertial reference frame;
2. the aircraft mass and mass distribution are constant;
3. perturbations from steady flight are small;
4. initial conditions are straight-line flight with forces and moments balanced;
5. the XZ-plane is a plane of symmetry;
6. the airframe is a rigid body;
7. the flow is quasi-steady;
8. the effect of the engine gyroscopics is negligible; and
9. the thrust is constant.

The state matrices were provided for a coupled 6-Degree-of-Freedom (DOF) linear model. Because we were interested primarily in the longitudinal mode, we decoupled the longitudinal mode from the lateral-directional mode by simply partitioning the state and control matrices. The eigenvalues of the decoupled matrices were compared to the coupled matrix eigenvalues to insure that the model had not been significantly altered. The controls available to the RQAS for the logitudinal mode were the flaps and the elevators. The controls available to the pilot were the standard elevator, rudder, and ailerons. The flap on the C-402B is a split flap, capable of deflecting only in the positive direction. However, as stated earlier, the assumption was made that flap control would be available to the RQAS for both positive and negative deflections.

2.1 COORDINATE REFERENCE SYSTEMS

The state-matrix equations for this project were furnished by NASA in the body-axis system. The body-axis system is an orthogonal, right-hand set of axes with its origin fixed at the aircraft's center of mass, as shown in Figure 2.1. The X-axis is oriented along the body centerline, pointing out the nose of the aircraft, the Y-axis is out the right wing; and the Z-axis completes the set, out the bottom of the aircraft. Elevator and rudder deflections are defined positive in terms of the right-hand rule, with respect to the deflection of the trailing edge. Positive aileron is defined as the deflection which creates a positive rolling moment. The XZ-plane is a plane of symmetry.

The normal lift and drag forces and stability derivatives are specified in the stability-axis system. The stability-axis system is an orthogonal, right-hand set of axes with its origin at the aircraft center of mass, as shown in Figure 2.2. The difference between the body- and stability- axis systems is that the X-axis for the stability axis system points directly into the projection of the relative wind onto the plane of symmetry of the aircraft, while the X-axis of the body-axis system points out the nose of the aircraft. The transformation between the two axis systems is represented by a rotation through the angle of attack about the Y-axis. Both coordinate reference systems are introduced here because discussions of the non-dimensional and dimensional stability derivatives refer to the stability-axis system, while discussion of instrument and sensor readings will refer to the body-axis system.

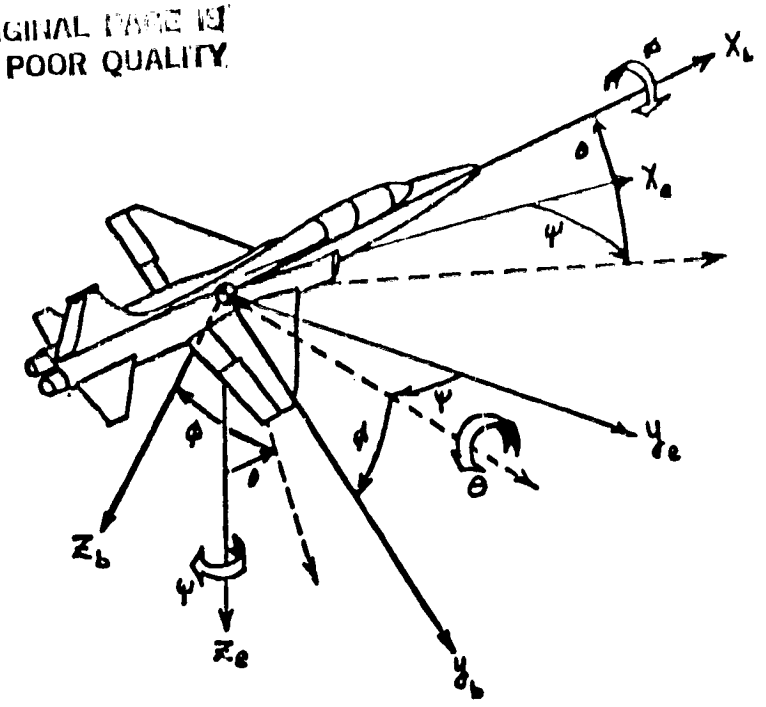

Figure 2.1 Body Axis Coordinate System

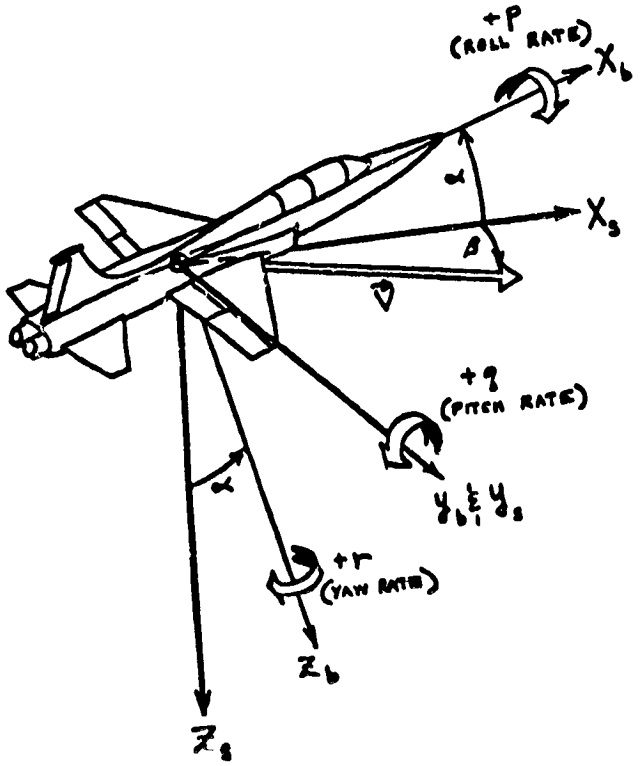

Figure 2.2 Stability Axis Coordinate System

2.2 ATMOSPHERIC TURBULENCE

The two forms of atmospheric turbulence which are commonly used to disturb aircraft in research on ride smoothing are discrete gusts (either step, ramp or 1-cosine) and statistically random gusts. The discrete gusts are normally used for evaluation of worst-case response to single large gusts, while detailed designs and evaluations are normally based on the random gust-field analysis. A discussion of random gust fields can be found in reference [12]. Provisions in this research effort were made to allow any time history of turbulence to be used for the disturbance. For this study, the random gust fields have been assumed to be homogeneous and locally isotropic above 500 feet. It is also assumed that Taylor's hypothesis applies, i.e. the gust field is frozen in time and space. The assumptions of homogenity and frozen field permit the turbulence to be treated as independent of time, thereby permitting stationary statistical methods to be applied to the analyses.

Two distinct formulations of atmospheric turbulence exist for use in statistical studies of gust response, the Dryden and the Von Karman models. Both models are very similar in the low frequency range, but they differ slightly in the high frequency asymptotes (due to a power of 2 in the denominator of the Dryden form, while the Von Karman form has a non-integer power of 11/6 in the denominator). The Dryden form is rational and can be modeled easily in the time domain, while the Von Karman form is irrational and can not be easily modeled analytically. The Dryden form has been more widely used in the past, but the current trend is toward the Von Karman model. Although the Von Karman model is recommended for frequency domain

analyses because it more accurately matches experimental data, both models yield simialr results for flying qualities evaluations. Because of the desire to compare time and frequency domain responses from the digital simulation, and because only the Dryden form could be modeled analytically for both the KU-FRL hybrid and the NASA LaRC moving base simulations, the Dryden model was selected to be the primary turbulence model for this research. The modeling of the Dryden gust field in state matrix form is detailed in reference [14].

2.3 ACTUATOR MODEL

The RQAS design and evaluation process included the servo actuator dynamics in all three types of simulation. The actuators were modeled as simple first-order lags, with unity steady-state gains, represented by

$$\frac{\delta_e}{U_e} = \frac{sbw}{S + sbw}, \tag{2.2}$$

where

δ_e = actual elevator position,

and U_e = elevator position command,

sbw = servo Bandwidth.

The actuator dynamics were included so that actual servo movements, rates and RMS values could be used in the performance evaluations. In addition, the servo bandwidth (BW) was one of the variables investigated as an important design parameter in the parametric studies.

3. DESIGN AND EVALUATION PROGRAM

3.1 GENERAL DESCRIPTION

The Interactive Control Augmentation Design (ICAD) program described here has been developed specifically for the design of ride quality systems for commuter aircraft. However, the ICAD program was intended to be general enough for any type of control system design, whether optimal or classical, continuous or sampled data. This flexibility is accomplished by combining existing control system analysis routines with highly interactive design looping and flexible graphics to give the control engineer a complete, self-contained, interactive design and analysis tool. The design and evaluation procedure employed by the ICAD program is pictured in Figure 3.1 and described below. Table 3.1 summarizes the capabilities of ICAD.

The aircraft model, flight parameters, and gust environment are input as data files. Other data files contain information for the control augmentation routines; see Appendix B for details on data file content and format. The designer selects program options and design modifications interactively and views the results in graphic or tabular form.

The control algorithm design procedures which make up the ICAD program are adopted from two NASA programs: CONTROL [15] and ORACLS [16]. CONTROL subroutines are utilized for classical design techniques, including root locus and bode plot methods. The ORACLS package of subroutines is used to design optimal linear quadratic full state feedback controllers. Both design procedures are integrated with time history and frequency response evaluation procedures to form an interactive design and evaluation program.

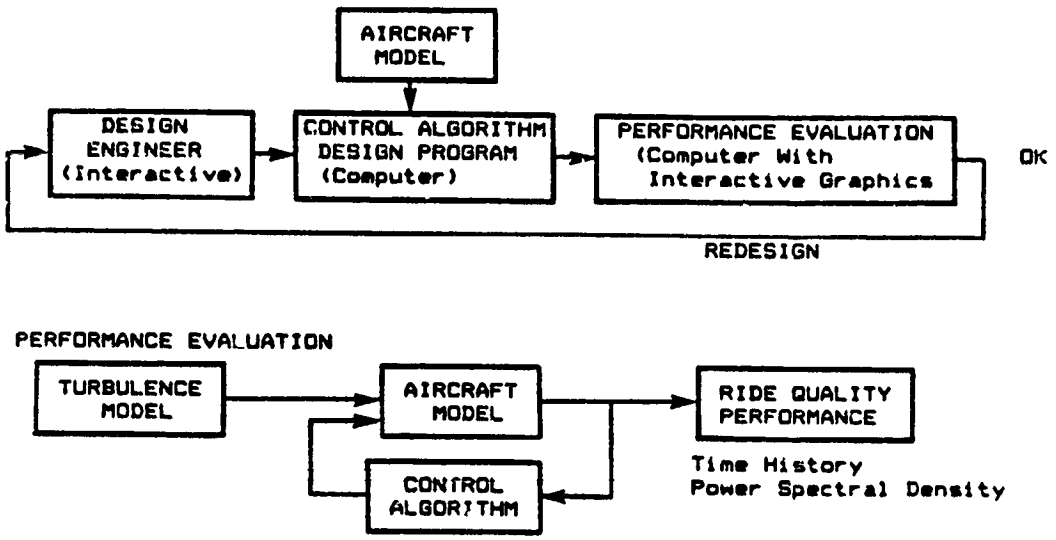

Figure 3.1 Design and Evaluation Procedure

Table 3.1 ICAD Analysis and Design Tools

Function	Tools	Evaluation Data
Analysis (Open and Closed Loop)	Time Histories (for all outputs and controls)	Maximum Values RMS Values Maximum Rates
	Bode Diagrams (for any combination of outputs and states/disturbances	Eigenvalues Zeroes Transfer Function Polynomials
	Power Spectral Densities* (for any combination of outputs and disturbances)	RMS Responses to - Dryden gust field - Von Karman gust field
Optimal Design	Linear Quadratic Gaussian (LQG) Regulator - Standard Optimal Regulator - Control Rate Weighting	Feedback gains all analysis above
Classical Design	Block Diagram Control System Design	Feedback gains all analysis above
	Root Locus - s-plane* - z-plane* - w'-plane*	

* indicates graphics available

The performance evaluation portion of ICAD can produce several types of data for use by the control designer. These include

1) Time Histories, including peak, rate and RMS values,

2) Frequency Responses, and

3) Power Spectral Densities, including RMS values.

1) Time histories can be generated for any output variable, as a response to a time history of gust disturbances and/or control movements. The open loop response as well as any number of augmented system responses can be overlaid for direct comparison of system performance. In addition, the responses can be overlaid on a time history design response envelope for time domain analysis. Examples of these plots appear in Chapter 4.

2) Frequency responses can be generated for any combination of control or disturbance inputs and any set of outputs. For example, vertical gust (w-gust) and elevator position (delta-e) might be chosen as transfer function inputs, and vertical acceleration (Az) and pitch attitude angle (Theta) might be chosen as outputs. These choices would result in the following tranfer functions:

1) Az / w-gust
2) Az / delta-e
3) Theta / w-gust
4) Theta / delta-e

As with the time histories, multiple Bode plots can be overlaid for direct comparison of frequency domain characteristics, such as phase and gain margin.

3) The power spectral density (PSD) of any output variable's response to turbulence can also be generated. This feature is specifically advanta-

geous to ride quality work. Graphics capabilities, similar to those described above, are available for PSDs.

This program is implemented in Fortran on the Harris 500 computer at the University of Kansas. The hardware available at the KU-FRL is pictured in figure 3.2. The Harris computer, combined with the efficiency of the Fortran 77 compiler, and the Tektronix 4025 high-speed graphics terminals, forms a system which provides the responsiveness necessary for an interactive design program, such as the ICAD program. Hard copy plots of screen graphics are available at the Harris facility. Remote "smart" terminals at the KU-FRL also provide interactive and hardcopy graphics, over high speed modem connections. These terminals provide the designer with added flexibility and accessability. The KU Academic Computer Center's Honeywell 60/66 mainframe was used for initial software development, and is available for a back-up to the Harris, but without the fast responsive and graphics capabilities needed for an interactive design program.

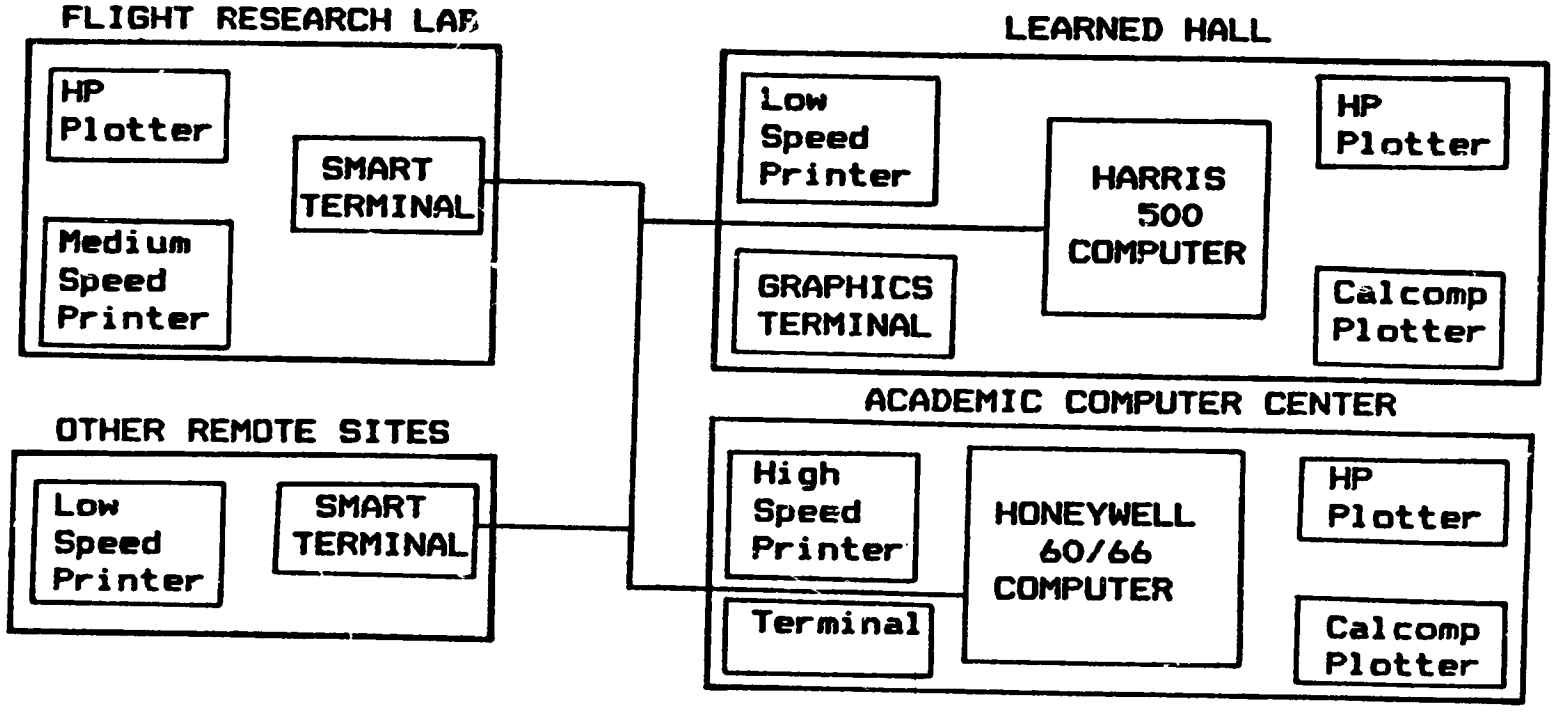

Figure 3.2 Hardware Resources of the University of Kansas

3.2 PROGRAM FLOW AND METHOD OF ANALYSIS

The ICAD Program analysis consists of the following six parts:

1. Input of system matrices and flight parameters, and definition of the output variables.
2. Augmentation of the open loop dynamics with the desired servo dynamics.
3. Analysis of the response of the open loop system.
4. Discretization of the system matrices for use in the time histories and for digital designs.
5. Development of a feedback gain matrix using either optimal or classical techniques.
6. Analysis of the response of the closed loop system.

The basic flow of the program is shown in Figure 3.3. The following sections discuss each of these operation.

3.2.1 INPUT OF MATRICES

The unaugmented aircraft is modeled as a set of matrix linear differential equations of the form

$$\dot{x} = A\,x + B\,u + D\,w, \tag{3.1}$$

where x = state vector,

u = control positions vector,

w = disturbance vector,

A = basic system matrix,

B = control matrix, and

D = disturbance matrix.

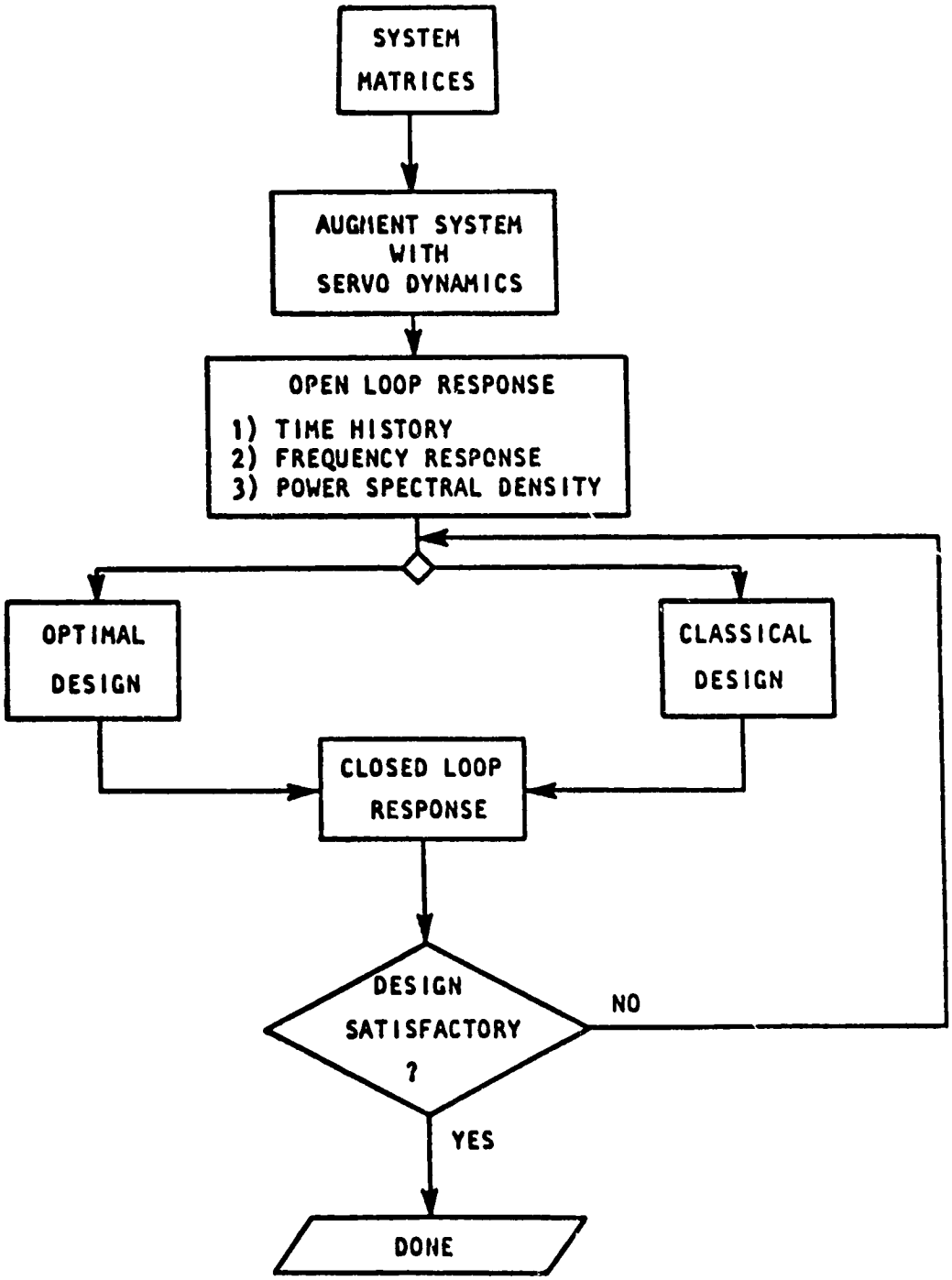

FIGURE 3.3 Basic Program Flow

The output of the system is modeled by

$$y = H1\ x + G1\ \dot{x} + FU1\ u. \tag{3.2}$$

The ICAD program input files contain the matrices A, B, D, H1, G1, and FU1, as described in Appendix B. By substituting equation 3.1 for x in equation 3.2, ICAD automatically forms the following output equation:

$$y = H\ x + FU\ u + GD\ w, \tag{3.3}$$

where H, FU, and GD = output matrices.

3.2.2 AUGMENTATION OF SERVO DYNAMICS

The basic system equations described above do not include servo dynamics. In order to better represent real systems, servo response to control system commands must be included. The ICAD Program allows any linear servo transfer function to be added to the basic system. The servo augmented system is then used for all time history simulations, and for classical control system design. For optimal control system design, the unaugmented system is used, so that the program will not consider control positions as optimal control feedback variables. However, evaluation of optimal designs is conducted with servos. A generalized block diagram of the servo augmentation, and the resulting system, is presented in Figure 3.4. Reference 15 and Appendix B contain the information required for servo augmentation setup. The servo augmented system of differential equations is

$$\begin{bmatrix} \dot{x} \\ \dot{u} \end{bmatrix} = \begin{bmatrix} A & B \\ 0 & -BW\ I \end{bmatrix} \begin{bmatrix} x \\ u \end{bmatrix} + \begin{bmatrix} 0 \\ BW\ I \end{bmatrix} uc + \begin{bmatrix} D \\ 0 \end{bmatrix} w, \tag{3.4}$$

and the corresponding output equation is

$$y = [H \quad FU] \begin{bmatrix} x \\ u \end{bmatrix},$$

where sbw is the servo Bandwidth. The equivalent shortened notation is

$$\dot{xc} = AC\ xc + BC\ uc + DC\ w \tag{3.5}$$

$$y = HC\ xc + FUC\ uc + GDC\ w,$$

where:

- **xc** = augmented state vector, with actual servo control positions as the added states,
- **uc** = commanded servo control position,
- **AC** = augmented system matrix,
- **BC** = control matrix (based on commanded controls),
- **DC** = augmented disturbance matrix,
- **HC,FUC,GDC** = augmented continuous output matrices.

The AC and BC matrices include the servo dynamics, which dictate the difference between actual control surface positions (which are part of the xc vector) and the commanded control positions (which make up the uc vector). This set of system and output equations represents the continuous dynamics of the open loop system, to which either analog or sampled data design methods can be applied.

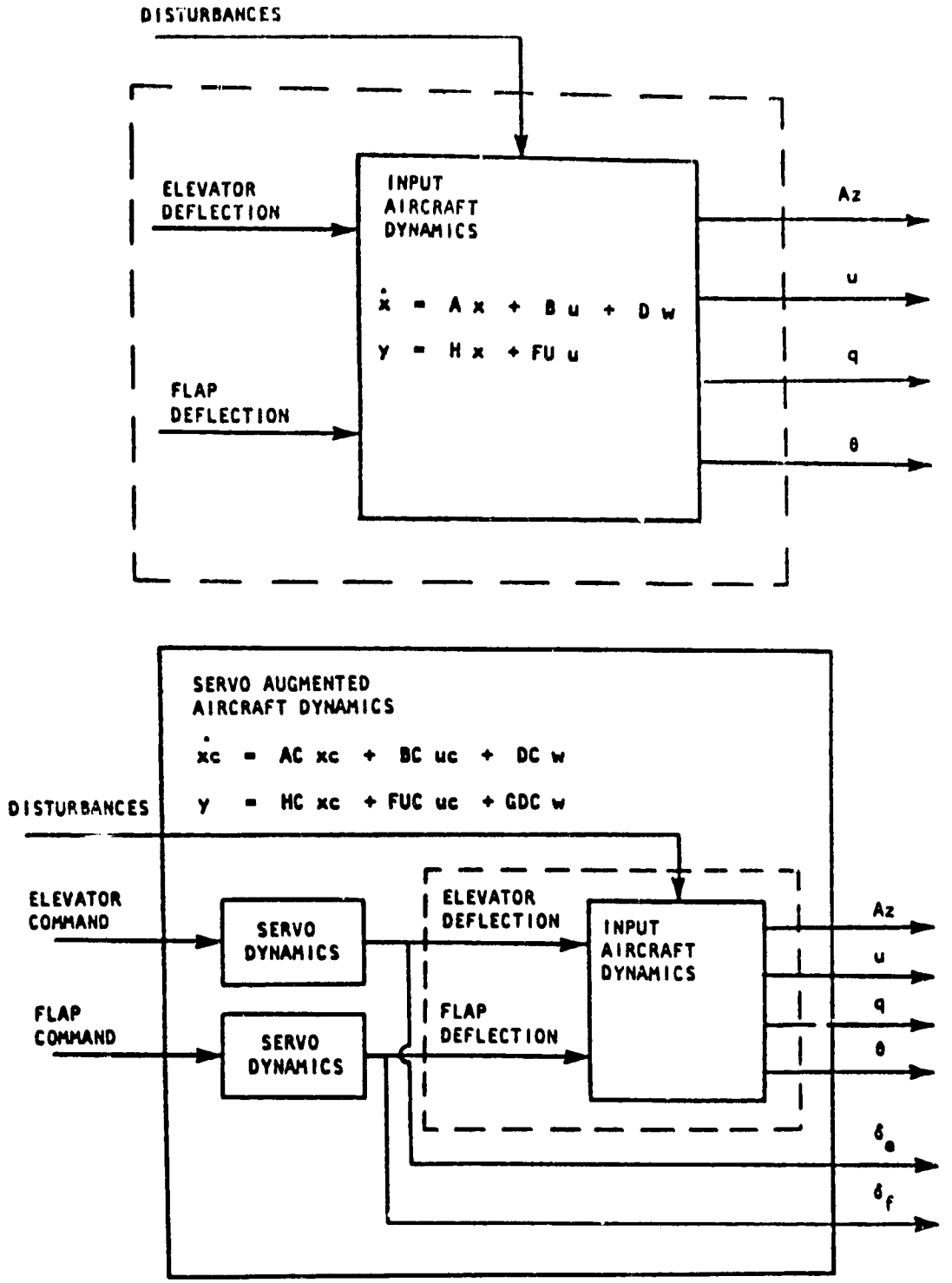

FIGURE 3.4 Servo Augmentation Procedure

3.2.3 ANALYSIS OF THE OPEN LOOP SYSTEM

The analysis of the open loop response provides a performance comparison for closed loop designs. This analysis consists of an open loop time history and open loop power spectral density calculation.

3.2.3.1 OPEN LOOP TIME HISTORY

Four inputs to the open loop time history can be specified, including up to two open loop control inputs and up to two gust disturbances. These control commands and/or gust disturbances are input through a data file. For the design of ride quality systems, the data file includes a time history of gusts which simulate a Dryden gust field. There are no pilot commands, and, because this is an open loop analysis, the control system commands are zero, so the system can be represented by

$$\dot{xc} = AC\ xc + DC\ w, \text{ and} \tag{3.6}$$

$$y = HC\ xc + GDC\ w. \tag{3.7}$$

The result of the simulation is a time history of the output variables (y) as the aircraft is flown through a Dryden gust field. Because of the specific application to ride quality, RMS values of all the variables are calculated as part of the time history simulation. Vertical acceleration is the most important variable in the ride quality of an aircraft, so it is included in the output vector. Any other desired variable can be included in the output vector to evaluate the control system performance. Because ICAD plots outputs (entries in the y vector) rather than states (entries in

the xc vector), the number of variables selected for plotting is independent of the states and controls.

3.2.3.2 OPEN LOOP FREQUENCY RESPONSE

As described in section 3.1, any set of control inputs or disturbances can be combined with any set of outputs for transfer function analysis. The designer is presented with the possible transfer function inputs and outputs (as labeled in a data file) and may choose as many of each as desired. Open loop magnitude and phase plots for the specified transfer functions are calculated and made available for immediate display. The open loop frequency responses are also stored for later comparison with the frequency responses of closed loop designs.

3.2.3.3 OPEN LOOP PSD

If the disturbance (w) is random turbulence, then an open loop transfer function (such as vertical acceleration response to vertical gust) can be combined with a turbulence spectrum (in our case, either the Dryden or the Von Karman forms) and the system response to that gust field can be computed. This is the power spectral density (PSD) technique. This method is especially useful in ride quality analysis, because, although the RMS acceleration is often used to measure system performance, the frequency content is also important. For instance, the accelerations that cause motion sickness are limited to a narrow range of frequencies.

CONTROL subroutines are used to calculate transfer functions between inputs and outputs specified by the user. These transfer functions are

then excited by either the Dryden or the Von Karman gust field spectrum using the equation

$$Po(\omega) = |G(j\omega)|^{1/2} * Pi(\omega), \tag{3.8}$$

where $Po(\omega)$ is the output spectral density at frequency ω and $Pi(\omega)$ is the excitation spectrum that models the gust field. $|G(j\omega)|$ is the magnitude of the transfer function frequency response. The ICAD Program calculates the frequency response and output power spectrum simultaneously and graphically displays the results. As with the time histories, the application of this technique to ride quality systems requires that RMS response to gust inputs be calculated. This is accomplished by the following

$$RMS = [\int_{-\infty}^{+\infty} Po(\omega)\ d\omega\ ]^{1/2}. \tag{3.9}$$

The square root of the value calculated by a numerical integration of the PSD over the selected frequency range yields the RMS. By applying this procedure to the Az/wg (vertical acceleration to vertical gust) transfer function, an RMS similar to that obtained from the time history can be calculated. RMS control activity in response to turbulence is another possible output that would apply to ride quality studies.

3.2.4 DISCRETIZATION

Two discretizations of the continuous system are formed. The first is a discrete model for the time history simulation, and the second is a discrete model for use in both the design and analysis of sampled data feedback control systems. The discretization of the continuous system for

time history simulation is based on a time interval that is small enough to approximate the control inputs as constants over the chosen period. This time interval is represented by Δt and is used to calculate the transition matrix, as shown below.

$$\mathbf{ACDT} = \exp(\mathbf{AC}\ \Delta t). \tag{3.10}$$

This matrix, and the assumption that the control inputs are constant over Δt, permits the calculation of a discrete control power matrix and a discrete disturbance matrix, as

$$\mathbf{BCDT} = {}_0\int^{\Delta t} \mathbf{ACDT}\ \mathbf{BC}\ dt, \tag{3.11}$$

and

$$\mathbf{DCDT} = {}_0\int^{\Delta t} \mathbf{ACDT}\ \mathbf{DC}\ dt. \tag{3.12}$$

The transition and discrete control power matrices are then used to update the state and output vectors as shown below.

$$\mathbf{xc}_{n+1} = \mathbf{ACDT}\ \mathbf{xc}_n + \mathbf{BCDT}\ \mathbf{uc}_n + \mathbf{DCDT}\ \mathbf{w}_n, \tag{3.13}$$

and

$$\mathbf{y}_n = \mathbf{HC}\ \mathbf{xc}_n + \mathbf{FUC}\ \mathbf{uc}_n + \mathbf{GDC}\ \mathbf{w}_n, \tag{3.14}$$

where

ACDT = system matrix discretized by Δt,

BCDT = control power matrix discretized by Δt,

DCDT = disturbance matrix discretized by Δt.

In this manner, disturbance, control, and state vectors are updated

every Δt. A suitable choice of Δt must be made based upon the requirements of the simulation. For the purpose of this design study, a Δt of .01 sec accurately simulates the continuous time response.

The discretization of the continuous system for the design of sampled data control systems and for generation of digital frequency responses is defined by the sample time (Ts) of the sampled data system. This discretization is identical to that of the time simulation, except that the control inputs and disturbances are assumed to be constant for a period of time equal to Ts. This choice of time period for the basis of discretization is accurate for sampled data systems that are based on zero order hold controls and for disturbances that do not have significant frequency content above 1/(2*Ts) Hz. For RQAS application, the maximum Ts is 0.1 sec, so disturbances with frequencies below 5 Hz should be accurately represented. Both the Dryden and Von Karman gust spectrums contain very little gust intensity above this frequency so that this approximation should be sufficiently accurate. The discrete equations for the states and the outputs are shown below.

$$xc_{n+1} = ACD\ xc_n + BCD\ uc_n + DCD\ w_n \tag{3.14}$$

$$y_n = HC\ xc_n + FUC\ uc_n + GDC\ w_n \tag{3.15}$$

where:

ACD = system matrix discretized by Ts,

BCD = control power matrix discretized by Ts,

DCD = disturbance matrix discretized by Ts.

3.2.5 CLOSED LOOP SYSTEM DESIGN METHODS

Both optimal and classical techniques may be used to design the control system. These techniques are described in sections 3.2.5.1 and 3.2.5.2.

3.2.5.1 OPTIMAL TECHNIQUES

The optimal control system designs are based on the Linear Quadratic Guassian (LQG) methods contained in the ORACLS computer program originated by NASA. ICAD utilizes selected subroutines from ORACLS to calculate full state optimal feedback gain matrices based upon specified state (Q) and control (R) weighting matrices. The standard system and output equations, and the cost functional for the LQG design approach are, respectively,

$$\dot{x} = A\,x + B\,u \tag{3.17}$$

$$y = H\,x \tag{3.18}$$

$$J = {}_0\int^{\infty}(Q'\ y\ Q + R'\ u\ R)\ dt \tag{3.19}$$

Any system that can be represented in the above form can be handled by the ICAD Program. The only limitation is that the outputs must be linear functions of the states, because the weighting matrices are applied to the outputs and the controls rather than to the states and the controls. Methods of applying this approach so that linear combinations of states and control positions, specifically acceleration, can be made into outputs for RQAS design are discussed in Chapter 4.

To use the optimal design option of the ICAD Program, initial Q and R weighting matrices are entered from the main data file. The first pass

through the program generates a design based on these weighting factors, and the design engineer can evaluate his design using time history or frequency response information in the design loop. The designer can then modify the **Q** and **R** matrices to create and evaluate another design. Graphics and numerical data are made available to the system designer both on the terminal screen and in the four output data files that are created by the program (see Table 3.1). The design engineer can continue to cycle through the program until a satisfactory design has been generated.

3.2.5.2 CLASSICAL TECHNIQUES

Subroutines from CONTROL are used to develop designs based on classical analysis. Feedback loops are defined in a user-specified block diagram, which is entered from a data file according to the CONTROL protocol (see Reference 15 for details on these methods). Root loci can be generated, based on one or two feedback loops that can contain any state or any linear combination of states. S-plane root loci are generated for continuous systems, and both z- and w'- plane root loci are generated for sampled data systems. The user can look at the root loci and choose a value for each of two feedback gains. The selected gains for the feedback loops are then converted into the state feedback gain matrices needed for the closed loop analysis. The resulting closed loop responses can be evaluated and another pass through the design loop can be executed, in a manner similar to that of the optimal procedure. However, for classical designs only the two feedback gains may be changed interactively; the feedback loops and feedback variables are fixed until the program is restarted.

If the original gain ranges were not adequate, new root loci for different ranges of feedback gains can be generated.

3.2.6 CLOSED LOOP RESPONSE

For the open loop time histories, uc was a null vector. For the closed loop, uc is calculated as a linear combinations of the states by the feedback gain matrix, the F matrix. The same approach was used for the closed loop analyses as was used for the open loop, except that now the system control vector, uc, is no longer a null vector.

3.2.6.2 CLOSED LOOP TIME HISTORY

All the open loop matrices are valid for closed loop analysis, if logic is added to update the controls based on the feedback gain matrix.

$$\dot{xc} = AC\ xc + BC\ uc + DC\ w, \tag{3.20}$$

and

$$y = HC\ xc + FUC\ uc + GC\ w, \tag{3.21}$$

where

$$uc = -F\ x. \tag{3.22}$$

When modeling a sampled data system, the controls in uc are fed back only after a specified time delay (Td) and are held constant until the next control value is output, which occurs Ts seconds later. As detailed in the discretization explanation in section 3.2.3.2, the "continuous" time history between control commands from the digital control system is computed for every Δt. The closed loop time history can be plotted on the CRT alone

or with any previous open or closed loop runs to evaluate various designs. RMS values, computed similarly to those of the open loop case, are also available for comparison.

3.2.6.2 CLOSED LOOP FREQUENCY RESPONSE AND PSD

The closed loop frequency responses and PSDs can be generated in response to random turbulence inputs and compared to open loop and other closed loop designs. For this analysis, all matrices are the same as those of the open loop case except the A matrix, which is calculated as the closed loop system equivalent A matrix, ACL. Since, in the closed loop case, uc can be calculated from xc, the system can be represented as shown below for excitation by disturbances.

$$\dot{xc} = ACL\ xc + DC\ w, \tag{3.23}$$

where

$$ACL = AC - BC\ F\ .$$

For sampled data systems, this equation is

$$xc_{n+1} = ACLD\ xc_n + DCD\ w_n. \tag{3.24}$$

where:

ACLD = discretized closed loop system matrix.

The output equation is the same for both sampled data and continuous systems,

$$y = HCL\ xc + GDC\ w, \tag{3.25}$$

where

HCL = closed loop output matrix.

Alternately, frequency response to control inputs can be calculated using the equations below, where **ucom** now represent commands coming from outside the control loop, if there are no disturbances.

$$\dot{xc} = \mathbf{ACLD}\ xc + \mathbf{BCD}\ ucom \quad \text{(for the continuous case)} \qquad (3.26)$$

$$xc_{n+1} = \mathbf{ACLD}\ xc_n + \mathbf{BCD}\ ucom_n \quad \text{(for the sampled data case)} \qquad (3.27)$$

and

$$y = \mathbf{HCL}\ xc + \mathbf{FUC}\ ucom \quad \text{(for both cases)} \qquad (3.28)$$

This capability was not used for RQAS design, because we were only concerned with system response to external disturbances. However, in order to attempt to make the ICAD program a general tool for use in control augmentation design as well as stability augmentation, this capability was included.

This completes the procedure needed to design and evaluate an analog or sampled data control system. As mentioned, this process can be repeated as many times as necessary, and analyses from all loops through the procedure can be compared. Appendix B is a detailed users manual for the ICAD program, which includes a list of all necessary inputs, descriptions of the output files generated, and step-by-step instructions for interactive usage.

4. OPTIMAL DESIGN

4.1 OVERVIEW

The majority of optimal controller designs are based on application of Linear Quadratic Guassian (LQG) synthesis which defines controls that minimize an infinite-time quadratic cost functional subject to the constraints of the differential equations of motion. The optimal design portion of the ICAD program is based on the ORACLS set of fortran subroutines, which are numerical linear algebraic procedures that apply LQG methods to optimal regulator designs [16]. A regulator is a controller that attempts to drive specified feedback variables to zero, which is precisely what is desired of a ride smoothing system with regard to accelerations.

4.1.1 CONTINUOUS SYSTEMS

The fundamental requirement for applying the ORACLS design tecnniques is that the dynamic system be represented as a linear, time invariant system of differential state and output vector equations,

$$\dot{x} = A\,x + B\,u \tag{4.1}$$

and

$$y = H\,x\,.$$

When the minimization is performed on an infinite-time cost functional, as is normally the case, a constant feedback gain control law

results. The feedback controls become a linear combination of the states,

$$u = K\,x \tag{4.2}$$

where K is a constant gain matrix [17]. This constant gain matrix is found by minimizing the continuous cost functional

$$J = {}_0\int^{\infty} [\, x'\,Q\,x + u'\,R\,u \,]\,dt \tag{4.3}$$

where Q is a positive semi-definite state weighting matrix and R is a positive definite control weighting matrix. The solution to this cost functional is defined by the matrix P which satisfies the reduced-matrix Ricatti equation

$$A'\,P + P\,A - P\,B\,R^{-1}\,B'\,P + Q = 0 \tag{4.4}$$

so that the gain matrix becomes

$$K = R^{-1}\,B'\,P. \tag{4.5}$$

The output variables are limited to linear combinations of the states because of the desire to apply the Q weighting matrix to the output variables rather than to the states. This approach will create a direct cause and effect relationship between changes in the weighting matrices and the system performance as defined by the output variables. The designer can then weight a single variable of interest, rather than weighting each of the state variables separately to get the desired effect. The cost func-

tional with the weighting on the outputs and the output limitation is

$$J = \int_0^{\infty} [\, y' Q y + u' R u \,]\, dt. \tag{4.6}$$

The reason for limiting the outputs to a linear combination of the states is that the theory and methodology used to solve the Ricatti equation require that the cost functional must be applied to the states and controls, so that the final cost functional becomes

$$J = \int_0^{\infty} [\, x' H'QH x + u' R u \,]\, dt, \tag{4.7}$$

where H'QH is the weighting matrix on the states.

The ICAD Program described in the previous chapter permits the outputs of the dynamic system to be made up linear combinations of the state and control variables,

$$y = H x + FU u \tag{4.8}$$

in order to allow more flexibility in defining the system outputs, specifically so that acceleration could be made an output. However, for general application of ORACLS subroutines as discussed above, the outputs are limited to only a linear combination of the states. This limitation appears severe; but, as will be shown in the next section, any outputs that can be expressed in the form of equation 4.8 can also be manipulated into the form required for optimal design. Therefore any problem that can be set up with outputs that are linear combinations of states and controls can then be analyzed by the optimal control section of the ICAD program.

4.1.2 DISCRETE SYSTEMS

The discrete state and output vector difference equations, assuming that the controls, u_n, are constant over each Ts, are

$$x_{n+1} = \Phi\, x_n + \Gamma\, u_n, \qquad (4.9)$$

$$y_n = H\, x_n,$$

where

$$\Phi = \exp[A\, t],$$

$$\Gamma = \{ {}_0\int^{Ts} \Phi\, dt\}\, B.$$

The discrete cost functional becomes

$$J = \sum_{n=1}^{\infty} [x'_n\, QD\, x_n + 2\, x'_n\, M\, u_n + u'_n\, RD\, u_n] \qquad (4.10)$$

where the discrete state, control and cross weighting matrices are

$$QD = {}_0\int^{Ts} \{\Phi'(t)\, Q\, \Phi(t)\}\, dt \qquad (4.11)$$

$$RD = Ts\, R + {}_0\int^{Ts} \{\Gamma'(t)\, Q\, \Gamma(t)\}\, dt$$

$$M = {}_0\int^{Ts} \{\Phi'(t)\, Q\, \Gamma(t)\}\, dt$$

The solution to the discrete Ricatti equation and the gain matrix becomes

$$P = \Phi' P \Phi - (\Gamma' P \Phi + M')'\, (RD + \Gamma' P \Gamma)^{-1}\, (\Gamma' P \Phi + M') + QD, \qquad (4.12)$$

$$K = (RD + \Gamma' P \Gamma)^{-1}\, (\Gamma' P \Phi + M'). \qquad (4.13)$$

The designer inputs the continuous weighting matrices and the sample time (Ts), and the ICAD program does all of the conversions to discrete matrices and equations. Thus the engineer designs using continuous output and control weighting matrices, and doesn't have to worry about discrete weighting and cross weighting functions.

4.2 APPLICATION TO ROAS DESIGN

The primary variables of interest in the design of any ride smoothing system are the accelerations. As described in chapter 3 and the previous section, the implementation of optimal control design in the ICAD program permits direct weighting of the outputs rather than the states. To reiterate, the purpose of weighting the outputs rather than the states is to permit the designer maximum flexibility in selecting his own weighted variables rather than automatically being forced to weight the states. The outputs may be a single state variable or they may be some combination of states and controls, e.g. acceleration. However, output weighting can be used only if the outputs are limited to linear combinations of the states. Acceleration (Az) is the linear combination of preturbation states (q,θ), and a state derivative ($\dot{\alpha}$) shown below

$$Az = U_0\dot{\alpha} - U_0 q + g \sin \theta_0 \theta. \tag{4.14}$$

Alternately, by substituting the state differential equation into (4.14), Az can be represented as a combination of states and controls

$$Az = U_0[Z_\alpha \alpha + Z_u u + Z_q q + Z_\theta \theta + Z_{\delta e}\delta e + Z_{\delta f}\delta f] - U_0 q + g \sin \theta_0 \theta, \tag{4.15}$$

where the Z variables are the elements from the state and control matrices.

4.2.1 STANDARD OPTIMAL REGULATOR

The standard form of the aircraft state equations do not include the control surface positions as states, and so acceleration cannot be included as an output. Since acceleration is not an output, it cannot be weighted

directly even though it is the primary design variable. The desired reductions in accelerations could be attemped by weighting each of the states relative to its contribution to the total acceleration. However, one of the great attractions of using weighting matrices in optimal control is that changes in the **Q** or **R** matrices are directly reflected in changes to the weighted variable. Reducing accelerations by weighting the states rather than weighting the accelerations lacks the desired direct relationship between the weighting matrices and the system performance. Therefore an alternative representation of the system to include acceleration as an output was sought, so that the desired direct weighting matrix to performace relationship could be established.

4.2.2 STATE AUGMENTED OPTIMAL REGULATOR

The problem of how to make the accelerations an output can be solved by augmenting the state vector with the control surface deflections. This augmentation can be accomplished in either of two ways. The state vector can be augmented by adding the servo dynamics into the problem. In this approach, the control specified by the design is a command to the servo, and the actual surface deflection is a state variable. The other approach is to convert the system to a rate command rather than a position command system. In this case the servo dynamics are not part of the design, but the actual surface deflection is a state variable because the commanded variable is the derivative of the surface deflection rather than the surface deflection.

4.2.2.1 STATE AUGMENTATION BY SERVO DYNAMICS

The first method to augment the state vector would be to include the servo dynamics in the equations of motion. This is already done by the ICAD program to account for the servo dynamics in the system performance in the time history evaluations. The servo-augmented system of state and outputs equations is

$$\begin{bmatrix} \dot{x} \\ \dot{u} \end{bmatrix} = \begin{bmatrix} A & B \\ 0 & -sbw\ I \end{bmatrix} \begin{bmatrix} x \\ u \end{bmatrix} + \begin{bmatrix} 0 \\ sbw\ I \end{bmatrix} uc\ , \tag{4.16}$$

and

$$y = [H \quad FU] \begin{bmatrix} x \\ u \end{bmatrix}$$

where sbw is the servo Bandwidth. The equivalent shortened notation is

$$\dot{xc} = AC\ xc + BC\ uc, \tag{4.17}$$

$$y = HC\ xc,$$

where

$xc' = \{ \alpha, u, q, \theta, \delta_e, \delta_f \}$,

$uc' = \{ U_e, U_f \}$, (U are commands to the servos)

$y' = \{ Az, \alpha, q, \theta, \delta_e, \delta_f \}$,

AC is the A matrix augmented by the B Matrix and the servo dynamics,

BC is a zero matrix augmented by the servo dynamics,

and

HC is the H matrix augmented by the FU matrix.

The disadvantage of this approach is that it adds two more states that have to be sensed for the full state feedback control laws generated by the

optimal design program. However it does permit acceleration to be included in the output vector and so to be weighted directly to simplify the design process.

4.2.2.2 STATE AUGMENTATION BY RATE COMMAND

An alternate approach to augmenting the state vector is to assume perfect servos, but to command the control surface deflection rate rather than the control surface deflection. In this approach, the accelerations can again be represented as a pure linear combination of the states. The augmented state and output equations would be

$$\begin{bmatrix} \dot{x} \\ \dot{u} \end{bmatrix} = \begin{bmatrix} A & B \\ 0 & I \end{bmatrix} \cdot \begin{bmatrix} x \\ u \end{bmatrix} + \begin{bmatrix} 0 \\ I \end{bmatrix} \quad uc \,, \tag{4.18}$$

and

$$y = [H \quad FU] \begin{bmatrix} x \\ u \end{bmatrix}$$

The equivalent shortened notation would be

$$\dot{xp} = AP\ xp + BP\ up, \tag{4.19}$$

and

$$y = HC\ xp,$$

where

$xp' = \{ \alpha, u, q, \theta, \delta_e, \delta_f \}$,

$up' = \{ \dot{\delta}_e, \dot{\delta}_f \}$,

$y' = \{ Az, \alpha, q, \theta, \delta_e, \delta_f \}$,

AP is equal to **AC** except the bottom two rows are all zero,

BP is a zero matrix augmented by the identity matrix for the rates.

and

HC is the same as **HC** in equation (4.17).

This method of state augmentation has two distinct features in addition to the capability to represent the accelerations as linear combinations of the states. The first is that the designer can now put a separate weight on the control surface deflections and the control surface deflection rates. This change adds another degree of flexibility in the design process. Even though the control deflection and its rate are not independent, the separate weighting factors can aid in tailoring the designs to specific rate or deflection limits.

The second feature is that the servo dynamics are not included in the design process, and so the optimal designs are based on perfect servos. Therefore the calculated control position commands from the previous cycle can be used as estimates for the actual control positions without significantly distorting the results. For general aviation application it is desireable to minimize the number of feedback loops, and hence the sensing requirements, to limit system complexity and cost.

The obvious disadvantage is that servos are typically designed for position commands and not rate commands. However this does not pose a significant problem for either analog or digital implementation. Further discussion on this topic is included in the next section where the details of this control law implementation are discussed. Because actual implementation of this aproach can be readily handled and this approach requires two fewer sensors, the command rate digital system was chosen as the primary design approach.

4.3 CONTROL RATE WEIGHTING DESIGN

Control rate weighting (CRW) was originally developed to provide the ability to weight the control positions and rates separately, and for the beneficial effect this had on system design [18]. Control rate command, a different name for the same thing, was introduced in the previous section primarily as a way to augment the state vector with the control positions so that acceleration could be made into an output. Thus the principal purpose of the CRW design approach. i.e. to permit separate weighting of the control and control rate by including a low pass filter in the feedback loop, is merely a collateral benefit to RQAS applications. The development of this approach will first be discussed in the continuous domain and then in the discrete domain.

4.3.1 CONTINUOUS CONTROL RATE WEIGHTING

The system equations for this approach have already been presented in the previous section (4.18, 4.19). The cost functional for weighting the states, the control position, and the control rate in the continuous domain for the CRW method is

$$J = {}_0\int^{\infty} [x' Q x + u' R u + \dot{u}' S \dot{u}] dt. \qquad (4.20)$$

Putting the above cost functional into terms of the rate command augmentation equations would yield:

$$J = {}_0\int^{\infty} [xp' HC' QP HC xp + up' S up] dt, \qquad (4.21)$$

where

$$QP = \begin{bmatrix} Q & 0 \\ 0 & R \end{bmatrix},$$

and

$$xp' = [x' \quad u']$$

$$u_p = \dot{u}.$$

Now when the gain matrices are found, the system controls are rate commands rather than position commands

$$up = \dot{u} = - F \; xp = -[F_1 \quad F_2] \begin{bmatrix} x \\ u \end{bmatrix}. \tag{4.22}$$

The implementation of this rate command would be handled in the continuous domain by simply integrating the commanded rate with an operational amplifier circuit prior to sending the signal to the position servo. However, implementation on a digital system is more complex, and is discussed in the next section.

4.3.2 DISCRETE CONTROL RATE WEIGHTING

The discretization of a linear system of equations, as discussed earlier, is done based upon a time interval over which the control is assumed to be constant. For a sampled data system, that time period is the sample time (Ts). The system differential equation becomes a difference equation, and the controls are treated as zero order holds. The fundamental point to keep in mind here is that the control is assumed to remain constant over the period of time used for discretization.

4.3.2.1 DESIGN

To apply the discretization process to the CRW approach, we start with equation (4.19). Discretizing the state and control equation separately results in the state and control difference equations

$$x_{n+1} = AD\ x_n + BD\ u_n \tag{4.23}$$

and

$$u_{n+1} = u_n + \Delta t\ up_n.$$

Putting this back into a single matrix equation we get:

$$\begin{bmatrix} x \\ u \end{bmatrix}_{n+1} = \begin{bmatrix} AD & BD \\ 0 & I \end{bmatrix} \begin{bmatrix} x \\ u \end{bmatrix}_n + \begin{bmatrix} 0 \\ \Delta t I \end{bmatrix} up_n . \tag{4.24}$$

When the continuous cost functional is transformed into a discrete cost functional, the cross weighting matrix appears between the states and the controls so that

$$J = \sum_{n=1}^{\infty} [x'_n\ QD\ x_n + 2\ x'_n\ M\ up'_n + up'_n\ RD\ up_n]. \tag{4.25}$$

This discrete cost functional is minimized subject to the constraints of the discrete system equations to provide a feedback gain matrix as in the continuous case, so that the system controls are

$$up_n = -F \begin{bmatrix} x \\ u \end{bmatrix}_n \tag{4.26}$$

The key thing to remember here is that the control vector, up, represents the control rate, $\dot{u}$. The gain matrix, which is the solution for a particular set of **Q** and **R** matrices, can be used to calculate the desired or optimum control rates for that design. The next step is to convert the desired control rates to control positions for implementaion.

4.3.2.2 IMPLEMENTATION

Because of the discretization process assumptions, the control variable in this problem, i.e. the control rate, remains constant over the discretization time period, Ts. Therefore the control position over any given sample period is a ramp function. To implement a ramp function on a position servo requires an approximation. As shown in equation 4.23, the desired control position at any given time during the sample period (which is the time period used to discretize the system equations) is the previous servo position plus the desired rate times the amount of time elapsed. Thus any portion of the final value of the desired servo position can be easily calculated. Any value between the initial and final values could be chosen as the position output to approximate the desired ramp function over the entire sample period. The two parameters necessary to consider when trying to approximate the desired rate command for the discrete CRW design are the computational delay time (Td, defined as the amount of time between reading the sensors, and outputting the new commands to the servos), and the portion of the final ramp value to use as the position command.

Several implementation schemes are possible when trying to approximate the desired ramp function. With perfect (infinitely fast) servos and small Td, the best approximation would be to use 50% of the final value of the ramp function. However, with a longer Td, the best approximation would be 100% of the final value of the ramp (see Figure 4.1a,b). With perfect servos, the control implementation becomes a tradeoff between the Td and the percent of the final value sent to the servo. It is possible to overcontrol the system with fast servos and small Td's if a large per cent of the final value is used without using some extra delay (Figure 4.1c). The most common approximation to date is presented in reference [19], where 100% of the final value of the ramp is used for the position command, but the command is delayed until the end of the sample period (Figure 4.1d).

When the servo dynamics are included, the servo bandwidth and rate limit become additional implementation considerations. With low to mid range bandwidth servos (10-20 rad/sec) the probability of over controlling the system when using the full ramp value for the servo position decreases significantly, even when very small Td are used (see Figure 4.2). It is therefore possible to use the ramp final value for the position command without delaying the signal output until the end of the sample period. If the servo bandwidth becomes very much higher than that selected for the nominal value in this study, the chance of over-driving the controls again reappears. This situation could be prevented by reducing the percent of the final value used, or by delaying the control output. However, for this application, the servo command was fixed at the full value and the design parameters then were limited to the Ts, Td, and servo bandwidth.

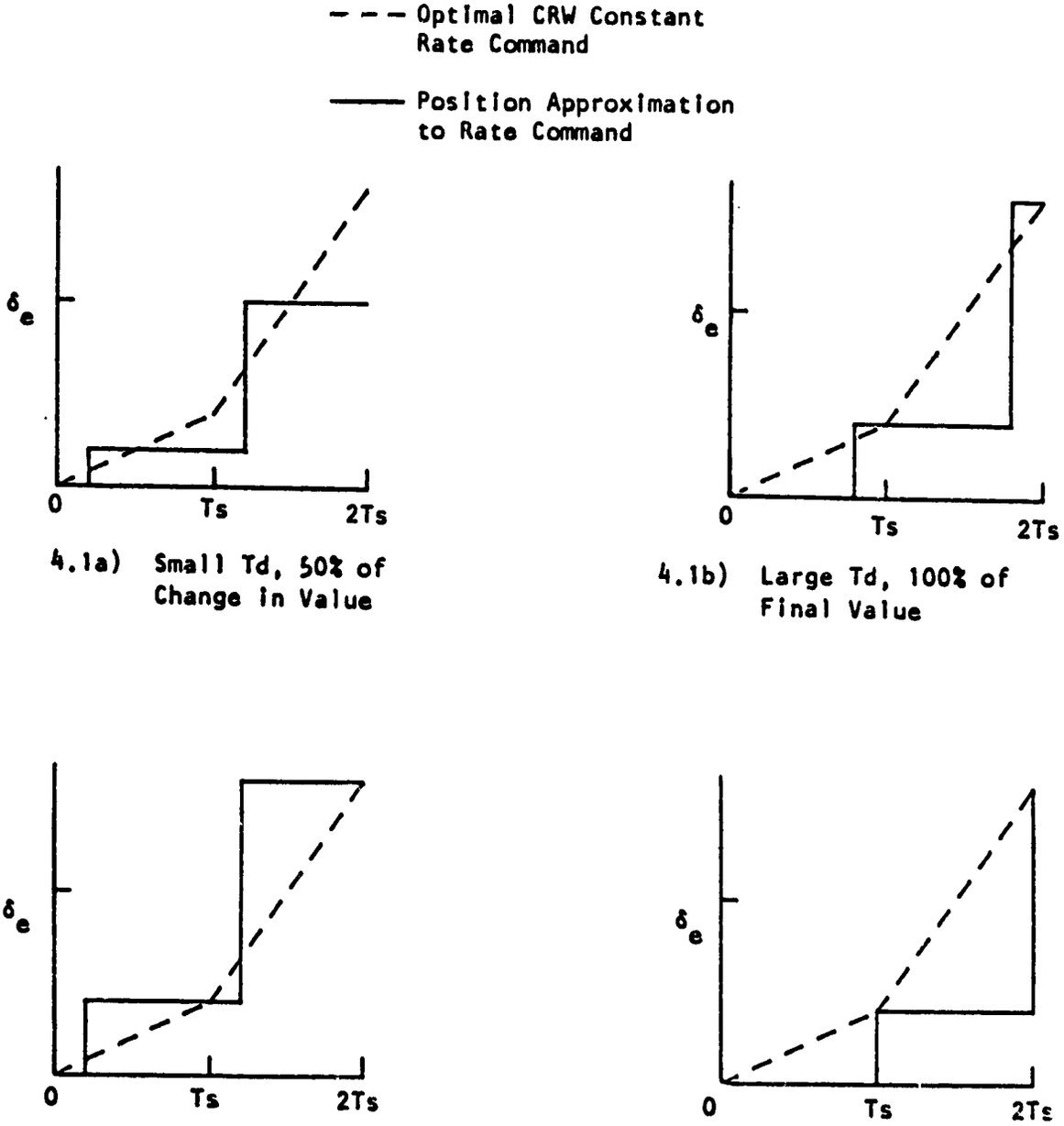

4.1a) Small Td, 50% of Change in Value

4.1b) Large Td, 100% of Final Value

4.1c) Small Td, 100% Final Value (Overcontrol)

4.1d) Td=Ts, 100% Final Value (Common Implementation)

Figure 4.1 Control Rate Weighting Command Implementation with Perfect Servos

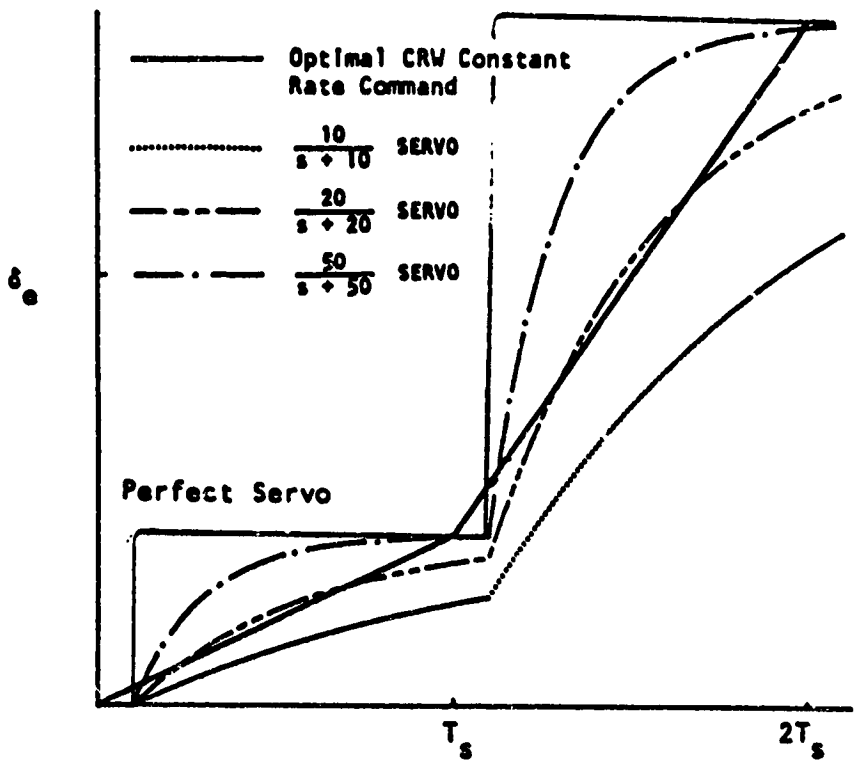

FIGURE 4.2 Control Rate Weighting Command Implementation
Small Td, 100% Final Value, Various Servo Models

4.4 DETAILED OPTIMAL POINT DESIGNS

The five flight conditions selected to represent a cross-section of a typical commuter aircraft mission included one takeoff, two climb, one cruise, and one approach configuration, Table 4.1. Emphasis was placed on the takeoff, climb and approach phases of flight because that is where the turbulence is strongest, and because commuter aircraft typically spend a relatively high percentage of their operating time in these mission phases. Optimal full state feedback designs were generated for these five configurations using the CRW design approach.

Table 4.1 Cessna 402B Flight Conditions

Configuration	Altitude(ft)	TAS(kts/fps)	Flaps(deg)
Takeoff	Sea level	109/184	0
Climb	Sea Level	125/211	0
Climb	5000	134/227	0
Cruise	20000	212/358	0
Approach	Sea Level	95/160	30

4.4.1 EVALUATION AND DESIGN

The actual design of the ROASs for the selected flight conditions was greatly simplified by the decision to set up the problem as described in the previous section, with the acceleration as one of the output variables. This section will include a discussion of the approach used to evaluate the

basic and augmented aircraft, and a brief step-by-step description of the actual design procedure used to generate the five optimal point designs to be discussed in section 4.4.2.

4.4.1.1 EVALUATION

In the past, PSD analyses have been a standard tool for evaluating the performance of the ride quality systems. As described in chapter 3, transfer functions of the system can easily be combined with the Dryden or Von Karman gust spectra to generate open and closed loop PSD plots. These PSD plots have the advantage of providing both a frequency distribution and an RMS value of the vertical acceleration. Although we have included frequency domain analyses in the evaluation process, the primary evaluation tool for our RQAS designs has been time domain analysis.

The fundamental reason behind the selection of time history simulation rather than frequency domain analysis for evaluation of our RQAS's performance was the selection of a digital rather than analog control system. Time history simulation permits accurate modeling of the discrete aspects of the system, e.g. zero-order holds for the controls, and computational delay times. Time domain analysis also permits analysis of more variables, and more features of those variables, e.g. both the servo commands and the servo outputs can be examined, and the peak, rate and RMS values for any desired variable are all available. Frequency domain analyses permit calculation of only the RMS value. Although RMS acceleration was the primary evaluation variable, peak values of the acceleration and flap deflection, as well as the maximum flap rate and flap RMS values were used

to evaluate the candidate designs. For these reasons, time history simulation formed the basis for the majority of our evaluations.

An example of the quantitative data from the ICAD program which is available to the design engineer for evaluation is shown in Table 4.2 for the takeoff flight configuration. For each cycle through the design process, the **Q** and **R** weighting matrices, the feedback gain matrix, and the maximum value, maximum rate and the RMS for all of the outputs are printed on the terminal screen and saved in a data file. Also included in the quantitative data are the eigenvalues (in the S plane for continuous or the Z and W' planes for discrete systems) and the RMS acceleration calculated from the appropriate S-plane or W'-plane PSD response.

Visual inspection and qualitative evaluations of both time history and frequency domain responses were made using both the screen graphics and hardcopy features of the ICAD program. Samples of the acceleration, elevator, and flap time history plots for the basic and augmented aircraft for the takeoff configuration are shown in Figures 4.3-4.5. Equivalent plots could be generated for any output variable.

4.4.1.2 DESIGN

The reason for choosing the CRW control strucure was to be able to include the acceleration in the output vector. The elements of the output vector were then ordered according to their importance. In this way the weighting process would start at the top left corner of the weighting matrix, and proceed down the diagonal to provide a methodical approach to determining the proper weights for each output. This setup permitted

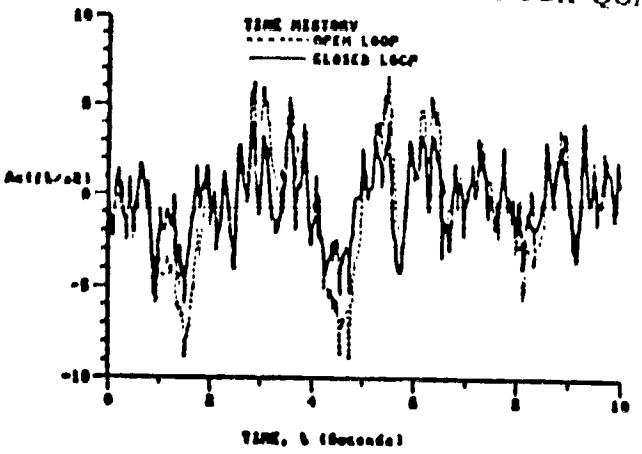

FIGURE 4.3 Vertical Acceleration (Sample Time History Plot)

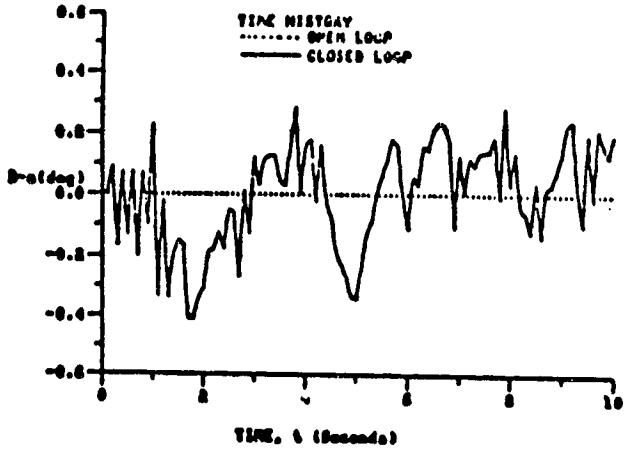

FIGURE 4.4 Elevator Position (Sample Time History Plot)

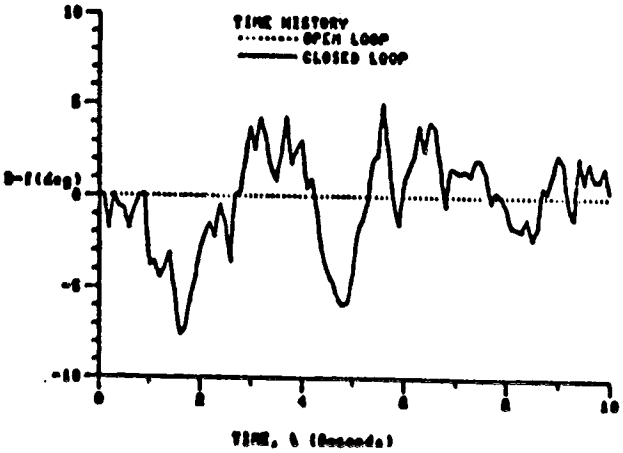

FIGURE 4.5 Flap Position (Sample Time History Plot)

TABLE 4.2 SAMPLE OPTIMAL DESIGN OUTPUT

```
TITLE OF THIS RUN:  FLGT 1 - NOMINAL  (MODEL A)
THE ALTITUDE IS:                      500.     ft
THE AIRSPEED IS:                      183.86   ft/sec
THE SAMPLE TIME IS:                   0.100    sec
THE DELTA TIME IS:                    0.010    sec
THE TURBULENCE INTENSITY IS:          6.00     ft/sec

                THIS IS AN OPEN LOOP RESPONSE.
     Az(ft/s2) Alfa(deg)  Q(deg/s) Thet(deg)  D-e(deg)  D-f(deg)
 MAX    -8.817     2.366    -1.322    -1.144     0.000     0.000
RATE  -124.685    33.182    -6.313     1.322     0.000     0.000
 RMS     3.095     0.872     0.551     0.605     0.000     0.000
THE EIGENVALUES OF THE SYSTEM ARE
  Z-REAL     Z-IMAG     W'-REAL    W'-IMAG   FREQUENCY   DAMPING
0.515923   0.000000  -6.386562   0.000000   6.386562   1.000000
0.809889   0.000000  -2.100803   0.000000   2.100803   1.000000
0.999542   0.015149  -0.003431   0.151556   0.151594   0.022631
0.999542  -0.015149  -0.003431  -0.151556   0.151594   0.022631
0.367879   0.000000  -9.242343   0.000000   9.242343   1.000000
0.367879   0.000000  -9.242343   0.000000   9.242343   1.000000
          3.50 ft/sec^2 IS THE RMS VALUE FROM THE DIGITAL PSD

********** THIS IS DIGITAL DESIGN NUMBER   1
    Q    MATRIX       6 ROWS       6 COLUMNS
1.000000   0.000000   0.000000   0.000000   0.000000   0.000000
0.000000   0.150000   0.000000   0.000000   0.000000   0.000000
0.000000   0.000000   0.750000   0.000000   0.000000   0.000000
0.000000   0.000000   0.000000   0.000100   0.000000   0.000000
0.000000   0.000000   0.000000   0.000000   0.100000   0.000000
0.000000   0.000000   0.000000   0.000000   0.000000   0.010000
    R    MATRIX       2 ROWS       2 COLUMNS
  0.050000     0.000000
  0.000000     0.100000
    FCL  MATRIX       2 ROWS       6 COLUMNS
-0.838816  -0.007035  -3.472487  -0.871027  17.427383  -0.092962
88.575622   0.141384  14.473325  13.268816 -17.855951  11.944615
                                COMPUTATIONAL DELAY TIME = 0.100
     Az(ft/s2) Alfa(deg)  Q(deg/s) Thet(deg)  D-e(deg)  D-f(deg)
 MAX    -7.105     2.604    -1.700    -1.678    -0.341   -14.414
RATE  -129.025    32.802    -7.564     1.699     2.601  -102.658
 RMS     2.403     0.949     0.697     0.916     0.144     5.263
THE EIGENVALUES OF THE SYSTEM ARE
  Z-REAL     Z-IMAG     W'-REAL    W'-IMAG   FREQUENCY   DAMPING
0.389104   0.332495  -7.235152   6.518994   9.738824   0.742918
0.389104   0.332495  -7.235152  -6.518994   9.738824   0.742918
0.314105   0.000000  10.438976   0.000000   0.438976   1.000000
0.889470   0.000000  -1.169956   0.000000   1.169956   1.000000
0.995260   0.005682  -0.047349   0.057087   0.074167   0.638404
0.995260   0.005682  -0.047349  -0.057087   0.074167   0.638404
          2.76 ft/sec^2 IS THE RMS VALUE FROM THE DIGITAL PSD
```

development of a direct and easy to use approach to optimal ROAS design as outlined below.

1. The first step was to establish initial **Q** and **R** weighting matrices as the design starting point. Units on all of the output variables were chosen so that maximums were as close as possible to the same magnitude. This was done so that all of the elements of the **Q** and **R** matrices could be kept within a couple orders of magnitude for numerical reasons.[1] The units used were ft/s2, deg, and ft/sec for the acceleration, angles, and velocity, respectively. The initial weighting matrices included 1.0 on the acceleration and 0.1 weights on the other outputs and controls.

2. The next step was to increase the weight on the acceleration until the resulting RMS value either stopped decreasing or started increasing. When this value for the acceleration weight factor was found, the **Q** and **R** set of matrices was normalized so that the acceleration weight was reset to 1.0.

3. The design was then fine tuned using the other weighting factors. Typically slight increases in the angle of attack and the pitch rate weighting factors were required to minimize the RMS accelerations.

1. For example, if the acceleration was 0.1 g and alpha was 5 deg, then for each to have equal impact on the cost functional the acceleration weight would have to be 2500 times larger than the angle of attack weight factor. This is because the contribution to the cost functional is the variable squared times the weighting factor, e.g. the ratio between the acceleration and the alpha weights would have to be [(5 x 5)/(.1 x .1)] This large difference between the elements of the weighting matrices can cause numerical problems in the solution of the Ricatti Equation.

4. The next step was then to adjust the control and control rate weighting factors to insure that physical limits for the control positions and servo rates were not violated. The flap deflection limit was 20 degrees, and the servo rate limit was 150 deg/sec.

5. The final step was then to go back to examine each of the weighting factors again, with the new control and control weights, to insure that the design point had not changed significantly.

6. An additional step would be taken for the final design after the actual flap control power is defined. This step would be to do a detailed tradeoff analysis to discover the relationship between ride quality improvements and the drag penalty (flap RMS deflection) and hardware cost (servo rate limit). An approach to this study would be to gradually decrease the control and control rate weights in order to establish a relationship between the flap activity and the RMS acceleration reductions. Figure 4.6 is an example of this type of information presented graphically. This particular example is for the take-off condition and it shows that the RMS reductions become negligible while the control activity continues to increase for reduced control weights. A detailed tradeoff analysis with the final RQAS design would indicate where on the curves would be the best compromise between acceleration reduction and flap RMS and rates.

This basic approach was applied to each of the flight conditions for both continuous and digital systems. The results of these point designs are presented in the following section.

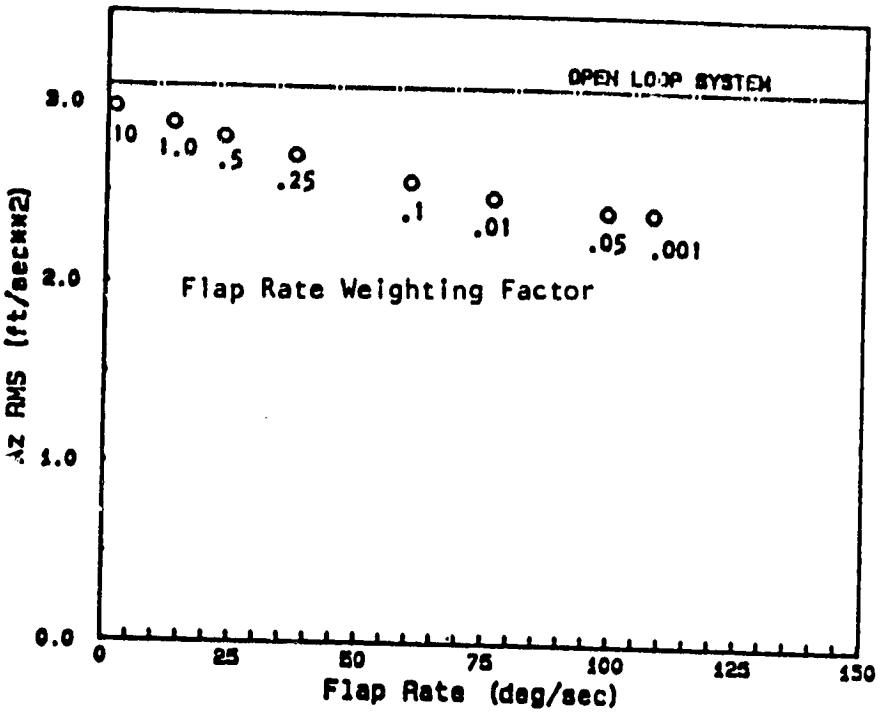

Figure 4.6a Effect Of Flap Rate On Az RMS

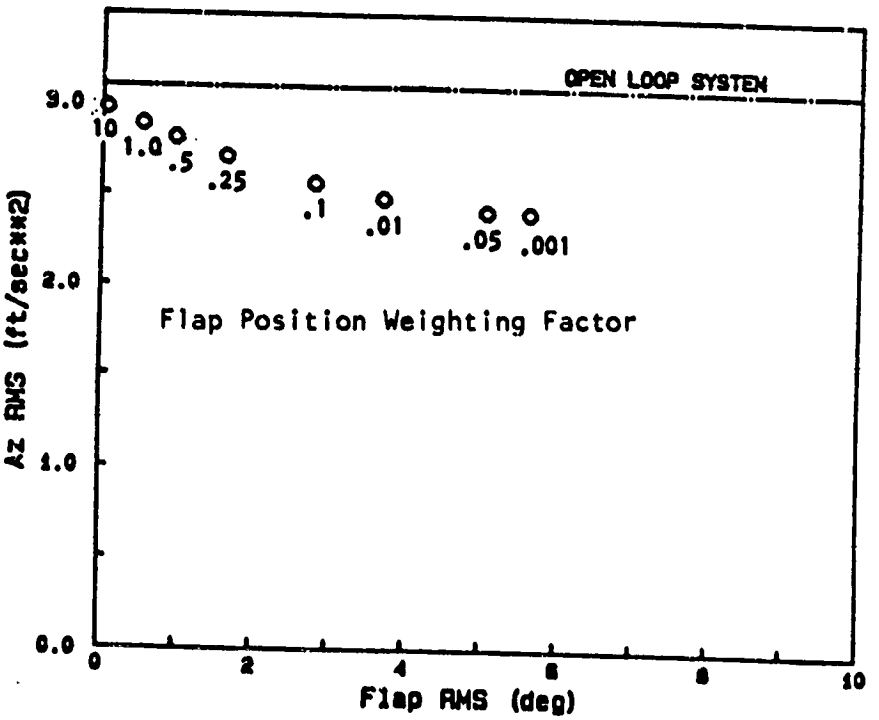

Figure 4.6b Effect Of Flap RMS On Az RMS

FIGURE 4.6 Effect of Flap Rate and Flap RMS on Az RMS

4.4.2 OPTIMAL POINT DESIGN DISCUSSION

There are two sets of point designs included in this summary. The aircraft state matrices are the same for both sets, but the flap control power differs by a factor of two. The first set of designs is for the original linear model, called Model A, derived from the NASA LaRC Cessna 402B nonlinear simulator[19]. The flap control power for Model A was only one-half of the actual flap power on the nonlinear simulation model. The second set of designs is for a linear model, called Model B, which has flap control power equal to the actual flap power on the simulator. Designs for both models, rather than just the design for the actual flap control power model, are presented for two reasons.

The first and primary reason is that the flap control power for the implementation of this system is not yet known. All our RQAS designs have been based on the assumption that the C-402B's flaps could be used for positive and negative direct lift control. However the C-402B has a split flap, so a redesign of the 402B's flap system to a bidirectional flap has been recognized as a necessity since the beginning of this project. Until that redesign is completed, it was decided to base all RQAS designs on the linear model derived from the C-402B simulator, with the assumption that the existing flaps could be made symmetric about zero degrees. The discrepancy between Model A and the actual C-402B simulator, Model B, was discovered during the moving base simulation study. Explanation of the reason for the difference in the two models is included in section 6.3.2.1. Because the only difference between the two models is the control power, and since the actual flap control power for the RQAS will not be known

until after the flap redesign has been completed, both designs will be presented here as possible configurations for the actual implementation of a RQAS design.

The second reason for presenting both sets of data is to show the design performance insensitivity to the control power differences. The control power had already been selected as one of the parameters for analysis in the detailed performance investigations. Therefore, when the error in the original model was discovered, it was felt worthwhile to present the detailed point designs for both sets of RQAS designs. As it turned out, both designs generated almost identical reductions in the RMS accelerations. The only real difference between them were the flap maximum values and deflection rates, and RMS values. Further details on this effect will be presented in the control power parameter study.

Only the results of the ICAD program digital simulations for the time histories and the analytic analysis of the PSDs are presented in this section. The results of the hybrid and NASA simulations are presented in Chapter 6.

4.4.2.1 ORIGINAL FLAP POWER DESIGNS (MODEL A)

The original linear models, Model A, provided from the nonlinear simulator as a basis for the control system designs included only one-half of the C-402B's flap control power. All the preliminary designs, up until the time of the NASA simulations, were done with these models. Tables E.1 through E.5, Appendix E, are the quantitative data summaries for the nominal designs for the five flight configurations. These Tables include:

1. The open loop time history peak, max rate and RMS for all the output variables.

2. The open loop eigenvalues, and the RMS acceleration from the PSD response.

3. The nominal RQAS design time history response.

   Ts = 0.1 sec,
   Td = 0.1 sec,
   Servo Bandwidth = 10 rad/sec

4. The prototype RQAS design time history response.

   Ts = 0.1 sec,
   Td = 0.06 sec,
   Servo Bandwidth = 10 rad/sec

5. The minimum Td RQAS design time history response.

   Ts = 0.1 sec,
   Td = 0.01 sec,
   Servo Bandwidth = 10 rad/sec

6. The nominal RQAS design eigenvalues and RMS acceleration from the PSD response.

The nominal parameters were chosen prior to the existence of the prototype controller, without knowing what the capability of the hardware control system would be. The nominal values of Ts and bandwidth were

chosen as reasonable values that would be representative of what could be expected for autopilot or augmentation system use. The Td was chosen to be the maximum possible so that the nominal designs would be conservative, with the expectation that the Td would be reduced and the prototype performance would be better than the nominal. The minimum Td designs were done to determine the best realistic performance available from a RQAS with the nominal Ts. After the prototype controller was built and tested, the actual Td was found to be 0.06 sec. The prototype designs were generated with this delay time for direct comparison to the hybrid and NASA simulations. The PSD responses model the RQAS designs with a full sample period delay, and so are comparable only to the nominal RQAS time history results.

The digital time history simulations are summarized in Table 4.3. The acceleration peak and RMS values, and the flap activity for three different RQAS designs discussed in the previous section are presented, and a continuous RQAS design is added for comparison. For the flight conditions most affected by turbulence -- the takeoff, climbs, and approach -- the RMS acceleration reductions range from 18 to 22% for the nominal design. The same four flight conditions show a reduction of from 22 to 28% for the prototype designs, and 26 to 37% for the minimum Td designs. The reduction for the cruise condition is 15% for the nominal, 20% for the prototype, and 29% for the minimum Td design. The cruise reductions are smaller than for the other conditions, as expected, because optimal controllers will have less effect on small disturbances than they will have on large disturbances.

TABLE 4.3 DIGITAL SIMULATION OPTIMAL DESIGN TIME HISTORY SUMMARY
(MODEL A)

	VERTICAL ACCELERATION PEAK (fps2)	% Decr	RMS (fps2)	% Decr	FLAP DEFLECTIONS PEAK (deg)	MAX RATE (deg/sec)	RMS (deg)
Takeoff @ SL							
OPEN LOOP	8.94		3.10				
NOMINAL	7.11	20.53	2.40	22.46	14.41	102.66	5.26
PROTOTYPE	6.39	28.52	2.26	26.98	14.54	102.09	5.35
MINIMUM Td	5.85	34.56	2.03	34.41	14.72	101.88	5.48
CONTINUOUS	4.59	48.66	1.63	47.33	14.48	102.42	5.98
Climb @ SL							
OPEN LOOP	9.66		3.72				
NOMINAL	8.56	11.38	2.91	21.73	9.21	123.91	4.17
PROTOTYPE	8.18	15.31	2.74	26.30	9.27	122.02	4.18
MINIMUM Td	7.94	17.80	2.49	33.03	9.26	122.65	4.19
CONTINUOUS	5.90	38.92	2.04	45.13	10.15	104.71	3.97
Climb @ 5000 ft							
OPEN LOOP	8.69		2.73				
NOMINAL	7.71	11.33	2.16	20.78	11.02	117.54	4.32
PROTOTYPE	7.34	15.58	1.97	27.75	11.12	117.42	4.40
MINIMUM Td	6.55	24.65	1.71	37.24	11.39	117.13	4.52
CONTINUOUS	5.05	41.91	1.41	48.31	12.96	93.55	4.23
Cruise @ 20000 ft							
OPEN LOOP	4.33		1.50				
NOMINAL	3.47	19.86	1.27	15.11	3.17	38.30	1.11
PROTOTYPE	3.35	22.75	1.19	20.45	3.18	38.60	1.11
MINIMUM Td	2.96	31.64	1.06	29.14	3.19	39.00	1.11
CONTINUOUS	2.87	33.72	.90	39.84	3.61	37.16	1.18
Approach @ SL							
OPEN LOOP	8.92		3.03				
NOMINAL	7.04	21.02	2.48	18.40	17.53	99.99	6.82
PROTOTYPE	6.91	22.54	2.38	21.53	17.55	99.47	6.82
MINIMUM Td	6.78	23.94	2.25	25.82	17.52	96.66	7.05
CONTINUOUS	5.53	37.97	2.01	33.73	10.26	101.90	4.50

NOMINAL: Ts = .1 sec
Td = .1 sec
Servo BW = 10 rad/sec

PROTOTYPE: Ts = .1 sec
Td = .06 sec
Servo BW = 10 rad/sec

MINIMUN Td: Ts = .1 sec
Td = .01 sec
Servo BW = 10 rad/sec

A consistent trend is already apparent due to the digital nature of the system, i.e. performance improves as the computational delay time decreases, a fact that is entirely consistent with trying to control random disturbances.

The flap activities are very high for all but the cruise condition, but are still within the limits of 20 deg and 150 deg/sec specified based on the the state-of-the-art of electromechanical servos as is discussed in Chapter 7, ROAS IMPLEMENTATION CONSIDERATIONS. The flap activities look excessive, until the fact is considered that only one-half of the normal control power is available to the ROAS. The elevator activities are not shown because the elevator is used very sparingly. For all flight conditions the peak elevator deflection was less than 1 degree, the maximum rate was under 10 deg/sec, and the RMS was less than .5 degrees.

The point designs for four out of the five flight conditions examined have very similar eigenvalues. As seen in Table 4.4, all but the cruise condition have short period damping of about .74, and phugoid damping in the range between .63 to .65. These very nearly critically damped roots compare to an overdamped short period and an extremely lightly damped (0.02 to 0.15) phugoid for the unaugmented aircraft. The short period natural frequencies are increased to between 8.5 to 9.9 rad/sec, while the phugoid natural frequencies are decreased to between 0.03 to 0.11 rad/sec.

TABLE 4.4 EIGENVALUE SUMMARY
(MODEL A)

TAKEOFF CONFIGURATION

W'-REAL	W'-IMAG	FREQUENCY	DAMPING
-7.235152	6.518994	9.738824	0.742918
-7.235152	-6.518994	9.738824	0.742918
-10.438976	0.000000	10.438976	1.000000
-1.169956	0.000000	1.169956	1.000000
-0.047349	0.057087	0.074167	0.638404
-0.047349	-0.057087	0.074167	0.638404

CLIMB (Sea Level) CONFIGURATION

W'-REAL	W'-IMAG	FREQUENCY	DAMPING
-7.034567	6.362747	9.485235	0.741633
-7.034567	-6.362747	9.485235	0.741633
-10.448573	0.000000	10.448573	1.000000
-2.146474	0.000000	2.146474	1.000000
-0.042161	0.048529	0.064285	0.655834
-0.042161	-0.048529	0.064285	0.655834

CLIMB (5000 ft) CONFIGURATION

W'-REAL	W'-IMAG	FREQUENCY	DAMPING
-7.293053	6.747095	9.935387	0.734048
-7.293053	-6.747095	9.935387	0.734048
-10.660500	0.000000	10.660500	1.000000
-1.095568	0.000000	1.095568	1.000000
-0.022776	0.026390	0.034860	0.653370
-0.022776	-0.026390	0.034860	0.653370

CRUISE CONFIGURATION

W'-REAL	W'-IMAG	FREQUENCY	DAMPING
-6.307067	4.677101	7.852030	0.803240
-6.307067	-4.677101	7.852030	0.803240
-10.472785	0.000000	10.472785	1.000000
-3.178820	0.000000	3.178820	1.000000
-0.030074	0.039873	0.049943	0.602162
-0.030074	-0.039873	0.049943	0.602162

APPROACH CONFIGURATION

W'-REAL	W'-IMAG	FREQUENCY	DAMPING
-6.423309	5.703391	8.589969	0.747769
-6.423309	-5.703391	8.589969	0.747769
-10.038295	0.000000	10.038295	1.000000
-0.072547	0.090290	0.115824	0.626352
-0.072547	-0.090290	0.115824	0.626352
-1.702065	0.000000	1.702065	1.000000

The result of the natural frequency and damping ratio changes are reflected in the PSD plot for the nominal design for the takeoff configuration as shown in Figure 4.7. The PSD plots for all five flight configurations show the same type of result and are included as Figures E.1 through E.5, Appendix E. An examination of these PSD plots shows that the typical result is a reduction in the acceleration content across the low to mid frequency range (.1-6 rad/sec) with a small increase in the upper range (6-10 rad/sec). The motion sickness frequency range is typically considered to be 0.1 to 1.0 Hz, (0.628 to 6.28 rad/sec) [20]. The range of reduced accelerations for the ROAS designs corresponds directly to the motion sickness range. The increase in the low amplitude high frequency bumps brought about by the active control system has been commonly referred to in prior research as the "cobblestone ride" effect [21]. The significant reduction of acceleration in the phugoid and short period ranges is somewhat offset by the slight increase at the higher frequencies. However, that increase is relatively small and would likely not be as uncomfortable to the passengers as the larger amplitude, lower frequency accelerations that have been reduced. An additional concern, other than the passengers' comfort, with the higher frequency accelerations would be in the area of structural mode excitation. For a small, relatively rigid aircraft such as the C-402B, flexible structural modes are of minimal concern; but, as the analysis is applied to larger and more flexible aircraft, excitation of the structural modes will become increasingly important [22].

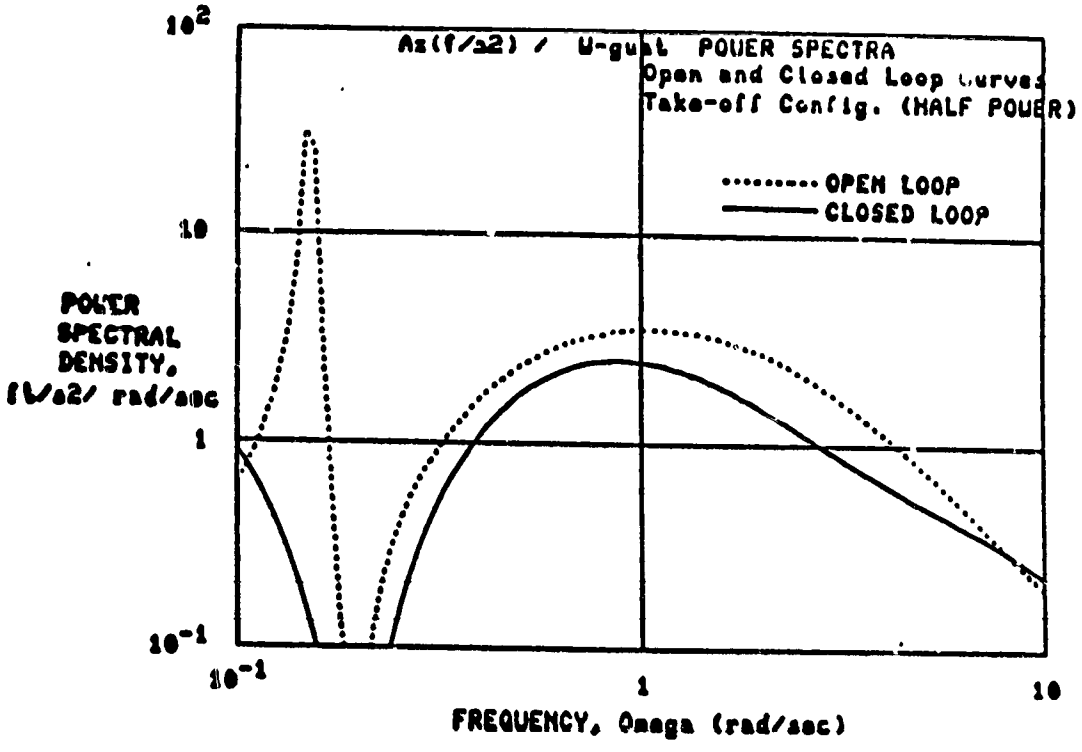

FIGURE 4.7 Takeoff Configuration PSD (Model A)

A comparison of the performance of the ROAS designs for the time history and PSD analyses is presented in Table 4.5. The only significant difference in the open loop responses occurs in the takeoff condition. The RMS value from the PSD response corresponds more closely to the values from the other simulations than the time history value does, so a likely explanation is that the time history gust file for this flight condition was not as good a representation of the Dryden gust field as the other gust disturbance files were. In all except the approach flight condition, the agreement in the percent reduction of RMS acceleration due to the ROAS is good. The large disagreement between the time history and PSD RMS acceleration values for the approach condition is apparently caused by the different frequency content of the time history and the PSD analyses.

The digital time history analysis is based on a 10 second gust field generated from a Dryden model. This period of time was chosen as a compromise between the digital computer time required for the simulation and the accuracy of the results. This simulation period can provide data on only a limited frequency range. The integration rate for the time simulation is 100 Hz, so frequencies can be sampled well above the upper limit of interest for this application of 10-20 rad/sec. The problem occurs on the lower end of the frequency range, where the low frequency PSD integration limit was 0.1 rad/sec. Based on the need to include at least one full period in order to cover the desired frequency, a 10 second gust field could represent frequencies as low as 0.628 rad/sec. In all but the approach flight condition, the low frequency energy (less then 0.628 rad/sec) left out of the time history was apparently equivalent to the high frequency content

TABLE 4.5 DIGITAL SIMULATION OPTIMAL DESIGN
TIME HISTORY-FREQUENCY REPONSE COMPARISON
(MODEL A)

	Time History Analysis		Freq Response	
	(fps2)	RMS % Decr	(fps2)	RMS % Decr
Takeoff @ SL				
OPEN LOOP	3.10		3.50	
NOMINAL	2.40	22.46	2.76	21.23
Climb @ SL				
OPEN LOOP	3.72		3.98	
NOMINAL	2.91	21.73	3.05	23.40
Climb @ 5000 ft				
OPEN LOOP	2.73		2.79	
NOMINAL	2.16	20.78	2.15	22.94
Cruise @ 20000 ft				
OPEN LOOP	1.50		1.50	
NOMINAL	1.27	15.11	1.30	13.50
Approach @ SL				
OPEN LOOP	3.03		3.10	
NOMINAL	2.48	18.40	2.28	26.28

(above 10 rad/sec) left out of the PSD analysis so that the results were very comparable. However, in the approach flight condition, there was a significant difference. To check the fact that this difference was indeed due to the frequency content difference, a PSD analysis was made for the frequency range 0.7-20 rad/sec and compared to the time history performance. The results of that test case showed comparable percentage reductions in both the time history and PSD analyses.

4.4.2.2 REVISED FLAP POWER DESIGNS (MODEL B)

The flap control power for four of the five flight configurations was twice as much for Model B as it was for Model A. Due to the circumstances described in Chapter 6, the approach condition remained the same in both models. The Model B RQAS designs contained control power terms which were equal to the control power on the simulator. In order to directly compare the two sets of designs, the data for Model B are presented in the same form as for Model A, except that the individual flight summaries are not included. The primary purpose of comparing the two models is to show the similarity in the performance, even though there is a factor of two difference in the control power terms. This similiarity will be further explored in the control power parameter study.

The digital time history simulations for the full flap power case are summarized in Table 4.6. There is no significant difference in the RMS acceleration reductions between this data and that presented for Model A. The only meaningful difference between the two sets of RQAS designs is that the Model B designs required about one-half of the control activity that

TABLE 4.6 DIGITAL SIMULATION OPTIMAL DESIGN TIME HISTORY SUMMARY
(MODEL B)

	VERTICAL ACCELERATION				FLAP DEFLECTIONS		
	PEAK		RMS		PEAK	MAX RATE	RMS
	(fps2)	% Decr	(fps2)	% Decr	(deg)	(deg/sec)	(deg)
Takeoff @ SL							
OPEN LOOP	8.94		3.10				
NOMINAL	7.09	20.70	2.40	22.46	7.17	53.55	2.57
PROTOTYPE	6.35	28.97	2.26	27.11	7.22	53.93	2.61
MINIMUM Td	5.78	35.32	2.02	34.73	7.32	53.58	2.66
CONTINUOUS	4.42	50.62	1.59	48.63	5.10	49.45	2.27
Climb @ SL							
OPEN LOOP	9.66		3.72				
NOMINAL	8.47	12.27	2.88	22.43	5.59	68.30	2.52
PROTOTYPE	8.13	15.86	2.70	27.49	5.66	67.92	2.55
MINIMUM Td	7.91	18.07	2.42	34.99	5.71	68.38	2.58
CONTINUOUS	5.94	38.49	2.01	45.97	5.10	49.45	2.27
Climb @ 5000 ft							
OPEN LOOP	8.53		2.75				
NOMINAL	7.14	16.32	2.14	22.22	5.35	47.49	2.10
PROTOTYPE	6.71	21.36	1.96	28.78	5.40	47.77	2.14
MINIMUM Td	6.13	28.17	1.72	37.52	5.51	47.39	2.19
CONTINUOUS	4.66	45.40	1.42	48.45	6.15	44.79	2.11
Cruise @ 20000 ft							
OPEN LOOP	4.33		1.50				
NOMINAL	3.44	20.58	1.27	15.11	1.75	20.98	.63
PROTOTYPE	3.35	22.75	1.18	21.26	1.76	21.10	.64
MINIMUM Td	3.08	28.91	1.04	30.61	1.78	21.16	.64
CONTINUOUS	2.56	40.83	.84	43.65	2.36	14.81	.95
Approach @ SL							
OPEN LOOP	8.92		3.03				
NOMINAL	7.04	21.02	2.48	18.40	17.53	99.99	6.82
PROTOTYPE	6.91	22.54	2.38	21.53	17.55	99.47	6.82
MINIMUM Td	6.78	23.94	2.25	25.82	17.52	96.66	7.05
CONTINUOUS	5.53	37.97	2.01	33.73	10.26	101.90	4.50

OPTIMAL NOMINAL: Ts = .1 sec
Td = .1 sec
Servo BW = 10 rad/sec

HARDWARE LIMITED: Ts = .1 sec
Td = .06 sec
Servo BW = 10 rad/sec

MINIMUM DELAY TIME: Ts = .1 sec
Td = .01 sec
Servo BW = 10 rad/sec

C-2

the Model A designs did. The change of the control activity by the reciprocol of the control power change would be normal and expected for a linear system. However, even though the model and the simulation are linear, the optimal solution to the Ricatti equation is nonlinear so this almost proportional change was not totally expected.

The eigenvalue summary is presented in Table 4.7. There is a great similarity for the eigenvalues of both systems, both in the damping ratios and the natural frequencies. The PSD plot for the full power nominal design for the takeoff configuration is shown in Figure 4.8. The full set of PSD plots for the Model B designs are included as Figures E.6 through E.10 in Appendix E. A comparison of the Model B PSD plots to the Model A PSD plots shows that the same frequency response characteristics are apparent in both. There is so little difference between the two sets of plots that they are indistinguishable in a visual inspection.

A comparison of the time history to PSD performance of the ROAS is presented in Table 4.8. Just as before, the only differences are for the takeoff configuration for the open loop, and the approach configuration for the augmented system. The reasons for these differences are the same as those given for Model A.

TABLE 4.7 EIGENVALUE SUMMARY
(MODEL B)

TAKEOFF CONFIGURATION

W'-REAL	W'-IMAG	FREQUENCY	DAMPING
-7.179389	6.546084	9.715701	0.738947
-7.179389	-6.546084	9.715701	0.738947
-10.401377	0.000000	10.401377	1.000000
-1.272836	0.000000	1.272836	1.000000
-0.048801	0.058307	0.076035	0.641827
-0.048801	-0.058307	0.076035	0.641827

CLIMB (SL) CONFIGURATION

W'-REAL	W'-IMAG	FREQUENCY	DAMPING
-7.262707	6.514562	9.756353	0.744408
-7.262707	-6.514562	9.756353	0.744408
-10.573930	0.000000	10.573930	1.000000
-1.670707	0.000000	1.670707	1.000000
-0.042003	0.049249	0.064728	0.648923
-0.042003	-0.049249	0.064728	0.648923

CLIMB (5000 ft) CONFIGURATION

W'-REAL	W'-IMAG	FREQUENCY	DAMPING
-7.240542	6.743911	9.894735	0.731757
-7.240542	-6.743911	9.894735	0.731757
-10.617063	0.000000	10.617063	1.000000
-0.023826	0.027181	0.036146	0.659172
-0.023826	-0.027181	0.036146	0.659172
-1.203098	0.000000	1.203098	1.000000

CRUISE CONFIGURATION

W'-REAL	W'-IMAG	FREQUENCY	DAMPING
-6.575168	4.540687	7.990661	0.822856
-6.575168	-4.540687	7.990661	0.822856
-10.558939	0.000000	10.558939	1.000000
-2.692514	0.000000	2.692514	1.000000
-0.028888	0.039276	0.048755	0.592504
-0.028888	-0.039276	0.048755	0.592504

APPROACH CONFIGURATION

W'-REAL	W'-IMAG	FREQUENCY	DAMPING
-6.423309	5.703391	8.589969	0.747769
-6.423309	-5.703391	8.589969	0.747769
-10.038295	0.000000	0.038295	1.000000
-0.072547	0.090290	0.115824	0.626352
-0.072547	-0.090290	0.115824	0.626352
-1.702065	0.000000	1.702065	1.000000

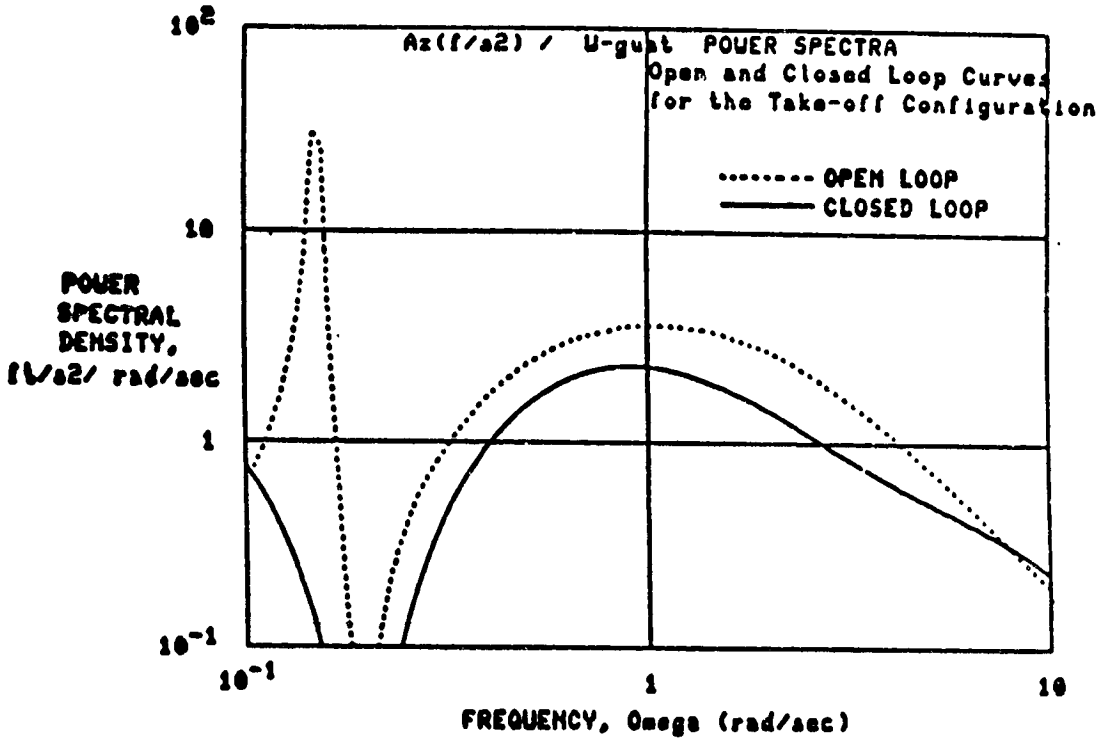

FIGURE 4.8 Takeoff Configuration PSD (Model B)

TABLE 4.8 DIGITAL SIMULATION OPTIMAL DESIGN
TIME HISTORY-FREQUENCY RESPONSE COMPARISON
(MODEL B)

	Time History RMS (fps2)	% Decr	Freq Response RMS (fps2)	% Decr
Takeoff @ SL				
OPEN LOOP	3.10		3.50	
NOMINAL	2.40	22.46	2.72	22.46
Climb @ SL				
OPEN LOOP	3.72		3.98	
NOMINAL	2.88	22.43	3.13	21.36
Climb @ 5000 ft				
OPEN LOOP	2.75		2.79	
NOMINAL	2.14	22.22	2.11	24.47
Cruise @ 20000				
OPEN LOOP	1.50		1.50	
NOMINAL	1.27	15.11	1.34	10.45
Approach @ SL				
OPEN LOOP	3.03		3.10	
NOMINAL	2.48	18.40	2.28	26.28

4.4.3 OPTIMAL POINT DESIGN SUMMARY

The performances of the optimal designs for both Models A and B are so similar that no distinction is made between them when presenting this summary. The norminal RQAS designs produced moderate reductions of 18-25% in the RMS accelerations for four flight conditions most affected by turbulence -- the takeoff, the two climb and the approach configurations. The reductions for the cruise condition are not as large, but the disturbances are not nearly as large either. The RQAS designs for all flight conditions show the same characteristics in the frequency domain of reducing the acceleration content across the low to mid frequency range while adding a small amount of low amplitude acceleration at the higher frequency range. This translates into a significant reduction in the motion sickness range, and a slight increase in the number of small high frequency bumps. The eigenvalues for all designs are also very similar, as would be expected from the similarity of the PSDs, with damping ratios ranging only from about .63 to .75 for both the short period and the phugoid.

The great similarity between these two sets of designs, with a factor of two difference in flap control powers, suggests that the final system performance will be relatively independent of the control power. The difference in the nominal, prototype, and minimum Td designs further suggests that performance will instead be strongly impacted by the digital parameters. The last section of this chapter is an investigation of the digital and implementation effects (including the control power), and the results support this preliminary conclusion.

4.5 PARAMETER STUDIES

After the nominal designs for the five conditions had been completed, a set of parameter studies to determine the impact of the selected parameters on the RQAS performance were conducted. The parameters included in these studies were:

1. the sample time (Ts);
2. the computational delay time (Td);
3. the servo bandwidth (BW); and
4. the elevator and flap control power.

The vertical RMS acceleration was the primary performance measure for these studies, but control rates and deflections were also examined to insure that established limits were not exceeded. The nominal designs formed the baseline for these studies both in terms of the parameter values and in terms of the **Q** and **R** weighting matrices. After the proper ratios of the outputs and controls had been found for each flight condition, in terms of weighting factors in the weighting matrices, these ratios were held constant throughout the parametric studies. In other words, the same **Q** and **R** matrices used to produce the nominal designs for each flight condition were also used for these parameter studies. To insure that this was a reasonable approach, new **Q** and **R** matrices were found using the design procedure outlined in Chapter 4, for a variety of cases. There was never any significant difference between the performance for the cases using the nominal weighting matrices or the cases using the weighting matrices found for that specific set of parameters.

Each parameter study consisted of varying one parameter while holding all of the others constant. In this way the effect of each individual parameter was first analyzed independent of the effects of the other parameters. Thr Ts and the Td were investigated to gain better understanding of the digital effect on the RQAS designs, while the BW and the control powers were studied to gain better understanding of the RQAS system implementation considerations. After the effect of each individual parameter was investigated, three combinations of parameters were studied. The first combination was Ts and Td. For each of the Ts's analyzed, a full Td study was also done to determine the interaction between these two parameters. The second combination of parameters was BW and Td. For each different BW, two additional Td's were also examined to determine the relationship between the BW and Td. The final combination of parameters examined was BW, Ts, and Td. This study continued the previous BW examinations to see what effect the BW had on performance with smaller Ts's.

Parameter studies were done for both the Model A and B RQAS designs. Both parametric studies are included to show that the parameter trends, like the point design performances, are very similar. Throughout the remainder of this section each figure will consist of two parts, A and B. Part A will be for the Model A design, and part B will be for the Model B design. The results and conclusions of the individual and combined parameter studies will be integrated into a discussion of the overall design of a RQAS in the summary section of this chapter.

4.5.1 SAMPLE TIME

The purpose of the Ts investigation was to determine the performance improvements gained by decreasing the sample time from the nominal value of 0.1 seconds (10 Hz). The Ts's investigated were 0.1, 0.08, 0.06, 0.04, and 0.02 seconds. A plot of the RMS acceleration versus the Ts for the takeoff configuration is shown in Figure 4.9. The remaining flight conditions are shown in Figures E.11 through E.15, Appendix E. The continuous RQAS performance shown, on this figure and all remaining figures, is for the nominal bandwidth servo. The trend is as expected, i.e. performance improves and approaches that of the continuous system as the Ts decreases. The performance penalty (PP) paid by the digital system, defined as

$$PP = \frac{\%\ \text{Reduction by Continuous} - \%\ \text{Reduction by Digital}}{\%\ \text{Reduction by Continuous}},$$

ranged for the different flight conditions from a PP = 0.45-0.55 for a Ts of 0.1 second, to a PP = 0.05-0.10 for a Ts of 0.02 seconds. The variation is very nearly linear so that the design choice of the Ts becomes a linear tradeoff between sample rate and acceleration reduction. The choice of Ts will therefore depend only upon the speed of the digital controller, and the amount of other digital processing required of it, if it isn't dedicated to the RQAS function.

Figures E.11 through E.15 show that the trends are the same for all of the flight conditions. The trends for Model A and Model B also have the same characteristics, reinforcing the conclusion from the point designs that control power affects only the control activity and not the other aspects of the RQAS performance.

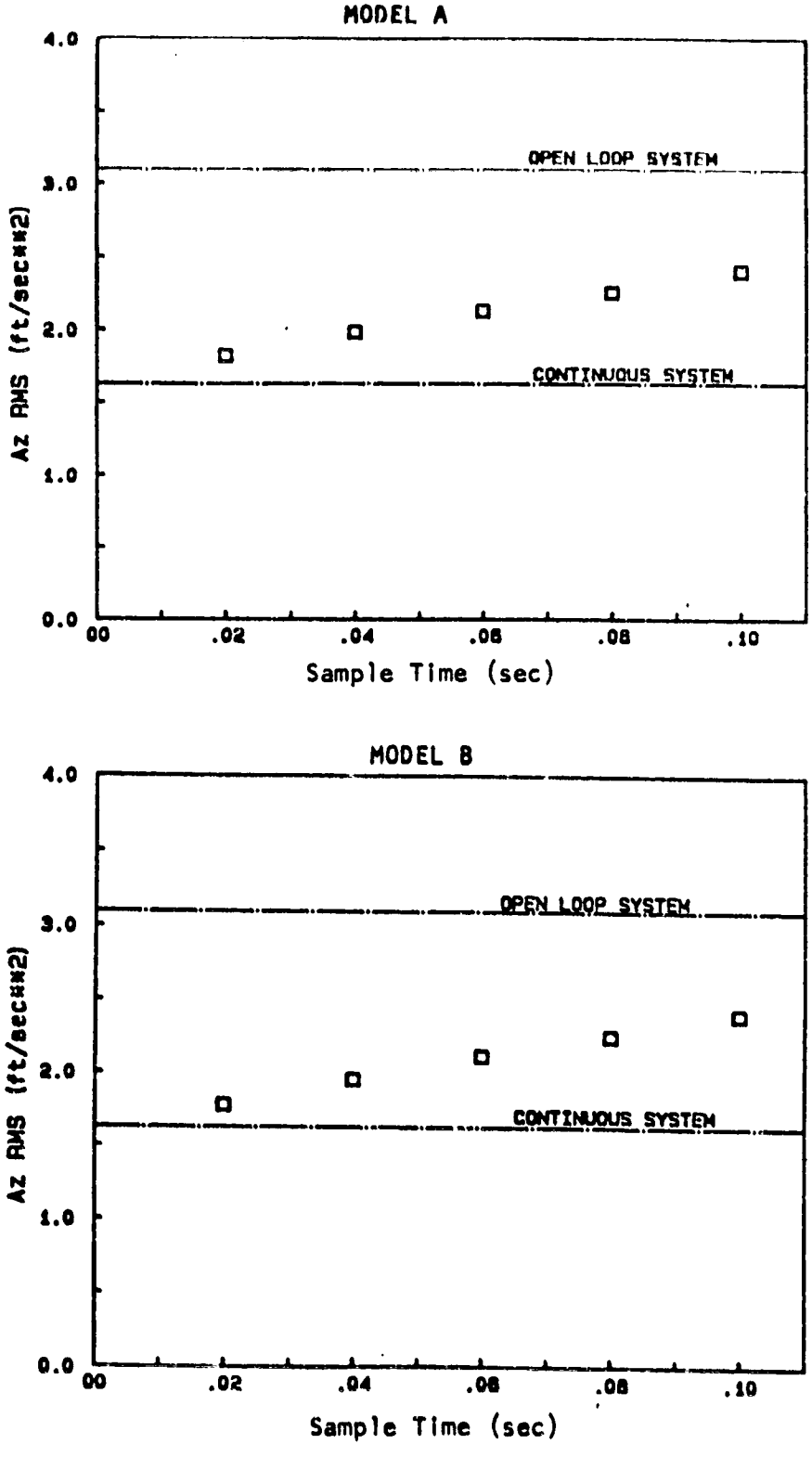

FIGURE 4.9 Effect of Sample Time - Takeoff Configuration

4.5.2 COMPUTATIONAL DELAY TIME

The purpose of the Td study was to investigate the effect that reducing Td from the nominal value of 0.1 second would have on the system performance. The main questions were: would a reduction in the Td cause over-control of the system as discussed in section 4.4.2.2; and would a reduction in Td improve performance as much as an equivalent reduction in the Ts?

The Td's investigated included 0.1, 0.08, 0.06, 0.04, 0.02, and 0.01 seconds for the initial study. The effect of reducing Td was similar for all flight conditions, as was the effect of a reduction of Ts, so only the plot for the takeoff condition is presented as Figure 4.10. This plot shows that reducing Td also reduces the RMS acceleration for the relatively slow nominal servo (BW = 10 rad/sec), as expected. However, Td reductions do not have as strong of an effect as similar reductions of Ts, as shown by the lower slope of the Td data. Using the same definition of PP as for the Ts study, the penalties paid by the digital RQAS designs for the different flight conditions ranged from a PP of 0.45-0.55 for Td = 0.1 seconds, to a PP of 0.18-0.27 for Td = 0.02 seconds, and finally to a PP of 0.15-0.24 for Td = 0.01 seconds.

In addition to the Td analyses done with all other parameters held to their nominal values, a similar Td analysis was performed for each of the Ts's investigated in the Ts parameter study. The purpose of this study was to try to define the combined effect and tradeoff between reducing Ts

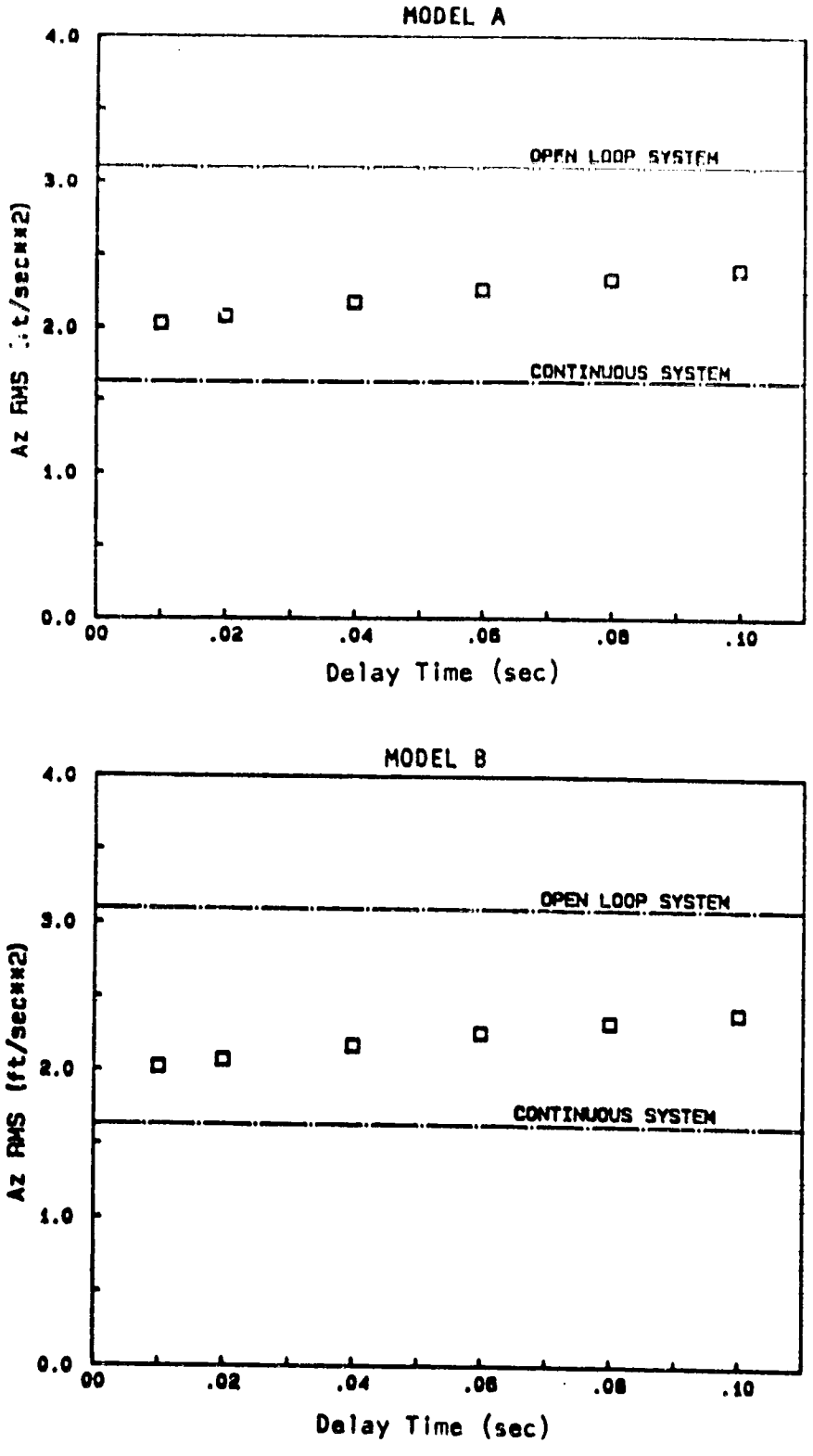

FIGURE 4.10 Effect of Delay Time - Takeoff Configuration (Ts = 0.1 sec)

or Td and reducing both Ts and Td. Plots similar to Figure 4.10 are included in Appendix E for Ts = 0.08, 0.06, 0.04 and 0.02, with Td starting at the Ts value and decreasing to 0.01 seconds. Again because of the similarity of the data for all the flight conditions, only those data for the takeoff condition are shown as Figures E.16 through E.19. The same general effect is seen for the Td reduction within each of the given Ts's as was seen with the nominal Ts, i.e. a reduction in Td reduces the RMS acceleration. However, a trend is apparent that the smaller Ts becomes, the more powerful a reduction of Td becomes, so that a reduction in either Ts or Td becomes almost equivalent.

To better show this trend, a composite of all the Td plots is presented as Figure 4.11. Each separate Ts is represented by a different symbol, and the one symbol of each type that is darkened in represents the case when the Td = Ts. The slope of each of the Td variations within a given Ts is always smaller than the slope of the Ts variation. However, the slope of the Td variations for the smaller Ts begin to approach the slope of the Ts variation.

The conclusions of these Ts and Td studies are that Ts and Td reductions both cause performance improvements, and that the Ts effect on these improvements is more powerful than the Td effect. However, as Ts decreases, reductions in Td become nearly equal to further reductions in Ts. This means that a small sample period decrease can be combined with a large reduction in Td to produce acceleration reductions equivalent to those realized from large Ts reductions. This combination of Ts and Td reductions would permit microprocessor time to be available during part of

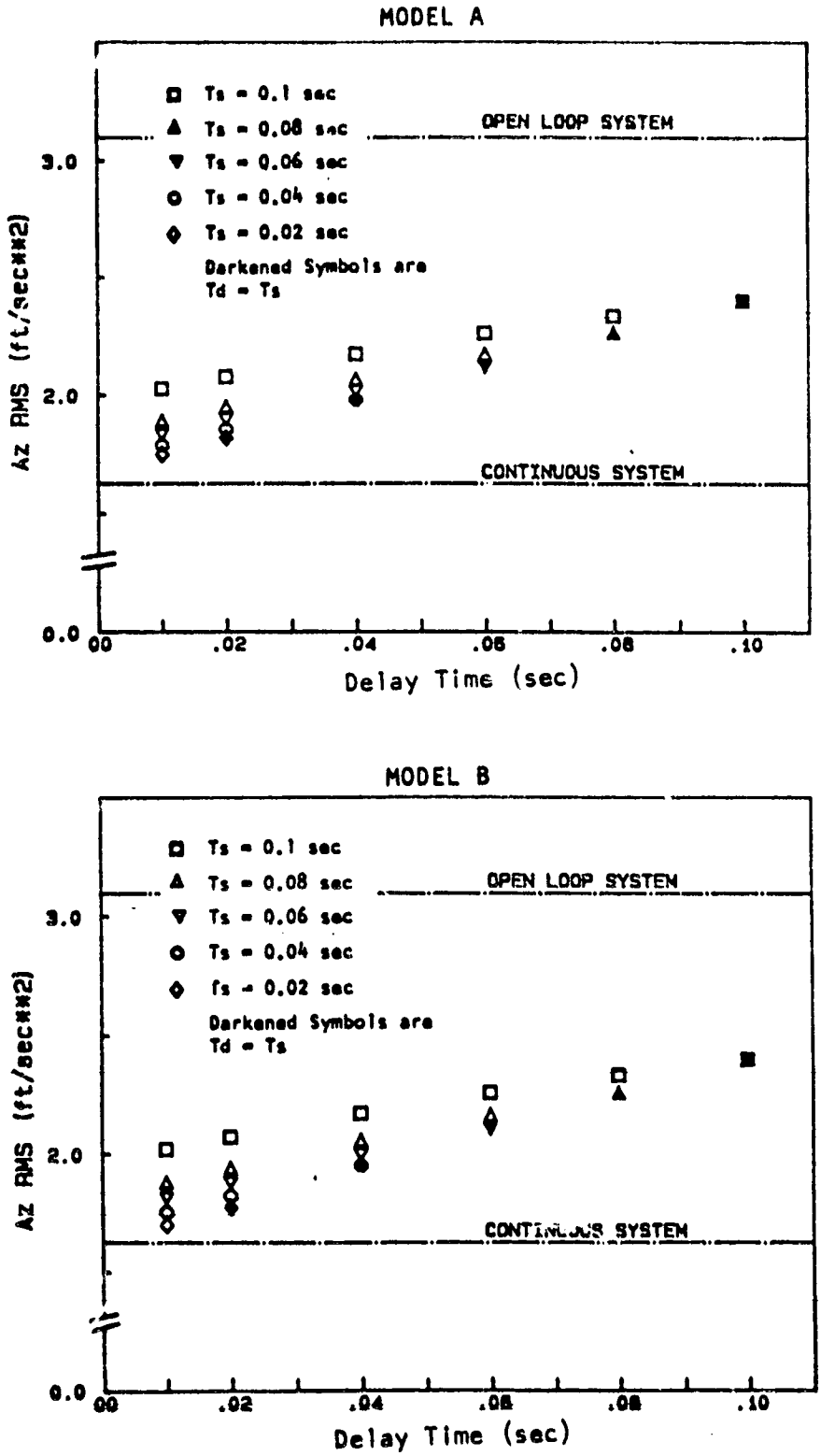

FIGURE 4.11 Effect of Composite Sample and Delay Time

each sample period for other tasks, if desired. If the microprocessor is dedicated to the RQAS, then there is no advantage to not reducing the Ts to the minimum possible value based on the processor speed.

As in all the previous data, there is no significant difference between the Model A and B designs for the digital systems, even further substantiating the conclusion that a control power change only impacts the control activity, and not the other performance characteristics.

4.5.3 SERVO BANDWIDTH

The purpose of the servo BW investigation was to determine the trade-off between higher BW servos, which translates into higher hardware costs, and acceleration reductions. The nominal servo for this project has been a 10 rad/sec BW servo, but much higher BW servos are available if the payoff warrants the investment. The servo BWs examined were 5, 10, 20, 30, 40, 50, and 100 rad/sec. Although realistic servos, even for extremely high performance, high cost applications are limited to about 75 rad/sec, the 100 rad/sec BW servo was included to see whether the system could be over-controlled as predicted earlier.

The initial phase of the BW investigations examined the effect of various servos on the nominal RQAS designs. The nominal design for the take off configuration is represented by the square symbols on Figure 4.12. The other flight configurations are included in Appendix E, Figures E.21 through E.25. For the nominal RQAS designs, the servo bandwidth has very little effect, due to the fact that the control output has already been delayed by a full sample period and a fast servo can't help to make up that delay. Please note that the continuous RQAS performance shown is the performance of a RQAS continuous design with a 10 rad/sec servo. The performance at the nominal BW is projected across the entire BW axis merely as a reference for the digital RQAS designs. The actual performance of a continuous system would also be expected to be a function of the servo BW, and probably a stronger function of BW than the digital systems.

The second phase of the BW study kept the nominal Ts and both nominal control powers, but Td is reduced to 0.06 and 0.01 seconds. The triangles

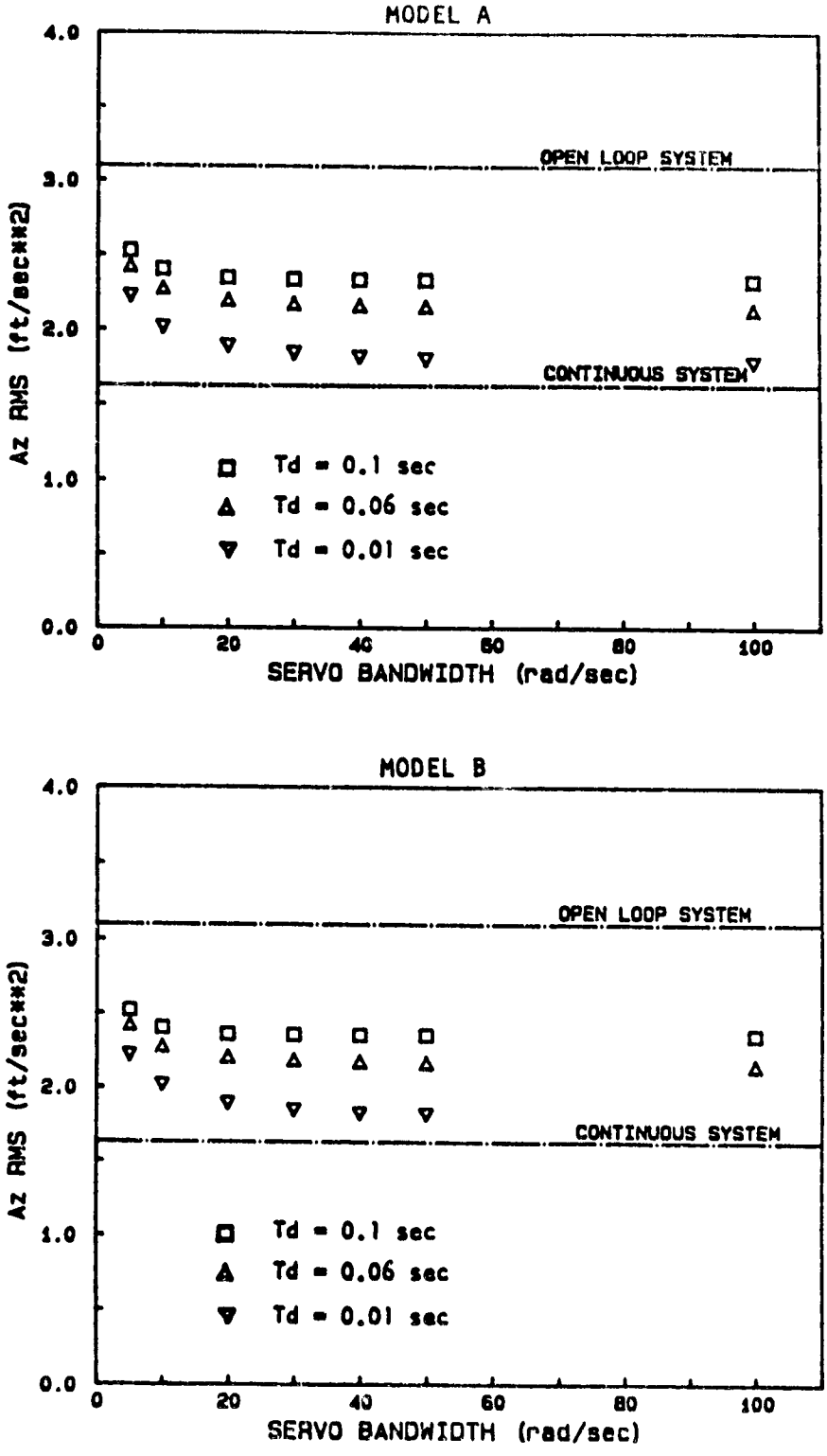

FIGURE 4.12 Effect of Servo Bandwidth - Takeoff Configuration

and the inverted triangles in the servo BW study plots represent the 0.06 and 0.01 Td's, respectively. The BW becomes increasingly important as Td is decreased. At Td = 0.06 seconds there are significant performance improvements up to a BW of 20 rad/sec (3.2 Hz). For Td = 0.01 seconds slight improvements continue through a BW of about 30 rad/sec (about 4.8 Hz).

The over-control of the system predicted in section 4.3.2.2 does occur, but only at Td = 0.01 seconds, and very high BW's. Several data points for the 100 rad/sec servo are missing from the figures because the performance of the RQAS caused an increase in RMS acceleration value that was off the scale. Figure 4.13 shows an example of what is meant by over-control, when the combination of small Td and high BW result in more control deflection than is desired. This figure shows what increasing the BW does to the actual control movement when compared to the desired control movement. For the 50 rad/sec servo, the control deflection is much larger than the optimal control would be, resulting in an over-control of the system. The climb at sea level configuration shows the beginning of this effect with an increase in the RMS value starting at the 50 rad/sec servo. However, the high dynamic pressure, low control activity cruise configuration does not exhibit evidence of the over-control even for the 100 rad/sec BW servo, and Td = 0.01 seconds.

The phenomenon of over-control is the one instance where there seems to be a difference between the Model A and Model B designs. The low control power (Model A) case exhibits over-control for only 2 out of 5 flight conditions, while the full power case shows it for 4 out of 5.

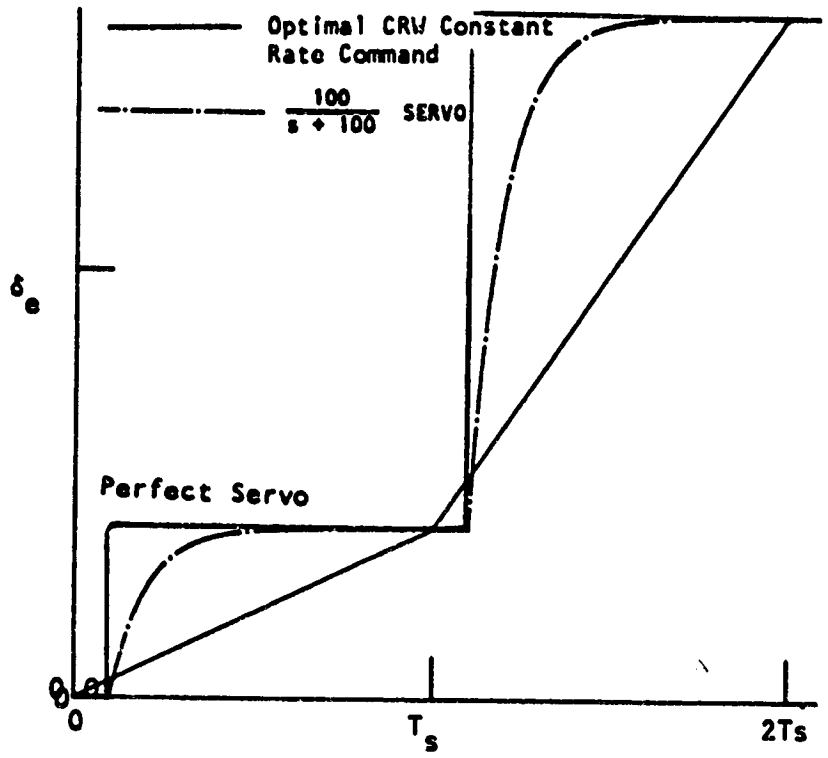

FIGURE 4.13 Example of Overcontrol with Small Td and High Bandwidth

The final phase of the BW study involved a change in Ts, Td and BW from the nominal designs. The objective of this investigation was to determine what effect a combined reduction in Ts and Td would have at different servo BWs. Figure 4.14 presents performance data for only the takeoff configuration for the three Ts and Td combinations listed below:

1. the squares are for a Ts of 0.10 and a Td of 0.06 seconds;
2. the triangles are for a Ts of 0.06 and a Td of 0.06 seconds (the prototype controller limit); and
3. the inverted triangles are for a Ts of 0.06 and a Td of 0.01 seconds.

Using the numbers above to refer to the three cases, there is a significant improvement going from case 1 to 2, but there is an even greater improvement going from case 2 to 3. The significance of this is that as Ts or Td, or both Ts and Td decrease, the importance of BW increases. The result is that, as the digital system approaches the continuous one, the BW becomes an increasingly important parameter. However, BW requirements never exceed reasonable limits for this type of application.

A second result of this study is that as Ts decreases the control power does begin to have some effect. For case 1 there is virtually no difference between the performance of the two different control power designs, while for case 2 there is a slight difference of about 3%. For case 3 a more noticeable difference is beginning to show up, almost 6%. Although the difference between the two control power RQAS designs is still fairly insignificant, a trend is starting to become evident that, as the

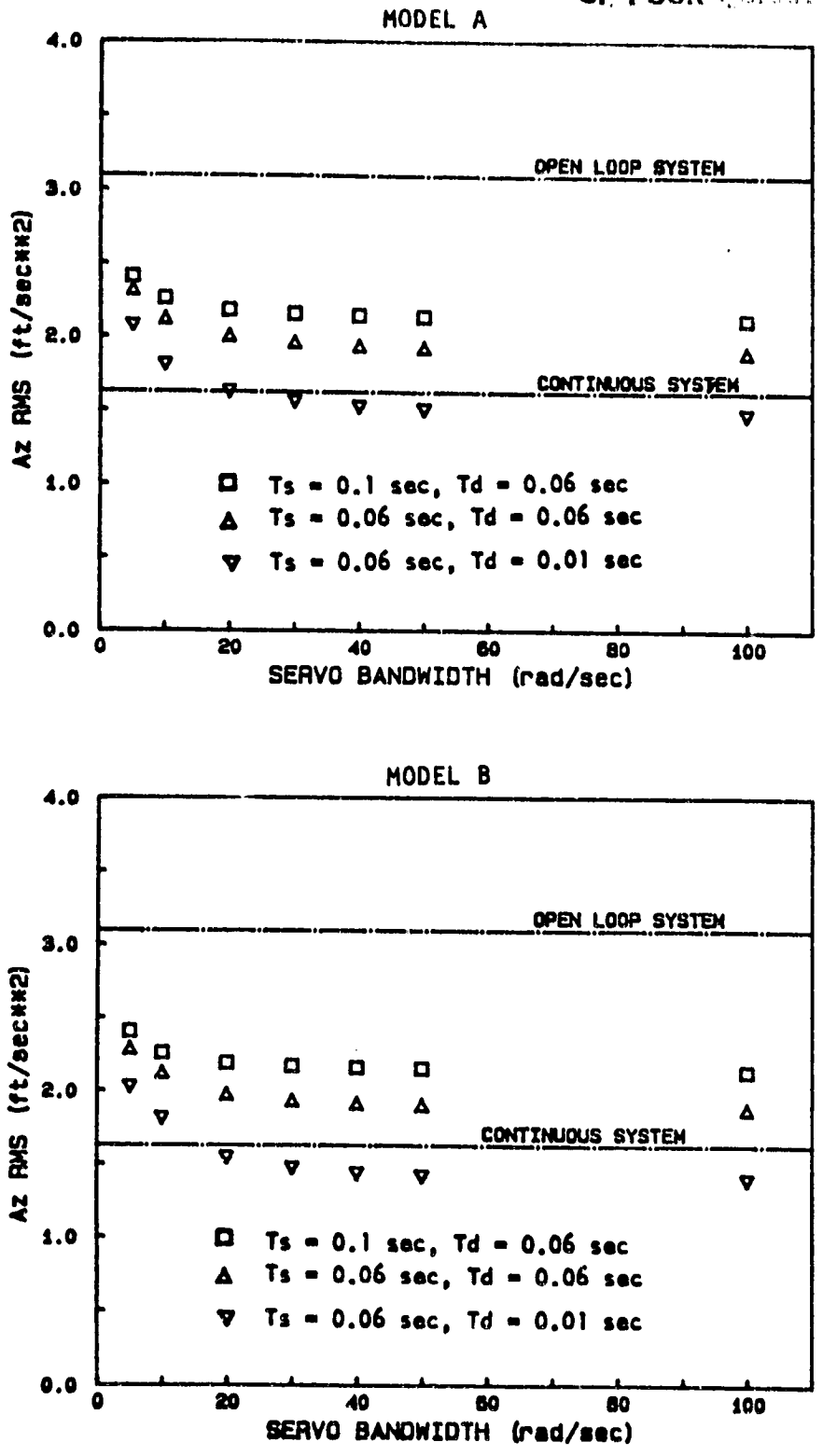

FIGURE 4.14 Increased Servo Bandwidth-Reduced Ts and Td Effect

digital system approaches a continuous one, the control power is beginning to impact the performance in areas other than in merely the control activity.

A third result is that the over-control condition no longer occurs. With reduced Ts, the control implementation used for this design effort can be used with even the highest BW servos and the minimum Td without fear of over-controlling the system. The reason for this is that as Ts decreases, the amount of excess control for any given BW servo will decrease.

4.5.4 ELEVATOR AND FLAP CONTROL POWER

The control power study consisted of examining the effect of reducing the elevator power to 20% of the original elevator power, and increasing the flap control power to twice the original. The reason for looking at a system with reduced elevator power was a desire to use only dedicated control surfaces for the RQAS. If only a small portion of the elevator control power is needed, then a split portion of the elevator surface, independent of the primary control system could be dedicated to the RQAS. The use of a separate split elevator surface was recommended in the feasibility study as being attractive both because the split surface would not be a primary flight control, and the split surface movements would not be connected to the pilot's controls and cause feedback to him. The reason for examining the effect of doubling the flap control power is that the C-402B now has a relatively inefficient split flap. It is reasonable to expect that a flap designed for the RQAS would be designed to be more efficient, and thus to have more control power. Examining the effect of increased flap control power will determine whether or not it would be beneficial to spend extra time, effort, and money to generate a highly efficient direct lift system.

As has been shown in the point design summaries, the elevator is used very little by the RQAS. Cutting the elevator power by a factor of five increases the RMS amount of elevator used by a factor of about 2-3. The elevator activity is still below 2 degrees peak, 1 degree RMS, and 20 deg/sec for all the flight conditions. It is entirely reasonable to expect to successfully implement an optimal design RQAS with only a small

dedicated portion of the existing elevator.

An initial flap control power examination has already been presented by carrying both Model A and B RQAS designs through the entire point design and parameter investigation process. The consistant result throughout this entire process has been that, for nominal digital RQAS designs, control power affects only the control activity, and not the other aspects of performance until Ts is reduced at least to 0.06 seconds or less. To insure that this trend continued to higher than normal control powers, the design with control twice that of Model B was done. Data for Model A (half), Model B (full) and the double control power design are shown in Table 4.9. As shown by the data in this table, the only benefit from an increase in flap control power is a reduction in the servo rate and displacement, but no significant reduction in RMS acceleration.

TABLE 4.9 FLAP CONTROL POWER SUMMARY
(MODEL B - TAKEOFF CONFIGURATION)

	VERTICAL ACCELERATION				FLAP DEFLECTIONS		
	PEAK		RMS		PEAK	MAX RATE	RMS
	(fps2)	% Decr	(fps2)	% Decr	(deg)	(deg/sec)	(deg)
MODEL A							
OPEN LOOP	8.94		3.10				
NOMINAL	7.11	20.53	2.40	22.46	14.41	102.66	5.26
PROTOTYPE	6.39	28.52	2.26	26.98	14.54	102.99	5.35
MINIMUM Td	5.85	34.56	2.03	34.41	14.72	101.88	5.48
MODEL B							
OPEN LOOP	8.94		3.10				
NOMINAL	7.09	20.70	2.40	22.46	7.17	53.55	2.57
PROTOTYPE	6.35	28.97	2.26	27.11	7.22	53.93	2.61
MINIMUM Td	5.78	35.32	2.02	34.73	7.32	53.58	2.66
DOUBLE FLAP POWER							
OPEN LOOP	8.94		3.10				
NOMINAL	7.25	18.90	2.40	22.58	4.57	31.56	1.56
PROTOTYPE	6.30	29.53	2.24	27.74	4.63	31.08	1.60
MINIMUM Td	5.60	37.36	1.97	36.45	4.73	31.66	1.65

4.6 OPTIMAL DESIGN SUMMARY

The optimal designs for the nominal system (Ts = 0.1 sec, Td = 0.1 sec, Servo BW = 10 rad/sec, and both one-half and full flap control power) produced about 18-22% RMS acceleration reduction at the high turbulence flight conditions (take-off, climb, and approach) and about 15% at the low turbulence cruise condition. By reducing both Ts and Td, the digital parameters of the RQAS, to .06 seconds, and increasing the servo BW to 20 rad/sec (equivalent to current autopilot servos) the reductions could be increased to better than 35%. By keeping Ts = 0.06 seconds, and further reducing Td to 0.01 seconds, the reductions could be increased to over 50%. These reductions compare to about 45-48% for a continuous system with the nominal 10 rad/sec BW servos.

The elevator activity is minimal for all designs, and implementation of a split surface pitch control appears feasible. The flap activities for the full C-402B control power designs stay below 70 deg/sec for the rate, 7 degrees for the peak, and 2.75 degrees for the RMS for all except the approach condition. Rates of 100 deg/sec, peaks of 17 degrees, and RMS of almost 7 degrees occur there, because of the loss of flap efficiency about the 30 degree trim deflection. For the Model A designs, the maximum rates, maximum deflections and RMS for the flaps are 120 deg/sec, 15 degress, and 5.48 degrees, respectively. Although the control activity for the Model A RQAS designs is high, it must be remembered that only one-half of the control was used in these designs.

A comparison of the performance of our RQAS, with a nominal Ts, to a past ride smoothing effort is presented in Table 4.10. Detailed ride

TABLE 4.10 RQAS - STOL RIDE SMOOTHING SYSTEM COMPARISON
(MODEL B, MODERATE TURBULENCE,
WITH RMS VERTICAL ACCELERATION IN g's)

	RQAS DESIGNS				BOEING STOL DESIGN
	Ts=.1 sec Td=.1 sec	Ts=.1 sec Td=.06 sec	Ts=.1 sec Td=.01 sec	Continuous	Continuous
TAKEOFF	.118	.111	.097	.078	
CLIMB @ SL	.142	.133	.119	.099	
CLIMB @ 5000 ft	.097	.089	.078	.064	
CRUISE	.082	.076	.067	.054	.06
DESCENT					.09
APPROACH	.122	.117	.111	.087	.11

smoothing systems were designed for low wing-loaded STOL transports by the Boeing Co. in the early 1970's [10]. Acceptable levels of RMS acceleration were set for this study at 0.11g (3.54 ft/s2) for a gust intensity with the probability of exceedence of 0.001. This criteria corresponds to a satisfactory rating by about 75% of the passengers [23]. A summary of the full flap power point design performance for the 0.001 probability of exceedence is presented for comparison to the STOL designs. The Boeing designs were continuous systems with high rate (100 deg/sec) and high BW servos (30 rad/sec). Both the Boeing and our continuous systems meet this criteria readily for all flight conditions. However, for the digital systems with the nominal Ts and Td, only the climb at 5000 ft and the cruise configurations meet the desired level of performance. By reducing Td, only the takeoff configuration can be added to those designs that can meet the established criteria.

The RQAS designs for all of the flight conditions can meet the criteria by reducing the Ts and Td to the prototype digital controller values. Table 4.11 shows that the prototype designs can meet or exceed the criteria of 0.11g for the vertical acceleration RMS. This entire comparison is done with the nominal servos; and, as shown in the servo parameter study, performance would improve for the RQAS designs with servo BW increased to 20 rad/sec. The purpose of this brief discussion was to provide a basis of comparison of the performance of the digital RQAS designs to one previous analog ride smoothing system.

The next Chapter will be a presentation of the classical RQAS designs, including the design approach, the point designs, and the parametric studies.

TABLE 4.11 RQAS PERFORMANCE: REDUCED Ts and Td
(MODEL B - 0.001 Probability of Exceedance)

	RMS Acceleration (in g's)				
	Open Loop	Ts=0.1 sec Td=0.1 sec	Ts=0.1 sec Td=0.01 sec	Ts=0.06 sec Td=0.06 sec	Ts=0.06 sec Td=0.01 sec
TAKEOFF	.152	.118	.097	.104	.090
CLIMB at SL	.183	.142	.119	.125	.110
CLIMB at 5000 ft	.125	.097	.078	.083	.070
CRUISE	.097	.082	.067	.072	.062
APPROACH	.150	.122	.111	.112	.107

5. CLASSICAL DESIGN

This chapter presents an alternate form of control system design that uses either the root locus method or the frequency response method of Bode to aid in the design of the active ride augmentation system. These designs are frequently referred to as classical control designs to distinguish them from the modern or optimal control designs discussed in the previous chapter. In this chapter, the root locus method will be used to design the active ride augmentation system. For this purpose, appropriate subroutines from the NASA CONTROL program [15] have been incorporated in the ICAD program to allow designs using root locus techniques in the z- or w'-domain for digital control systems, or in the s-domain for continuous control systems.

These CONTROL subroutines provided the capability to calculate eigenvalues and transfer functions, and to generate root loci, root contours, frequency responses, and power spectra for open- and closed-loop systems. In the analyses of digital flight control systems, the CONTROL program first discretizes the aircraft, servo, and sensor dynamics and any analog feedback loops so that the entire system, including the digital controller, will have a common discrete representation. In the discretization process, CONTROL automatically accounts for the sampling and zero order hold effects. External inputs to the aircraft and the digital controller can also be defined, if desired. External inputs to the aircraft are considered as sampled continuous inputs, whereas, external inputs to the digital controller are considered discrete inputs separated in time by the sample time, Ts. The discretized system is then described by vector difference

equations which are algebraically equivalent to vector differential equations that describe continuous systems. The same computer algorithms used for continuous systems can then be used for the discrete system. The resulting discrete transfer functions are z-transform transfer functions.

The ICAD program automatically converts from the z-domain to the w'-domain so that w'-plane analysis can also be used in the design of digital flight control systems. This conversion to the w'-domain is accomplished by means of the bilinear transformation scaled with a factor Ts/2,

$$w' = \frac{2}{Ts}\,\frac{z-1}{z+1} \quad . \tag{5.1}$$

The factor 2/Ts which appears in equation 5.1 ensures that the w'-plane will approach the s-plane as the sample time approaches zero. If the w'-plane root locus is used to analyse digital control systems as if it were actually an s-plane root locus, the sample time must be restricted to a maximum of 0.1 seconds, or else distortion of the root loci will occur. An example of this is given in Figure 5.1 where constant damping loci are shown for different sample times for two different values of the damping ratio. From this figure, it is clear that higher values of the sample time distort the s-plane straight line damping loci of a continuous system. However, if the sample time is restricted to 0.1 seconds or less, this distortion does not occur and s-plane methods can be applied to the w'-plane in the design of digital control systems.

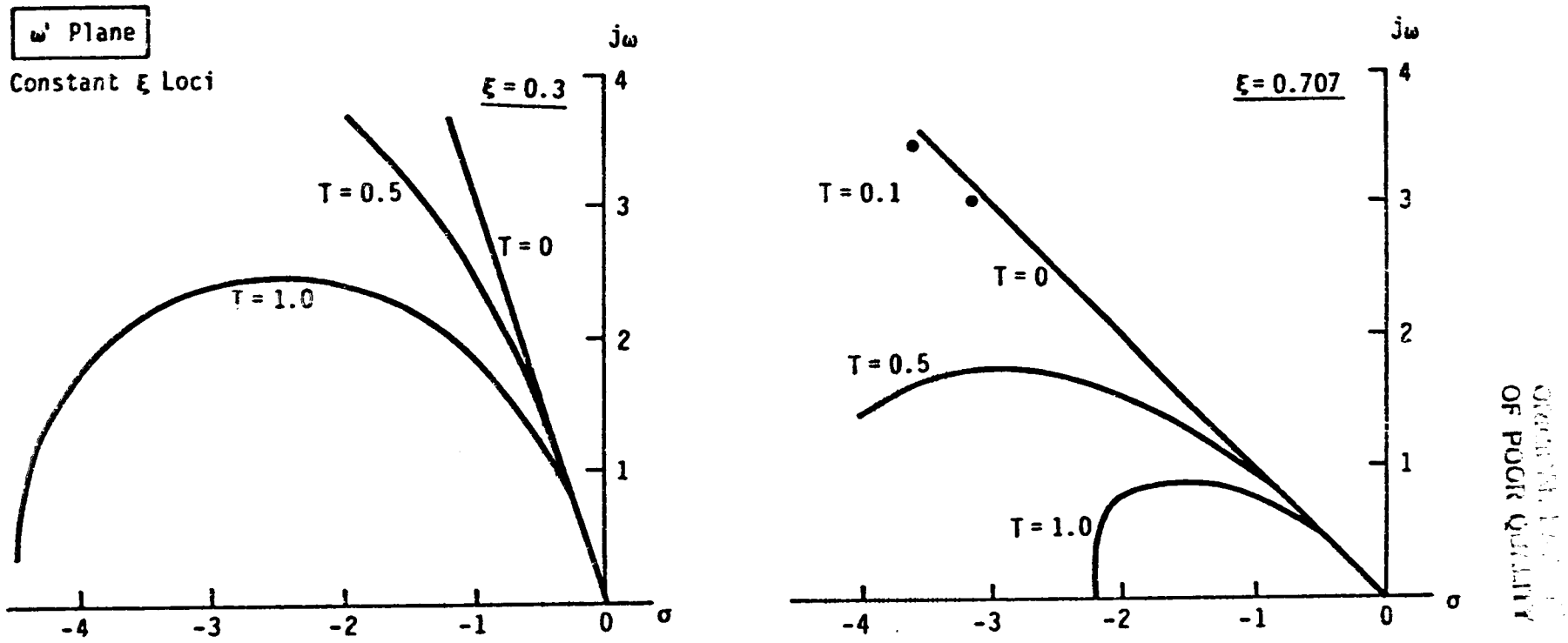

FIGURE 5.1 Constant Damping Ratio Root Loci in the W' Plane

All the designs in this chapter were done in the w'-plane. Proper selection of the sample time insures that the w'-plane root loci used in the design of digital control systems will have a marked similarity to the s-plane root loci. The w'-plane root locus will then not only have a geometrical resemblance to the s-plane root locus, but the actual root and gain values will also be similar. In the limit, when the sample time and the computational delay time approach zero, the w'-plane will approach the s-plane. The design engineer, by using the w'- plane, can therefore draw on more extensive experience with the s-plane root loci to help facilitate the digital designs.

5.1 DESIGN APPROACH

One of the ways in which the classical designs differ from the optimal designs is in the number of feedback loops. The classical designs can utilize limited feedback instead of the full state feedback required for the optimal designs. To keep the classical designs simple, the number of feedback loops were limited to two loops: an inner loop for controlling the vertical accelerations, and an outer loop to correct the handling quality deficiencies resulting from the inner loop closure.

Although no handling qualities specifications exist for commercial or regional aircraft, the current industry accepted standards as defined in military specifications F-8785C [24] were used and applied to both the unaugmented and augmented aircraft in order to determine compatibility with minimum acceptable levels of aircraft dynamic mode parameters such as the short period mode damping, etc. For this purpose, the Cessna 402B was defined as a class 1 (light utility) aircraft, with the goal of satisfying level 1 (clearly adequate) flying qualities for category B (climb, cruise, descent) and category C (takeoff, approach) flight phases.

With the root locus method the design engineer can relocate the eigenvalues of the augmented aircraft to favorable positions (as specified in the military specifications) by making use of the two loop closures and some combination of proportional, integral, and derivative control. The proportional control is

$$u_i = Ke_i, \tag{5.2}$$

where u_i is the control command, and e_i the error signal. The associated

transfer function is

$$D(z) = K \tag{5.3}$$

The integral control is

$$u_i = u_{i-1} + Ke_i \tag{5.4}$$

and has a transfer function,

$$D(z) = K/(1-z^{-1}). \tag{5.5}$$

The derivative control is

$$u_i = K(e_i - e_{i-1}) \tag{5.6}$$

and has a transfer function,

$$D(z) = K(1-z^{-1}). \tag{5.7}$$

A combination of these control structures will allow various types of compensation such as lead, lag-lead and others. Initially the designs were based on proportional control only. Integral and/or derivative control was not required for the Cessna 402B aircraft.

The nominal point designs were generated with sample and computational delay times of 0.1 and 0.01 seconds, respectively. The relatively small delay time compared to the sample time was selected for the nominal designs for two reasons. First, with small delay times, the eigenvalues from the root loci would more accurately predict the performance attained in the digital simulation; and second, the small delay time would permit more of the microprocessor duty cycle to be available for the addition of other advanced stability augmentation system (SAS) and autopilot functions. The effect of varying the nominal values of Ts and Td will be discussed later. Furthermore, sensor dynamics were neglected in the nominal designs, because sensor response is normally of high enough frequency so as to not influence

the aircraft dynamics. Typical sensors have undamped natural frequencies of 20 Hz and higher [25], whereas, the aircraft dynamic frequencies of interest do not exceed 1.5 Hz. The servos for the nominal designs were represented as having first order dynamics with a bandwidth of 10 rad/sec. The response of the system due to varying the servo bandwidth will be presented later.

All the designs in this chapter were done for the Model A aircraft defined in the previous chapter. The Model A aircraft has half the standard Cessna 402B flap control power. Since the system is linear, the full flap control power (Model B) designs should give equivalent performance with half the gain of the Model A designs in the flap control loop, and the flap control activity should subsequently be halved. Therefore, the performance attained by the Model A designs presented in this chapter should also be attained by the Model B designs with the exception that the flap maximum rate, maximum deflection and RMS values will be halved. The control power effect is further discussed in section 5.5.4 where the elevator and flap control power parameter studies are presented.

5.2 SELECTION OF FEEDBACK LOOPS

To control the vertical accelerations, feedback of angle of attack (α) and vertical accelerations (Az) to both the flaps and the elevator were examined as discussed below. In addition it became necessary to also examine the effects of attitude angle (θ) and pitch rate (q) feedback to both the flaps and the elevator. Although θ- and q-feedbacks were not expected to provide much attenuation of the vertical accelerations, their effects on the aircraft were still examined primarily to gain a better understanding on how they could be efficiently used as an outer loop to not only remedy possible handling qualities deficiencies but also to provide further reductions in the vertical accelerations, if at all possible. Alpha and vertical acceleration feedback to both the flaps and the elevator provided the primary solution to the active ride augmentation problem in regional aircraft as explained below.

The effect of vertical acceleration feedback to the direct lift flaps is intuitively obvious. The net effect of this loop closure is approximately similar to increasing the mass of the aircraft, and will therefore artificially increase the wing loading of the aircraft. The acceleration response of the aircraft will then be reduced.

Angle of attack feedback to the direct lift flaps will try to maintain alpha and therefore C_L constant following an alpha gust.

Vertical acceleration feedback to the elevator increases the short-period resonant frequency of the aircraft to the zone where the gust power spectrum is decaying at the rate of 40 dB/decade. Therefore, the higher the aircraft effective short-period resonant frequency, the lower the

magnitude of the response to turbulence. Note that this system can cause potential structural resonance problems if the aircraft short period resonant frequency is allowed to increase to high values in flexible aircraft.

The effect of feeding back the angle of attack to the elevator is to increase the magnitude of M_α directly, which is equivalent to increasing the static stability of the aircraft.

Loop closures involving pitch rate and attitude angle were not considered as primary means of controlling the vertical accelerations. Pitch rate feedback did not give as high a percentage reduction in the vertical accelerations as the angle of attack or vertical acceleration systems. This is because of the relatively low contribution of the pitch rate term to the vertical accelerations for this aircraft.

The attitude control system will tend to hold the pitch attitude constant in the presence of disturbances since the reference for stabilization is the horizon. Consequently this rigidity in attitude prohibits any weathercocking tendency of the aircraft to nose into the wind, and thereby reduce accelerations.

It is important to note that although pitch rate and attitude angle systems cannot be used as primary means of reducing the vertical accelerations, they are mostly used in active ride augmentation system designs as outer loops to improve the handling qualities deficiencies arising in the augmented aircraft due to the inner loop closure. They can also be effectively used to improve any handling qualities deficiencies which may be present in the unaugmented aircraft itself.

5.3 DETAILED DESIGN FOR THE TAKEOFF CONFIGURATION

Having decided on the essential loop closures for controlling the vertical accelerations, the designer is left with the task of selecting a system that will give the maximum reduction in the vertical accelerations without demanding excessive control activity. Factors such as the aircraft pitch response to turbulence, sensor requirements, etc. will also have to considered in selecting the best overall system. In this section, the detailed design for the takeoff configuration will be performed. Designs for the other Cessna 402B flight conditions are presented in section 5.4.

5.3.1 UNAUGMENTED 402B DYNAMICS AT TAKEOFF

Figure 5.2 shows a pole-zero plot of the Cessna 402B in a takeoff configuration at sea level. Note that this is a s-plane plot since the aircraft response without the digital control is a continuous function of time. Table 5.1 summarizes the dynamic characteristics of this aircraft. The phugoid damping ratio does not satisfy the military specification for level 1 flying qualities requirement. The control system must therefore also increase the phugoid damping to level 1 requirements.

The n/α term in Table 5.1 is approximately equal to $-Z_\alpha/g$ and is defined [12] as the steady-state, normal acceleration change, per unit angle of attack (as obtained by an incremental elevator deflection at constant speed: true airspeed and Mach number).

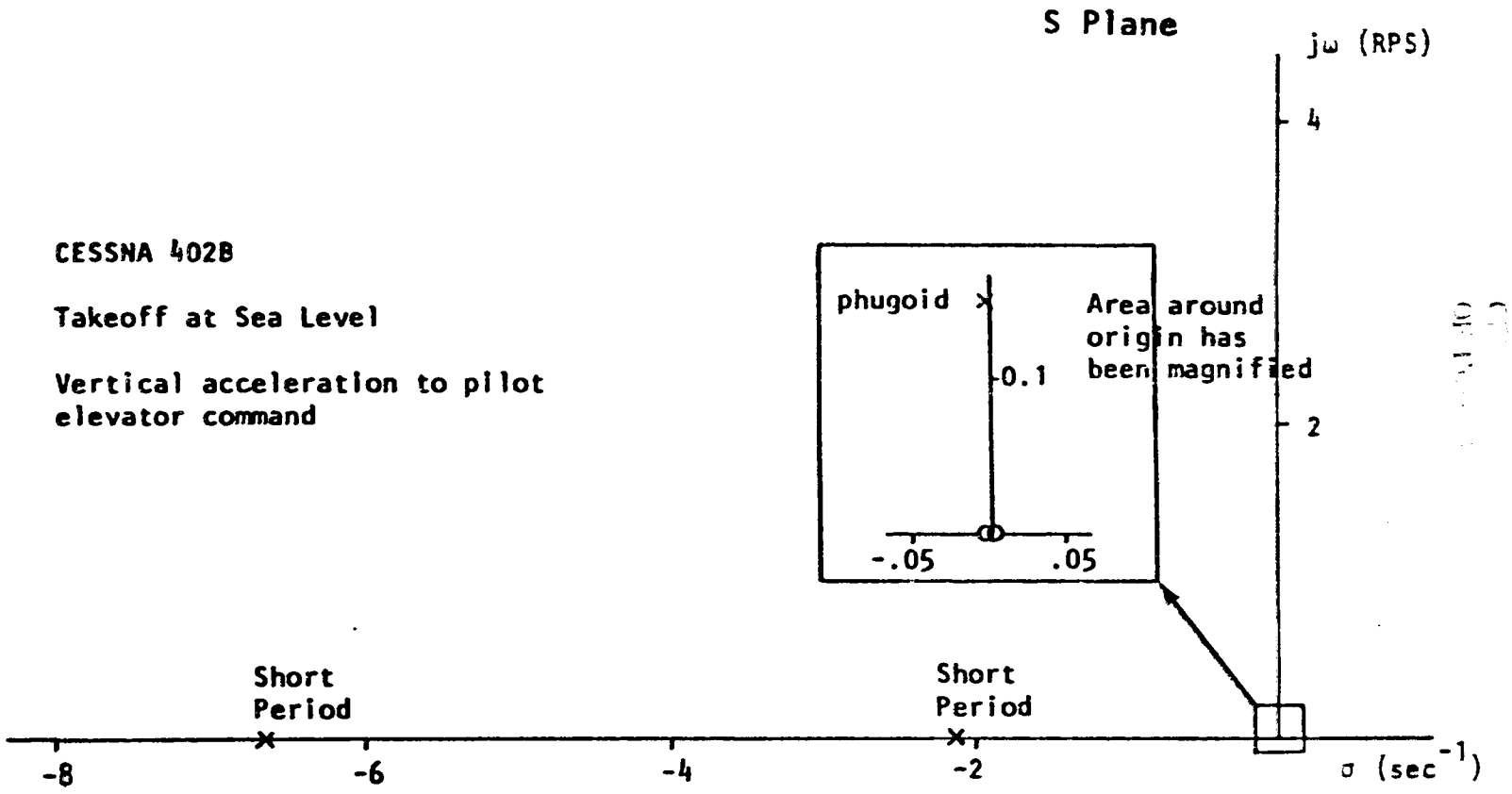

FIGURE 5.2 Eigenvalue-Zero Plot of the 402B at Takeoff

Table 5.1 Cessna 402B Dynamics During Takeoff

Dynamic Mode	Military Specifications	Actual
Short Period:		
damping	0.35-1.30	1.16*
undamped frequency, rad/sec; (n/α= 6.9)	α 1.0-5.0	3.66*
Phugoid:		
damping	> 0.04	0.02
undamped frequency, rad/sec	unspecified	0.15

* The actual short period mode values shown are for an equivalent second order system since the unaugmented 402B has two real short period eigenvalues at -2.1 and -6.6 for the takeoff configuration. Application of the Military Specifications will require these equivalent values.

5.3.2 VERTICAL ACCELERATION SYSTEMS

5.3.2.1 FEEDBACK TO THE DIRECT LIFT FLAPS

Figure 5.3 shows the block diagram of the vertical acceleration to the direct lift flap, digital control system. The effect c this system is in an approximate sense similar to increasing the mass of the aircraft, and the major effect on the aircraft dynamics can be anticipated on this basis. The root locus diagram of this system is shown in Figure 5.4.

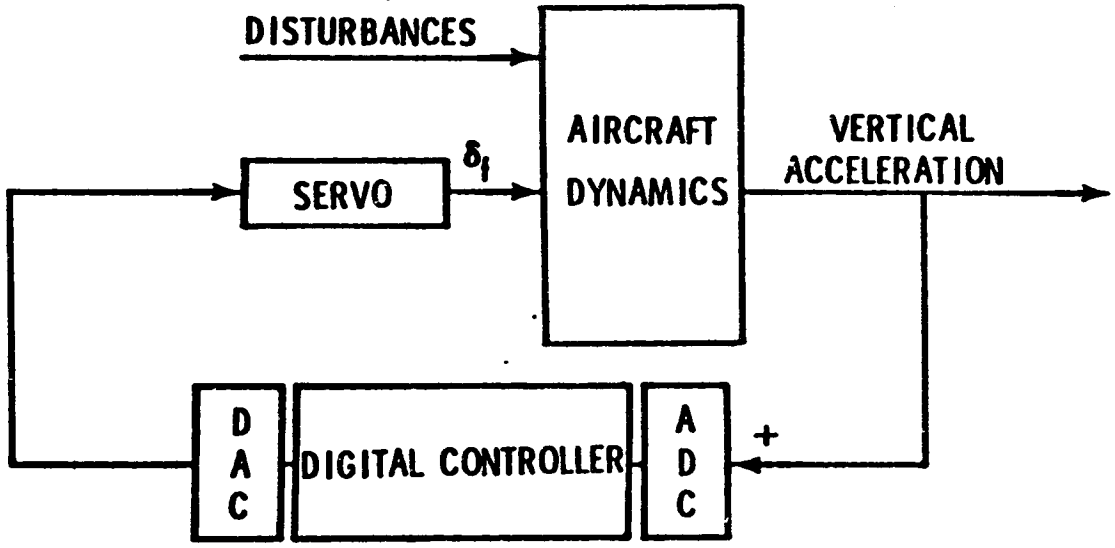

FIGURE 5.3 Block Diagram of a Digital Direct Lift Control System Using Acceleration Feedback

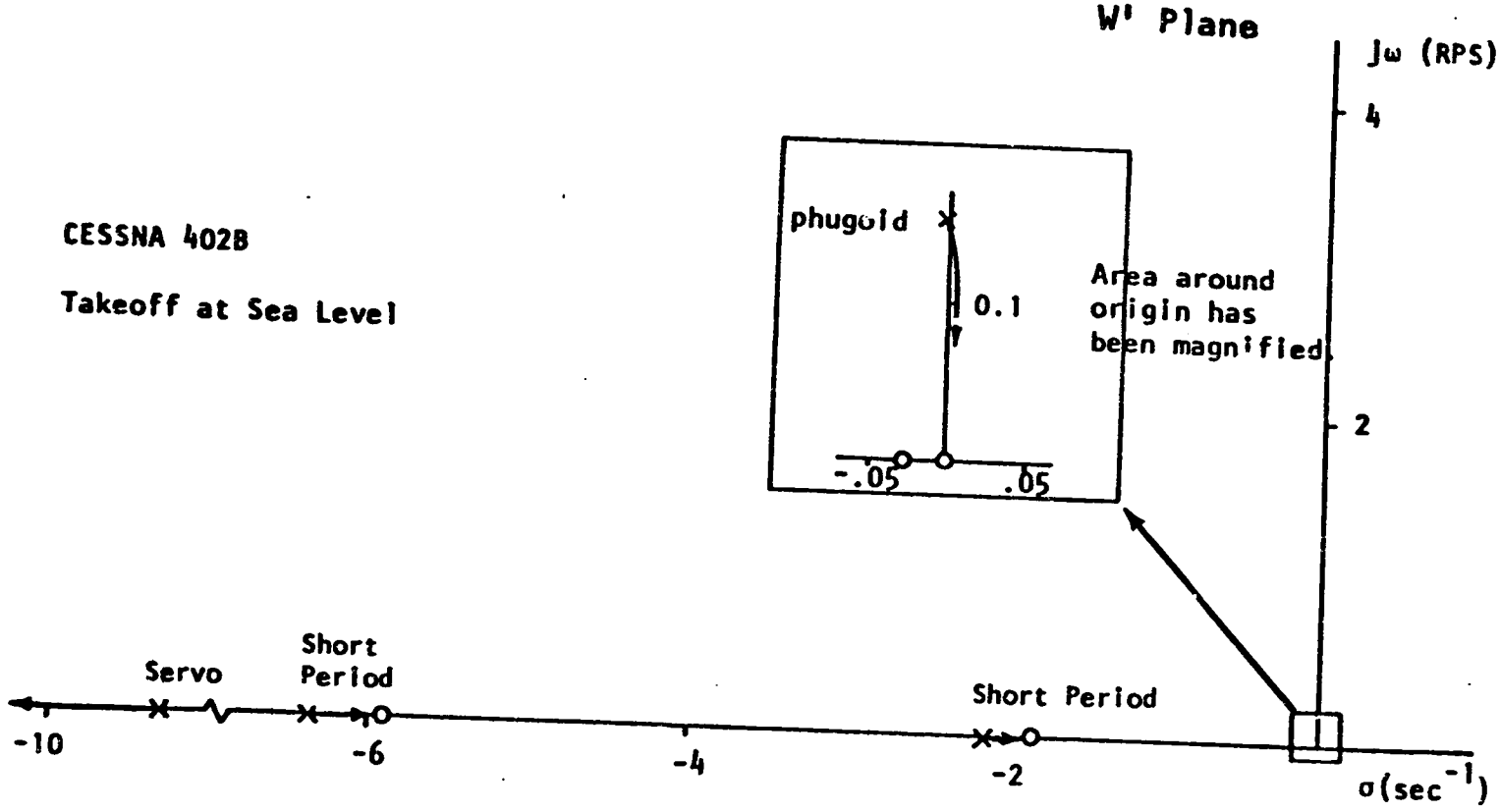

FIGURE 5.4 Root Locus for the Digital Direct Lift Control System of Figure 5.3

Notice that with increasing gain values, the phugoid mode crosses the imaginary axis. Although the phugoid is unstable, the undamped frequency decreases, resulting in a very slow divergence in this mode so the pilot will have more time to correct this deficiency. However, in terms of the military specifications, this mode will be able to satisfy only level 3 flying qualities requirement. The short period equivalent undamped frequency is decreased. This decrease in the equivalent undamped frequency implies a less rapid response of the augmented aircraft to disturbances in this particular mode. The effect of the servo on the aircraft dynamics will become less important as the servo eigenvalue moves towards infinity.

Ignoring the phugoid mode stability, the performance of this system is summarized in Table 5.2 and Figure 5.5. With increasing gain values, this system gives increased reductions in the vertical accelerations, although the slope of Figure 5.5 tends to level off at the higher gains. The increased levels of acceleration reduction are accompanied by an increased amount of control activity. The control activity, however, does not level off with increased gain values. This means that although significant amounts of reduction can be achieved, the penalty in terms of the control activity will be higher. The control rate activity in this system will be the restricting factor in the amount of reductions that can be attained in the vertical accelerations.

TABLE 5.2 PERFORMANCE OF THE Az TO DELTA-F SYSTEM

Gain	RMS accel. (ft/sec^2)	Percentage Reduction	Flap Control Activity Max (deg)	Rate (deg/s)	RMS (deg)
0.00	3.10	0.0	0.0	0.0	0.0
0.01	2.75	11.0	3.5	26.0	1.3
0.02	2.52	18.6	6.4	51.8	2.3
0.03	2.34	24.3	8.8	83.8	3.1
0.04	2.21	28.6	10.[illegible]	119.2	3.8
0.05	2.11	31.8	12.5	156.7	4.4
0.06	2.04	34.0	13.7	194.8	4.8
0.07	2.00	35.4	14.6	249.5	5.3

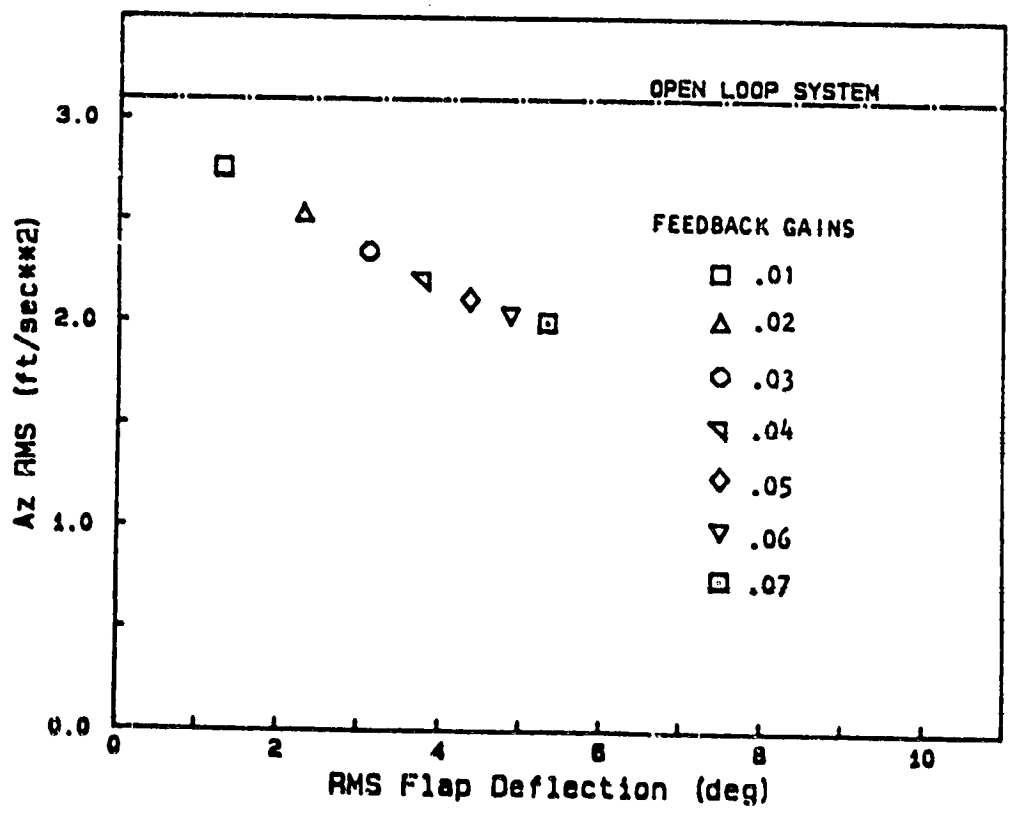

FIGURE 5.5 RMS Az Variation With Direct Lift Flap RMS Deflection

5.3.2.2 FEEDBACK TO THE ELEVATOR

Figure 5.6 shows the block diagram of the vertical acceleration to elevator, digital control system. The effect of this system would be to increase the short period resonant frequency of the aircraft to the frequency range where the gust power spectrum is decaying at the rate of 40 dB/decade. The magnitude of the aircraft response to turbulence will therefore be reduced.

The root locus diagram of this system is shown in Figure 5.7. With increasing gain values, the two short period eigenvalues approach each other on the real axis before leaving this axis. As the gain values are further increased, the undamped frequency of this mode increases, speeding up the response in the short period mode. The short period damping decreases and will result in increased pitch oscillations in the presence of disturbances. Eventually the aircraft will become unstable as the eigenvalues cross the imaginary axis. The phugoid mode undamped frequency decreases as the gain is increased thereby increasing the period of this oscillation. The phugoid damping decreases and this mode soon becomes unstable. The servo eigenvalue approaches the finite zero. The close proximity of this eigenvalue-zero pair together with the now slightly greater separation of the servo eigenvalue from the origin indicates that the servo effect on the aircraft dynamics will become less important. The performance of this system is summarized in Table 5.3 and Figure 5.8. This system gives a negligible reduction in the vertical accelerations. Although not shown, the pitch response to turbulence has also increased. However, the elevator control activity is minimal.

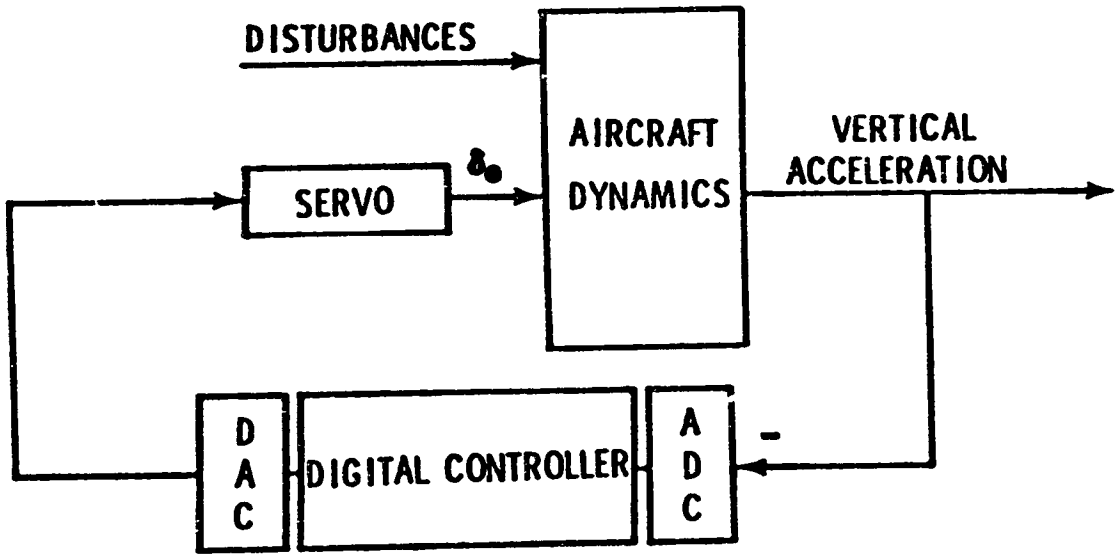

FIGURE 5.6 Block Diagram of a Digital Attitude Control System Using Acceleration Feedback

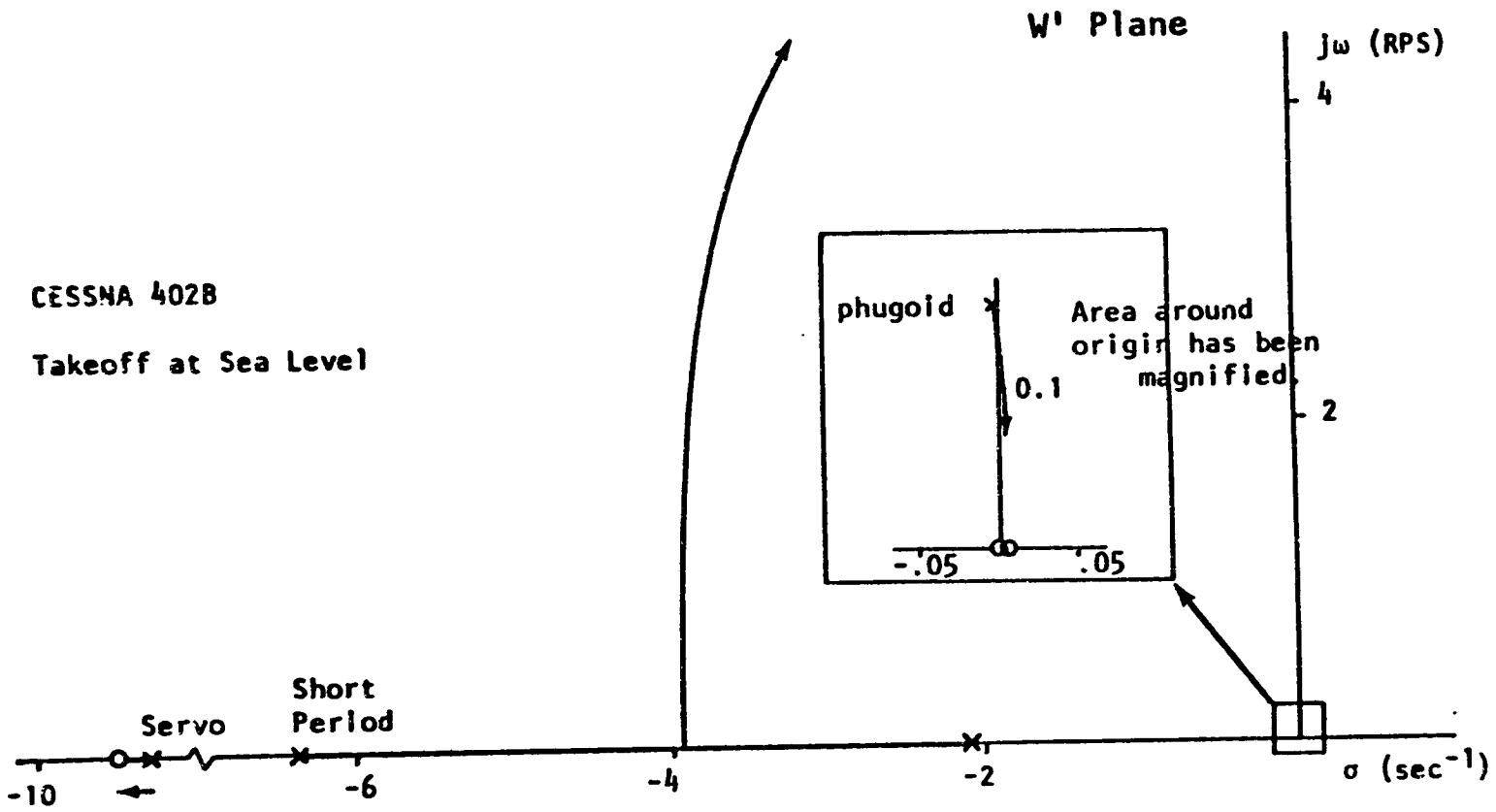

FIGURE 5.7 Root Locus for the Digital Attitude Control System of Figure 5.6

TABLE 5.3 PERFORMANCE OF THE Az TO DELTA-E SYSTEM

Gain	RMS accel. (ft/sec^2)	Percentage Reduction	Elevator Control Activity Max (deg)	Rate (deg/s)	RMS (deg)
0.000	3.10	0.0	0.0	0.0	0.0
0.001	3.00	3.1	0.36	3.02	0.14
0.002	2.94	5.0	0.72	6.55	0.28
0.003	2.91	6.0	1.07	10.54	0.41
0.004	2.90	6.2	1.37	14.82	0.54
0.005	2.93	5.3	1.60	19.20	0.67

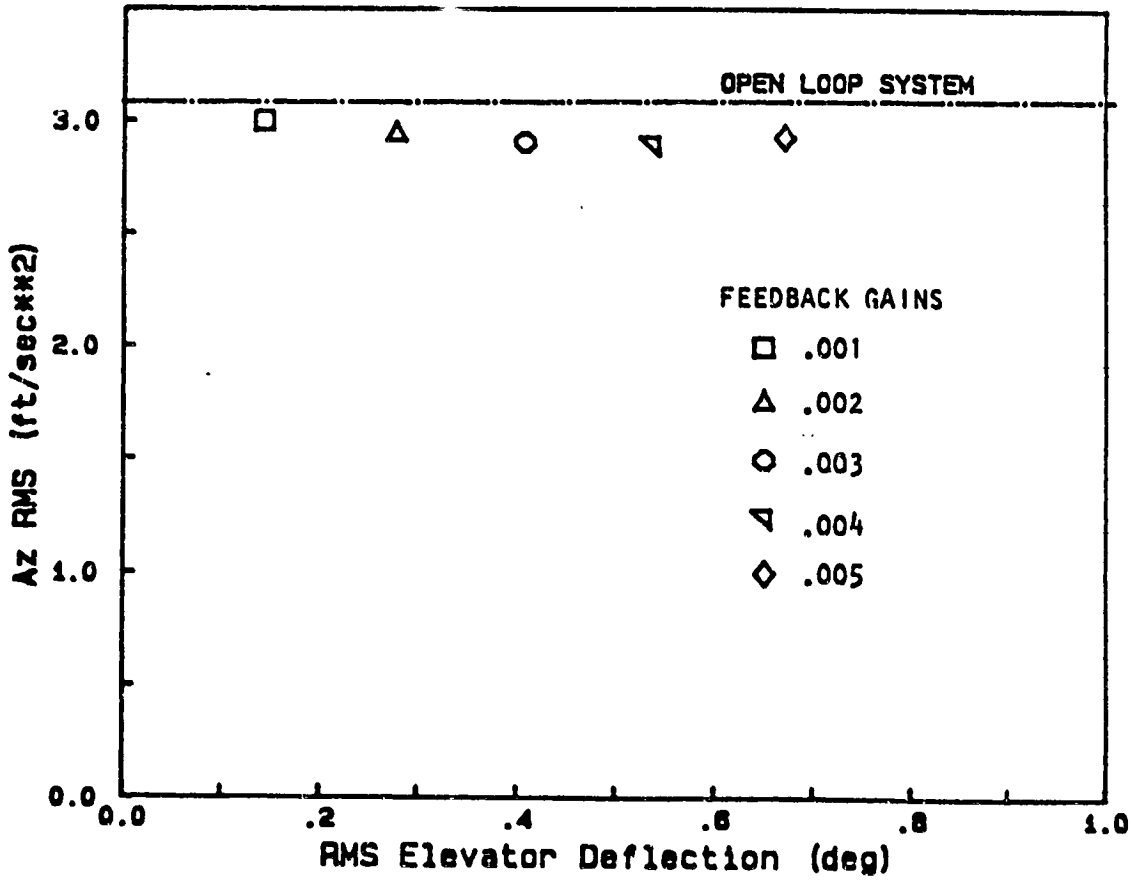

FIGURE 5.8 RMS AZ Variation with Elevator RMS Deflection

5.3.3 ANGLE OF ATTACK SYSTEMS

5.3.3.1 FEEDBACK TO THE DIRECT LIFT FLAPS

Figure 5.9 shows the block diagram of the angle of attack to the direct lift flap, digital control system. This system will tend to maintain alpha and thus C_L constant following an alpha gust.

The root locus diagram of this system is shown in figure 5.10. With increasing gain values, the phugoid mode undamped frequency increases causing a reduction in the period of oscillation associated with this mode. The phugoid mode damping also increases, satisfying the military specification on level 1 flying qualities requirement. The short period mode remains real although it's equivalent undamped frequency decreases. This decrease in the equivalent undamped frequency will be higher than in the vertical acceleration to direct lift flap system since the finite zeroes are now separated at a greater distance from the short period eigenvalues. The response to disturbances will therefore be less rapid compared to the vertical acceleration to direct lift flap system. The influence of the servo on the aircraft dynamics will become less important as the servo eigenvalue moves to infinity.

The performance of this system is summarized in Table 5.4 and Figure 5.11. With increasing gain values, this system gives increased reductions in the vertical accelerations. However, a limit is soon approached and any further gain increase degrades the performance of this system, both in terms of reductions in the vertical accelerations and increases in the control requirements.

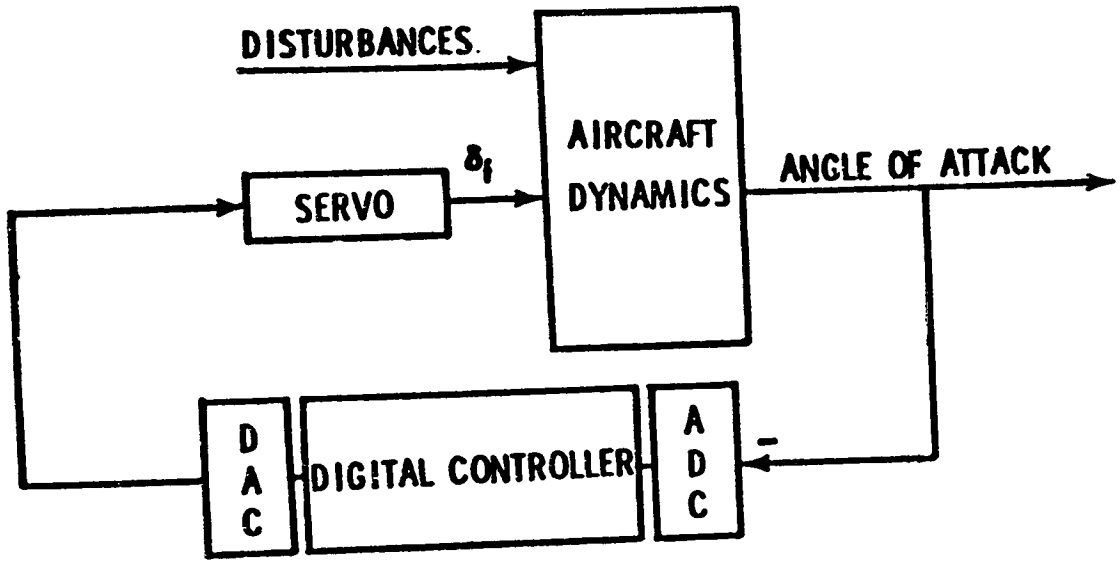

FIGURE 5.9 Block Diagram of a Digital Direct Lift Control System Using Angle of Attack Feedback

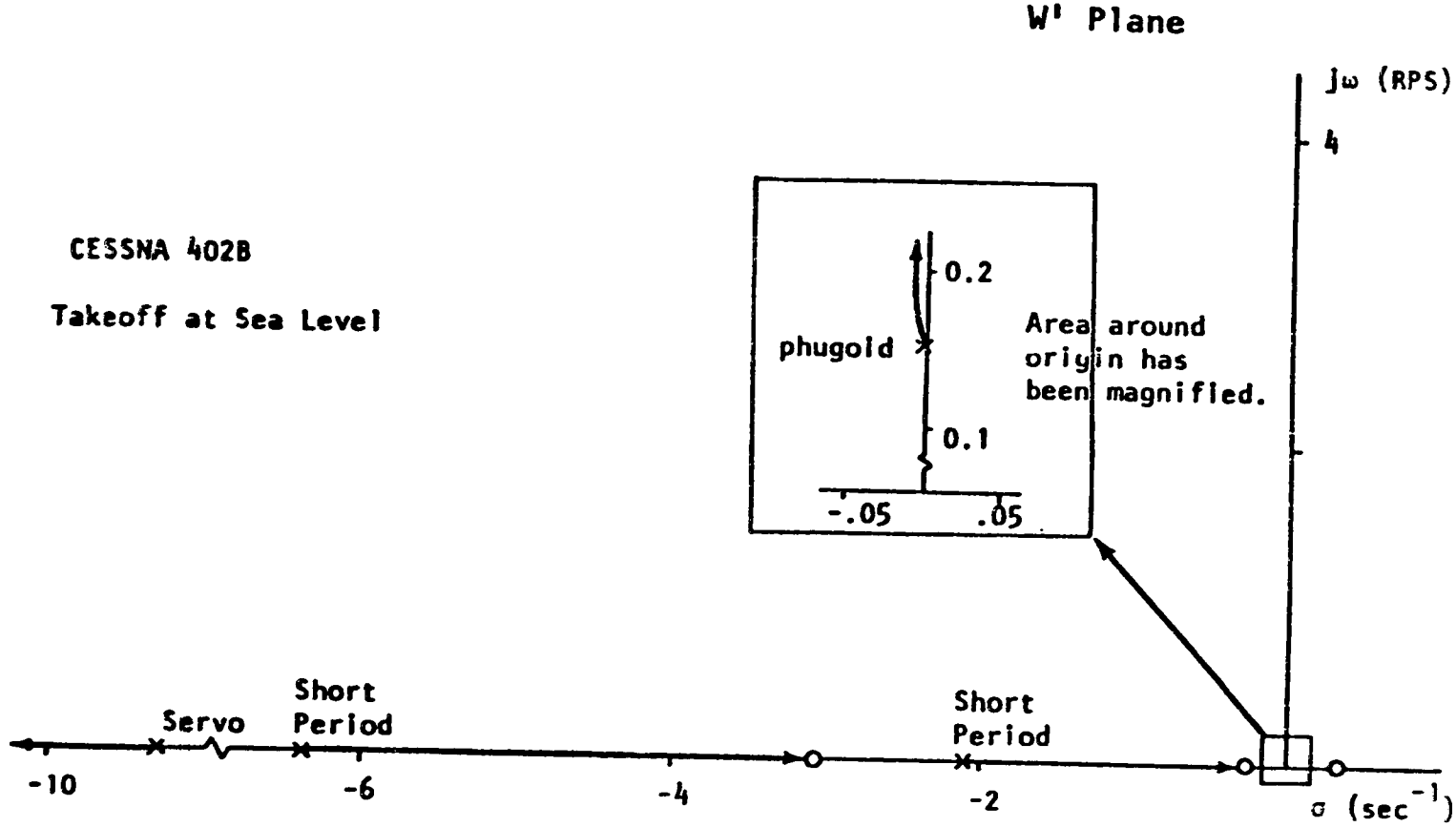

FIGURE 5.10 Root Locus for the Digital Direct Lift Control System of Figure 5.9

TABLE 5.4 PERFORMANCE OF THE ALPHA TO DELTA-F SYSTEM

Gain	RMS accel. (ft/sec^2)	Percentage Reduction	Flap Control Activity Max (deg)	Rate (deg/s)	RMS (deg)
0.0	3.10	0.0	0.0	0.0	0.0
0.05	2.59	16.5	5.67	36.24	2.26
0.10	2.25	27.4	11.76	70.52	4.75
0.15	2.23	27.9	18.33	102.60	7.50
0.20	2.64	14.7	25.43	132.30	10.50

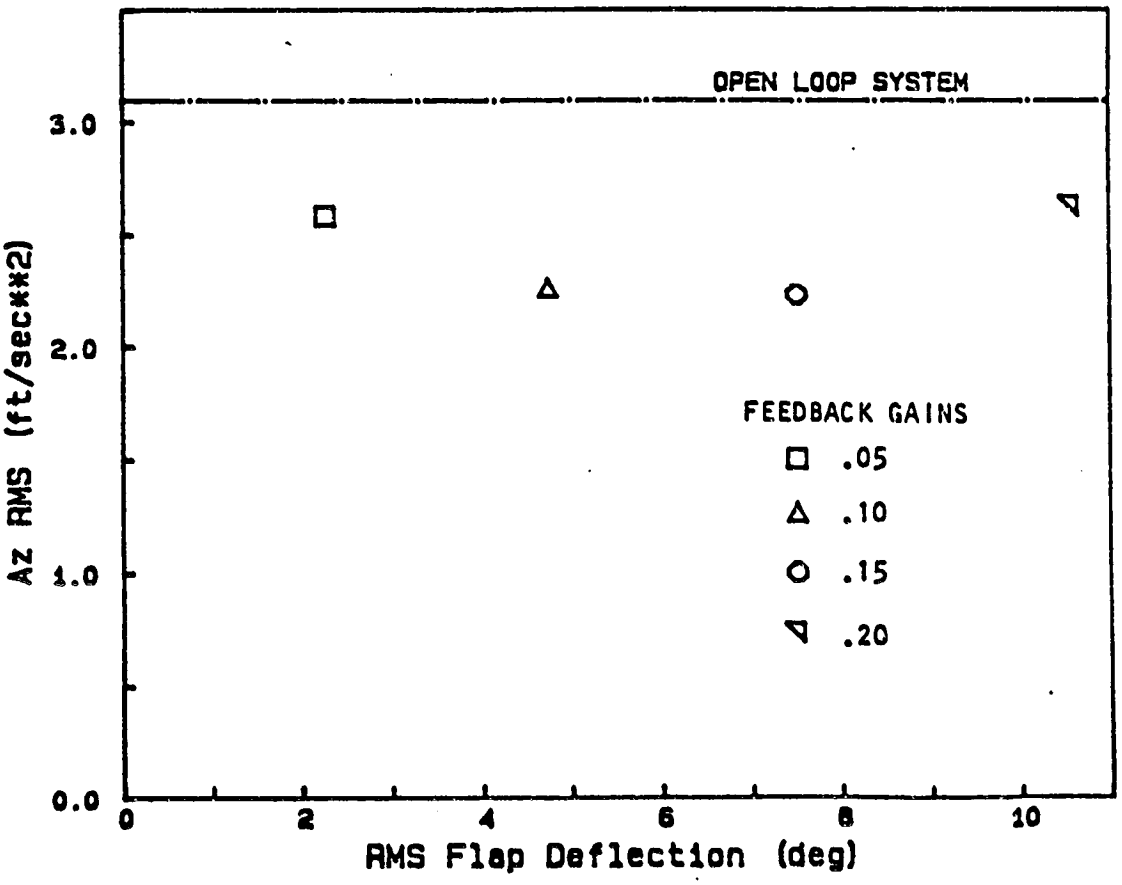

FIGURE 5.11 RMS Az Variation with Direct Lift Flap RMS Deflection

5.3.3.2 FEEDBACK TO THE ELEVATOR

Figure 5.12 shows the block diagram of the angle of attack to elevator digital control system. The effect of this system would be to increase the magnitude of M_α directly and thereby increase the static stability of the aircraft.

The root locus diagram of this system is shown in Figure 5.13. The phugoid mode undamped frequency increases as the gain is increased thereby decreasing the period of this oscillation. The damping, however, decreases and this mode immediately becomes unstable. The increase in the undamped frequency will result in a more rapid divergence of this mode. The two short period eigenvalues approach each other on the real axis before leaving this axis. As the gain values are further increased, the undamped frequency of this mode increases. This will cause an increase in speed in the short period pitch response of the aircraft. The decrease in the short period damping will cause increased pitch oscillations in the presence of disturbances. Eventually the aircraft will become unstable as the eigenvalues cross the imaginary axis. The influence of the servo on the aircraft dynamics will become less important as the servo eigenvalue moves towards infinity.

The performance of this system is summarized in Table 5.5 and Figure 5.14. This system gives a negligible reduction in the vertical accelerations. Although not shown, the pitch response to turbulence in both the short period and phugoid modes has also increased. Demands on the elevator activity are, however, small.

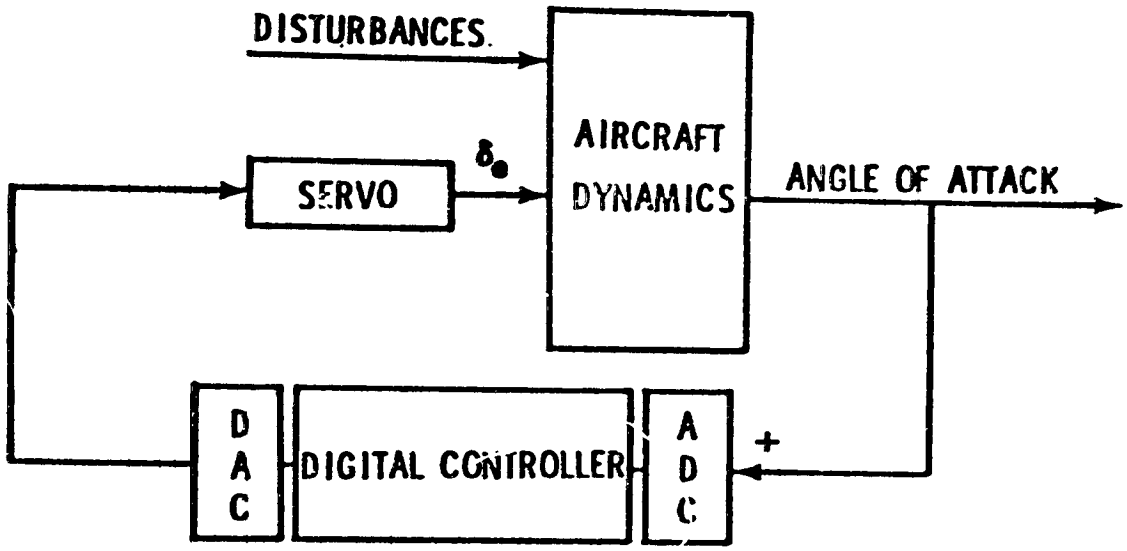

FIGURE 5.12 Block Diagram of a Digital Attitude Control System Using Angle of Attack Feedback

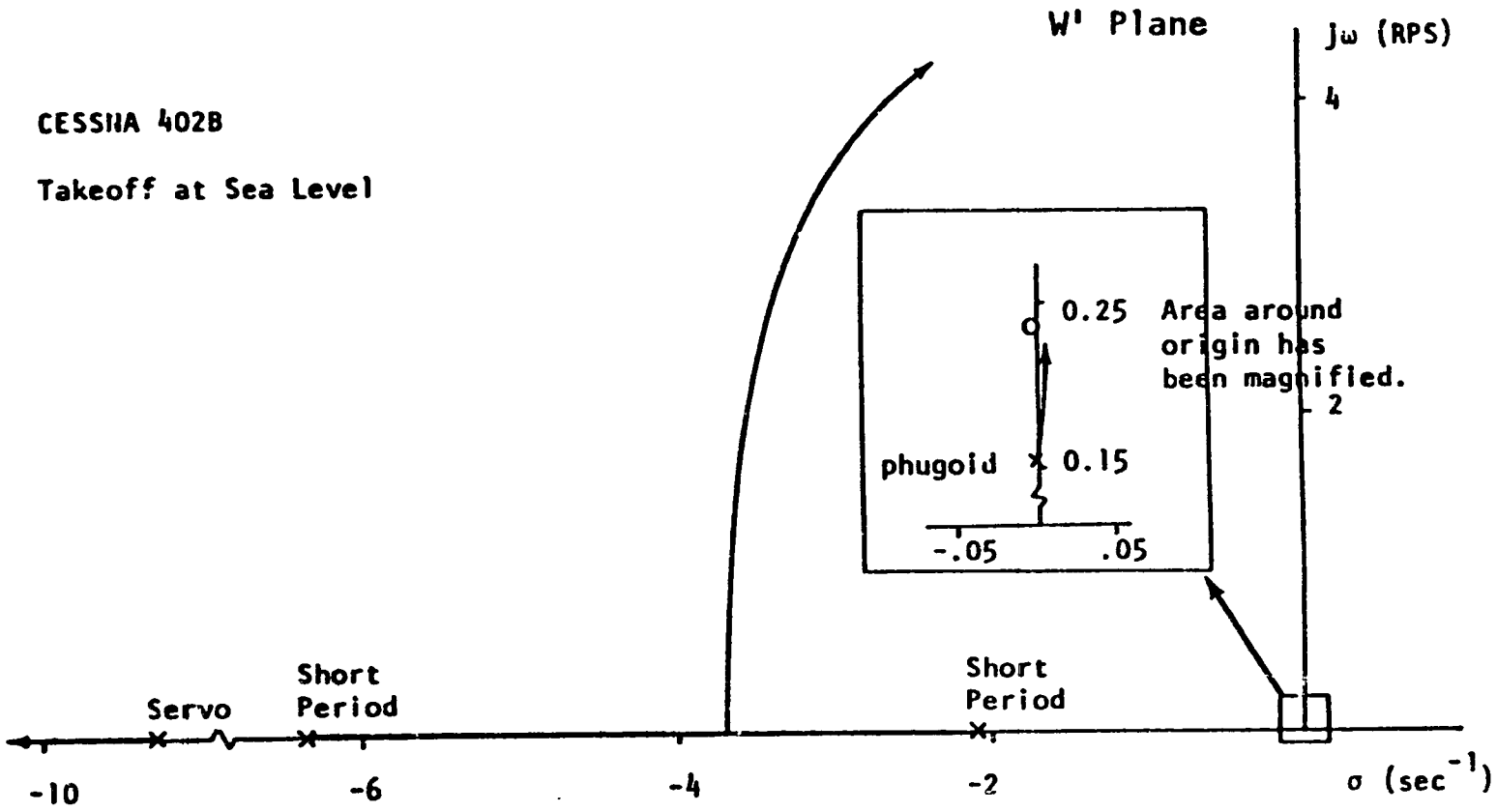

FIGURE 5.13 Root Locus for the Digital Attitude Control System of Figure 5.12

TABLE 5.5 PERFORMANCE OF THE ALPHA TO DELTA-E SYSTEM

Gain	RMS accel. (ft/sec^2)	Percentage Reduction	Elevator Max (deg)	Control Rate (deg/s)	Activity RMS (deg)
0.000	3.10	0.0	0.0	0.0	0.0
0.004	3.00	3.1	0.42	3.22	0.17
0.008	2.95	4.6	0.86	6.96	0.32
0.012	2.94	4.9	1.30	11.15	0.45
0.016	2.96	4.3	1.68	15.63	0.59

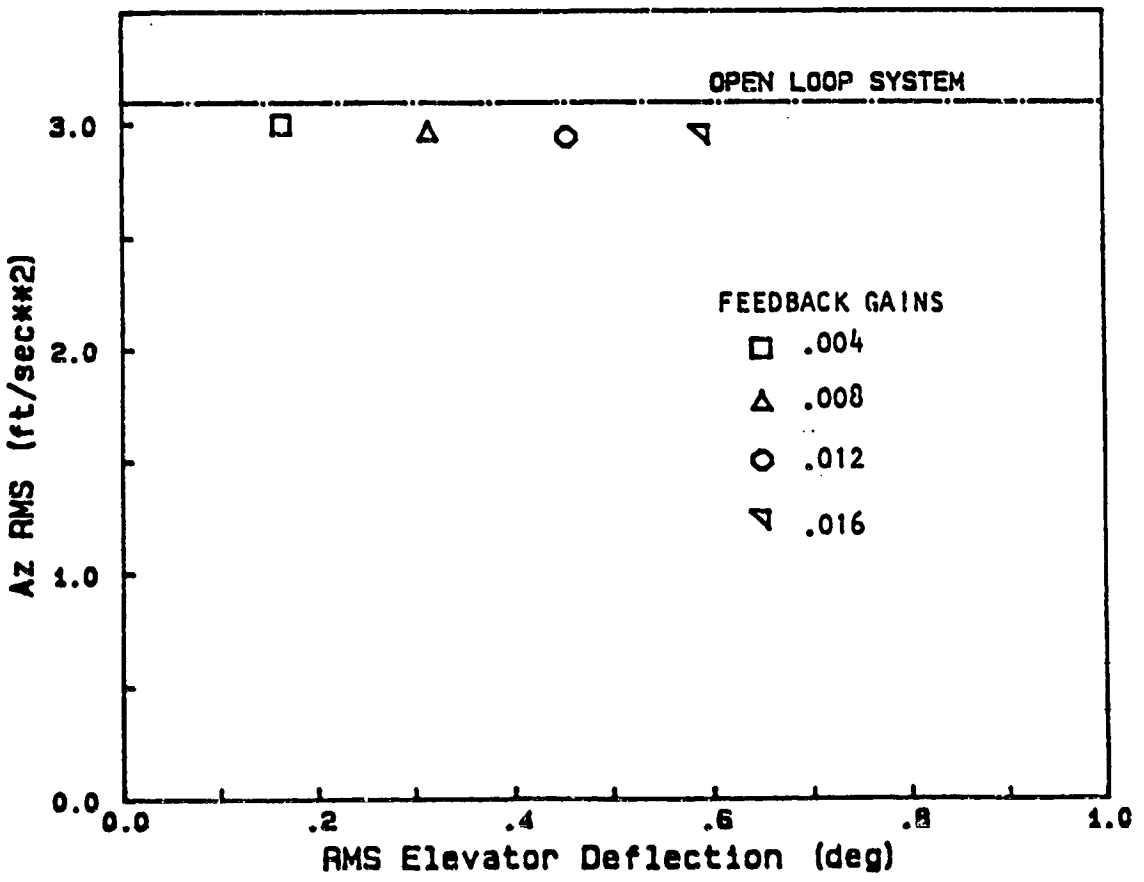

FIGURE 5.14 RMS Az Variation with Elevator RMS Deflection

5.3.4 SELECTION OF THE VERTICAL ACCELERATION CONTROL SYSTEM

A comparison of the four vertical acceleration control systems is shown in Table 5.6. In all tables to follow, Gain 1 refers to the value of the gain in the feedback to the elevator, and Gain 2 refers to the value of the gain in the feedback to the direct lift flaps. The comparison in table 5.6 is based on the maximum reductions that could be attained in the vertical accelerations while keeping the control activity within realizable values. For the direct lift flaps, the control activity should not exceed maximum and rate values of 20 deg. (15 deg. for the approach) and 150 deg/sec., respectively.

Referring to Table 5.6, the vertical acceleration and angle of attack systems to the elevator can be eliminated from implementation considerations since they provide minimal reductions in the vertical accelerations. The two direct lift systems give overall higher reductions in the vertical accelerations.

The vertical acceleration to direct lift flap system does much better than the angle of attack system in terms of higher percentage reductions in the RMS vertical acceleration values. The RMS flap deflection value in the vertical acceleration system is less than the value of the angle of attack system. Therefore, the drag penalty due to the direct lift flaps will be much smaller. The maximum flap deflection is also lower in the vertical acceleration system and the RMS pitch rate value is less.

The vertical acceleration system has destabilized the phugoid mode. Although the angle of attack system has increased the phugoid damping, it is not sufficient enough to satisfy the military specification on level 1

TABLE 5.6 PERFORMANCE COMPARISON OF THE VERTICAL ACCELERATION CONTROL SYSTEMS

UNAUGMENTED AIRCRAFT:

	Az(ft/s2)	Alfa(deg)	Q(deg/s)	Thet(deg)	D-e(deg)	D-f(deg)
MAX	-8.939	2.394	-1.615	1.123	0.000	0.000
RATE	-126.660	33.263	-23.191	-1.580	0.000	0.000
RMS	3.095	0.877	0.614	0.583	0.000	0.000

Z-REAL	Z-IMAG	W'-REAL	W'-IMAG	FREQUENCY	DAMPING
0.515923	0.000000	-6.386562	0.000000	6.386562	1.000000
0.809889	0.000000	-2.100803	0.000000	2.100803	1.000000
0.999542	0.015149	-0.003431	0.151556	0.151594	0.022631
0.999542	-0.015149	-0.003431	-0.151556	0.151594	0.022631
0.367879	0.000000	-9.242343	0.000000	9.242343	1.000000
0.367879	0.000000	-9.242343	0.000000	9.242343	1.000000

VERTICAL ACCELERATION TO DIRECT LIFT FLAP SYSTEM:

GAIN1= 0.000000 GAIN2= 0.048000

COMPUTATIONAL DELAY TIME = 0.010

	Az(ft/s2)	Alfa(deg)	Q(deg/s)	Thet(deg)	D-e(deg)	D-f(deg)
MAX	-6.000	2.486	-2.111	1.917	0.000	-12.168
RATE	-144.776	33.174	8.440	-2.110	0.000	-148.923
RMS	2.128	0.939	0.861	1.066	0.000	4.260

Z-REAL	Z-IMAG	W'-REAL	W'-IMAG	FREQUENCY	DAMPING
-0.272499	0.000000	-34.982762	0.000000	34.982762	1.000000
0.537116	0.000000	-6.022764	0.000000	6.022764	1.000000
0.822006	0.000000	-1.953819	0.000000	1.953819	1.000000
1.000257	0.011287	0.003206	0.112837	0.112883	-0.028400
1.000257	-0.011287	0.003206	-0.112837	0.112883	-0.028400
0.367879	0.000000	-9.242343	0.000000	9.242343	1.000000

RMS Az REDUCTION IS 31.2%

VERTICAL ACCELERATION TO ELEVATOR SYSTEM:

GAIN1= 0.004000 GAIN2= 0.000000

COMPUTATIONAL DELAY TIME = 0.010

	Az(ft/s2)	Alfa(deg)	Q(deg/s)	Thet(deg)	D-e(deg)	D-f(deg)
MAX	-7.502	-2.178	3.827	2.858	-1.373	0.000
RATE	-125.605	33.415	21.008	3.825	-14.819	0.000
RMS	2.904	0.828	1.568	1.322	0.538	0.000

TABLE 5.6 CONTINUED

Z-REAL	Z-IMAG	W'-REAL	W'-IMAG	FREQUENCY	DAMPING
0.362529	0.000000	-9.357180	0.000000	9.357180	1.000000
0.679508	0.304403	-3.059013	4.179340	5.179232	0.590631
0.679508	-0.304403	-3.059013	-4.179340	5.179232	0.590631
0.999721	0.010355	-0.002252	0.103572	0.103597	0.021734
0.999721	-0.010355	-0.002252	-0.103572	0.103597	0.021734
0.367879	0.000000	-9.242343	0.000000	9.242343	1.000000

RMS Az REDUCTION IS 6.2%

ANGLE OF ATTACK TO DIRECT LIFT FLAP SYSTEM:

GAIN1= 0.000000 GAIN2= 0.140000

COMPUTATIONAL DELAY TIME = 0.010

	Az(ft/s2)	Alfa(deg)	Q(deg/s)	Thet(deg)	D-e(deg)	D-f(deg)
MAX	-5.720	2.552	-2.452	2.430	0.000	-16.979
RATE	-126.355	33.049	-8.028	-2.451	0.000	96.380
RMS	2.200	0.970	1.090	1.260	0.000	6.929

Z-REAL	Z-IMAG	W'-REAL	W'-IMAG	FREQUENCY	DAMPING
0.279710	0.000000	-11.257071	0.000000	11.257071	1.000000
0.605531	0.000000	-4.913880	0.000000	4.913880	1.000000
0.837242	0.000000	-1.771769	0.000000	1.771769	1.000000
0.998881	0.022081	-0.008759	0.221032	0.221205	0.039595
0.998881	-0.022081	-0.008759	-0.221032	0.221205	0.039595
0.367879	0.000000	-9.242343	0.000000	9.242343	1.000000

RMS Az REDUCTION IS 28.9%

ANGLE OF ATTACK TO ELEVATOR SYSTEM:

GAIN1= 0.012000 GAIN2= 0.000000

COMPUTATIONAL DELAY TIME = 0.010

	Az(ft/s2)	Alfa(deg)	Q(deg/s)	Thet(deg)	D-e(deg)	D-f(deg)
MAX	-8.184	-2.161	3.562	2.401	-1.300	0.000
RATE	-126.008	33.470	16.817	3.562	-11.154	0.000
RMS	2.942	0.801	1.435	1.142	0.457	0.000

Z-REAL	Z-IMAG	W'-REAL	W'-IMAG	FREQUENCY	DAMPING
0.267629	0.000000	-11.554972	0.000000	11.554972	1.000000
0.704229	0.254644	-2.958455	3.430433	4.529937	0.653090
0.704229	-0.254644	-2.958455	-3.430433	4.529937	0.653090
0.999908	0.019590	0.000994	0.195898	0.195900	-0.005074
0.999908	-0.019590	0.000994	-0.195898	0.195900	-0.005074
0.367879	0.000000	-9.242343	0.000000	9.242343	1.000000

RMS Az REDUCTION IS 4.9%

flying qualities requirement. The equivalent undamped short period frequency of the angle of attack system is now less than the vertical acceleration system.

Based on the above discussion, the angle of attack system can be considered inferior when compared to the vertical acceleration system. The angle of attack system has a further serious disadvantage in terms of the sensor requirements. The angle of attack sensor [25] senses an indicated angle of attack because of the disturbances which exist near the airframe. Consequently, the true angle of attack must be computed from the indicated angle which requires additional data, usually, the indicated airspeed and mach number, to perform this computation. Also, the characteristics of the alpha-sensors are difficult to predict by analysis, so flight test programs are often required to determine a suitable location for the sensor, to determine the sensor characteristics, etc..

The vertical acceleration to direct lift flap system is clearly the best overall system in controlling the vertical accelerations. It was therefore selected for the active ride augmentation. As noted earlier, this system destabilized the phugoid mode and decreased the equivalent short period undamped frequency. To correct these deficiences, a second (outer) loop closure to the elevator was made.

The acceleration system, as noted earlier, will in an approximate sense increase the mass of the aircraft and thereby artificially increase the wing loading of the aircraft. This agrees with past studies [2] where low wing loading has been considered the primary design characteristic contributing to poor ride quality.

5.3.5 EFFECT OF THE SECOND LOOP CLOSURE

To stabilize the aircraft phugoid mode and to increase the equivalent short period undamped frequency, an attitude hold system, that is, an attitude angle to elevator system was required. The attitude hold system will tend to hold the pitch attitude constant in the presence of disturbances since the reference for stabilization is the horizon. Due to this rigidity in attitude, the effect on the vertical acceleration reductions of the direct lift system will be negligible.

Figure 5.15 shows the block diagram of the multi-loop direct lift system with digital control. The effect on the aircraft dynamics is illustrated in the root locus diagram of Figure 5.16.

Note that the phugoid mode is rapidly stabilized and the damping increases considerably to easily satisfy the military specification on level 1 flying qualities requirement. Some degradation in the short period damping, however, results.

The performance of this system is summarized in Table 5.7. The attitude hold system, as expected, has a negligible effect on the vertical acceleration reductions. Also, the phugoid mode has been rapidly stabilized while the short period mode is still real. The demand on the elevator control activity is extremely small.

The effect of including the attitude hold system was to satisfy the military specification on level 1 flying qualities requirement, without adversely affecting the vertical acceleration reductions. Further reductions in the vertical accelerations, if possible, would therefore be highly desirable.

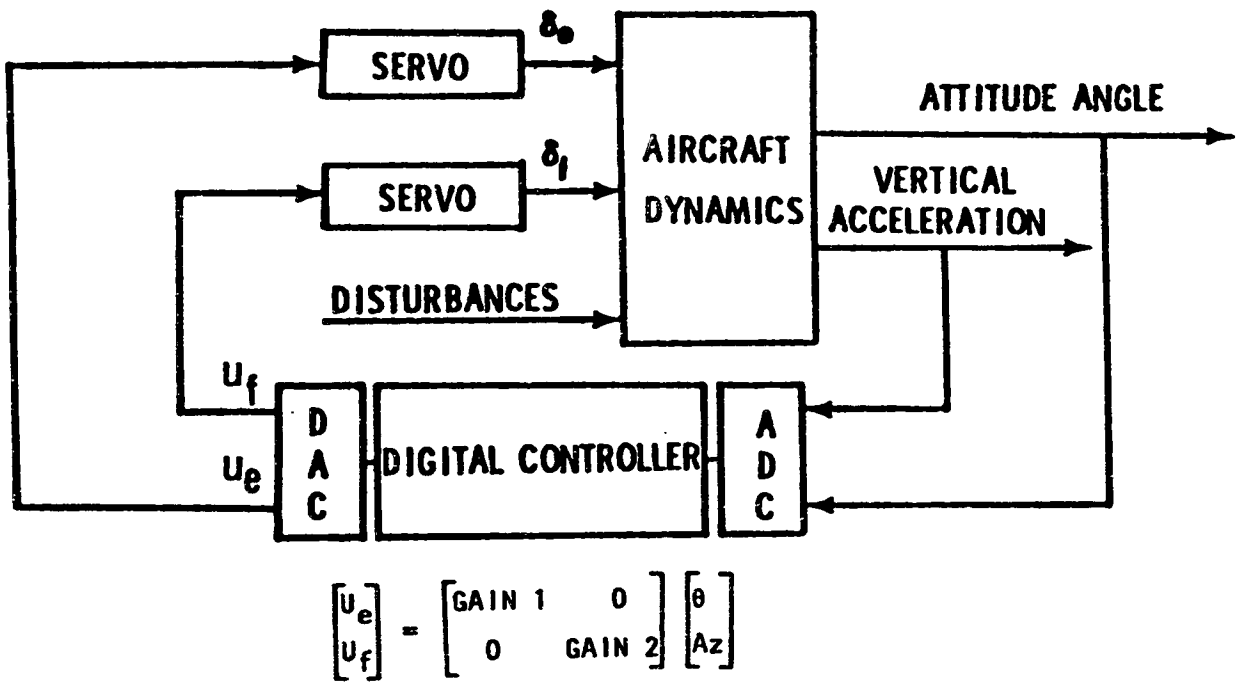

FIGURE 5.15 Block Diagram of a Digital Direct Lift Plus Attitude Hold Control System.

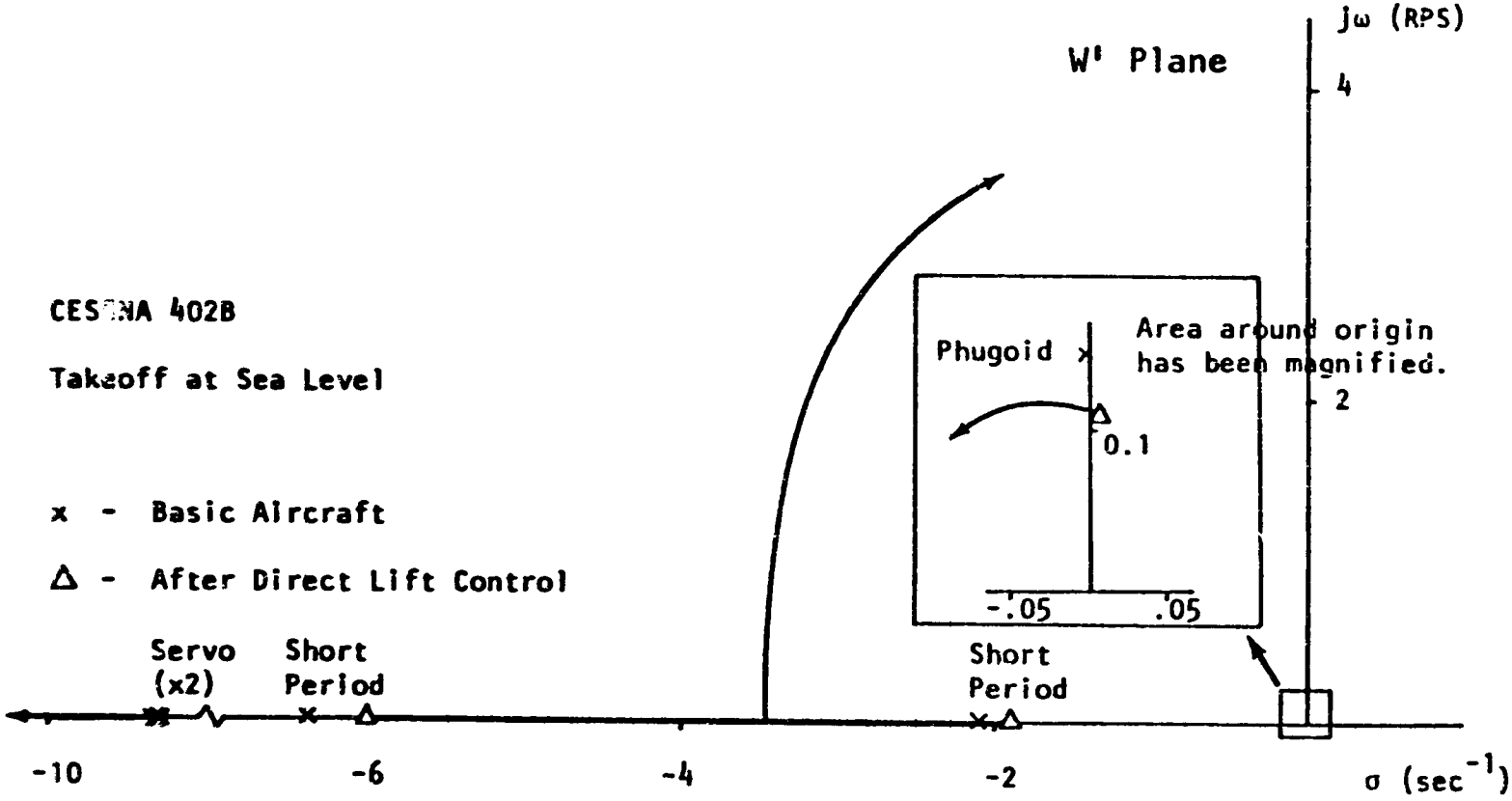

FIGURE 5.16 Root Locus for the Digital Multiloop Control System of Figure 5.15

TABLE 5.7 PERFORMANCE OF THE
Az TO DELTA-F AND THETA TO DELTA-E SYSTEM

UNAUGMENTED AIRCRAFT:

	Az(ft/s2)	Alfa(deg)	Q(deg/s)	Thet(deg)	D-e(deg)	D-f(deg)
MAX	-8.939	2.394	-1.615	1.123	0.000	0.000
RATE	-126.660	33.263	-23.191	-1.580	0.000	0.000
RMS	3.095	0.877	0.614	0.583	0.000	0.000

Z-REAL	Z-IMAG	W'-REAL	W'-IMAG	FREQUENCY	DAMPING
0.515923	0.000000	-6.386562	0.000000	6.386562	1.000000
0.809889	0.000000	-2.100803	0.000000	2.100803	1.000000
0.999542	0.015149	-0.003431	0.151556	0.151594	0.022631
0.999542	-0.015149	-0.003431	-0.151556	0.151594	0.022631
0.367879	0.000000	-9.242343	0.000000	9.242343	1.000000
0.367879	0.000000	-9.242343	0.000000	9.242343	1.000000

AFTER DIRECT LIFT CONTROL:

GAIN1= 0.000000 GAIN2= 0.048000

COMPUTATIONAL DELAY TIME = 0.010

	Az(ft/s2)	Alfa(deg)	Q(deg/s)	Thet(deg)	D-e(deg)	D-f(deg)
MAX	-6.000	2.486	-2.111	1.917	0.000	-12.168
RATE	-144.776	33.174	8.440	-2.110	0.000	-148.923
RMS	2.128	0.939	0.861	1.066	0.000	4.260

Z-REAL	Z-IMAG	W'-REAL	W'-IMAG	FREQUENCY	DAMPING
-0.272499	0.000000	-34.982762	0.000000	34.982762	1.000000
0.537116	0.000000	-6.022764	0.000000	6.022764	1.000000
0.822006	0.000000	-1.953819	0.000000	1.953819	1.000000
1.000257	0.011287	0.003206	0.112837	0.112883	-0.028400
1.000257	-0.011287	0.003206	-0.112837	0.112883	-0.028400
0.367879	0.000000	-9.242343	0.000000	9.242343	1.000000

RMS Az REDUCTION IS 31.2%

WITH ATTITUDE HOLD SYSTEM:

GAIN1= 0.001000 GAIN2= 0.048000

COMPUTATIONAL DELAY TIME = 0.010

	Az(ft/s2)	Alfa(deg)	Q(deg/s)	Thet(deg)	D-e(deg)	D-f(deg)
MAX	-6.103	2.503	-2.039	1.752	-0.100	-12.253
RATE	-144.789	33.169	8.644	-2.038	0.161	-148.358
RMS	2.117	0.914	0.859	0.897	0.051	4.232

TABLE 5.7 CONTINUED

Z-REAL	Z-IMAG	W'-REAL	W'-IMAG	FREQUENCY	DAMPING
-0.272514	0.000000	-34.983868	0.000000	34.983868	1.000000
0.584950	0.000000	-5.237390	0.000000	5.237390	1.000000
0.796198	0.000000	-2.269265	0.000000	2.269265	1.000000
0.998024	0.011667	-0.019097	0.116902	0.118451	0.161218
0.998024	-0.011667	-0.019097	-0.116902	0.118451	0.161218
0.349156	0.000000	-9.648160	0.000000	9.648160	1.000000

RMS Az REDUCTION IS 31.5%

GAIN1= 0.002000 GAIN2= 0.048000

COMPUTATIONAL DELAY TIME = 0.010

	Az(ft/s2)	Alfa(deg)	Q(deg/s)	Thet(deg)	D-e(deg)	D-f(deg)
MAX	-6.148	2.520	-1.970	1.611	-0.184	-12.335
RATE	-144.807	33.158	8.869	-1.970	0.313	-147.914
RMS	2.110	0.902	0.855	0.791	0.090	4.218

Z-REAL	Z-IMAG	W'-REAL	W'-IMAG	FREQUENCY	DAMPING
-0.272529	0.000000	-34.984972	0.000000	34.984972	1.000000
0.644591	0.000000	-4.322161	0.000000	4.322161	1.000000
0.753496	0.000000	-2.811572	0.000000	2.811572	1.000000
0.335044	0.000000	-9.961555	0.000000	9.961555	1.000000
0.996029	0.011617	-0.039114	0.116627	0.123011	0.317975
0.996029	-0.011617	-0.039114	-0.116627	0.123011	0.317975

RMS Az REDUCTION IS 31.8%

GAIN1= 0.003000 GAIN2= 0.048000

COMPUTATIONAL DELAY TIME = 0.010

	Az(ft/s2)	Alfa(deg)	Q(deg/s)	Thet(deg)	D-e(deg)	D-f(deg)
MAX	-6.152	2.535	-1.952	1.518	-0.260	-12.413
RATE	-144.829	33.141	9.113	-1.951	0.467	-147.576
RMS	2.105	0.895	0.850	0.718	0.122	4.210

Z-REAL	Z-IMAG	W'-REAL	W'-IMAG	FREQUENCY	DAMPING
-0.272543	0.000000	-34.986083	0.000000	34.986083	1.000000
0.706013	0.068753	-3.408458	0.943376	3.536601	0.963767
0.706013	-0.068753	-3.408458	-0.943376	3.536601	0.963767
0.323488	0.000000	-10.223164	0.000000	10.223164	1.000000
0.994255	0.011258	-0.056978	0.113228	0.126756	0.449506
0.994255	-0.011258	-0.056978	-0.113228	0.126756	0.449506

RMS Az REDUCTION IS 31.9%

5.3.6 THE ACTIVE RIDE AUGMENTATION SYSTEM

To further reduce the levels of vertical accelerations, it was decided to implement a vertical acceleration to elevator control system in conjunction with the direct lift and attitude hold control systems. The attitude hold system would stabilize the phugoid mode and increase its damping to level 1 flying qualities requirements. The short period mode would then remain real although its equivalent undamped frequency will be slightly increased. The vertical acceleration to elevator control system can then increase the short period mode undamped frequency and at the same time improve the vertical acceleration reductions of the direct lift system. Note that the vertical acceleration to elevator system will tend to increase the aircraft's pitch response to turbulence and care shou'd be taken not to aggravate this situation.

Figure 5.17 shows a block diagram of this multiloop digital control system. Here, the accelerometer signal to the elevator is first inverted before been summed with the theta signal of the stabilized gyro.

The effect on the aircraft dynamics of this system is illustrated in the root locus diagram of Figure 5.18. The phugoid mode is again rapidly stabilized and the damping is increased considerably. The phugoid mode undamped frequency decreases slightly. Any desired value of the short period undamped frequency can also be attained. Due to the vertical acceleration feedback to the elevator, the short period mode eigenvalues leave the real axis at a greater distance from the origin. Overall, the short period mode undamped frequency will be higher compared to having an

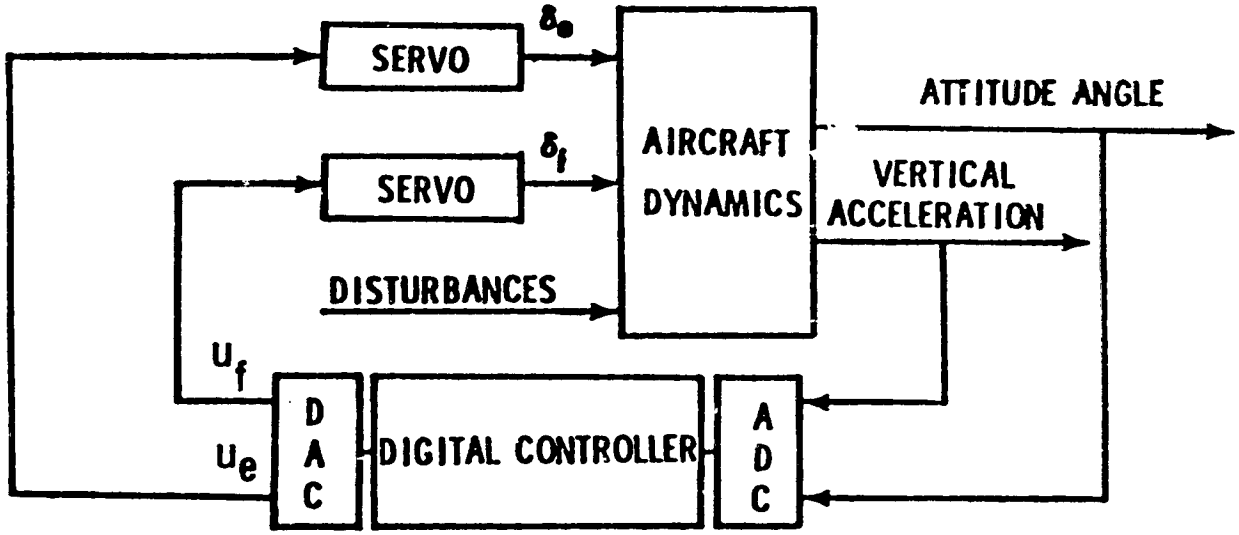

$$\begin{bmatrix} U_e \\ U_f \end{bmatrix} = \begin{bmatrix} \text{GAIN 1} & -\text{GAIN 1} \\ 0 & \text{GAIN 2} \end{bmatrix} \begin{bmatrix} \theta \\ A_z \end{bmatrix}$$

FIGURE 5.17 Block Diagram of the Digital Active Ride Augmentation System

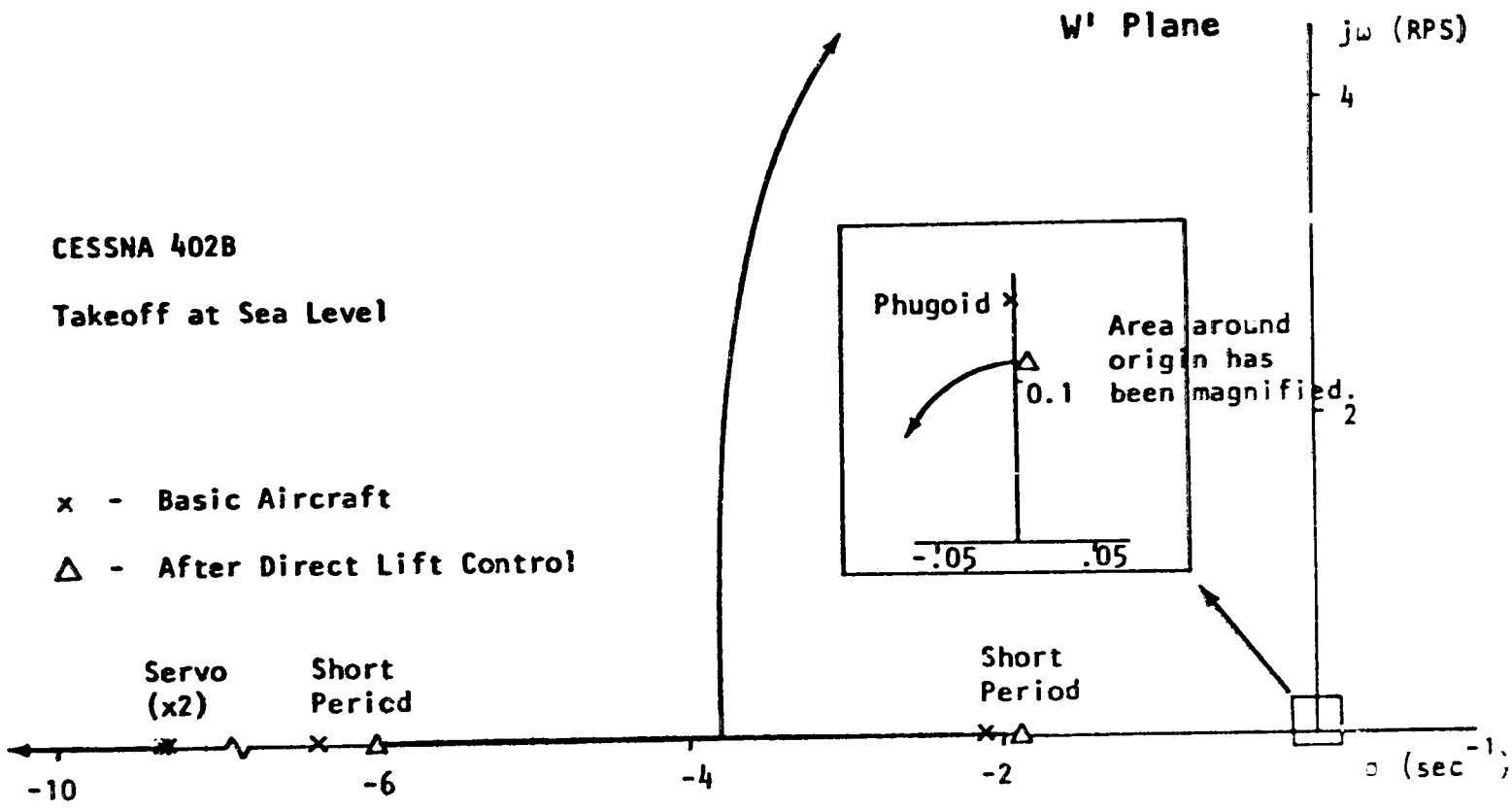

FIGURE 5.18 Root Locus for the Digital Active Ride Augmentation System of Figure 5.17

attitude hold system only. Consequently, higher values of undamped frequencies will result in the aircraft having a rapid pitch response in the presence of disturbances. Note that the short period damping decreases and increasing gains will eventually make the aircraft unstable. The servo eigenvalues remain real and their effect on the aircraft dynamics will become less important as they move further away from the origin.

The performance of this system is summarized in Table 5.8. With this system, increasing gains in the elevator loop, leads to further reductions in the vertical accelerations. The elevator control activity is, however, extremely small suggesting that excessive elevator control power exists. Notice that the flap deflection, both in terms of RMS and maximum values, decreases. Increasing gains in the elevator loop leads to a slight increase in the aircraft's short period pitch response in the presence of turbulence. However, the long term pitch response decreases as the phugoid mode damping increases and approaches critical damping.

By referring to this table, the design engineer can select the combination of gains which will give the maximum reductions in the vertical accelerations while simultaneously satisfying the military specification on level 1 flying qualities requirements. In order to maximize the performance of this system, the gain value in the feedback to the direct lift flaps should be chosen to take complete advantage of the available direct lift flap rate authority. The upper gain value in the feedback to the

TABLE 5.8 PERFORMANCE OF THE Az TO DELTA-F AND Az PLUS THETA TO DELTA-E SYSTEM

UNAUGMENTED AIRCRAFT:

	Az(ft/s2)	Alfa(deg)	Q(deg/s)	Thet(deg)	D-e(deg)	D-f(deg)
MAX	-8.939	2.394	-1.615	1.123	0.000	0.000
RATE	-126.660	33.263	-23.191	-1.580	0.000	0.000
RMS	3.095	0.877	0.614	0.583	0.000	0.000

Z-REAL	Z-IMAG	W'-REAL	W'-IMAG	FREQUENCY	DAMPING
0.515923	0.000000	-6.386562	0.000000	6.386562	1.000000
0.809889	0.000000	-2.100803	0.000000	2.100803	1.000000
0.999542	0.015149	-0.003431	0.151556	0.151594	0.022631
0.999542	-0.015149	-0.003431	-0.151556	0.151594	0.022631
0.367879	0.000000	-9.242343	0.000000	9.242343	1.000000
0.367879	0.000000	-9.242343	0.000000	9.242343	1.000000

AFTER DIRECT LIFT CONTROL:

GAIN1= 0.000000 GAIN2= 0.048000

COMPUTATIONAL DELAY TIME = 0.010

	Az(ft/s2)	Alfa(deg)	Q(deg/s)	Thet(deg)	D-e(deg)	D-f(deg)
MAX	-6.000	2.486	-2.111	1.917	0.000	-12.168
RATE	-144.776	33.174	8.440	-2.110	0.000	-148.923
RMS	2.128	0.939	0.861	1.066	0.000	4.260

Z-REAL	Z-IMAG	W'-REAL	W'-IMAG	FREQUENCY	DAMPING
-0.272499	0.000000	-34.982762	0.000000	34.982762	1.000000
0.537116	0.000000	-6.022764	0.000000	6.022764	1.000000
0.822006	0.000000	-1.953819	0.000000	1.953819	1.000000
1.000257	0.011287	0.003206	0.112837	0.112883	-0.028400
1.000257	-0.011287	0.003206	-0.112837	0.112883	-0.028400
0.367879	0.000000	-9.242343	0.000000	9.242343	1.000000

RMS Az REDUCTION IS 31.2%

ADDING ELEVATOR CONTROL:

GAIN1= 0.002000 GAIN2= 0.048000

COMPUTATIONAL DELAY TIME = 0.010

	Az(ft/s2)	Alfa(deg)	Q(deg/s)	Thet(deg)	D-e(deg)	D-f(deg)
MAX	-5.869	2.331	-2.673	2.021	-0.604	-11.492
RATE	-141.322	33.286	14.305	-2.673	-6.370	-146.359
RMS	2.062	0.862	1.148	0.995	0.195	4.014

TABLE 5.8 CONTINUED

Z-REAL	Z-IMAG	W'-REAL	W'-IMAG	FREQUENCY	DAMPING
-0.222026	0.000000	-31.415610	0.000000	31.415610	1.000000
0.680294	0.125096	-3.674145	1.762521	4.075024	0.901625
0.680294	-0.125096	-3.674145	-1.762521	4.075024	0.901625
0.996909	0.010344	-0.030417	0.103758	0.108124	0.281319
0.996909	-0.010344	-0.030417	-0.103758	0.108124	0.281319
0.334385	0.000000	-9.976345	0.000000	9.976345	1.000000

RMS Az REDUCTION IS 33.4%

GAIN1= 0.004000 GAIN2= 0.048000

COMPUTATIONAL DELAY TIME = 0.010

	Az(ft/s2)	Alfa(deg)	Q(deg/s)	Thet(deg)	D-e(deg)	D-f(deg)
MAX	-5.502	2.211	3.446	2.192	-1.093	-10.995
RATE	-137.826	33.262	21.496	3.445	-13.294	147.385
RMS	2.023	0.811	1.399	0.982	0.368	3.851

Z-REAL	Z-IMAG	W'-REAL	W'-IMAG	FREQUENCY	DAMPING
-0.169644	0.000000	-28.172128	0.000000	28.172128	1.000000
0.673837	0.226194	-3.468613	3.171428	4.699918	0.738016
0.673837	-0.226194	-3.468613	-3.171428	4.699918	0.738016
0.310056	0.000000	-10.533041	0.000000	10.533041	1.000000
0.995214	0.009296	-0.047544	0.093406	0.104810	0.453617
0.995214	-0.009296	-0.047544	-0.093406	0.104810	0.453617

RMS Az REDUCTION IS 34.6%

GAIN1= 0.006000 GAIN2= 0.048000

COMPUTATIONAL DELAY TIME = 0.010

	Az(ft/s2)	Alfa(deg)	Q(deg/s)	Thet(deg)	D-e(deg)	D-f(deg)
MAX	-5.283	2.115	3.965	2.316	-1.406	-10.619
RATE	-133.997	33.153	29.067	3.968	-20.309	147.576
RMS	2.015	0.781	1.646	0.980	0.536	3.784

Z-REAL	Z-IMAG	W'-REAL	W'-IMAG	FREQUENCY	DAMPING
-0.115052	0.000000	-25.200388	0.000000	25.200388	1.000000
0.664398	0.296304	-3.294446	4.146985	5.296306	0.622027
0.664398	-0.296304	-3.294446	-4.146985	5.296306	0.622027
0.288085	0.000000	-11.053861	0.000000	11.053861	1.000000
0.994217	0.008429	-0.057640	0.084783	0.102521	0.562231
0.994217	-0.008429	-0.057640	-0.084783	0.102521	0.562231

RMS Az REDUCTION IS 35.0%

elevator is then limited to prevent violation of the level 1 flying qualities requirement in the aircraft short period undamped frequency, and to keep the aircraft short period pitch response to turbulence within reasonable limits.

Based on these considerations, the gain values were selected as $K_{Az} = 0.048$, and $K_{-Az+\theta} = 0.004$ resulting in a 35% reduction in the RMS vertical accelerations.

Although the augmented aircraft short period and phugoid modes undamped frequencies and damping now satisfy the military specification for level 1 flying qualities, the pilot will still have difficulty in maneuvering the aircraft due to interference from the RQAS. This interference from the RQAS will arise when the pilot, by commanding the elevator, introduces accelerations in the aircraft response. The direct lift control system will try to counteract these accelerations, causing the pilot to exert a considerable amount of effort in an attempt to accomplish the desired maneuver. Some type of control augmentation will, therefore, have to be added to allow maneuvering of the aircraft, as if the automatic controls had not been introduced.

Figure 5.19 illustrates the performance of this system on the vertical acceleration reductions. An examination of the PSD and Time History plots shows that although the automatic controls have reduced the number of high amplitude, low frequency peaks, the number of low amplitude, high frequency peaks has increased. Therefore, although the effect of the automatic controls has in an approximate sense artificially increased the wing loading, there is a difference. An inherent increase in the wing

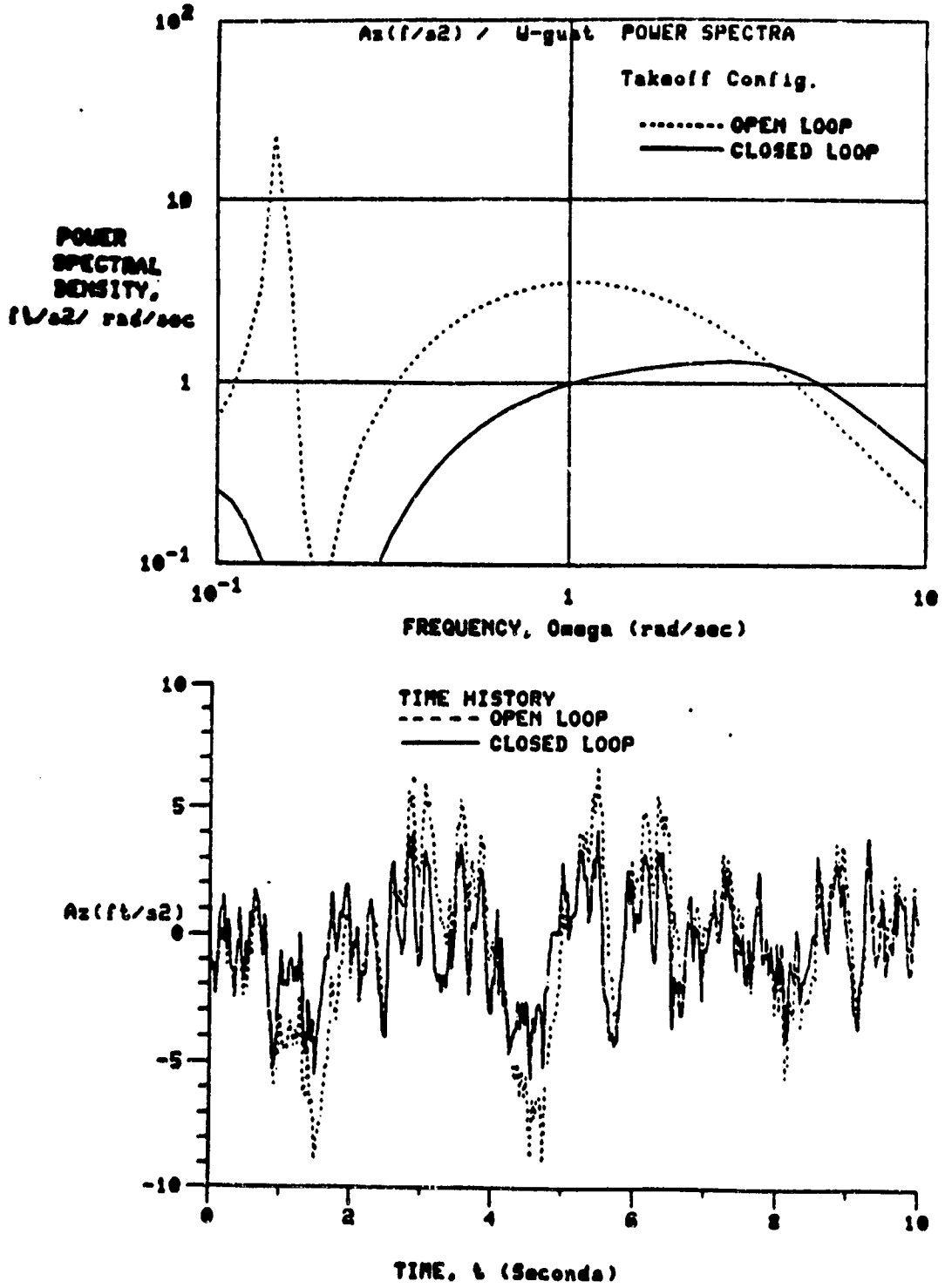

FIGURE 5.19 Power Spectral Density and Time History Plot of the Vertical Acceleration

loading will reduce the number of low amplitude and also the high frequency peaks [7].

However, an examination of the PSD plot shows that this increase in the acceleration content in the upper frequency range (5-10 rad/sec) is relatively small. Also, since motion sickness occurs in the middle frequency range (0.6-6 rad/sec), the effect of the low amplitude, high frequency peaks on the passenger ride comfort will be small. Notice that the active control system has reduced the acceleration content in the motion sickness frequency range (0.6-6 rad/sec), and also at the phugoid frequency.

5.4 DESIGNS FOR THE OTHER FLIGHT CONDITIONS

Five flight conditions were selected to represent a cross section of the flight envelope. These included the takeoff configuration, as well as two climb, one cruise, and one approach configurations Again, emphasis was placed on the takeoff, climb and approach phases of flight, because that is where the turbulence is worst, and because regional aircraft typically spend a relatively high percentage of their operating time there. These five flight conditions are summarized in Table 5.9.

Table 5.9 Cessna 402B Flight Conditions

Configuration	Altitude(ft)	TAS(kts/fps)	Flaps(deg)
Takeoff	Sea level	109/184	0
Climb	Sea level	125/211	0
Climb	5000	134/227	0
Cruise	20000	212/358	0
Approach	Sea level	95/160	30

The designs for the remaining four other flight conditions were generated using root locus techniques as before. The vertical acceleration to direct lift flap system was first designed to give the maximum reductions in the vertical accelerations. The attitude hold and the vertical acceleration to elevator systems were then included to satisfy the military specifications on level 1 flying qualities requirements and to provide further reductions in the vertical accelerations. In the approach to

landing the maximum flap deflection was limited to ± 15 degrees since the landing flaps are required to be down 30 degrees in this flight phase.

Tables E.6 through E.10, Appendix E, summarize the performance of the direct lift control system for the five flight conditions. The point designs for the other flight conditions have very similar characteristics compared to the takeoff flight condition. For both of the climb configurations, the flap rate restriction sets the limit on further vertical acceleration reductions. This is, however, not the case with the cruise configuration. In the approach to landing configuration, both the maximum allowed flap deflection and also the flap rate restriction limit further reductions in the vertical accelerations.

The time history simulations are summarized in table 5.10. This table includes the following designs:

1. The open loop system response.
2. The nominal design with:

   Ts = 0.10 sec
   Td = 0.01 sec
   Servo Bandwidth = 10 rad/sec

3. The prototype design, which is the design realizable with the hardware and software that is the prototype controller.
4. The continuous system design, which assumes an analog controller.

TABLE 5.10 DIGITAL SIMULATION CLASSICAL DESIGN TIME HISTORY SUMMARY

	VERTICAL ACCELERATION PEAK (fps2)	% Decr	RMS (fps2)	% Decr	FLAP DEFLECTIONS PEAK (deg)	MAX RATE (deg/sec)	RMS (deg)
Takeoff @ SL							
OPEN LOOP	8.94		3.10				
NOMINAL	5.45	39.09	2.01	35.16	11.10	151.48	3.89
PROTOTYPE	6.13	31.45	2.25	27.42	11.86	146.94	4.12
CONTINUOUS	4.49	49.80	1.44	53.55	13.29	149.40	4.90
Climb @ SL							
OPEN LOOP	9.66		3.72				
NOMINAL	7.80	19.26	2.41	35.26	10.70	150.15	3.84
PROTOTYPE	7.66	20.70	2.68	27.96	10.97	153.00	4.04
CONTINUOUS	5.38	44.30	1.89	49.22	11.10	154.20	4.42
Climb @ 5000 ft							
OPEN LOOP	8.53		2.75				
NOMINAL	5.78	32.24	1.70	38.21	10.88	151.50	3.47
PROTOTYPE	5.98	29.89	1.95	29.09	9.49	125.80	3.30
CONTINUOUS	4.00	53.08	1.18	57.12	10.42	151.60	4.33
Cruise @ 20000 ft							
OPEN LOOP	4.33		1.50				
NOMINAL	4.15	4.11	1.01	32.75	3.83	94.95	1.31
PROTOTYPE	3.37	22.15	1.19	20.67	3.37	55.05	1.16
CONTINUOUS	1.46	66.40	.48	68.25	5.35	119.16	1.87
Approach @ SL							
OPEN LOOP	8.92		3.03				
NOMINAL	6.32	29.10	2.17	28.35	15.10	144.00	5.61
PROTOTYPE	6.52	26.91	2.36	22.11	13.89	153.10	5.34
CONTINUOUS	5.29	40.62	1.89	37.82	14.92	134.20	5.79

NOMINAL: Ts = .1 sec
Td = .01 sec
Servo BW = 10 rad/sec

PROTOTYPE: Ts = .1 sec
Td = .06 sec
Servo BW = 10 rad/sec

As for the optimal designs, the continuous system designs are included for comparison. In any case, the continuous system performance represents the levels of vertical accelerations reductions that are realizable for digital systems with extremely fast hardware and software. After the completion of the prototype controller, the prototype designs were generated for comparison to the hybrid and NASA simulations.

The performance improvements for the takeoff, climb, and cruise configurations are very similar, achieving about 33 to 38% reductions for the nominal design. The reduction for the approach condition is slightly less being 28%. It is apparent from this table that performance improves as the computational delay time decreases, and this performance improvement is more for flight conditions involving high dynamic pressures.

The point designs for four out of the five flight conditions have very similar eigenvalue characteristics. From Table 5.11, it is seen that all but the cruise condition have short period damping greater than 0.707, the critical damping value. The phugoid damping has been increased to the range between .29 to .45 and satisfies the military specification on level 1 flying qualities requirement for this mode. The short period undamped frequencies are within the range 4.2 to 5.5 rad/sec, while the phugoid undamped frequencies are decreased to between .06 to .15 rad/sec.

TABLE 5.11 EIGENVALUE SUMMARY

TAKEOFF CONFIGURATION

W'-REAL	W'-IMAG	FREQUENCY	DAMPING
-28.172128	0.000000	28.172128	1.000000
-3.468613	3.171428	4.699918	0.738016
-3.468613	-3.171428	4.699918	0.738016
-10.533041	0.000000	10.533041	1.000000
-0.047544	0.093406	0.104810	0.453617
-0.047544	-0.093406	0.104810	0.453617

CLIMB (Sea Level) CONFIGURATION

W'-REAL	W'-IMAG	FREQUENCY	DAMPING
-32.515527	0.000000	32.515527	1.000000
-3.866089	2.637414	4.680021	0.826084
-3.866089	-2.637414	4.680021	0.826084
-10.209328	0.000000	10.209328	1.000000
-0.036907	0.094444	0.101399	0.363979
-0.036907	-0.094444	0.101399	0.363979

CLIMB (5000 ft) CONFIGURATION

W'-REAL	W'-IMAG	FREQUENCY	DAMPING
-50.523805	0.000000	50.523805	1.000000
-3.579260	2.984481	4.660282	0.768035
-3.579260	-2.984481	4.660282	0.768035
-10.161213	0.000000	10.161213	1.000000
-0.031560	0.084234	0.089952	0.350857
-0.031560	-0.084234	0.089952	0.350857

CRUISE CONFIGURATION

W'-REAL	W'-IMAG	FREQUENCY	DAMPING
-62.156293	0.000000	62.156293	1.000000
-3.383870	4.392395	5.544701	0.610289
-3.383870	-4.392395	5.544701	0.610289
-9.987553	0.000000	9.987553	1.000000
-0.026398	0.056025	0.061933	0.426235
-0.026398	-0.056025	0.061933	0.426235

APPROACH CONFIGURATION

W'-REAL	W'-IMAG	FREQUENCY	DAMPING
-17.534502	0.000000	17.534502	1.000000
-3.177245	2.701898	4.170748	0.761793
-3.177245	-2.701898	4.170748	0.761793
-0.043683	0.142395	0.148945	0.293285
-0.043683	-0.142395	0.148945	0.293285
-9.748261	0.000000	9.748261	1.000000

5.5 PARAMETER STUDIES

The parameters examined for impact on the active ride augmentation system performance included: the sample time (Ts); the computational delay time (Td); the servo bandwidth (BW); and the elevator and flap control power. The performance measure used for the parameter study evaluation was the RMS vertical acceleration. Each parameter was varied over the selected range while holding all the other parameters constant. For each parameter variation, the gains were adjusted to give the maximum reductions in the RMS vertical accelerations.

5.5.1 SAMPLE TIME

The purpose of the sample time investigation was to determine the performance improvements gained by reducing the sample time from the 0.1 second used as the nominal. The sample times investigated were 0.1, 0.08, 0.06, 0.04, and 0.02 seconds. Figure 5.20 illustrates the effect of varying the sample time on the vertical acceleration reductions for the takeoff configuration. The plots for the other flight conditions are presented as Figures E.26 through E.30 in Appendix E. As the sample time is reduced, the digital control system performance approaches that of the continuous control system.

Clearly, lower sample times improve the system performance. There will, however, be a limit in the minimum value of the sample time that can selected. This value will depend on the speed of the digital controller, and the amount of other digital processing required, if additional auto-pilot and stability augmentation system functions are later included.

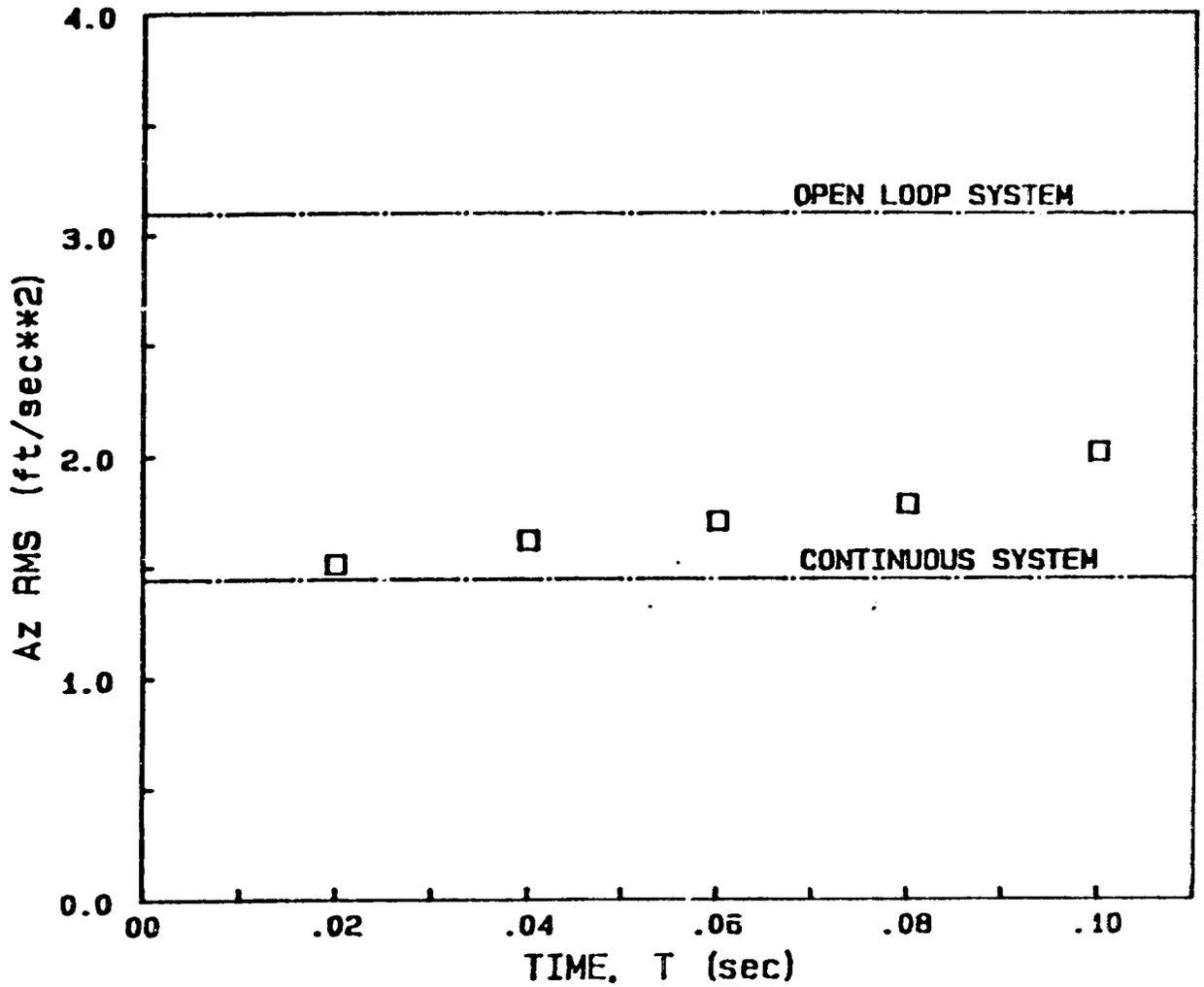

FIGURE 5.20 Effect of Sample Time - Takeoff Configuration

5.5.2 COMPUTATIONAL DELAY TIME

The purpose of the computational delay time study was to investigate how sensitive the system performance would be if the delay time was increased from the nominal value of 0.01 second. If the performance is not degraded by a significant amount, it may be advantageous to use slower hardware and software. The advantages would then be lower hardware and software development costs. The computational delay times investigated were 0.01, 0.02, 0.04, 0.06, 0.08, and 0.1 seconds.

An examination of the root locus plot for the takeoff configuration with a full sample time delay (Td=0.1sec.=Ts) shows that the aircraft dynamics are not significantly changed near the origin (see Figure 5.21 and compare with Figure 5.18). The full sample time delay introduces two fast eigenvalues at -20 on the real axis. One fast eigenvalue is associated with each of the two loop closures. With the vertical acceleration to direct lift flap feedback, both the short period and phugoid modes behave in the same manner as before, that is, without any computational time delays. However, for the same values of the gain K_{Az}, the undamped frequencies of these two modes is now very slightly reduced. Although not shown, the servo and the fast eigenvalues are first real and approach each other before leaving the real axis. With increasing gain values the damping of these two eigenvalues will decrease and their undamped frequencies will increase. If care is not taken, this interaction between the fast eigenvalue and the servo eigenvalue will lead to a very rapid destabiliz-

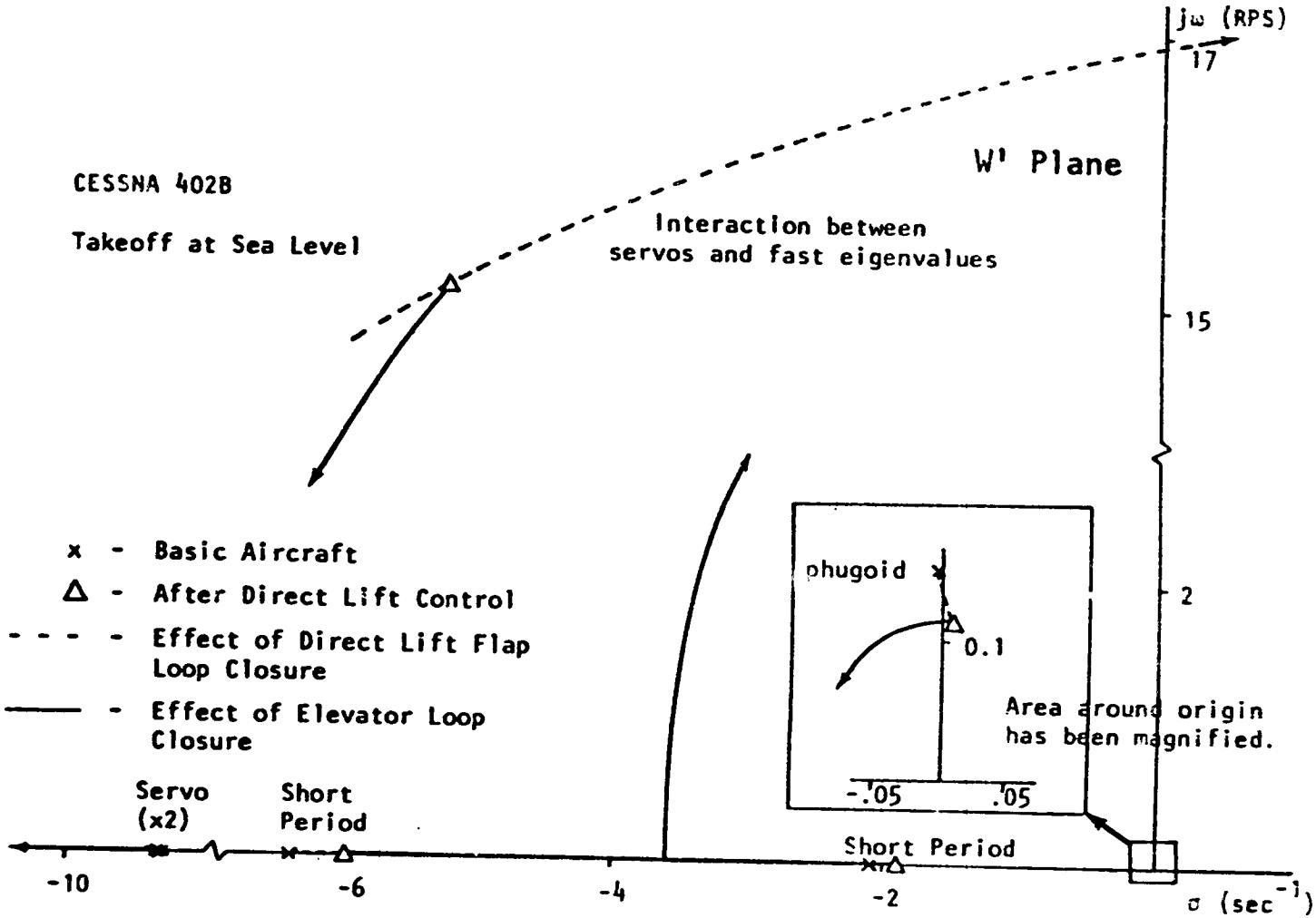

FIGURE 5.21 Effect of the Full Sample Time Delay on the Root Locus for the Digital Control System of Fig 5.16

ation of the aircraft. The effect of the second loop closure on the short period and phugoid modes is also virtually unchanged. However, this second loop closure introduces another fast eigenvalue and a servo eigenvalue in the system. With increasing gains, these two newly introduced eigenvalues remain real and are sufficiently separated from the aircraft dynamic modes to not cause any significant interferences in the aircraft response to disturbances. The previous interaction of the servo and the fast eigenvalues due to the direct lift flap loop closure will now move away from the imaginary axis. Increasing gain values will increase the separation of this eigenvalue from the aircraft dynamic mode eigenvalues, resulting in less and less interference with the aircraft dynamic response to disturbances. However, as before, significant gain increases in the feedback to the elevator will now cause the aircraft to become unstable as the short period mode eigenvalues cross the imaginary axis.

Figure 5.22 illustrates the effect of increasing the computational delay time on the vertical acceleration reductions for the takeoff configuration. The effect is very similar on the other flight configurations, as shown in Figures E.31 through E.35 in Appendix E. Clearly low delay times will be required for improved system performance. This, again requires faster hardware and software.

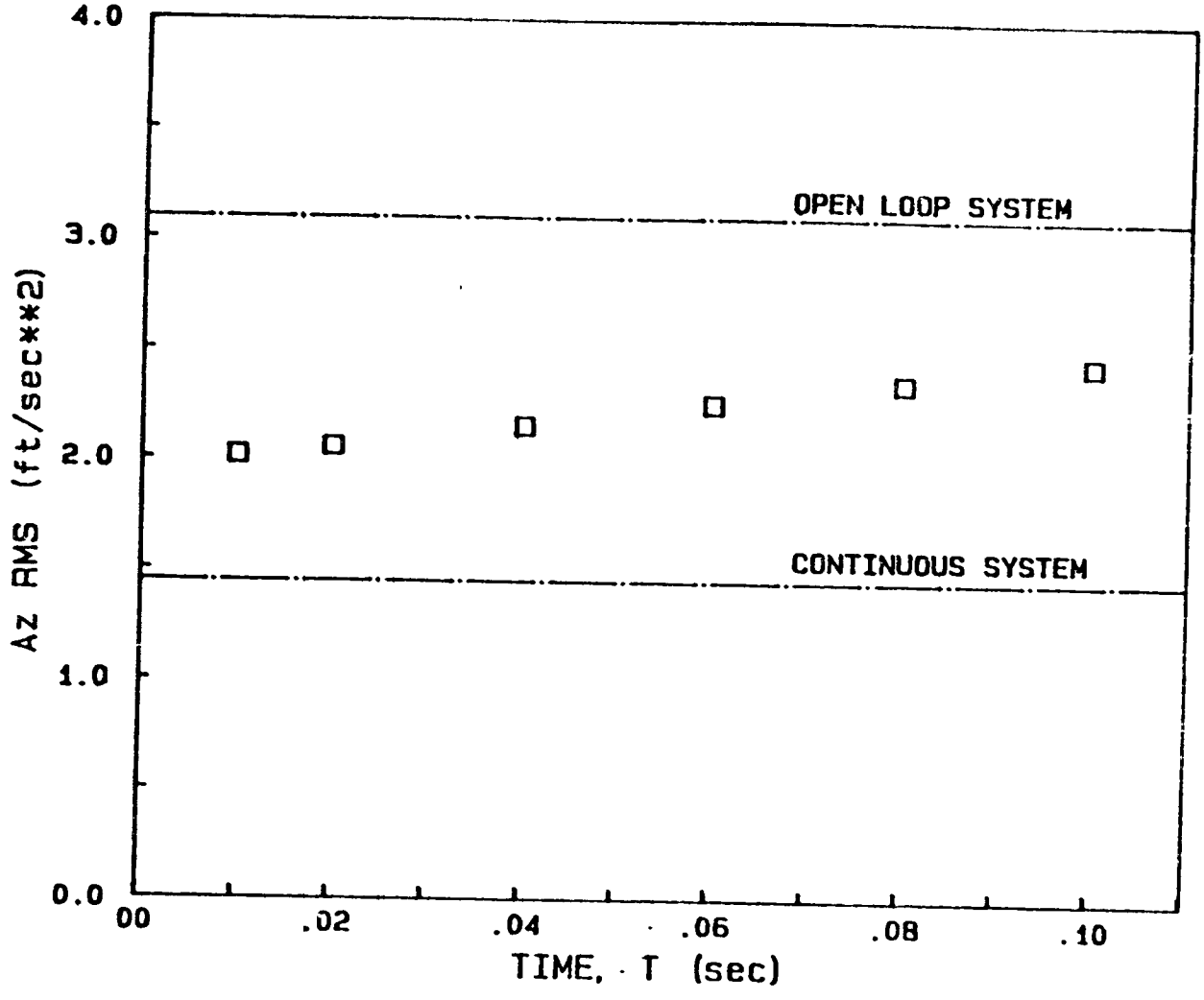

FIGURE 5.22 Effect of Delay Time - Takeoff Configuration

5.5.3 SERVO BANDWIDTH

The purpose of this study was to determine if higher bandwidth servos significantly improve the ROAS performance. An increase in the servo bandwidth usually results in an exponential increase in the servo cost. The servo bandwidths investigated were 5, 10, 20, 30, and 50 rad/sec. The sample time and delay time were 0.1 and 0.01 seconds, respectively. Looking at the root locus plot with the nominal value of 10 rad/sec (figure 5.18), it is evident that opting for higher bandwidth servos will not significantly affect the aircraft dynamic response to disturbances as the servo eigenvalues have already become well separated from the aircraft dynamic mode eigenvalues due to the gain increases. Higher bandwidth servos will increase this separation and significant performance improvement cannot, therefore, be really expected. Figure 5.23 shows the effect of the servo bandwidth on the vertical acceleration reductions on the takeoff configuration. Again the effect is very similar for all the flight configurations, as shown in Figures E.36 through E.40. As expected, not much performance improvement could be gained with higher bandwidth servos. Only for the approach flight condition, where the flap control power is very low, does increased servo bandwidth improve the performance.

Given the choice, it is much better to opt for faster hardware and software, than for a higher bandwidth servo. Faster sampling and reduced delay times significantly improve the system performance for all of the flight conditions. Also the associated costs will be lower for faster computers than for high bandwidth servos.

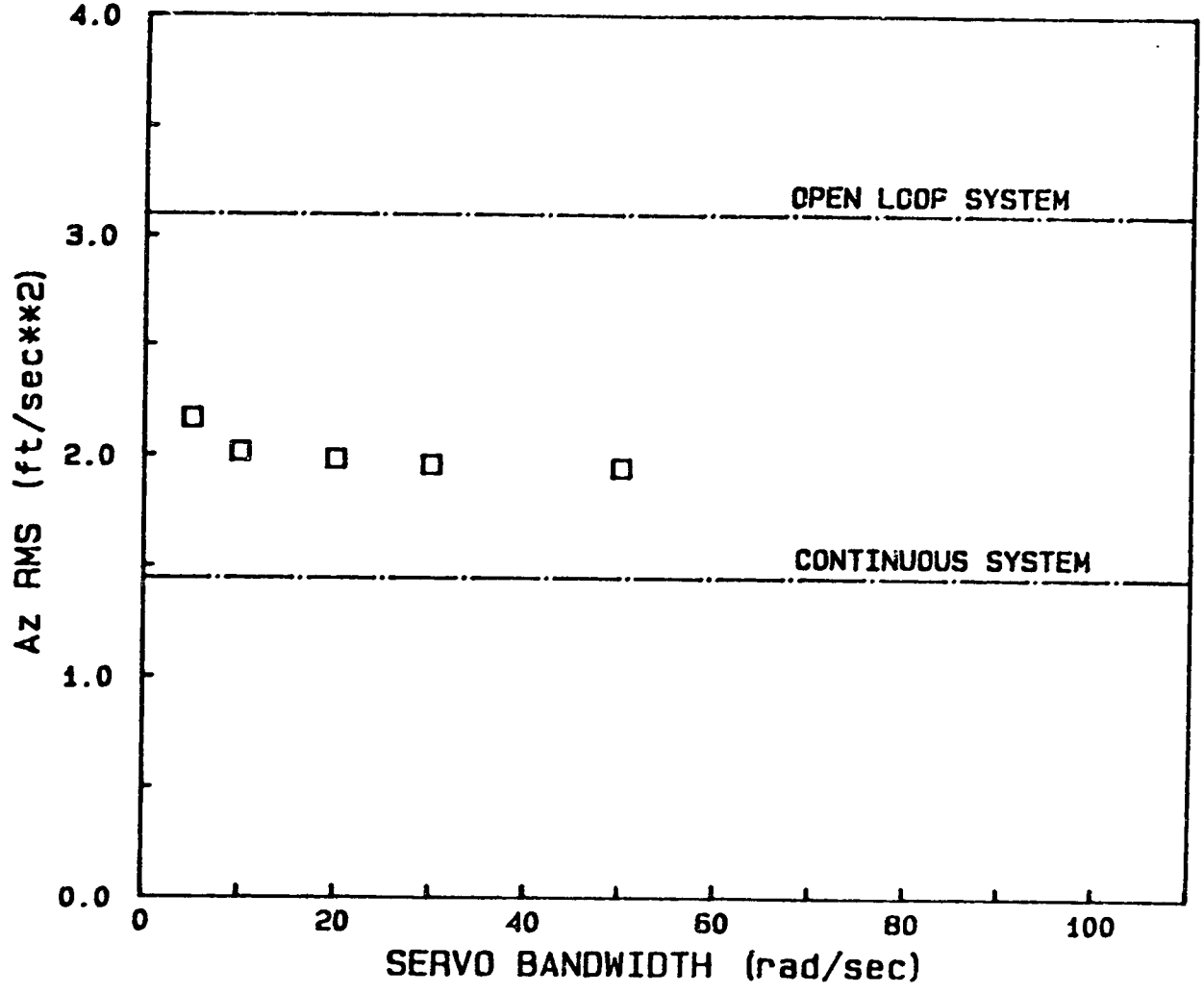

FIGURE 5.23 Effect of Servo Bandwidth - Takeoff Configuration

5.5.4 ELEVATOR AND FLAP CONTROL POWER

In this study, the effect of reducing the elevator control power and the effect of increasing the flap control power were investigated.

The reason for looking at the system with reduced elevator power was to see if only a small portion of the elevator could be used for the active ride augmentation function. Mechanizing the ride augmentation system with a dedicated separate surface control elevator would have several advantages. One of the primary ones would be the lack of feedback to the control column of the RQAS commands, as is inherent in the reversible control system autopilots used on regional aircraft. Also, separate surface control would permit a reduction in reliability and redundancy requirements, and the later addition of other advanced SAS and autopilot functions.

The reason for doubling the flap power was to see if an increase in the flap control power would significantly improve the system performance. The Cessna 402B at present has split landing flaps which will have to be redesigned to allow both up and down deflections for the active ride augmentation function. Examining the effect of increased flap control power will determine whether it is really beneficial to spend the extra time, effort, and money to develop highly efficient direct lift flaps.

Both control power studies are simplified by the fact that the system is linear. This means that if the control power is doubled and the corresponding gains are halved, then the control activity will be halved while

giving the same performance. Consider a dynamic system described in state space form as

$$\dot{x} = Ax + Bu \tag{5.8}$$

$$u = Kx \tag{5.9}$$

On substituting equation 5.8 into 5.7 gives

$$\dot{x} = Ax + BKx \tag{5.10}$$

It is clearly evident that if the control power, as decribed by **B**, is doubled, then, for the same system response, the gains as described by **K** will have to be halved. The control activity will subsequently be halved while the system response remains the same.

In the design of the active ride augmentation system, it was observed that the elevator activity was extremely small. From Tables E.6 through E.10, it is seen that the takeoff configuration demands the most elevator activity. In this configuration, the elevator maximum, RMS, and rate values are 1.09 deg, 0.37 deg, and 13.29 deg/sec, respectively. If the elevator control power is reduced by 20%, then the elevator control activity will increase by 500% and the resulting maximum, RMS, and rate values will be 5.45 deg, 1.9 deg, and 66.45 deg/sec, respectively. Note that these values are for the takeoff configuration and for all other flight conditions they will be far smaller. It is, therefore, entirely reasonable to implement an active ride augmentation system with only a small dedicated portion of the existing elevator.

Doubling the flap control power will, in a similar manner, reduce the flap control activity by half while still giving the same vertical acceleration reductions. Table 5.12 summarizes the effect of attempting even further reductions in the vertical accelerations with this increased control power. As with the bandwidth investigation, only the approach flight condition shows that an increase in flap control power yields any significant improvement in ROAS performance.

Although the increased flap control power has most benefited the approach to landing configuration, an attempt must be made to ensure that increased flap power is made available in the redesign of the direct lift flaps. Then, in other flight conditions, this increased flap power can be used to reduce the amount of flap control activity and thereby reduce the servo rate and displacement requirements. In the approach configuration, the increased flap power can be used to provide further vertical acceleration reductions. This must be done since the approach to landing is the most important flight phase in terms of the passenger's mean reaction to the total trip [2]. This is because a memory decay occurs such that a passenger's overall reaction to the flight is a stronger function of the later portions of the flight than at the beginning.

5.12 PERFORMANCE IMPROVEMENTS WITH TWICE THE DIRECT LIFT FLAP CONTROL POWER

Flight Condition	RMS Vertical Acceleration Reductions	
	Standard Flap Control Power	Double Flap Control Power
Takeoff at Sea Level	35%	39%
Climb at 500 ft	35%	38%
Climb at 5000 ft	38%	39%
Cruise at 20000 ft	33%	33%
Approach at Sea Level	28%	37%

5.6 CLASSICAL DESIGN SUMMARY

With the nominal values of Ts=0.1 sec., Td=0.01 sec., BW=10 rad/sec and half direct lift flap control power (model A) as defined in the optimal designs, the system performance as measured by the percentage vertical acceleration reductions is 33-38% for the takeoff, climb and cruise configurations, and 28% for the approach configuration. The low flap control power caused by the 30 degree trim deflection of the flap in the approach configuration demands a higher direct lift flap control activity and a limit is soon reached in terms of the maximum allowed flap deflection of 15 degrees. From all of the flight conditions analyzed, the approach to landing flight condition demands the most direct lift flap control activity with 15.1 degrees of maximum deflection and 5.6 degrees of RMS deflection. The takeoff configuration demands the most elevator control activity with maximum, RMS and rate values of 1.09 deg, 0.37 deg, and 13.29 deg/sec, respectively. In terms of the continuous system performance the vertical acceleration reductions are 50-58% for the takeoff and climb configurations, 68% for the cruise configuration, and 38% for the approach configuration. Again, the maximum allowed direct lift flap deflection restricts even greater percentage reductions to be realized in the approach to landing configuration.

All of these designs are based on turbulence levels having a probability of exceedance of 0.01. If a goal of satisfying at least 85% of the passengers at this level of turbulence is set, only the nominal designs for the cruise and the 5000 ft climb meet this criteria [2]. However, for the takeoff and the 500 ft climb, a sample time of 0.04-0.06 sec. and a compu-

tational delay time of 0.01 sec. is required if the servo bandwidth is to remain at 10 rad/sec. The approac' configuration requires a still lower sample time of 0.02 sec., with the present flap control power. In the redesign of the direct lift flaps, if the present flap effectiveness can be doubled then the nominal sample time of 0.1 sec. will suffice. If the flap effectiveness could be increased by only 50% then a sample time of 0.04-0.06 sec. will be sufficient. If the flap effectiveness cannot be increased then a servo bandwidth of 20 rad/sec will be required to keep the sample time in the range 0.04-0.06 sec.

It should be noted that trying to satisfy more than 85% of the passengers should not be attempted, because it becomes increasingly difficult to satisfy even more passengers. Even if the vertical accelerations could be reduced to zero, 6% of the passengers will still not be satisfied with the ride. Consequently, increasing the percent of passengers satisfied criteria will lead to an over design of the active ride augmentation system.

Table 5.13 summarizes the gain requirements for the nominal designs. It is evident that gain scheduling will be required for the different flight conditions.

TABLE 5.13 GAIN REQUIREMENTS

Takeoff at Sea Level	Gain 1 = 0.0040	Gain 2 = 0.0480
Climb at 500 ft	Gain 1 = 0.0022	Gain 2 = 0.0385
Climb at 5000 ft	Gain 1 = 0.0024	Gain 2 = 0.0500
Cruise at 20000 ft	Gain 1 = 0.0017	Gain 2 = 0.0350
Approach at Sea Level	Gain 1 = 0.0020	Gain 2 = 0.0585

NOTE: Gain 1 is the feedback gain to the elevator
Gain 2 is the feedback gain to the direct lift flaps

6. ADDITIONAL SYSTEM TEST AND VALIDATION

The digital time and frequency domain analyses done as an integral part of the ICAD program provided the foundation for the evaluation of the different RQAS designs' performance. This digital simulation modeled as closely as possible the analog system and the analog-digital interfaces. However, the digital simulation using the perturbation equations represented a discrete rather than a sampled data system. Furthermore, the digital simulation could not provide evaluation of the RQAS designs for piloted flight, either for flight between the trim points or for handling quality evaluations about the trim points. To correct these deficiencies, two additional simulations were done to validate the RQAS design performance.

These two additional simulations were a hybrid simulation at the KU-FRL, and a moving base simulation at NASA LaRC. The hybrid simulation was done to provide a development testbed for the prototype digital controller, and to more realistically test the RQAS designs as actual sampled data systems. The final step in the validation process was a full 6 DOF, nonlinear, moving base simulation done on the NASA LaRC C-402B real-time system (RTS) [26]. The first objective of this simulation was to test the 3 DOF linear RQAS designs on the full 6 DOF, nonlinear, full variable (rather than perturbation) model, and the second was to perform "pilot in the loop" handling quality evaluations.

This chapter is divided into three parts. The first part is a discussion of the prototype digital controller. The second part describes the hybrid simulation and the results of that effort, and the final section describes the NASA simulation and results of that effort.

6.1 PROTOTYPE CONTROLLER

The discussion of the prototype controller is divided into three parts. The first part provides a description of the microcomputer which formed the basis for the prototype. The second part discusses the interface between the analog aircraft system and the digital controller, and the final part briefly describes the control law implementation on the microcomputer.

6.1.1 MICROCOMPUTER

The microprocessor for the prototype controller was a standard Zenith Z-100, a general purpose business/education/research/home microcomputer. This microcomputer was not a dedicated, specially designed digital control system, but rather an off the shelf model which also served as a smart terminal for operating the ICAD program, a program development and data analysis tool, and a word processor. The fact that a general purpose microcomputer was used for the prototype controller had a direct bearing on the computational delay and sample times. A dedicated, specially designed digital controller could be expected to be at least an order of magnitude faster than this unit. However, one of the reasons for building a prototype controller was to demonstrate the economic and technical feasibility of digital control systems for application to general aviation aircraft. The successful implementation of the digital control laws on this standard desktop microcomputer, which cost less than $1700, certainly demonstrates both the desired technical and economic feasibility.

6.1.2 SYSTEM ANALOG-DIGITAL AND DIGITAL-ANALOG INTERFACES

The hardware components of the prototype controller, other than the microcomputer itself, are the analog-to-digital (ADC) and digital-to-analog (DAC) converters. One of the primary reasons for selecting the Z-100 microcomputer was the fact that it uses a standard S-100 internal communication buss. The S-100 buss is an IEEE specified standard communication interface for microcomputers. Selecting a computer with this industry standard buss provided a wide choice of off the shelf ADC/DAC interfaces at a fraction of the cost of specially designed and built converters. Specifically, the combined ADC/DAC board used in the prototype controller cost $455, as compared to $500-700 each for separate ADC and DAC interfaces priced for the Pro-Log STD Buss, a more specialized research and industry buss. Thus, the entire hardware cost for the prototype controller was under $2200, a feasible investment even for general aviation use.

Even at this relatively low cost, the technical specifications of the ADC/DAC board far exceed any possible requirements that could derive from a ROAS application. The ADC can sample at a nominal 50KHz rate, while the DAC has a nominal dynamic refresh rate of 250KHz. These rates are both well over an order of magnitude higher than could ever be used on a ROAS application, e.g a sample rate of 100 Hz (Ts = 0.01 seconds) for 20 variables would require only 2000 samples per second. The resolution for both the ADC and DAC is 12 bits, which translates into .0146 degrees over a dynamic range of -30 to +30 degrees. This is much higher resolution than would be needed for ROAS applications, and indeed exceeds the accuracy of most available sensors. This detailed technical information is offered as

C-3

further proof of the technical and economic feasibility of digital RQAS for general aviation applications.

6.1.3 CONTROL ALGORITHM IMPLEMENTATION

The software development of the control algorithm was done in a high level language, specifically Z-BASIC, rather than in assembly language. The use of BASIC in programming the control laws greatly shortened the development and testing time, and further reduced the difficulty and cost of the digital controller implementation. However, Basic does have the disadvantage of providing slower program execution.

Following checkout of the program, the control algorithm was compiled to speed up the program execution and reduce the Td. The prototype did a single pass through the control law in 0.06 seconds, so that is the value of Td used for the digital prototype designs. The commands were sent to the aircraft model as soon as they were calculated, i.e. without adding to the delay time as was described in Chapter 4. This implementaion was chosen because the results of the Td parameter study indicated that smaller Td's provided better performance. Further reductions in the Td could be made by reprogramming the control algorithm in a more efficient language, such as Fortran, or ultimately in assembly language. Still further reductions in delay time could be achieved by hardware additions to the Z-100, or by switching to a dedicated, faster microcomputer. All of these steps, to reduce Td and improve the RQAS performance, could be done easily and at relatively low cost.

6.2 HYBRID SIMULATION

The two purposes for doing a hybrid simulation were to provide a testbed for the development of the prototype digital controller, and to test the RQAS point designs as realistically as possible, i.e. with an analog system and a digital controller. A flow chart of the hybrid simulation is shown in Figure 6.1. This simulation consisted of the analog elements -- the aircraft, the servos, and the Dryden gust field -- programmed on an EAI TR-48 analog computer; and the digital RQAS provided by the prototype controller. Appendix C provides a detailed discussion of real-time analog simulation and the analog computer, and the prototype digital controller was described in the previous section. Therefore only a brief summary of the equations, characteristics, and assumptions concerning the analog simulation is presented in subsection 6.2.1. Subsection 6.2.2 provides a description of the test procedure and equipment, and the final subsection describes the results, and compares the results from the digital and the hybrid simulations.

6.2.1 ANALOG SIMULATION

The equations used for the analog simulation were the same linear, small perturbation equations used in the digital simulation. However, solving them as differential equations rather than as difference equations removed any possible distortions due to correlations between model and gust field integration step sizes, sample times, delay times, etc. As in the digital simulation, no sensor dynamics, noise, or bias were included in

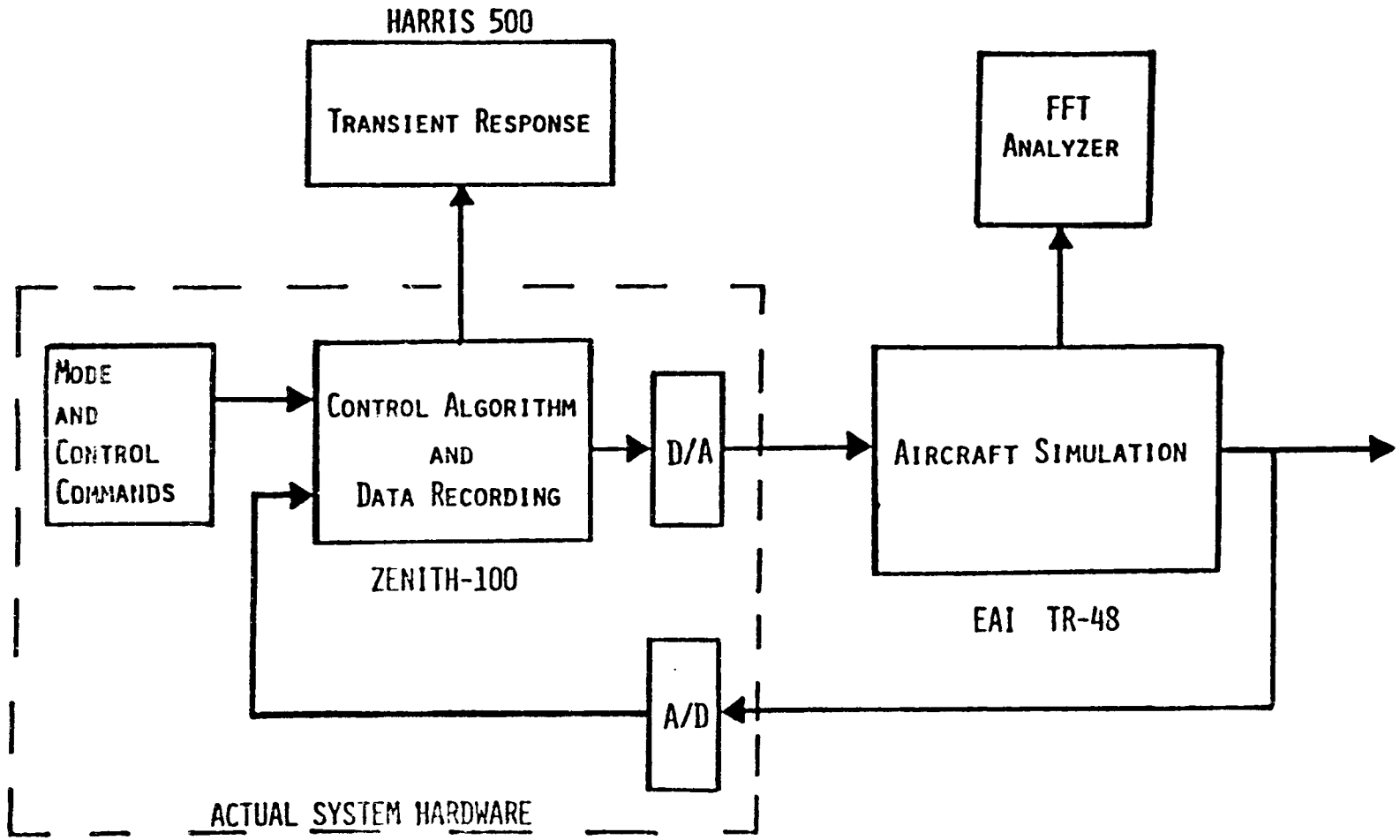

Figure 6.1 Real Time Hybrid Simulation

the analog model. The aircraft and servo states were directly available from the analog computer as deterministic perturbation variables. Because the RQAS designs have been formulated as regulators based on the given trim conditions, the perturbation states read from the analog computer were the error values used directly in the control computations. This feature simplified the implementation of the control laws, but also limited the scope of the simulation to testing at only the five specific flight conditions.

The first task on the hybrid simulator, following verification of the model, was to implement and checkout the digital controller. The capability to very easily time scale the analog computer paid a special dividend for this task. As mentioned earlier, the control algorithm was developed in BASIC, normally an interpretive language. An interpreted program is much slower than a compiled version, and the prototype controller was not fast enough to keep up with the 10 Hz sampling rate when the algorithm was run in the interpreter mode. However, by slowing the analog time down by a factor of 10, the control algorithm could be tested in the interpretive mode. A powerful feature of an interpretive language is the ability to check program flow and variable values at any time during the execution of the program. This feature was especially useful during the code development phase for the control of and communication with the ADC's and DAC's. After the control algorithm development and checkout was completed, the BASIC program was compiled into machine code to increase the speed of execution, and the analog simulation was returned to operation in real time for the actual design evaluation tests.

The next task was the test and evaluation of the RQAS designs implemented on the prototype controller for the five flight conditions. Each flight condition was treated as a separate simulation because the use of perturbation equations precluded moving very far away from each trim condition. In addition, the stability derivatives, in the form of state and control matrix elements, were sufficiently different to require resetting the analog computer for each flight condition. No piloted flight was attempted, both because of the use of perturbation equations and because of a lack of any realistic way of putting commands into the system and of visualizing the resultant aircraft movements. All of the hybrid simulation was done prior to the discovery of the flap control power discrepancy, so only Model A designs were tested on the hybrid simulator; and because of the control law implementation on the prototype controller, only the designs with Td =0.06 seconds were tested.

6.2.2 TEST AND EVALUATION PROCEDURE

The hybrid tests were intended to as closely parallel the digital simulations as possible so that direct comparisons could be made between the two simulations. The first step in the normal procedure was to collect response data on the unaugmented aircraft performance in both the time and frequency domains. Then the prototype controller was turned on and a set of time history and PSD data were collected for the augmented system. The data collection and evaluation procedures for the time and frequency domains are presented separately in the next two subsections.

6.2.2.1 TIME HISTORY DATA COLLECTION AND EVALUATION

The duration of the sample for the time history analysis for the hybrid simulation was 50 seconds, as compared to 10 seconds on the digital simulation. The danger of using too short a time period for performance evaluation is that excitation of the phugoid might be overlooked. A gust duration of only 10 seconds had been used with confidence in the digital simulation for three reasons:

1) These disturbance time histories were generated to tight tolerances for average and RMS values to insure use of a representative portion of a statistical Dryden gust field.

2) Only a single gust field was used for each flight condition so that the unaugmented and augmented systems were excited by a common disturbance. Their performances were thus directly comparable.

3) The reductions calculated for the time history were substantiated by the PSD reductions.

However, the gust disturbances for the analog simulation were generated from continuous white noise and the disturbances could not be checked for statistical properties prior to the sample. Furthermore, these gust time histories were not reproducible. For these two reasons, the analysis period was extended to insure that the low frequency data (around the phugoid frequency range) were included in the time history analysis. To further insure that the low frequency content was not neglected in the time history analysis, the results of several time histories were averaged.

Another change between the digital and hybrid time history evaluations was the data collection sample rate. The data samples were collected at only 10 Hz for the hybrid simulation as compared to 100 Hz for the digital

time history simulation. However, based on the low frequency range of concern -- 0 to 2 Hz for the hybrid simulation -- the 10 Hz rate is more than adequate. The numerical data analysis was performed using the same subroutines used in the ICAD program for the digital analysis, to further insure comparability.

In addition to recording the quantitative data for later analysis, immediate time plots for qualitative review were available on the Fast Fourier Transform (FFT) analyzer described in the next section. A sample of the CRT display, showing time history data for both an unaugmented and augmented system, is shown as Figure 6.2.

FIGURE 6.2 SAMPLE TIME HISTORY PLOT FROM THE FFT ANALYZER

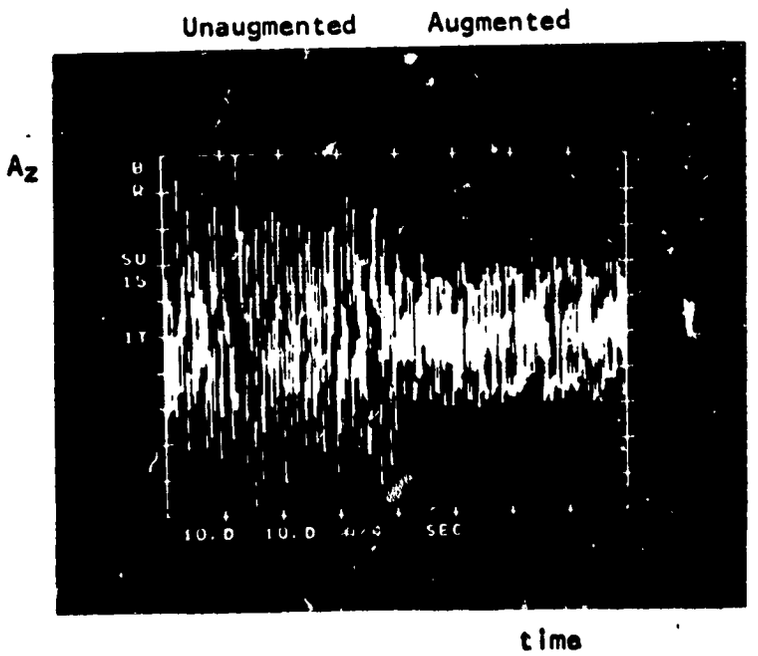

6.2.2.2 FREQUENCY DOMAIN DATA COLLECTION AND EVALUATION

The frequency domain analysis was done in real time on a Nicolet Scientific Corporation Model 660B Dual Channel FFT Analyzer. The availability of this equipment was an unplanned but very beneficial circumstance for this research project. This equipment was bought for another NASA research project at the KU-FRL examining noise reduction methods in general aviation aircraft. This FFT analyzer could display both instantaneous and averaged PSDs, in addition to Bode plots, and the time history data already mentioned. These data were available for real time viewing on the built-in CRT, and in hardcopy form on an X-Y plotter. This FFT analyzer also performed the calculation of the RMS value so that the entire frequency domain analysis was done in real time.

The PSD plots generated for the hybrid simulation are the average of 15 separate 200 second PSD samples taken and calculated by the FFT analyzer described above. The sample rate of the FFT for PSDs is a function of the frequency range specified (0 to 2 Hz), and was in this case 5.12 Hz. This odd sampling frequency is a result of the FFT internal data collection and analysis characteristics. The purpose in mentioning the sample rates is to point out the difference between the time and frequency domain sample rates on the hybrid simulation. These sample rates will also later be compared to the time and frequency domain sample rates used on the NASA simulation.

6.2.3 HYBRID SIMULATION RESULTS

The results of the hybrid simulation for the prototype designs are first presented for the time domain and then for the frequency domain. These results are then compared to each other, and then to the results from the digital simulation.

6.2.3.1 TIME HISTORY RESULTS

Time history summaries of the prototype controller's performance are presented in Table 6.1 for the optimal design and in Table 6.2 for the classical design. The summaries for the hybrid simulation are presented in the same format as the digital simulation summaries in chapters 4 and 5. Only the prototype design, the design constrained by the actual computational delay time of the prototype controller, was tested on the hybrid.

All of the hybrid simulations were done with the original C-402B model, Model A. However, based on the similarity of the Model A and B RQAS designs in the optimal RQAS digital simulations, the use of the Model A designs for the hybrid simulation shouldn't distort the general results at all. The Model A and B results of the digital simulations indicated that the frequency distribution and the RMS acceleration reductions were almost identical for the different control powers, and that the only change was in the control surface activity. The assumption is therefore made that the same characteristics would apply to the Model A and B RQAS designs on the hybrid simulator.

TABLE 6.1 HYBRID SIMULATION OPTIMAL DESIGN TIME SUMMARY
(MODEL A)

	VERTICAL ACCELERATION PEAK (fps2)	% Decr	RMS (fps2)	% Decr	FLAP DEFLECTIONS PEAK (deg)	MAX RATE (deg/sec)	RMS (deg)
Takeoff @ SL							
OPEN LOOP	8.79		3.50				
PROTOTYPE	4.76	45.87	2.36	32.47	9.17	69.90	3.88
Climb @ SL							
OPEN LOOP	8.73		3.65				
PROTOTYPE	5.22	40.18	2.46	32.60	10.89	90.00	4.47
Climb @ 5000 ft							
OPEN LOOP	6.03		2.61				
PROTOTYPE	2.62	56.49	1.59	39.13	6.27	39.84	2.62
Cruise @ 20000 ft							
OPEN LOOP	3.19		1.43				
PROTOTYPE	1.57	50.78	.95	33.66	2.39	22.48	1.07
Approach @ SL							
OPEN LOOP	7.85		3.23				
PROTOTYPE	4.68	40.39	2.41	25.39	17.03	77.51	7.30

PROTOTYPE: Ts = .1 sec
Td = .06 sec
Servo BW = 10 rad/sec

TABLE 6.2 HYBRID SIMULATION CLASSICAL DESIGN TIME HISTORY SUMMARY
(MODEL A)

	VERTICAL ACCELERATIONS				FLAP DEFLECTIONS		
	PEAK		RMS		PEAK	MAX RATE	RMS
	(fps2)	% Decr	(fps2)	% Decr	(deg)	(deg/sec)	(deg)
Takeoff @ SL							
OPEN LOOP	8.79		3.50				
PROTOTYPE	4.22	51.99	2.26	35.43	9.07	93.99	4.17
Climb @ SL							
OPEN LOOP	8.73		3.65				
PROTOTYPE	4.26	51.20	2.56	29.86	7.05	118.87	3.62
Climb @ 5000 ft							
OPEN LOOP	6.03		2.61				
PROTOTYPE	3.09	48.74	1.67	36.06	5.17	41.81	2.38
Cruise @ 20000 ft							
OPEN LOOP	3.19		1.43				
PROTOTYPE	1.51	52.66	.95	33.57	1.44	17.64	.78
Approach @ SL							
OPEN LOOP	7.85		3.23				
PROTOTYPE	4.91	37.46	2.40	25.70	12.28	76.03	6.76

PROTOTYPE: Ts = .1 sec
Td = .06 sec
Servo BW = 10 rad/sec

The data in Tables 6.1 and 6.2 show that the ROAS designs for the five flight conditions all produced significant reductions in RMS acceleration, ranging from 25% in the approach condition to 39% in the climb at 5000 ft condition. The peak and RMS flap rates are well below the maximum limits (20 degrees and 150 deg/sec, respectively) established in the design phase, except for the approach condition, where the maximum deflection is 17 degrees. The large peak and high RMS flap activity for the approach condition is again attributed to the low flap control power for this trim condition. For this simulation, the reductions in the peak accelerations, ranging from 40 to 56%, were significantly larger than the reductions in the RMS, which ranged from 25 to 39%. The difference in the reductions in the peak and the RMS accelerations could have a significant effect on the passengers' opinion of the ride improvement which may not be fully accounted for when considering only the RMS reductions.

6.2.3.2 FREQUENCY DOMAIN RESULTS

The Dryden spectrum from the analog simulation for the takeoff flight condition is shown in Figure 6.3, and it compares extremely well to the theoretical spectrum also plotted. The PSD plots for the optimal and classical ROAS designs for the takeoff configuration are presented in Figure 6.4. The PSD plots for all five flight conditions are shown in Figures E.41 through E.45. The optimal designs are shown as part A and the classical designs are part B. Both optimal and classical ROAS designs show a significant reduction in the acceleration in the PSD plots for all the flight conditions. The frequency range from 0.1 to 1.0 Hz (0.628 to 6.28

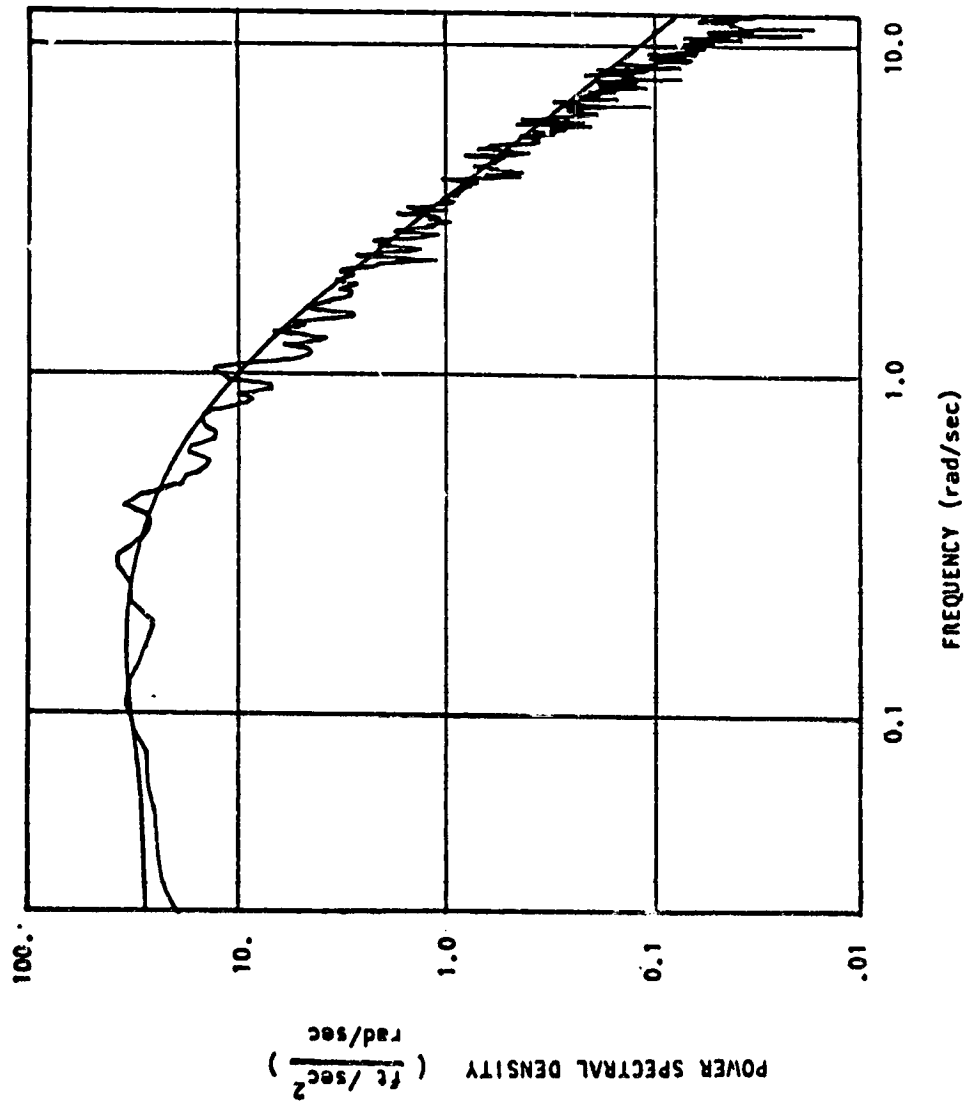

Figure 6.3 Experimental and Theoretical Dryden Gust Spectra

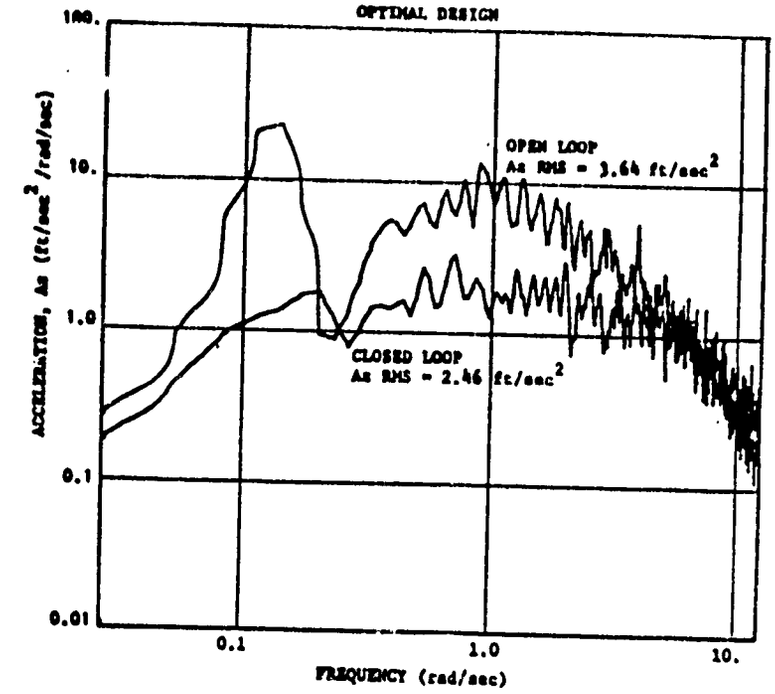

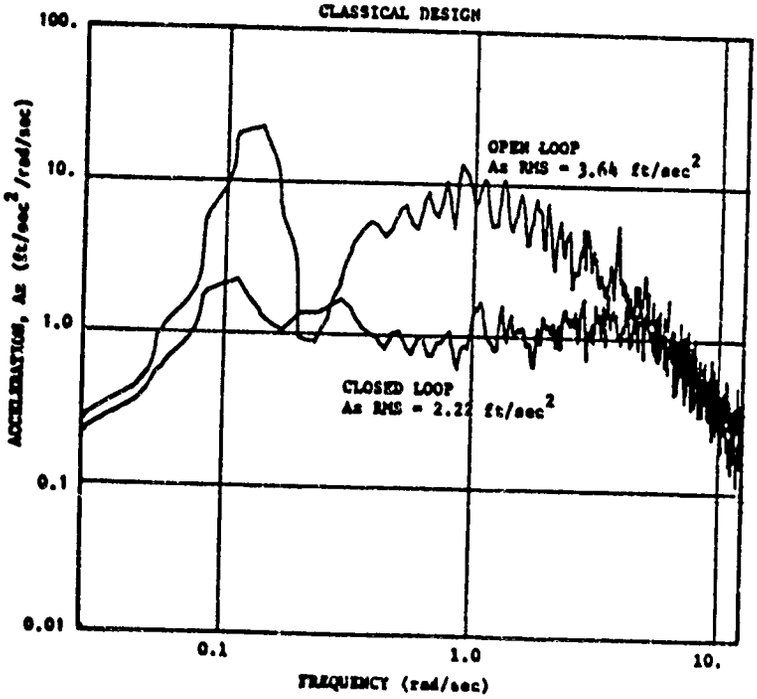

FIGURE 6.4 Hybrid Simulation PSD - Takeoff Configuration (Model A)

rad/sec) is of particular interest because this range is normally associated with motion sickness. Both the optimal and classical designs show a reduction over this range for all of the flight conditions. The slight increase in the accelerations above the motion sickness range, referred to as a "cobblestone ride" effect, is again evident in these PSD plots, as it was in the digital PSD plots.

6.2.4 PERFORMANCE COMPARISONS

Two different comparisons of the data will be presented. First the the time history response will be compared to the frequency domain. The purpose of this comparison is to further substantiate the use of time history data for evaluation of performance to random disturbances. The second comparison will examine the results from the two different types of simulations. The purpose of this comparison is to validate the performance predicted on the digital evaluation with a more realistic mixture of continuous and digital components.

6.2.4.1 TIME AND FREQUENCY RESPONSE COMPARISON

Summaries of the time and frequency domain results from the hybrid simulations are presented in Tables 6.3 and 6.4 for the optimal and classical designs, respectively. The magnitudes of the time history and frequency response RMS accelerations for both the basic and augmented aircraft agree very well. The time and frequency comparisons for the hybrid simulation are better correlated than for the digital simulation for two reasons. First, the digital time history simulation was of 10 seconds, while the

TABLE 6.3 HYBRID SIMULATION OPTIMAL DESIGN
TIME HISTORY-vs-FREQUENCY RESPONSE COMPARISON
(MODEL A)

	Time History Analysis RMS (fps2)	% Decr	Freq Response RMS (fps2)	% Decr
Takeoff @ SL				
OPEN LOOP	3.50		3.64	
PROTOTYPE	2.36	32.47	2.46	32.42
Climb @ SL				
OPEN LOOP	3.65		3.72	
PROTOTYPE	2.46	32.60	2.42	34.95
Climb @ 5000 ft				
OPEN LOOP	2.61		2.67	
PROTOTYPE	1.59	39.13	1.51	43.45
Cruise @ 20000 ft				
OPEN LOOP	1.43		1.33	
PROTOTYPE	.95	33.66	.86	35.34
Approach @ SL				
OPEN LOOP	3.23		3.13	
PROTOTYPE	2.41	25.39	2.27	27.48

PROTOTYPE: Ts = .1 sec
Td = .06 sec
Servo BW = 10 rad/sec

TABLE 6.4 HYBRID SIMULATION CLASSICAL DESIGN
TIME HISTORY-vs-FREQUENCY RESPONSE COMPARISON
(MODEL A)

	TIME HISTORY RMS (fps2)	% Decr	FREQUENCY RESPONSE RMS (fps2)	% Decr
Takeoff @ SL				
OPEN LOOP	3.50		3.64	
PROTOTYPE	2.26	35.43	2.22	39.01
Climb @ SL				
OPEN LOOP	3.65		3.72	
PROTOTYPE	2.56	29.86	2.36	36.64
Climb @ 5000 ft				
OPEN LOOP	2.61		2.67	
PROTOTYPE	1.67	36.06	1.58	40.82
Cruise @ 20000 ft				
OPEN LOOP	1.43		1.33	
PROTOTYPE	.95	33.57	.89	32.58
Approach @ SL				
OPEN LOOP	3.23		3.13	
PROTOTYPE	2.40	25.70	2.23	28.75

PROTOTYPE: Ts = .1 sec
Td = .06 sec
Servo BW = 10 rad/sec

hybrid simulation was 50 seconds long. Even though there was limited low frequency acceleration in the augmented aircraft PSDs, a longer sample will more accurately include whatever low frequency accelerations are there. Second, the digital analysis compared the RMS acceleration from a randomly excited time history to the RMS value calculated from an analytic PSD, while the hybrid analysis compared experimental time history and PSD results. The comparison of experimental-to-analytic data would not be expected to be as well correlated as two sets of experimental data.

6.2.4.2 DIGITAL TO HYBRID COMPARISON

Only the time history data for the digital and hybrid simulations are directly comparable, because the analytic method used for calculating the PSD in the digital evaluation phase did not permit evaluation of designs with a Td which was not an integral part of the sample period. However, the general shapes of the PSD plots from both simulations compared well, especially when considering that the digital plots are analytic and the FFT plots are experimental. The differences are that the sharp peak at the phugoid frequency and the deep valley between the phugoid and short period frequencies for the basic aircraft are less pronounced in the experimental plot. The augmented system PSD plots for both simulations show the same general performance, i.e. an overall reduction of acceleration across the entire frequency range, except for the "cobblestone ride" effect cited previously.

Table 6.5 shows a comparison of the time history data for the two simulations. The basic aircraft responses in the two simulations are very

TABLE 6.5 DIGITAL-VS-HYBRID OPTIMAL DESIGN COMPARISON
(MODEL A)

	DIGITAL SIMULATION VERTICAL ACCELERATION				HYBRID SIMULATION VERTICAL ACCELERATION			
	PEAK		RMS		PEAK		RMS	
	(fps2)	% Decr	(fps2)	% Decr	(fps2)	% Decr	(fps2)	% Decr
Takeoff @ SL								
OPEN LOOP	8.94		3.10		8.79		3.50	
PROTOTYPE	6.39	28.52	2.26	26.98	4.76	45.87	2.36	32.47
Climb @ SL								
OPEN LOOP	9.66		3.72		8.73		3.65	
PROTOTYPE	8.18	15.31	2.74	26.30	5.22	40.18	2.46	32.60
Climb @ 5000 ft								
OPEN LOOP	8.69		2.73		6.03		2.61	
PROTOTYPE	7.34	15.58	1.97	27.75	2.62	56.49	1.59	39.13
Cruise @ 20000 ft								
OPEN LOOP	4.33		1.50		3.19		1.43	
PROTOTYPE	3.35	22.75	1.19	20.45	1.57	50.78	.95	33.66
Approach @ SL								
OPEN LOOP	8.92		3.03		7.85		3.23	
PROTOTYPE	6.91	22.54	2.38	21.53	4.68	40.39	2.41	25.39

PROTOTYPE: Ts = .1 sec
Td = .06 sec
Servo BW = 10 rad/sec

similar. The only consistent difference between the open loop simulations was that the peak accelerations are typically higher in the digital simulation than in the hybrid simulation. The difference in the maximum values recorded may partially be due to the lower sample rate used for data recording for the hybrid simulation. The slower sampling rate may have missed some of the maximum values because they occured between samples.

The one consistent difference in the ROAS performance in the two time history simulations is that the performance of the ROAS was better in the hybrid simulation for every flight condition. This performance improvement ranged from 4 to 13 % more reduction of the RMS acceleration on the hybrid than on the digital simulation. The performance improvement is even more significant when the reductions of peak accelerations are compared. The peak reductions on the digital simulation ranged only from 15 to 28%, while on the hybrid the comparable reductions were from 40 to 56%. Part of this difference may be attributed to the slower sample rate on the hybrid, as was mentioned in the open loop discussion, but that can only account for a small part of the difference. It is possible that the difference in peak values and the reduction in peak values may in some way be due to the difference between modeling the system in a discrete and in a continuous manner. However this could not be substantiated.

6.3 NASA MOVING BASE SIMULATION

The two objectives of this final phase of simulation were to test the longitudinal RQAS designs on a full 6 DOF, nonlinear model, and to perform initial handling qualities evaluations on a piloted simulation. The RQAS function was provided by the KU-FRL prototype controller used for the hybrid simulation. The equipment that made up the NASA simulation system is shown in Figure 6.5. The Cessna 402B is simulated on the NASA CDC mainframe computer for real time digital integration of the equations of motion (EOM). However, the state and control variables are passed between the CDC and the prototype controller as analog signals. All time history and frequency domain data were collected and analyzed on the NASA computer and transfered to the KU Harris 500 computer for additional analysis. The first subsection is a brief description of the NASA LaRC C-402B moving base simulator, and the second subsection describes the test and evaluation procedure. The third and fourth subsections present the results of the automatic mode, and the piloted simulations, respectively.

6.3.1 NASA CESSNA 402B SIMULATOR

The linear perturbation models used to generate the RQAS point designs were derived from this 6 DOF, nonlinear simulation. This simulation model was developed from aerodynamic data adjusted from full scale wind tunnel data on a similar configuration, a Cessna 310, using analytical and empirical techniques. Lift and drag estimates were adjusted based on flight test data. The model nonlinearity stems from the variation of the stability derivatives as a function of flight conditions.

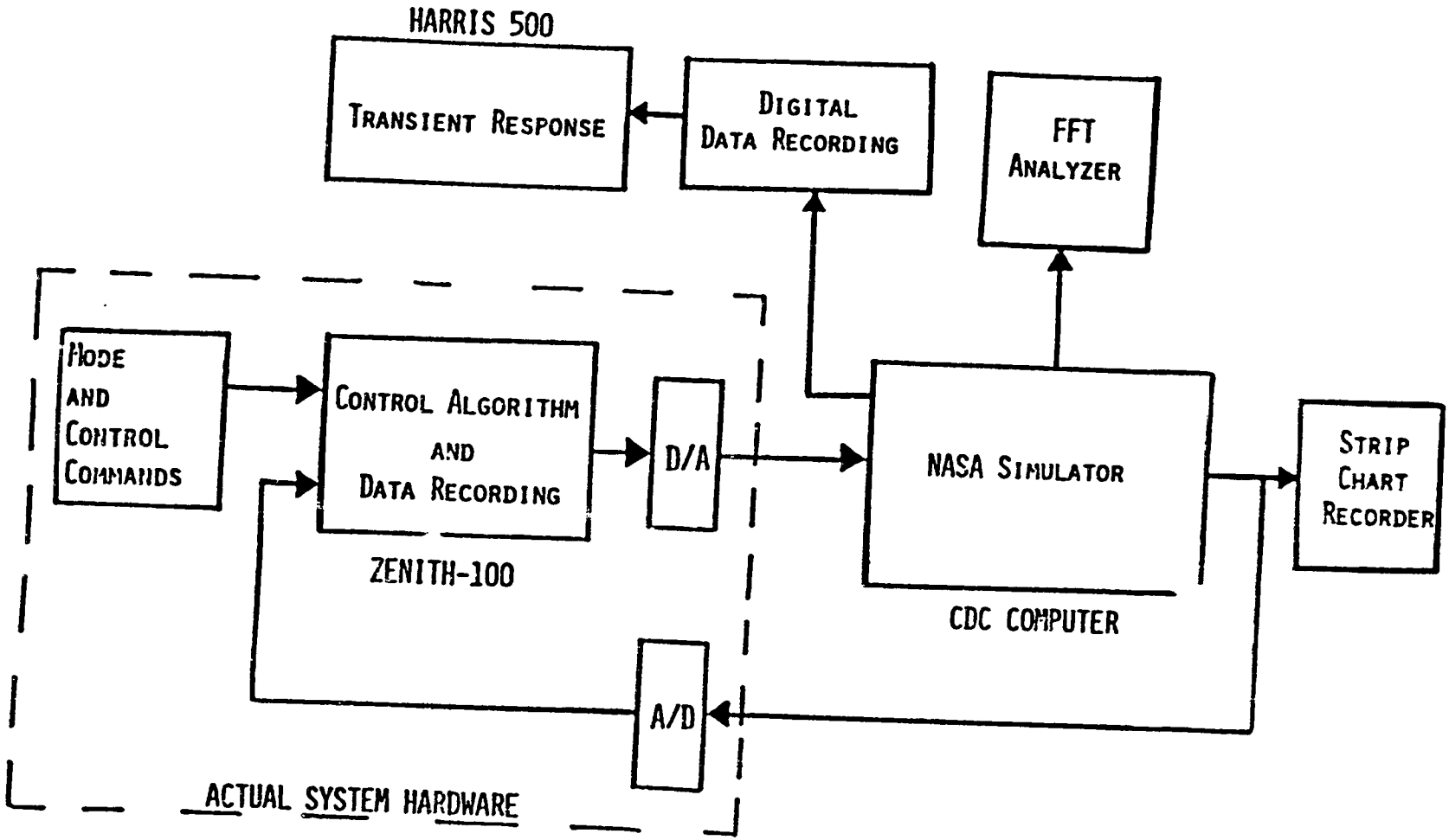

FIGURE 6.5 NASA Simulation Flow Diagram

The simulations of the aircraft, servos, and Dryden gust field were done on the NASA Real-Time System (RTS) digital computer at an iteration rate of 32 Hz. The total state variable EOM, rather than the perturbation equations, are used on the RTS simulation model. However, the perturbation states were generated for the RQAS by the RTS computer by subtracting the trim values from the total, so the perturbation states were passed to the prototype controller. ADCs and DACs are part of the RTS to make all inputs and outputs analog signals, including those signals between the CDC and Z-100 digital computers. The analog-digital and digital-analog conversions were done by the digital computers on each end of the communication channels to most closely emulate a continuous aircraft-digital controller sampled data system.

6.3.2 TEST AND EVALUATION PROCEDURES

Two different sets of tests were done on the NASA simulator. The first set was the unpiloted, or automatic mode, RQAS design performance evaluations. These tests were intended to parallel as closely as possible both the digital and hybrid simulations, and were done for optimal RQAS designs for all five flight conditions. These tests are discussed in the Automatic Mode Simulation section. The second type of test was a piloted simulation, which was done to provide data on the handling qualities of the augmented aircraft. The test and evaluation procedures for the piloted simulations were very different than for any of the other simulations, and are described in section 6.3.2.2.

6.3.2.1 AUTOMATIC MODE SIMULATIONS

The purpose of this set of tests was to validate the performance of longitudinal mode RQAS, which had been designed based on linear 3 DOF models, on a full 6 DOF, nonlinear simulation model, using the prototype controller to provide the ride augmentation. The procedures for these tests and evaluations were very similar to those used for the hybrid simulation. The main difference was that the data collection and evaluation sample rate for both the time history and frequency domain data was 32 Hz, and sample duration was 128 seconds.

When the first tests were run, the initial Model A RQAS designs produced little or no reduction in the RMS acceleration, except in the approach configuration. The cause of this lack of performance was diagnosed to be a difference in the control power between Model A, for which the RQAS designs had been made, and the NASA simulation model. The NASA model had more control power than the RQAS design models, so the prototype controller commanded too much control deflection for the simulation. The result was an over-control situation which produced little or no reduction in RMS values.

At the time of the NASA simulation, the reason that the NASA linearization program had provided the incorrect control powers was not known, so hand calculated estimates of the proper control power were made, and new optimal designs were created. These designs, because they were based on estimates, are called the approximate full power (Model C) designs. Only data for these Model C designs are presented for the NASA simulations. The Model B modified matrices were derived by the NASA lin-

earization program after the NASA simulation effort had been completed.[2]

The real significance of the above occurrence is not that there was a discrepancy between the model used for design and the model used for simulation, or that this difference was uncovered. The real significance is that upon discovery of a major model error, the model could be redefined, new designs made, and the objectives of the simulation program could still be met, because of the capabilities built into the ICAD program. The discovery and diagnosis of the problem was done during the first 3 days of a 5 day period alloted to this project on the C-402B simulator. The redesigns of the optimal RQASs were done by telephone access to the ICAD program from the NASA LaRC simulation facility. The Z-100, which had been taken to NASA LaRC to use as the prototype controller, was used as a remote terminal. Evaluations of all five optimal RQAS designs for Model C were completed, and a limited amount of piloted simulation was still accomplished in the remaining two days. The ability to quickly provide redesigns for the controller enabled us to achieve the objectives and salvage this simulation program. This type of design flexibility and response could be even more critical in a flight test program.

2. The difference in the control powers was traced to the fact that the original linear models (Model A) had been derived prior to the simulator program change which provided symmetric flap control power for both + and - deflections. The linearization program requires + and - control deflections about the trim point for control power calculations. All but the approach flight condition had a trimmed flap setting of 0 degrees. Since deflection was limited to + deflections, when - flap movements were input by the linearization program, the actual deflection was zero degrees. The control power derived for Model A was thus one half of what it should have been with the symmetric flap. Only the approach configuration, because the trimmed flap deflection was 30 degrees rather than zero, had the proper flap control power.

6.3.2.2 PILOTED SIMULATIONS

The approach used on the piloted simulations was pretty much the same as would be used for any handling quality evaluation. The pilot for these simulations was Perry Deal, a veteran test pilot from the NASA LaRC Flight Operations Branch. The test pilot first performed an evaluation of the basic aircraft using his own preselected series of maneuvers, first without the atmospheric turbulence and then with. The pilot then repeated this two step evaluation with the RQAS on. No time histories or frequency response data were colleted. The data presented are the pilot comments and ratings based on the Cooper-Harper rating scale.

6.3.3 AUTOMATIC MODE SIMULATION RESULTS

Because of the discrepancy in the flap control power cited previously, only the optimal RQAS designs could be modified in time to perform the simulation tests. Therefore, only data for the optimal RQAS designs are included in this chapter, using Model A designs for the approach condition and Model C designs for the other four flight conditions. The approach flap control power was correct for the original model (Model A) and so that design was used for this flight condition. The estimated (Model C) flap power for the lift turned out to be low by 5-10%, and the pitching moment was low by 50%, when compared to the final Model B values. The time history results will be presented first, followed by the frequency response results. Finally, the time and frequency data from the NASA simulation will be compared, and then the results from all three simulations will be compared.

6.3.3.1 TIME HISTORY RESULTS

Table 6.6 is a time history summary, for the approach flight condition, similar to those presented for the previous simulations. The acceleration reductions shown are lower than projected by the digital simulation in the ICAD program for the four flight conditions using Model C designs, the takeoff, two climb, and the cruise configurations. The Model C feedback gains were calculated based on less control power than the simulator actually had, resulting in excessive control movements. The data from the Model C designs provide an example of the performance degradation caused by the control power discrepancies, and emphasize the need to provide the designer with an accurate model of the aircraft. The open loop data from the NASA simulations are not affected by the error in the flap control power, and are directly comparable to the linear simulations.

6.3.3.2 FREQUENCY RESPONSE RESULTS

Due to the limited time left to do the simulations after the Model C designs were completed, only five samples were taken to average for the RQAS performance evaluations. This low number of samples resulted in more data scatter than in the hybrid PSD plots. To make the plots more readable and to show the performance differences between the basic and augmented aircraft, a smoothing routine was applied to the original data. Figure 6.6.A is the PSD plot generated from the 5 samples, and Figure 6.6.B is the same plot after a smoothing routine has been applied.

The smoothed PSD plots for all five flight conditions are shown as Figures E.46 through E.50 in Appendix E. There is a fundamental difference

TABLE 6.6 NASA SIMULATION OPTIMAL DESIGN TIME HISTORY SUMMARY
(MODEL C)

	VERTICAL ACCELERATION PEAK (fps2)	% Decr	RMS (fps2)	% Decr	FLAP DEFLECTIONS PEAK (deg)	MAX RATE (deg/sec)	RMS (deg)
Takeoff @ SL							
OPEN LOOP	11.27		3.00				
PROTOTYPE	8.78	22.07	2.64	11.96	9.91	48.49	2.86
Climb @ SL							
OPEN LOOP	12.32		3.54				
PROTOTYPE	9.57	22.34	3.01	15.04	8.37	46.81	2.18
Climb @ 5000 ft							
OPEN LOOP	6.85		2.03				
PROTOTYPE	5.50	19.80	1.57	22.71	6.99	29.78	2.01
Cruise @ 20000 ft							
OPEN LOOP	3.51		.97				
PROTOTYPE	2.85	18.85	.91	6.51	1.55	10.31	.42
Approach @ SL (Model A)							
OPEN LOOP	12.48		3.55				
PROTOTYPE	10.77	13.72	2.82	20.57	11.46	99.91	4.13

PROTOTYPE: Ts = .1 sec
Td = .06 sec
Servo BW = 10 rad/sec

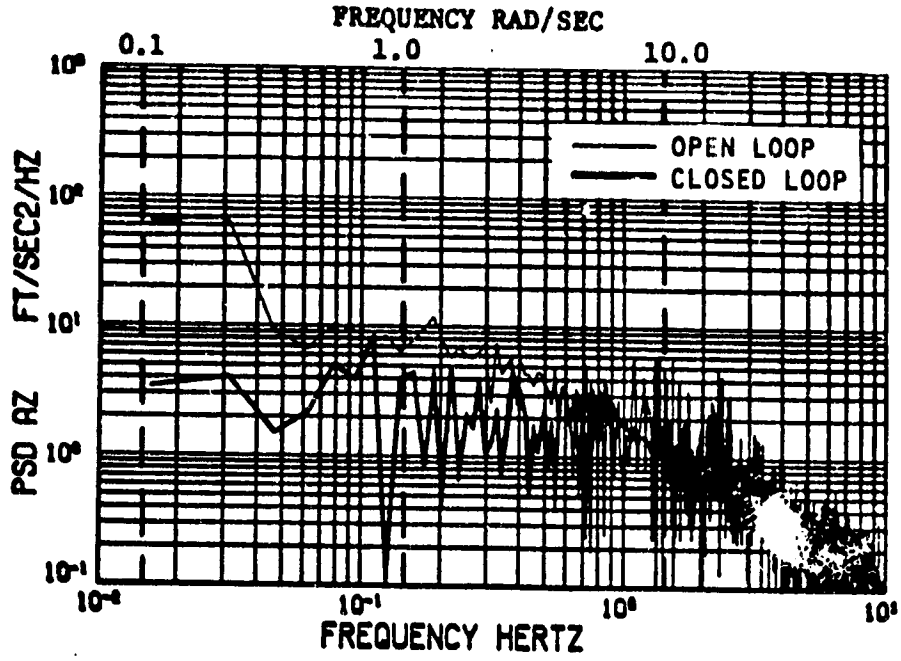

Figure 6. 6a

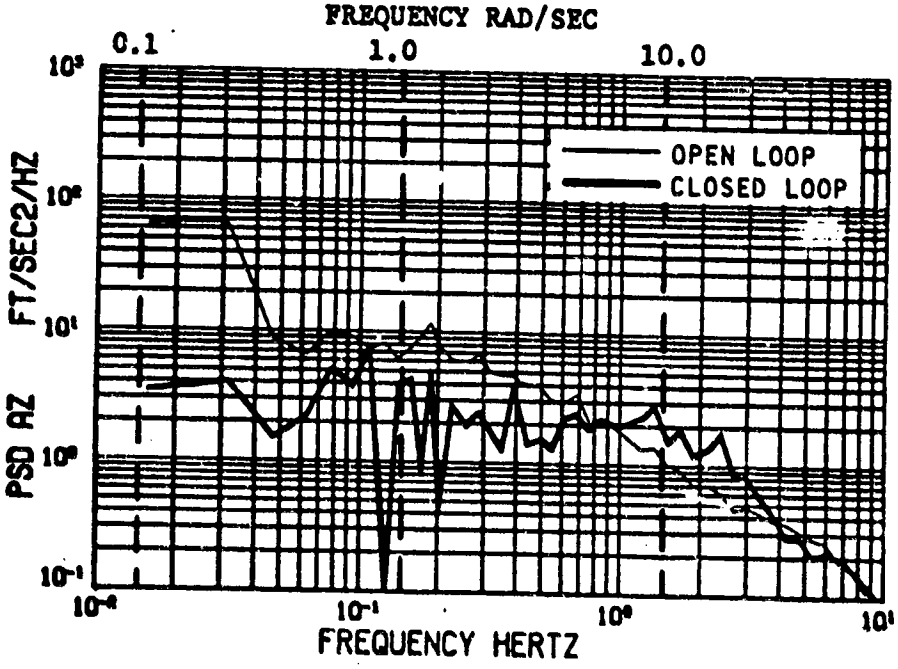

Figure 6. 6b

Figure 6. 6 NASA Simulation PSD - Takeoff Configuration (Approximate Full Power)

in the unaugmented aircraft data that will be discussed in the next section. The same reduction across the frequency range from 0.01 to 1.0 Hz is evident; however, the increase in the upper frequency range is larger and more pronounced.

6.3.3.3 PERFORMANCE COMPARISONS

The first comparison is again made between the time history and frequency response data for the NASA simulation. The second, and final, comparison made is between all three types of simulation. The purpose of this comparison is to validate the use of the digital simulation in the ICAD program for predicting performance trends rather than having to perform all three types of simulations for future designs.

6.3.3.3.1 TIME AND FREQUENCY DOMAIN COMPARISONS

The time and PSD performance evaluations, Table 6.7, again yield comparative results, as expected. The NASA data exhibit the least variation between the time and frequency data for any of the three simulations. The relationship between the digital and hybrid simulations was explained before. The variation between the time and frequency data for the hybrid is greater than for the NASA simulation due to sampling differences. The hybrid comparison used time and frequency data based on different sample rates, while the NASA analysis procedures used the same data for both the time and PSD analyses. Thus, the variations between the time and frequency domain are justified by the types of data compared, and by the sample rates used to collect that data.

TABLE 6.7 NASA SIMULATION OPTIMAL DESIGN
TIME HISTORY-vs-FREQUENCY RESPONSE COMPARISON
(MODEL C)

	TIME HISTORY RMS (fps2)	% Decr	FREQUENCY RESPONSE RMS (fps2)	% Decr
Takeoff @ SL				
OPEN LOOP	3.00		3.06	
PROTOTYPE	2.64	11.96	2.66	13.13
Climb @ SL				
OPEN LOOP	3.54		3.64	
PROTOTYPE	3.01	15.04	3.03	16.80
Climb @ 5000 ft				
OPEN LOOP	2.03		2.09	
PROTOTYPE	1.57	22.71	1.57	24.95
Cruise @ 20000 ft				
OPEN LOOP	.97		.98	
PROTOTYPE	.91	6.51	.91	6.87
Approach @ SL (Model A)				
OPEN LOOP	3.55		3.53	
PROTOTYPE	2.82	20.57	2.78	21.69

PROTOTYPE: Ts = .1 sec
Td = .06 sec
Servo BW = 10 rad/sec

6.3.3.3.2 DIGITAL - HYBRID - NASA COMPARISON

A comparison of the open loop, and prototype RQAS performances for the three different simulations is presented in Table 6.8. The NASA open loop RMS accelerations are significantly lower than the hybrid and digital values for all but the approach condition. The lower RMS values for the nonlinear simulation are attributed to the difference shown in Figure 6.7. The hybrid (and the digital which is not shown here) PSD approaches a 40 dB/dec asymtote at frequencies above 1.0 Hz (Figure 6.7A), but the non-linear NASA PSD does not (Figure 6.7B). For the four flight conditions in which the RMS acceleration for the NASA model is less than the hybrid, the difference appears to be that the acceleration in the region from 1 rad/sec to the 40 dB/dec asymtote is less for the nonlinear model. The plot begins decreasing earlier at a flatter slope, and so includes less acceleration in the range between 1 to 10 rad/sec.

The approach condition is the one condition which has a higher RMS acceleration value in the NASA PSD than in the hybrid. An examination of the two PSDs leads to the conclusion that the extra acceleration in the NASA PSD is concentrated in the phugoid range. The phugoid peak for the nonlinear model is 20 times larger than the peak in the linear models. The existence of a phugoid peak of this magnitude is not typical of an aircraft configured with flaps and gear down. No explanation of this high concentration of acceleration at this low frequency could be generated.

A comparison of the RQAS performance for the three simulations is more difficult, because the only common denominator is the approach condition. Although all the flight conditions are included in the table, the only

TABLE 6.8 DIGITAL-VS-HYBRID-VS-NASA OPTIMAL DESIGN COMPARISON
(MODEL A)

	DIGITAL SIMUALTION VERTICAL ACCELERATION				HYBRID SIMUALTION VERTICAL ACCELERATION				NASA SIMULATION VERTICAL ACCELERATION			
	PEAK		RMS		PEAK		RMS		PEAK		RMS	
	(fps2)	% Decr	(fps2)	% Decr	(fps2)	% Decr	(fps2)	% Decr	(fps2)	% Decr	(fps2)	% Decr
Takeoff @ SL												
OPEN LOOP	8.94		3.10		8.79		3.50		11.27		3.00	
PROTOTYPE	6.39	28.52	2.26	26.98	4.76	45.87	2.36	32.47	8.78	22.07	2.64	11.96
Climb @ SL												
OPEN LOOP	9.66		3.72		8.73		3.65		12.32		3.54	
PROTOTYPE	8.18	15.31	2.74	26.30	5.22	40.18	2.46	32.60	9.57	22.34	3.01	15.04
Climb @ 5000 ft												
OPEN LOOP	8.69		2.73		6.03		2.61		6.85		2.03	
PROTOTYPE	7.34	15.58	1.97	27.75	2.62	56.49	1.59	39.13	5.50	19.80	1.57	22.71
Cruise @ 20000 ft												
OPEN LOOP	4.33		1.50		3.19		1.43		3.51		.97	
PROTOTYPE	3.35	22.75	1.19	20.45	1.57	50.78	.95	33.66	2.84	18.85	.91	6.51
											MODEL C	
Approach @ SL												
OPEN LOOP	8.92		3.03		7.85		3.23		12.48		3.55	
PROTOTYPE	6.91	22.54	2.38	21.53	4.68	40.39	2.41	25.39	10.77	13.72	2.78	21.69

PROTOTYPE: Ts = .1 sec
Td = .06 sec
Servo BW = 10 rad/sec

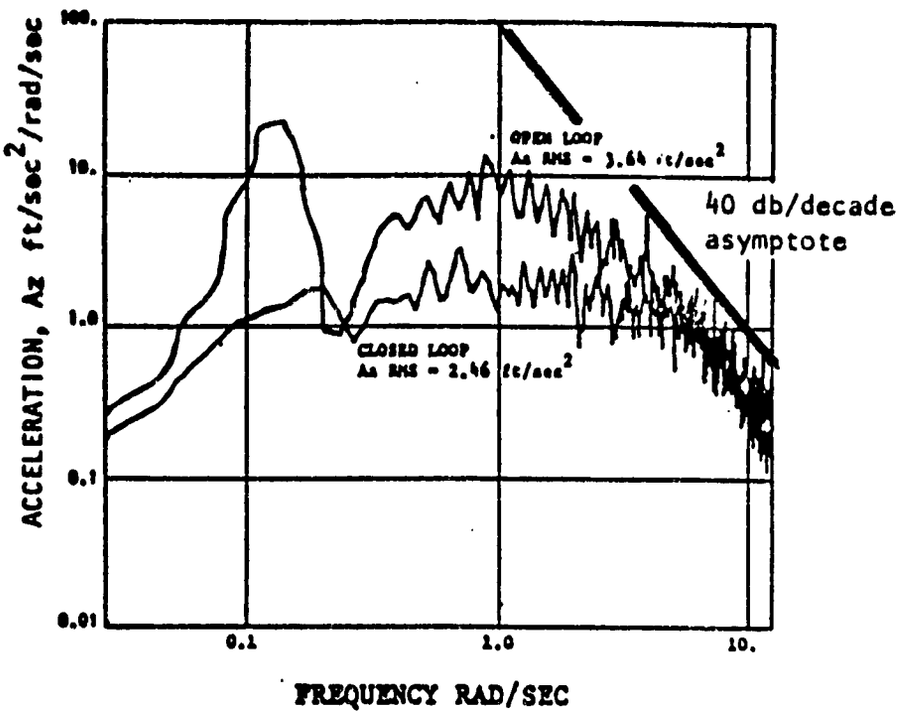

Figure 6.7 a Hybrid PSD

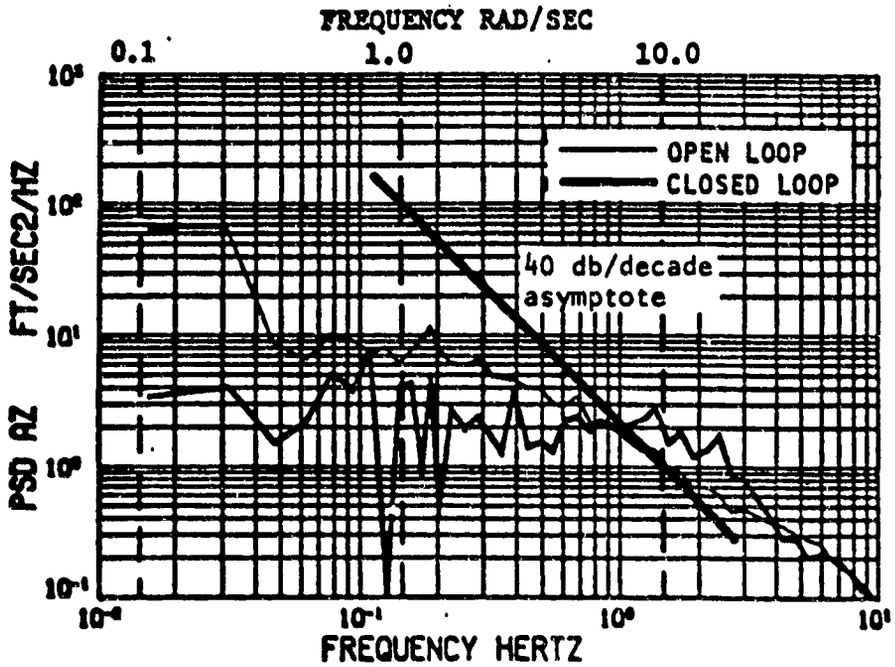

Figure 6.7 b NASA PSD

FIGURE 6.7 Hybrid And NASA PSD Plots- Takeoff Configuration

comparison will be made for the approach condition. Because the Model C designs performed almost identically to the Model A and B designs in the digital simulation, the conclusions drawn for the approach condition will be assumed to be indicative of the performance for all different designs.

For the approach condition, although there is a fairly large variation in the open loop RMS values, there is reasonably good agreement in the percentage reduction in all three simulations. The hybrid simulation shows the most reduction, especially in the peak values. The difference in the absolute RMS acceleration shown in this case is likely due to the open loop difference discussed above. The relative comparability between the percent reductions is a good indication that performance evaluations in the ICAD program provide good approximations on the relative performance of the RQAS to the open loop aircraft, even if the absolute values do not agree.

6.3.4 PILOTED SIMULATION RESULTS

Due to the time spent diagnosing the problem and getting the prototype controller to function on the NASA simulator the remaining time was sufficient for only a bare minimum of piloted simulation. A handling qualities evaluation was done for the approach condition and a very limited evaluation was done for the climb/cruise condition at 5000 ft.

The condition at 5000 ft is called a climb/cruise because of the way the aircraft was flown during the piloted simulation. Although the aircraft was set up for trim in a climb attitude, the evaluation was flown about a 5000 ft cruise condition. The level turns, climbing and descending turns, etc. were all flown from a cruise at 5000 ft in order to keep fairly close to the trim condition. Flight could not be permitted to deviate from the trim too far, because there was no provision in the control algorithm to periodically update the trim condition during flight.

The approach is the most demanding flight configuration, based on pilot workload, and is the only condition for which a proper RQAS design was available. The 5000 ft climb/cruise condition was the other configuration tested because its RQAS performance most closely approached the performance predicted by the digital and hybrid simulations. The results of these evaluations are summarized here, first for the approach and then for the climb/cruise configuration, with the test pilot's Cooper-Harper rating as the quantitative evaluation. The control feel evaluation parameters and the the basic maneuvers flown for the handling quality evaluations are shown in Table 6.9.

TABLE 6.9 CONTROL FEEL PARAMETERS AND HANDLING QUALITY MANEUVERS

CONTROL FEEL PARAMETERS EVALUATED

1. Stick Force
2. Breakout Force
3. Damping
4. Sensitivity
5. Gradient

HANDLING QUALITY MANUEVERS FLOWN FOR EVALUATION

1. 30 degree Bank Turn
2. Steady Climb - Full Throttle
3. Steady Descents
4. Climbing Turns
5. Descending Turns
6. Steady Trimmed Flight

6.3.4.1 APPROACH CONFIGURATION

An extensive handling quality evaluation was carried out for the unaugmented aircraft in the approach configuration with the turbulence off This evaluation included a complete control feel evaluation as well as a Cooper-Harper rating. The result of the control feel test was that all controls had satisfactory characteristics and accurately reflected the C-402B, except for the rudder pedals. The rudder pedal breakout force was too light and the sensitivity too high to properly represent the real aircraft. Some of the comments pertinent to the Cooper-Harper evaluation were that the spiral mode was almost neutral, and that there were deficiencies in the directional axis in both the Dutch Roll mode and the rudder control characteristics. The overall Cooper-Harper rating was 2½.

The next step was to evaluate the basic aircraft in turbulence. The principle comments for this simulation mode were that both the dutch roll and the phugoid were significantly aggravated by the turbulence. Accurate control and maintenance of trimmed flight was much more difficult. Because of excessive dutch roll and phugoid excitation and the resulting difficulty in holding trim, an overall Cooper-Harper rating of 4 was given to the basic aircraft in turbulence.

The third step was a control feel and handling quality check of the RQAS system with no turbulence. The stick force and gradient for longitudinal control increased, as expected, because the pilot now had to "fight" the RQAS to move away from trimmed flight. The results of the handling qualities maneuvers showed that the phugoid damping was improved, but that there was a strong nose down moment in all turns. There were also strong

restoring moments to any trim deviation. The overall Cooper-Harper rating for this mode was a 6.

The final step was the evaluation of the RQAS with turbulence. Only the handling quality maneuvers were flown for this condition. The main comments were that the phugoid was much better behaved, and thus pitch was more stable and trim was much easier to hold. However, there was again a strong restoring moment that opposed any maneuvers, and the longitudinal response was sluggish and resembled an attitude command system. A strong nose down moment occured in all turns, and there was some feedback to the control column, although not enough to make it overly objectionable. The overall rating of 5 was given for this mode.

6.3.4.2 CLIMB/CRUISE AT 5000 ft

Due to time constraints only an abbreviated handling qualities evaluation was done for this configuration. The flight duration was only sufficient to get a general impression, but not to do a full Cooper-Harper rating. The purpose of this test was to see if there were any gross differences between the performance in the approach configuration and in the climb/cruise configuration. The pilot comments and reactions to the four combinations of turbulence on/off and RQAS on/off were very similar to those described for the approach configuration.

6.3.5 NASA SIMULATION SUMMARY

The NASA simulations included automatic mode tests of optimal control RQAS designs for all five flight conditions, and piloted simulations for optimal RQAS designs on two flight conditions. Although simulations of both the optimal and classical RQAS designs in both the automatic and piloted modes had been planned, the limited simulations completed met the basic objectives set for this effort.

The performance of the RQAS designs on the 6 DOF, nonlinear simulator was comparable to both KU linear 3 DOF simulations on the only directly comparable configuration, and there was no excitation of the lateral-directional mode. The piloted simulations pointed out the problems that had been expected in the handling qualities. Even though problems had been expected in the handling qualities, they were not insurmountable. With just the basic control algorithm on the prototype controller, the handling qualities of the C-402B in light to moderate turbulence were only degraded form 4 to 5, on the Cooper-Harper scale. Design changes will be discussed in the next chapter that offer potential solutions to the handling qualities degradation problem.

7. ROAS IMPLEMENTATION CONSIDERATIONS

The final phase of this project involved an examination of the hardware requirements, and other areas that must be considered before actually implementing a ROAS on a C-402B or other commuter/regional or general aviation (GA) aircraft. The sensor, actuator, and digital controller requirements are presented in Section 7.1 and are compared to the current state-of-the-art. The second area that must be considered before continuing on to the implementation phase is what can be done to eliminate the degradation of the handling qualities caused by the ROAS. Any system that caused even the least deterioration in the handling of an aircraft would be turned down by the pilots. Section 7.2 presents two potential solutions to the handling qualities problem identified in the NASA piloted simulation.

7.1 HARDWARE REQUIREMENTS

The hardware considered in this section includes sensors, actuators and the digital controller. The number and type of sensors required depend upon whether the optimal or the classical design approach is chosen. The actuator requirements for both the optimal and the classical designs would be equivalent. Both design approaches use the flaps and the elevator, and have similar rate and displacement requirements. The microprocessor and hardware interface requirements are also very similar, in terms of speed and resolution. Both design approaches show the same trend of performance improvement due to faster computation times.

7.1.1 SENSORS

The designer of the classical ROAS has, by the judicious choice of the feedback loops, reduced the feedback requirements to two easily sensed variables. The only sensors needed for a classical ROAS implementation would be an accelerometer and a pitch attitude sensor (probably an attitude gyro). Numerous off the shelf accelerometers and attitude gyros that are currently used for commuter aircraft autopilots would satisfy the requirements for a ROAS application. There are no extra sensitivity, or other special features needed that would preclude use of off the shelf sensors.

The optimal ROAS is full state feedback designs and therefore require α, u, q, and θ sensors for implementation. The pitch attitude and pitch rate can of course be sensed by attitude and rate gyros, respectively, and the velocity can be acquired from the normal pitot static system. However, a good method for sensing the angle of attack on a commuter aircraft may not be available. The angle of attack is the primary variable in the flap control calculation, and the ROAS performance would be expected to be sensitive to proper measurement of α. An angle of attack vane could be used, but these vanes are subject to interference effects and inaccuracies if placed anywhere other than on a nose boom. Differential pressure methods of calculating α are available. However good α measurements require good differential pressure measurements, and good pressure measurements are normally made only well away from the aircraft. The most practical solution may be to estimate α based on the measurement of other variables.

One method of estimating not only angle of attack, but pitch angle and flight path angle, for unsteady flight, is based on the measurement of the three linear accelerations, pitch and yaw rates, the rate of climb, the airspeed and the roll angle [27]. This approach is much too complicated and requires too many sensors for commuter aircraft application. However it is an example of the fact that given any six independant motion variables, such as the three linear accelerations and the three angular rates, it is possible to calculate any other variable. A much simpler and more direct approach might be to calculate the perturbation α directly from the linear equations used to design the system. Normal sensors can provide the acceleration, the pitch rate and attitude, and the airspeed. The perturbation α could then be approximately calculated based on the two step process shown below

$$\alpha = \frac{1}{U_0} [\, A_z + U_0\, q - g \sin\theta_0 \theta \,] \qquad (7.1)$$

$$\alpha = \alpha_0 + {}_0\int^{Ts} \alpha \, dt = \alpha_0 + Ts\, \alpha$$

where

α =the perturbation angle of attack,

A_z =the perturbation vertical acceleration,

U_0 =the trim velocity,

q =the perturbation pitch rate,

θ =the perturbation pitch angle,

α_0 =the perturbation α from the previous sample period,and

Ts =the sample time.

This would be one way of estimating α that is direct and simple. More accurate and involved methods such as using a Kalman Filter to predict rather than estimate α would also be possible.

There are no unusual or difficult sensor requirements, other than possibly the angle of attack, that can not be met by hardware currently being used in commuter aircraft autopilots. Indeed, further advances in sensors such as multiple degree of freedom accelerometers based on fluidics, and laser gyros [28] may become available for commuter aircraft application in the future. This type of sensor represents the trend toward a limited number of moving parts to improve reliability and reduce life cycle costs. If these sensors become economically feasible for commuter aircraft, the possibility of sensing three accelerations and three angular rates as the basis for any possible motion variable becomes realistic. But even with the current state-of-the-art, there is no real difficulty meeting the sensing and estimation requirements for a RQAS installation.

7.1.2 ACTUATORS

The use of electromechanical actuators (EMA) has been assumed since the inception of this research. Hydraulic actuators were never considered because of the lack of a hydraulic system on almost all aircraft in the commuter/regional class. EMA are now being designed and flight tested on military aircraft as primary flight control actuators, and have been used for years as autopilot and trim actuators on military and commuter aircraft [29, 30, 30, 31, 32]. Because of advances in the use of rare earth magnetic materials, e.g. SmCo, and the application of microprocessors to provide

controlled electronic commutation, EMA are becoming faster, more powerful, and more reliable. For military applications, rate limits of 170 deg/sec for the no load case, and 113 deg/sec at full load for maximum torques of over 44,000 in-lbf have been attained.

Obviously a commuter aircraft application could afford neither the hardware cost nor the electrical power consumption needed to obtain the above performance. However, as shown by the various simulations and the calculations in Appendix D, maximum rates of less than 100 deg/sec and maximum torques of less than 2000 in-lbfs would be adequate for this application. A study of EMA in 1978 indicated that rates of 100 deg/sec were reasonable for application to light aircraft at that time, and EMA technology has progressed rapidly. Bandwidth requirements for RQAS application are comparable to existing autopilot characteristics. Commuter aircraft autopilot actuators typically have a bandwidth of 3 Hz (18.8 rad/sec), and the bandwidth parameter study done indicated that no performance gains were achieved with servo bandwidths above 20 rad/sec. If more bandwidth becomes necessary, the newer EMA are providing up to 12 Hz for some high performance military applications. Although this technology is not currently available to the commuter aircraft, it serves as an example of the progress in this field.

Thus, based on the torque, rate and bandwidth needed for an RQAS implementation, the state of the art of EMA can currently meet all requirements. The last item to be discussed in the area of hardware considerations is the digital controller.

7.1.3 DIGITAL CONTROLLER

The prototype digital controller developed for this project was based on a standard, multipurpose desktop microcomputer, the Z-100. The ADC and DAC capabilities were provided by a low cost, general purpose interface board, and the control algorithm was written in BASIC. Even at this low cost and low level of sophistication, the prototype controller was easily able to meet the sample rate required for the nominal RQAS designs.

The control algorithm used on the prototype controller was extremely simple. The only tasks it did were: read the state variables directly from the simulator; calculate the new control commands; and send these commands to the servos. In an actual system, the algorithm obviously becomes much more complicated. For example: the total rather than the perturbation variables would be the inputs; some of the states might have to be estimated or predicted; and other tasks such as updating the trim point, recalculating the gain matrices for gain scheduling, and error checking and fault diagnosis would have to be done. Each of these tasks would add to the execution time of the digital controller, so speed of the microprocessor may become a concern.

The computational time required for one loop through the prototype control algorithm was about 0.06 sec. Based on benchmarks run on the Z-100, converting to a faster software implementation, such as Fortran, would reduce the Td to less than 0.01 sec. Addition of a hardware floating point coprocessor to the Z-100 could provide an additional order of magnitude decrease in Td. Conversion to a faster, dedicated flight system could reduce this time even further. Therefore, the speed of the microprocessor

would impose no limitation at all on the implementation of a RQAS.

The other hardware in the digital controller, in addition to the microcomputer, is the ADC and DAC interface. As discussed in Chapter 6, even for the low cost models used in the prototype controller, the capabilities far exceeded any possible demands that the RQAS could place on them. There are therefore no technical limitations placed on the implementation of the RQAS designs by any of the hardware components.

7.2 HANDLING QUALITIES

Although the NASA simulations indicated that the aircraft handling qualities on a Cooper-Harper scale were degraded from a 2½ to a 6 in nonturbulent air, the rating were degraded only from a 4 to a 5 in turbulence. Regardless of the amount of degradation, it is doubtful that any augmentation system that reduced the controllability of the aircraft would be adopted. Therefore some method of restoring the handling qualities to at least the original level must be suggested before implementation can be seriously considered. Two potential solutions are offered.

A straightforward method of restoring controllability to the pilot was suggested by the test pilot during preliminary discussions. A very simple and yet effective method of keeping the RQAS from fighting the pilot inputs would be to simply turn off the system during manuevering flight. For example, one wing leveler that our test pilot had flown made turns so difficult to perform, a simple on/off button was put on the control column. Whenever the pilot wanted to make a turn, he disengaged the system while manuevering, and then reengaged it when back to level flight. This method would certainly restore controllability during maneuvers for a RQAS application. However, it also removes the benefit of the RQAS in the approach phase where ride smoothing and maneuverability are both required continuously.

A second approach to restoring open loop handling performance to the augmented system would be to artificially bias the state variables to reflect the effect of the pilot's commands. Simply stated, the pilot commands would be input to a model of the aircraft to predict what the

effect on the state variables should be. The inputs from the sensors to the controller would then be compared to these predicted states rather than the trim conditions to calculate the perturbed state or error values. In this way the controller in effect becomes a model following system rather than a simple regulator. A block diagram of the basic RQAS, and a modified RQAS is shown in Figure 7.1. The computational requirements of this approach are not overwhelming, but there is the disadvantage of requiring sensors for the control column and rudder movements. This approach could even use the RQAS to provide control augmentation in addition to the original stability augmentation if a properly designed model of the aircraft were used. Other than the additional sensors needed for the pilot control movements, this approach would only result in software additions to the existing control algorithm, and so would pose no implementation problems.

STANDARD RQAS BLOCK DIAGRAM

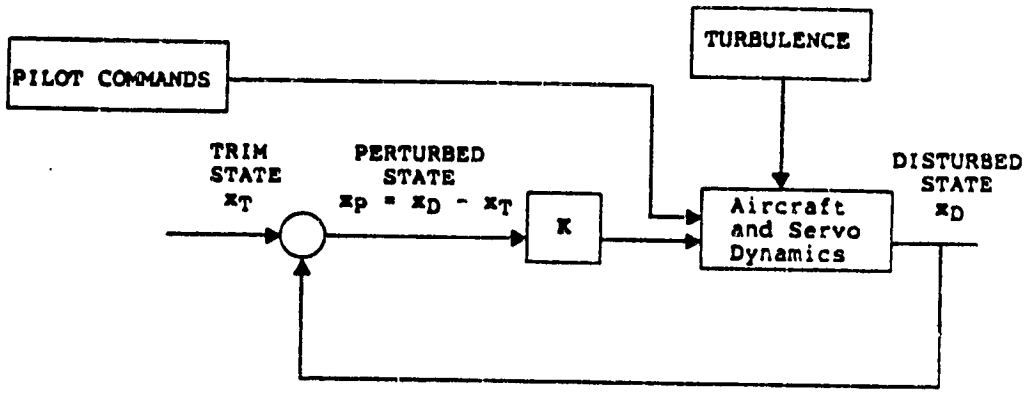

RQAS WILL "FIGHT" ANY COMMANDS BY PILOT THAT TRY TO CHANGE TRIM VARIABLE VALUES

RQAS WITH CAS MODIFICATION

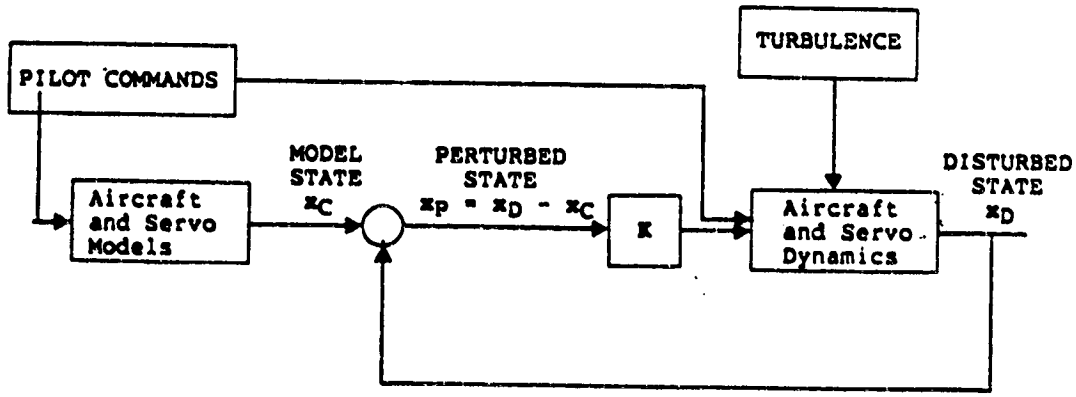

CAS MODIFICATION WILL CAUSE STATE VARIABLES TO BE COMPARED TO THE COMMANDED STATES RATHER THAN TO THE TRIM STATES, SO THAT THE RQAS WILL NO LONGER "FIGHT" PILOT INPUTS

FIGURE 7.1 Proposed Handling Qualities Modification

8. SUMMARY, CONCLUSIONS AND RECOMMENDED RESEARCH

The first section of this chapter presents the research objectives, tasks accomplished, and a brief summary of the results and conclusions. The last section presents a list of recommended research tasks that would lead to validation of a RQAS through a flight test program on the NASA Cessna 402B.

8.1 SUMMARY

The primary goals of this project were to generate detailed designs for a digital, longitudinal mode RQAS for a Cessna 402B; and to investigate the influence of selected parameters on the performance of those RQAS designs.

Detailed designs and extensive parametric examinations for the five flight conditions selected to represent a typical commuter aircraft mission profile have been completed. Two significant products of this effort deserve mention before proceeding to a summary of the research results. The ICAD program and the digital controller, although not directly part of the research goals, were indispensible research tools. Both the ICAD program and prototype controller are tools that can be used for the design and test of other stability or control augmentation systems. In particular, the power and flexibility of the ICAD program was instrumental in the successful completion of the NASA moving-base simulation. Both of these tools contributed immeasurably to the completion of the research tasks, and to the generation of the results summarized below.

The results of this project indicated that either an optimal or a classical digital, longitudinal mode RQAS could produce significant reductions in the vertical RMS acceleration through use of direct lift flaps and separate, split surface elevators. These reductions range from 20-25% (from open-loop RMS values of 0.085 to 0.116 g's) for low bandwidth servos (10 rad/sec) and low computer requirements (Ts = 0.1 and Td =0.1 seconds), to reductions over 50% for autopilot type servos (BW of 20 rad/sec) and modest computer requirements (Ts = 0.06, Td =0.01 seconds).

Although the performance of the optimal and the classical RQAS designs was very similar in reduction of RMS acceleration, there is one significant difference when considering application to commuter aircraft. The classical designs require only limited feedback (Az and θ) for implementation, while the optimal designs require full state feedback. The ability to implement a RQAS with fewer sensors, if other measures of performance are equal, would favor the classical designs in commuter applications.

The results of the parametric studies indicated that the RQAS performance was a very strong function of the digital parameters of the system (Ts and Td). These studies showed that RQAS performance improves with reductions in either Ts or Td, but that Ts has the stronger influence. The level of RMS acceleration reductions produced by a continuous system can be attained by a digital RQAS with autopilot type servos and the modest computer performance cited above. Within the linear model restrictions, neither the elevator nor the flap control power affect the acceleration reduction significantly. An increase in the flap control power, however, results in decreased activity in the flap RMS and deflection rate. Simil-

arly, the RQAS performance is not a strong function of the servo bandwidth. Performance improvements for the system effectively cease when the bandwidth is increased above about 20 rad/sec.

The results of the three different simulations were generally comparable, indicating that the abbreviated digital simulation done in the ICAD design and evaluation program provides a representative measure of the RQAS performance. There was adequate agreement in the comparison of the time history to frequency domain results in all the simulations to further substantiate use of the short digital time history simulation for the detailed designs.

The limited piloted simulation done on the NASA simulator confirmed the concern that a SAS designed as a acceleration regulator would cause a degradation of the piloted handling qualities of the aircraft. It stands to reason that a system designed to keep accelerations to zero will "fight" the pilot inputs that attempt to cause the aircraft to accelerate, either linearly or in turns. However, two possible fixes to this problem were suggested in Chapter 7, the more attractive of which would require only modification to the control algorithm to restore or improve the piloted handling qualities.

In summation, these RQAS designs offer technically and economically feasible application of a digital ride smoothing system to a Cessna 402B. Preliminary analyses of RQAS designs for other commuter aircraft indicate that performance similar to that experienced on the Cessna 402B can be expected.

8.2 RECOMMENDED RESEARCH

The next step in an orderly development of a RQAS for commuter aircraft should be a demonstration of the feasibility, and verification of the predicted performance by flight testing these RQAS designs. The specific tasks listed below are recommended as logical and appropriate research efforts to follow this project.

1. Proceed with detailed redesign of the direct lift flap system on the Cessna 402B. This design effort should include a detailed structural analysis, as well as consideration of the interaction between the control surface size and placement effects on the actuator requirements.
2. Proceed with a detailed study of the hardware required, and a detailed design of the avionics system for the flight test phase. This study should include an analysis of the sensor accuracies, sensitivities, and placement needed for implementation of a flight system as well as further definition of the digital computer requirements.
3. Continue with the analytic design of the RQAS. Include in this effort an examination of other potential control approaches, such as Limited State Feedback. Investigate methods of removing the control activity limitations imposed on the optimal design by the inclusion of the control positions in the formulation of the vertical acceleration. Generation of the final detailed RQAS designs will most likely require a more accurate model of the test vehicle, including, the final value of the control power of the direct lift flaps and the

split elevator surfaces. An examination of the feasibility and desirability of adding a lateral RQAS system should also be done.

4. Perform a detailed analysis of tha requirement for gain scheduling for the RQAS. Preliminary analysis indicates that gain scheduling will be required, but additional detailed simulation, either digital or hybrid, is required to substantiate that need. If gain scheduling is required, modify the control law software implementation to include that capability.

5. Investigate the effects of unsteady aerodynamics on the RQAS performance, particularly at conditions with less than full flap control power where high control rates are experienced. Also investigate what structural interactions that might be experienced at these high control rates. The effect of lags due to downwash on the horizontal tail should also be investigated.

6. Perform a detailed analysis and design of a control law modification to regain, or improve upon, the level of handling qualities associated with the basic aircraft. Include investigation of the use of a washout filter for handling qualities improvements.

7. Perform a detailed economic analysis of an RQAS implementation. Initially this should include a cost estimate of the structural modifications and the hardware costs for a flight test vehicle. Ultimately, this economic analysis should also include the operational costs due to added control surface movements generated by the RQAS.

8. Perform a flight test program of a digital, longitudinal mode RQAS.

References:

1. Woolley, D.; US Regionals Grow and Change. Interavia, May 1984, pp 478-480.

2. Downing, D.R.; Hammond, T.A.; Amin S.P.: Ride Quality Systems for Commuter Aircraft. NASA CR 166118. May 1983.

3. Phillips, W.H.; Kraft, C.C. Jr.: Theoretical Study of Some Methods for Increasing the Smoothness of Flight Through the Air. NACA TN-2416, 1951.

4. Zbrozek, F.: Theoretical Analysis of a Gust Alleviator Used on a Lancaster Aircraft and Comparison with Experiment. Royal Aircraft Establishment Report No. AERO 2645, Jan 1961.

5. Oehman, W. I.: Analytical Study of the Performance of a Gust Alleviation System with a Vane Sensor. NASA TN D-7431, Feb 1974.

6. Krag, B.: Active Control Technology for Gust Alleviation. Von Karman Institute Lecture Series 1979-1, Jan 1979.

7. Jones,J.G.; Fry, D.E.: Aircraft Ride Bumpiness and Design of a Ride Smoothing System. N-78-26053 17/2203, Royal Aircraft Establishment, 1977.

8. Cessna Aircraft Co.: Design of a Ride Comfort System on a Cessna 172K Aircraft. NASA CR 14013, Apr 1975.

9. Moynes, J.F.; Gallager, J.T.: Flight Control System Designer for Ride Quality of Highly Manuverable Aircraft. N78-26054 17/2204, Northrop Corp., 1978.

10. Holloway, R.B.; Thompson, G.O.; Rohling, W.J.: Prospects for Low Wing-Loading STOL Transports with Ride Smoothing. AIAA J. of Aircraft, Vol 9, No 8,Aug 1972.

11. Lapins, M.; Jacobson, I.D.: Application of Active Control Technology to Aircraft Ride Smoothing Systems. NASA CR 145980 May 1975.

12. Roskam, J.: Airplane Flight Dynamics and Automatic Flight Controls, Part I. Roskam Aviation and Engineering Corp. 1979.

13. Dicudonne, J.E.: Description of a Computer Program and Numerical Technique for Developing Linear Perturbation Models from Nonlinear Systems Simulations. NASA TM 78710, 1978.

14. Heath, R. E. II: State Variable Model of Wind Gusts. AFFDL/FGC-TM-72-12, July 1972.

15. Edwards, J.W.: A Fortran Program for the Analysis of Linear Continuous and Sampled-Data Systems. NASA TM X-56038, January 1976

16. Armstrong, E.S.: ORACLS - A Design System for Linear Multivariable Control, Marcel Dekker, Inc., New York, c.1980.

17. Ogata, K.: Modern Control Engineering. Prentice Hall, Inc., Englewood Cliffs, CA 1970.

18. Broussard, John, "The Design of Digital-Adaptive Controllers for VTOL Aircraft", Analytic Sciences Corporation, NASA CR-144912, March 1976

19. Broussard, John: Design, Implementation, and Flight Test of PIF Autopilots for General Aviation Aircraft. NASA CR-3709, July 1983

20. McKenzie, J.R.; Brumaghim, S. H.: Review of Ride Quality Needs of Industry and User Groups. NASA TM X-3295. August 1975.

21. Jones, J.G.: Ride Bumpiness and the Influence of Active Control Systems. N80-29991 20/2748, Royal Aircraft Establishment, 1980.

22. Roberts, P.A.; Swain, R.L.; Schmidt, D.K.; Hindsdale, A.J.: Effects of Control Laws and Relaxed Static Stability on Vertical Ride Quality of Flexible Aircraft. NASA CR-143843, April 1977.

23. Richards, L.G.; Kuhthau, A.R.; and Jacobson, I.D.: Passenge Ride Quality Determined from Commercial Airline Flights. NASA TM X-3295, 1975 Ride Quality Symposium, 11-12 Aug 1975.

24. MIL-F-8785C: Military Specification of Flying Qualities of Piloted Airplanes. November 1980.

25. Roskam, J.: Airplane Flight Dynamics and Automatic Flight Controls, Part II. Roskam Aviation and Engineering Corp. 1979.

26. Hoh, R.H.; Mitchell, D.G; Myers, T.T.:Simulation Model of the Cessna 402B. NASA CR-152176, July 1978.

27. Hosman, R.J.A.W.: A Method to Derive Angle of Pitch, Flight Path Angle, and Angle of Attack from Measurements in Nonsteady Flight. Report vth-156, Delft University od Technology, Apr 1971.

28. Roskam, J; See, M.J.: The State of the Art of General Aviation Autopilots: Now and in the Future. SAE Paper 810582, Apr 1981.

29. Eijsink, H.; Rice, M.; Roskam, J.: A Study of Low-Cost Reliable Actuators for Light Aircraft. KU-FRL Report 351; Apr 1978.

30. See, M.J.; Levy, D.; Roskam, J.: The State of the Art of General Aviation Autopilots. NASA CR 159371, Apr 1980.

31. Leonard, J.B.: Electromechanical Primary Flight Control Activation Systems for Fighter/Attack Aircraft. SAE Paper 82435, 1982.

32. Thompson, K.C.; Eitenmiller, K.G.: An Electromechanical Primary Flight Control Actuation System for Military Transport Aircraft. AIAA Paper 83-2195, 1983.

33. Cannon, M. R. : "Magnitude- and Time- Scaling of State Space Equations for Analog/Hybrid Computation." Simulation, July 1973, pp 23-28.

34. Eijsink, J.F.: On the Use of Electromechanical Actuators in Light General Aviation Aircraft. M.S. Thesis, University of Kansas, April 1978.

APPENDIX A THE AIRCRAFT MODEL

In this appendix, a three-view drawing and a linearized model of the Cessna 402B used for this study is presented. The linearized state space model shown here is for the takeoff (at sea level) flight condition. It was derived by NASA from a nonlinear simulation model using a standard NASA LaRC numerical technique [13]. This data is for the Model B as defined in the main text.

Figure A.1

THREE-VIEW DRAWING

*MAXIMUM HEIGHT OF AIRPLANE WITH NOSE GEAR DEPRESSED IS 11'10".

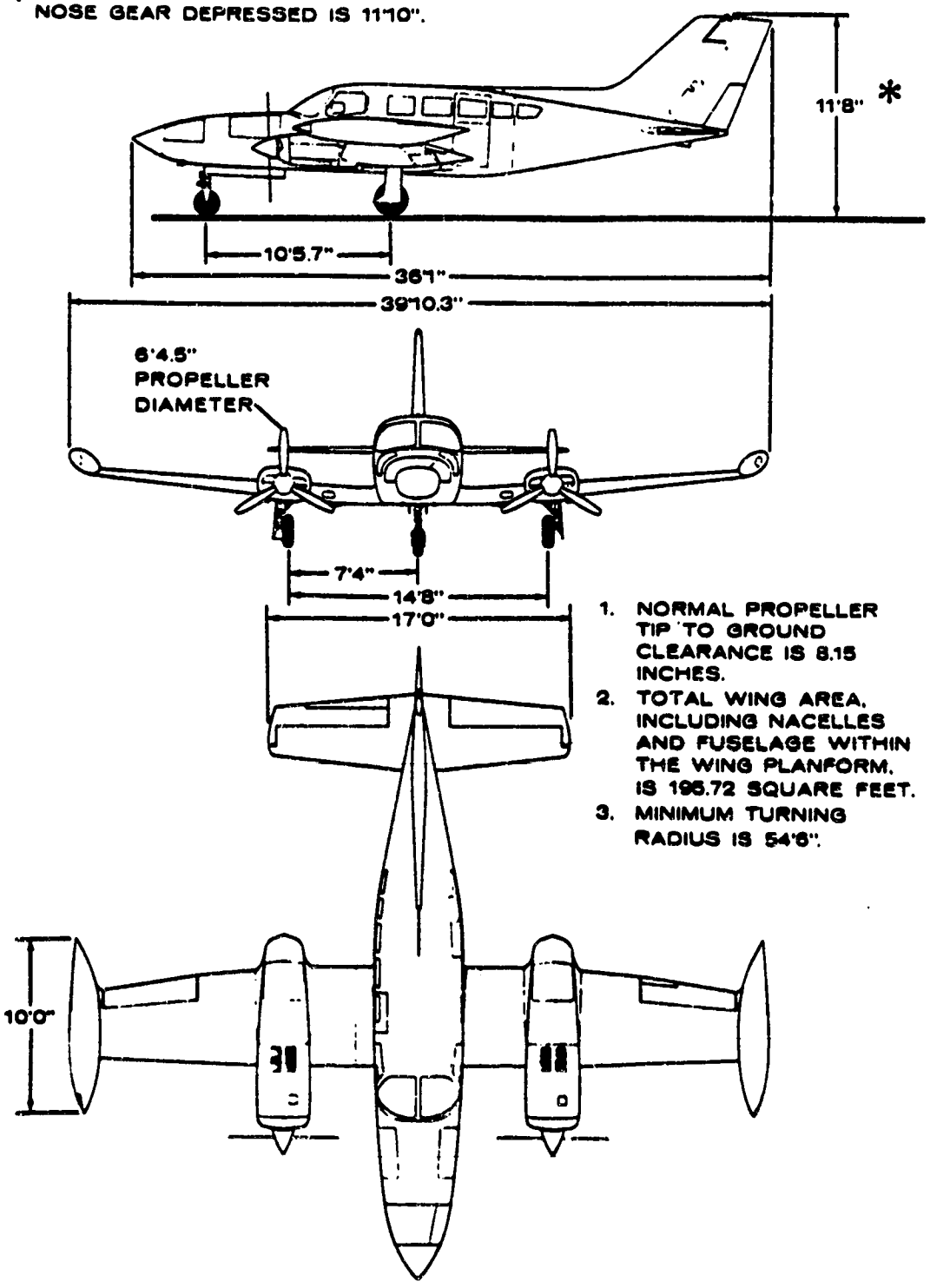

1. NORMAL PROPELLER TIP TO GROUND CLEARANCE IS 8.15 INCHES.
2. TOTAL WING AREA, INCLUDING NACELLES AND FUSELAGE WITHIN THE WING PLANFORM, IS 195.72 SQUARE FEET.
3. MINIMUM TURNING RADIUS IS 54'6".

```
CESSNA 402B TWIN ENGINE LT A/C      84/09/18.      08.41.48.

RUN NUMBER =          1    NTRM   =           7    WINDS  =           F    BANKTRM =           F    TRIMOK  =           T
TIME   = 0.

AIRCRAFT CONSTANTS : WT - (LBS), IXX - (SLUG-FT-FT), SW,BW,CBAR - (FT), CG - (% OF CBAR).
WEIGHT  =  .630000E+04    IXX     =  .111762E+05    IYY     =  .507780E+04    IZZ     =  .152460E+05    IXZ     = 0.
SW      =  .195700E+03    BW      =  .398600E+02    CBAR    =  .517000E+01    XCG     =  .250000E+00**

ATMOSPHERIC VARIABLES :  RHO - (SLUGS/FT-FT-FT), WINDMG - (FT/SEC), WINDAZ - (DEG), UWINDS - (FT/SEC).
RHO     =  .237072E-02    GBAR    =  .402234E+02    WINDMG  =  .100000E+02    WINDAZ  =  .450000E+02    UWINDS  = 0.
VWINDS  = 0.              WWINDS  = 0.              UGUSTS  = 0.              VGUSTS  = 0.              WGUSTS  = 0.

CONTROLS : PEDL - (IN), DWHEEL - (DEG), DPEDAL - (IN), DFLAP - (DEG), DE,DA,DR - (DEG),  , DGEAR,DTH,DPROP,DMIX - (0.,1.)
PEDL    =  .105385E+01    DWHEEL  =  .278449E+01    DPEDAL  = -.548879E+00    DFLAP   = 0.              DGEAR   = 0.
DE      =  .284238E+00    DA      =  .130094E+01    DR      = -.702586E+01    DTH(1)  =  .975000E+00    DTH(2)  =  .975000E+00
DPROP1  =  .100000E+01    DPROP2  =  .100000E+01    DMIX(1) =  .935941E+00    DMIX(2) =  .935941E+00    MR      = 0.
SEALEV  =             F   DETAB   = 0.              DATAB   = 0.              DPTAB   = 0.              BXR     = 0.
PWL     = 0.              STAWB   = 0.              DCWLFPL =  .100000E+01    DCWLFPR =  .100000E+01

AUXILLARY VARIABLES : VTOTAL - (FT/SEC),  GAMDEG - (DEGREES),  VIAS - (KNOTS),  ALTDOT - (FT/MIN),  VTOTKNT - (KNOTS)
ALPDEG  =  .673779E+01    BETADEG = -.290829E+01    VTRUE   =  .183862E+03    VTOTAL  =  .183862E+03    GAMDEG  =  .842536E+01
PSIDEG  =  .294000E+01    THEDEG  =  .151941E+02    PHIDEG  = 0.              VIAS    =  .109000E+03    ALTDOT  =  .161638E+04
VTOTKNT =  .108933E+03    LAMDEG  = -.137518E-05    EPSH    =  .672971E+01    ALPHRAD =  .489969E-03
ALPRAD  =  .117646E+00    ALPDOT  = -.170104E-07    BETARAD = -.507585E-01    BETADOT =  .889021E-08    VTOTDOT =  .173451E-05

STATE VARIABLES - BODY AXIS : UB - (FT/SEC), PB - (RAD/SEC), ANGLES - (RAD).
UB      =  .182349E+03    VB      = -.932894E+01    WB      =  .216076E+02    PB      = 0.              QB      = 0.
RB      = 0.              PSIRAD  =  .513127E-01    THERAD  =  .265187E+00    PHIRAD  = 0.              XE      = 0.
YE      = 0.              ALT     = 0.
UBDOT   =  .217019E-03    VBDOT   =  .154468E-05    WBDOT   = -.288823E-05    PBDOT   = -.169329E-06    QBDOT   =  .782345E-07
RBDOT   = -.228612E-06    PSIDOT  = 0.              THEDOT  = 0.              PHIDOT  = 0.              XEDOT   =  .181878E+03
YEDOT   = -.436525E-03    HDOT    =  .269398E+02

TOTAL AERO FORCES, MOMENTS, AND COEFFICIENTS IN THE BODY AXIS
FXAERO  =  .231925E+03    FYAERO  =  .392422E-03    FZAERO  = -.617900E+04    LAERDB  = -.184775E-02    MAERDB  =  .256087E+03
NAERDB  = -.345493E-02    CDRAGB  = -.294630E-01    CSIDEB  =  .384187E-07    CLIFTB  =  .784961E+00    CROLLB  = -.588892E-08
CPITCHB =  .629256E-02    CYAWB   = -.110111E-07

ENGINE PARAMETERS : THRUST - (LBS), BHP - (BRAKE H.P.), OMEGDT - (LBS/HR)
CTHRUST =  .180736E+00    THRUST1 =  .711352E+03    THRUST2 =  .711352E+03    RPM(1)  =  .270000E+04    RPM(2)  =  .270000E+04
OMEGDT1 =  .171120E+03    OMEGDT2 =  .171120E+03    BHP(1)  =  .296934E+03    BHP(2)  =  .296934E+03    DEGT(1) = -.937851E+02
DEGT(2) = -.937851E+02    SFC(1)  =  .125932E+03    SFC(2)  =  .125932E+03    LAMBDA1 =  .822701E-01    LAMBDA2 =  .822701E-01
PROPEFF1 =  .798817E+00   PROPEFF2 =  .798817E+00   DPBHP(1)= .995232E+00    DPBHP(2)= .995232E+00    BHPT(1) =  .298356E+03
BHPT(2) =  .298356E+03    BHPD(1) =  .298359E+03    BHPD(2) =  .298359E+03    LAMBDA1 =  .770000E-01    LAMBDA2 =  .770000E-01
MANPRS1 =  .345000E+02    MANPRS2 =  .345000E+02    RPM(1)  =  .270000E+04    RPM(2)  =  .270000E+04
PCTBHP1 =  .986357E+02    PCTBHP2 =  .986357E+02    THRHP1  =  .237196E+03    THRHP2  =  .237196E+03
FXENG   =  .141924E+04    FZENG   =  .992241E+02    LENGINE = 0.              NENGINE = -.256087E+03    NENGINE = 0.
```

** Center of Gravity is at 25% chord for all flight conditions.

AERODYNAMIC COEFFICIENTS IN THE STABILITY AXIS

LIFT PARAMETERS

CLABWFN	=	.285000E+01	CLAH	=	.192000E+01	CLALPDT	=	.106549E+02	CLDE	=	.119000E-01
CLE	=	.421582E-02	CLH	=	.928249E-03	CLO	=	.168305E+02	CLOH	=	.101000E+02
CLOMP	=	.125885E+02	CLWFN	=	.728243E+00	DCLACT	=	.370000E-01	DCLCT	=	.270000E+00
DCLFLAP	=	.186240E-16	DCLGEAR	=	0.	DCLWFMP	=	.495875E-01	CLIFTS	=	.782975E+00

DRAG PARAMETERS

CDWFMW	=	.611099E-01	DCDDB	=	0.	DDPHIP	=	.246385E+00	DCDFLAP	=	.392000E-17
DCDGEAR	=	0.	DCDCWL	=	.100000E-02	DCDEDF	=	0.	GFTHR	=	.100000E+01
CDRAGS	=	.631099E-01									

SIDE FORCE PARAMETERS

CYBETA	=	-.123569E-01	CYBETDT	=	.367207E-01	CYDR	=	.333702E-02	DCSIDE	=	-.119198E-01
CYDA	=	-.440000E-03	CSIDES	=	.384187E-07						

ROLL PARAMETERS

CLBETA	=	-.159821E-02	CLBETDT	=	-.138976E-01	CLDA	=	-.180698E-02	CLDR	=	.309592E-03
CLP	=	-.787908E+00	CLR	=	.183733E+00	DCROLL	=	0.	CROLLS	=	-.714371E-08

PITCH PARAMETERS

CMALPDT	=	-.279415E+02	CMREF	=	.629256E-02	CMO	=	-.413285E+02	CMWFN	=	.212922E-01
DCMACT	=	0.	CMOWFN	=	-.422000E+00	DCMFLAP	=	.880000E-18	DCMGEAR	=	.200000E-04
DCMWFMP	=	0.	DCMACT	=	0.	CPITCHS	=	.629256E-02			

YAW PARAMETERS

CNBETA	=	.238801E-02	CNBETDT	=	-.152851E-01	CNDA	=	.136087E-03	CNDR	=	-.139024E-02
CNP	=	-.719358E-01	CNR	=	-.164856E+00	DCYAW	=	-.299949E-02	CNREFS	=	-.102417E-07

AUXILLIARY PARAMETERS

DDPHIP	=	.246385E+00	KADBAR	=	0.	KDBAR	=	.627000E+00	KDBAR	=	.546000E+00
PDEDA	=	.620000E+00	QBARMI	=	.100000E+01	QBARMIP	=	.124638E+01	CD2VT	=	.140595E-01
BD2VT	=	.108397E+00	LENGTHM	=	.188000E+02	LENGTHMM	=	.188000E+02	XREF	=	.250000E+00

GEAR FORCES AND MOMENTS

FXGEAR	=	0.	FYGEAR	=	0.	FZGEAR	=	0.	LGEAR	=	0.
MGEAR	=	0.	NGEAR	=	0.						

ENGINE-OUT PARAMETERS

DCLEO	=	.108322E-01	DCDEO	=	.320000E-01	DCYEO	=	0.	DCRLEO	=	0.
DCMEO	=	0.	DCNBEO	=	0.						

CONTROL LOADER PARAMETERS

FCTOT	=	I	FCAERO	=	I	FCSTAT	=	I	FCDYN	=	I	FCDC	=	I
DETAB	= 0.													
FWTOT	=	I	TWDW	=	I	DATAB	= 0.							
FPTOT	=	I	DFPDP	=	I	DRTAB	= 0.							
FLNDSE	= 0.		DFLNDS	= 0.										

WINGS MOMENT COEFFICIENTS

CME	=	I	CMED	= -.310000E-02	CMEA	= -.240000E+00	CMEA2	= -.140000E+01	CMEDE	= -.730000E-02	
CMETAB	= -.880000E-02										
CMA	=	I	CMAD	= 0.	CMAA	= .170000E-02	CMADA	= -.330000E-02	CMADA	= -.400000E-02	
CMR	=	I	CMPD	= .189500E-02	CMRA	= .725000E-04	CMRDR	= -.725000E-03	CMRTAB	= -.234000E-02	

VALUES OF THE STATES, CONTROLS, AND STATE DERIVATIVES AT THE POINT AT WHICH THE PERTURBATION MODEL WAS GENERATED.

STATE				STATE DERIVATIVES				CONTROLS			
ALPHA	=	.11795	RAD	ALPDOT	=	-.00000	RAD/SEC	DE	=	.28424	DEG
VTOT	=	183.86187	FT/SEC	VTOTDOT	=	.00000	FT/SEC/SEC	DFLAP	=	0.00000	DEG
QB	=	0.00000	RAD/SEC	QBDOT	=	.00000	RAD/SEC/SEC	DA	=	1.30094	DEG
THETA	=	.26519	RAD	THETADOT	=	0.00000	RAD/SEC	DR	=	-7.02566	DEG
BETA	=	-.05076	RAD	BETADOT	=	.00000	RAD/SEC	THR	=	711.35216	LBS
PB	=	0.00000	RAD/SEC	PBDOT	=	-.00000	RAD/SEC/SEC	THL	=	711.35216	LBS
RB	=	0.00000	RAD/SEC	RBDOT	=	-.00000	RAD/SEC/SEC	DGEAR	=	0.00000	[0.,1.]
PHIRAD	=	0.00000	RAD	PHIDOT	=	0.00000	RAD/SEC				
PSIRAD	=	.03131	RAD	PSIDOT	=	0.00000	RAD/SEC				

ALTITUDE ABOVE SEA LEVEL	=	0.0000	FT
DYNAMIC PRESSURE, QBAR	=	40.2234	LBS/FT-FT
MEAN AERO CHORD, CBAR	=	5.1700	FT
WING SPAN, BW	=	39.8600	FT

VARIABLE DESCRIPTIONS AND UNITS

ALPHA	=	ANGLE OF ATTACK	RAD	DE	=	ELEVATOR DEFLECTION	DEG
VTOT	=	MAGNITUDE OF AIRSPEED	FT/SEC	DFLAP	=	FLAPS DEFLECTION	DEG
QB	=	PITCH RATE IN BODY FRAME	RAD/SEC	DA	=	AILERON DEFLECTION	DEG
THETA	=	PITCH ATTITUDE ANGLE	RAD	DR	=	RUDDER DEFLECTION	DEG
BETA	=	SIDESLIP ANGLE	RAD	DTHR	=	THRUST FROM RIGHT ENGINE	LBS
PB	=	ROLL RATE IN BODY FRAME	RAD/SEC	DTHL	=	THRUST FROM LEFT ENGINE	LBS
RB	=	YAW RATE IN BODY FRAME	RAD/SEC	DGEAR	=	GEAR DEPLOYMENT	[0.,1.]
PHI	=	ROLL ATTITUDE ANGLE	RAD				
PSI	=	HEADING ANGLE	RAD				

VTOTIC	= VTOT AT T = 0.	FT/SEC
CBAR	= A/C MEAN AERO CHORD	FT
BW	= A/C WING SPAN	FT
SW	= A/C WING AREA	FT**2
QBARIC	= .5 * RHO * VTOTIC**2	LBS/FT**2

NON-DIMENSIONALIZING EQUATIONS

ALPHA	(ND)	=	ALPHA		ALPDOT	(ND)	=	ALPDOT * .5*CBAR/VTOTIC
VTOT	(ND)	=	VTOT / VTOTIC		VTOTDOT	(ND)	=	VTOTDOT * .5*CBAR/VTOTIC**2
QB	(ND)	=	QB * .5*CBAR/VTOTIC		QBDOT	(ND)	=	QBDOT * .25*CBAR**2/VTOTIC**2
THETA	(ND)	=	THETA		THETADOT	(ND)	=	THETADOT * .5*CBAR/VTOTIC
BETA	(ND)	=	BETA		BETADOT	(ND)	=	BETADOT * .5*CBAR/VTOTIC
PB	(ND)	=	PB * .5*BW/VTOTIC		PBDOT	(ND)	=	PBDOT * .25*BW**2/VTOTIC**2
RB	(ND)	=	RB * .5*BW/VTOTIC		RBDOT	(ND)	=	RBDOT * .25*BW**2/VTOTIC**2
PHI	(ND)	=	PHI		PHIDOT	(ND)	=	PHIDOT * .5*BW/VTOTIC
PSI	(ND)	=	PSI		PSIDOT	(ND)	=	PSIDOT * .5*BW/VTOTIC

DE	(ND)	=	DE * PI / 180.
DFLAP	(ND)	=	DFLAP * PI / 180.
DA	(ND)	=	DA * PI / 180.
DR	(ND)	=	DR * PI / 180.
CDTHR	(ND)	=	DTHR / (QBARIC*SW)
CDTHL	(ND)	=	DTHL / (QBARIC*SW)

THE DIMENSIONAL A MATRIX

ALPDOT RAD/SEC	-1.173001	-.001735	.913369	-.024891	-.000000	.048850	.005788	.000000	-.000000
VTOTDOT FT/SEC/SEC	9.658804	-.027827	.000000	-31.784399	1.445273	-.000956	.000089	-1.576690	.000000
QDOT RAD/SEC/SEC	-9.497766	.000677	-7.532703	.078368	.000001	-.153803	-.018224	-.000000	.000000
THETADOT RAD/SEC	0.000000	0.000000	1.000000	0.000000	0.000000	0.000000	0.000000	0.000000	0.000000
BETADOT RAD/SEC	-.035231	.000021	-.000000	-.008790	-.154730	.117775	-.993916	.168800	-.000000
PDOT RAD/SEC/SEC	.315603	-.000109	.000000	.000321	-2.932215	-2.415530	.389164	-.000166	.000000
RDOT RAD/SEC/SEC	.090051	.000666	.000000	.000330	2.586163	-.330764	-.320586	-.000332	.000000
PHIDOT RAD/SEC	0.000000	0.000000	0.000000	0.000000	0.000000	1.000000	.271583	0.000000	0.000000
PSIDOT RAD/SEC	0.000000	0.000000	0.000000	0.000000	0.000000	0.000000	1.038223	0.000000	0.000000
	ALPHA RAD	VTOTAL FT/SEC	QB RAD	THETA RAD	BETA RAD	PB RAD/SEC	RB RAD/SEC	PHI RAD	PSI RAD

THE DIMENSIONAL B MATRIX

	DE RAD	DFLAPS RAD	DA RAD	DR RAD	DTHR LBS	DTHL LBS
ALPDOT RAD/SEC	-.180149	-.226209	-.000004	0.000000	-.000006	-.000006
VTOTDOT FT/SEC/SEC	.000000	.000000	.051465	-.390316	.005116	.005116
QDOT RAD/SEC/SEC	-18.824857	1.116317	.000013	0.000000	.000298	.000359
THETADOT RAD/SEC	0.000000	0.000000	0.000000	0.000000	0.000000	0.000000
BETADOT RAD/SEC	.000000	-.000000	-.005510	.041787	-.000000	-.000000
PDOT RAD/SEC/SEC	-.000000	.000000	-2.911990	.756197	-.000196	.000210
RDOT RAD/SEC/SEC	-.000000	.000000	-.091166	-1.586543	-.000608	.000522
PHIDOT RAD/SEC	0.000000	0.000000	0.000000	0.000000	0.000000	0.000000
PSIDOT RAD/SEC	0.000000	0.000000	0.000000	0.000000	0.000000	0.000000

THE A MATRIX EIGENVALUES

EIGENVALUES			TIME CONSTANT	DAMPING RATIO	UNDAMPED NATURAL FREQUENCY	PERIOD	TIME TO HALF
-.66193E+01	+	0. *I	.15107E+00				
-.24779E+01	+	0. *I	.40357E+00				
-.20976E+01	+	0. *I	.47902E+00				
.75402E-08	+	0. *I	-.13262E+09				
.37817E-01	+	0. *I	-.26443E+02				
-.35982E-02	+	.15183E+00*I		.23692E-01	.15187E+00	.41359E+02	.44729E+03
-.35982E-02	+	-.15183E+00*I					
-.23498E+00	+	.17722E+01*I		.13144E+00	.17878E+01	.34841E+01	.68492E+01
-.23498E+00	+	-.17722E+01*I					

APPENDIX B: ICAD DETAILED USERS MANUAL

B.1 THE INTERACTIVE RUN

Figure B.1 is a flow chart of the ICAD program. It shows that data describing the airplane (state matrix equations), data describing the flight condition and gust environment, and data needed for the augmentation procedures are input through data files. After data file input, optional open loop time history and PSD analyses are available, followed by entry into either the optimal or classical design loop. Each design loop iteration is followed by options to conduct time history and PSD analyses, which can then be viewed graphically and compared to any previous analyses in the run. Decision points in the flow of ICAD are resolved interactively, using detailed user prompts. An explanation of the various user prompts follows in sections B.1.1 and B.1.2. After reading these sections, the user is encouraged to experiment in order to gain experience with the various options available, as well as the default conditions.

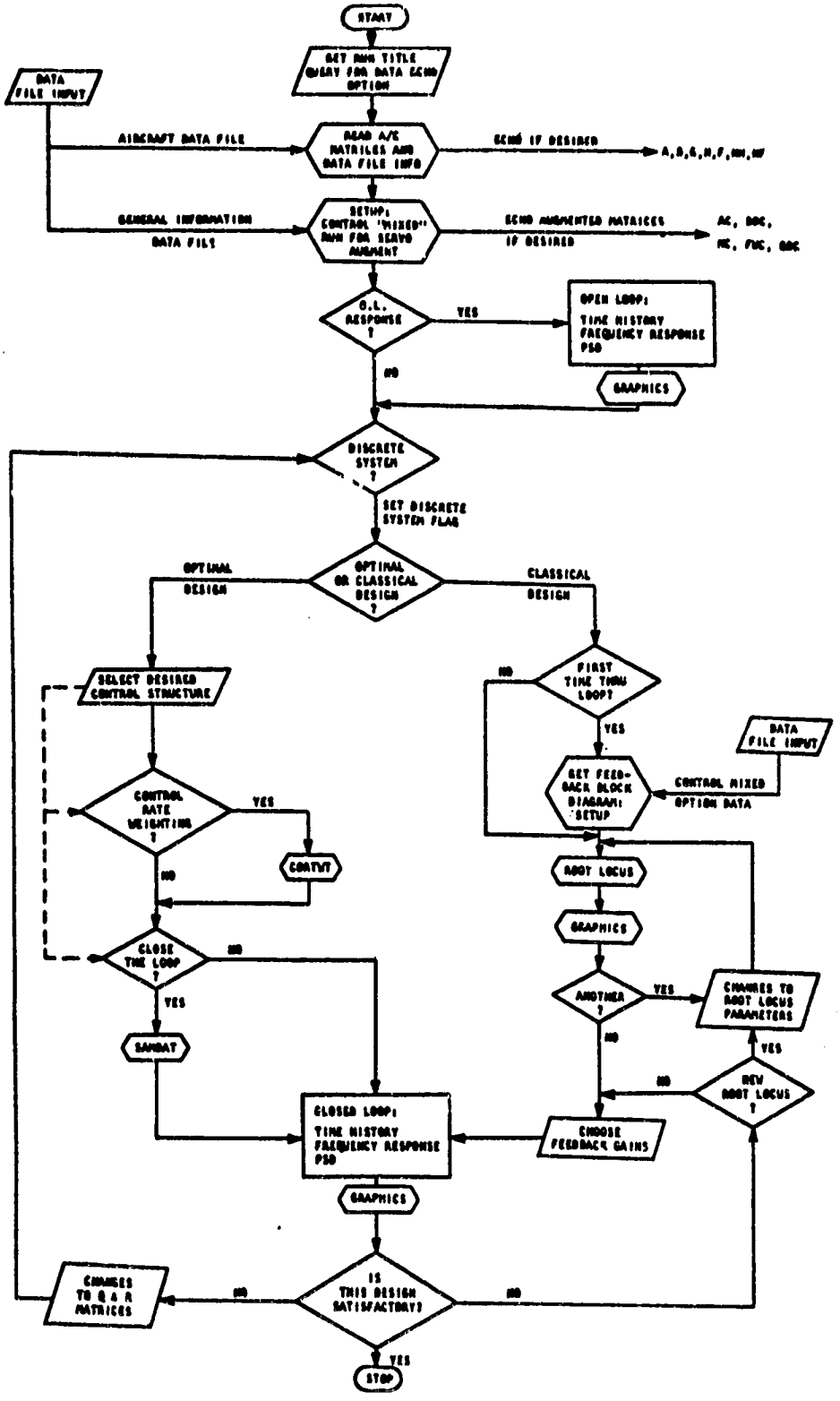

Figure A.1 ICAD Program Flow

The following pointers should be kept in mind while running ICAD:

1. The default responses to questions, when defaults exist, are given in angle brackets (< >). These responses can be affirmed by entering a carriage return (denoted hereafter by <cr>).

   Example:

   Do you want an Open Loop response? <Yes>

2. Most menu prompts allow I1 replies -- That is, a one digit integer followed by a <cr>.

3. A carriage return at any prompt for a number, whether integer or real, will be taken as a zero.

4. In response to a (Y/N) question, only upper case y's or n's are recognized. Any response beginning with these letters will also work. Any unrecognized response causes execution to continue using the default response. This feature allows a <cr> to be used to affirm the default.

   Thus, much of the run can be conducted by using carriage returns and integer entries between 1 and 5. It is strongly suggested that the user become accustomed to these procedures, which will increase the speed and ease of use of the program greatly.

5. In the program description which follows, "not implemented" indicates that the variable or option being described is no longer needed or is not yet verified. Options in this category should be avoided, and variables in this category should be entered as dummies that have no effect on program execution.

This description is organized as follows: Section B.1.1 contains an explanation of all the user prompts that occur in the primary flow of the ICAD Program. Section B.1.2 gives a similar explanation for the flow of the interactive graphics routines. Section B.2 then details the data files, their organization, content, and format. Section B.2 also describes the output files generated by ICAD.

B.1.1 USER PROMPT EXPLANATION

In these explanations, boldface represents prompts given by ICAD, and input formats appear in brackets [ ] after each prompt. All prompts are given in the order they appear during an execution of the program.

Enter the Title for the output of this run: [15A4]

The title entered here will appear in the run header, which contains the basic flight condition information. This header is printed to the summary file and the terminal.

Do you want an input matrix data echo? <No> [A1]

Selecting this option will cause the following matrices to be printed to the screen during execution:

Input matrices (**A**, **B**, **G1**, **H1**, **FU1**).
Servo augmented matrices (**AC**, **BDC**, **HC**, **FUC**, **GDC**).
Augmented matrices used for transfer function analysis
of control weight rating (CRW) designs (**APC**, **DPC**, **HDPC**, **FPC**).

Once set, this option can be defeated by typing an "8" at the "FOR THE PSD" prompt.

The data echo option also causes the input matrices to be echoed to the summary file. Two additional matrices are output to the summary file. **H** and **FU**. These are the matrices which make up the output equation used by

ICAD. ICAD creates H and FU to eliminate x from the output equation supplied by the user:

$$y = H1\,x + G1\,\dot{x} + FU1\,u$$

To eliminate x, the system equation is used:

$$x = A\,x + B\,u + D\,w$$

This results in the following equations for H and FU:

$$H = H1 + G1 \cdot A$$

$$FU = FU1 + G1 \cdot B$$

The GDC matrix also results from this calculation:

$$GDC = G1 \cdot D$$

Finally, the B and D matrices are combined to ease the handling of the sytems of equations:

$$BDC = \left| B \,;\, D \right|$$

Do you want an Open Loop reponse? <Yes> [A1]

A "Yes" response allows a time history and/or PSD analysis to be done on the open loop, servo augmented system.

Do you want a Time Reponse? <Yes> [A1]

In both the open and closed loop case, the option is available to skip the time history response. The following question is asked if a time history is desired (a "Yes" answer above):

Do you want extra printout? <No>[A1]

<N> No extra printout. This option minimizes screen printout. Only the time history state and control labels, their maximum time history values and rates, and their root mean squared values are printed out. All output files remain intact.

<Y> Extra printout. The values of the states at each time step are printed to the screen. The printout intervals conform to those set up in the general information data file (so that the screen printout is the same as the output to the output file assigned to logical unit number (LUN) 11 - see section B.2.2 for an explanation of NPRINT, NTIMES, T(1) and T(2)). The summary file will not recieve this printout -- it always recieves printout similar to that recieved on the screen during a "no extra printout" option.

Do you want a PSD? <Yes> [A1]

In both the open and closed loop case, the option is available to do a PSD/frequency response. If chosen, the first run through this procedure allows the user to choose the desired transrer functions to be analyzed during the rest of the run. This is done with the following prompts:

The available transfer function numerators are:
1. **Az(ft/s2)**
2. **Alfa(deg)**
3. **Q(deg/s)**
4. **Thet(deg)**
5. **D-e(deg)**
6. **D-f(deg)**

Enter desired numerators,
one at a time; append with zero: (2 DIGITS) [I2]

The numerator labels listed are only examples; these labels are supplied as inputs to ICAD. A label must be supplied for each variable in the output vector and for each control and disturbance (disturbances are shown below). Any set of I2 numbers from 1 to 6 will be accepted in response to the above prompt. A carriage return is to be entered after each number. The final zero can be achieved by hitting the carriage return only.

The available transfer function denominators are:
1. **COMD-E**
2. **COMD-F**
3. **W-gust**
4. **Q-gust**

Enter desired denominators,
one at a time; append with zero: (2 DIGITS) [I2]

Again, any set of I2 numbers, here between 1 and 4 inclusive, may be chosen; each followed by a carriage return and the final entry being a zero or carriage return.

The above set of prompts appears only the first time through the procedure. Below are PSD options which always appear. The extra printout options are:

FOR THE PSD
EIGENVALUES ONLY..... TYPE 1
EIGENVALUES AND ZEROES..... TYPE 2
EXTRA PRINTOUT..... TYPE 3 [I1]

<1> Eigenvalues only. This option defeats all screen and summary file output except the system eigenvalues and the RMS values calculated from the PSD for each transfer function. Output files are not changed by this

option.

<2> Eigenvalues and zeroes. This choice causes the eigenvalues of the system, and the zeroes of the chosen transfer functions, as well as the PSD computed RMS, to be written to both the screen and the summary file.

<3> Extra printout. All of the above outputs will be given, plus the PSD/frequency response values at the chosen frequency intervals (see section B.2 or Reference 15 for an explanation of IFREQ, FFREQ, and DELFRQ). This printout contains similar information to the output file assigned to LUN 12, but is formatted differently.

FOR THE SYSTEM EXCITATION
VON KARMAN SPECTRA..... TYPE 1
DRYDEN SPECTRA..... TYPE 2 <1> [I1]

This option allows the choice of the input power spectrum which will excite the various transfer functions. Both are gust field power spectra which excite the gust mode of the aircraft. The aircraft altitude and airspeed, which are required to compute the spectra, are data file inputs.

TEKTRONIX TERMINAL GRAPHICS; TYPE 1 TO BYPASS [I1]

This prompt will appear at two stages in the interactive run: once after each time history/PSD analysis, and once after each root locus analysis. A carriage return will allow entry into the applicable graphics routines, whose prompts and outputs are discussed in section B.1.2.

Do you want a Sampled Data System? <Yes> [I1]

A "Yes" answer to this prompt sets the proper flags for the design and analysis of a digital controller. A "No" response causes an analog controller to be generated.

FOR THE ACTIVE CONTROL SYSTEM
OPTIMAL DESIGN TECHNIQUES..... TYPE 1
CLASSICAL TECHNIQUES..... TYPE 2 <1> [I1]

This is the decision point between the two possible design loops. An explanation of the interactive options for the classical case will be given first, followed by the optimal techniques options.

B.1.1.1 OPTIONS - CLASSICAL TECHNIQUES

The first menu that appears on entry into the classical design loop is an echo of root locus parameters read from a data file by CONTROL, followed by the options to change those parameters.

N1= 1 N2= 1 GAIN1= 1.000000 GAIN2= 1.000000

CHANGES TO
N1..... TYPE 1
N2..... TYPE 2
GAIN1..... TYPE 3
GAIN2..... TYPE 4
NO MORE CHANGES.. TYPE 5 [I1]

This prompt allows the user to change the CONTROL root locus parameters before each calculation of the root locus. Thus, if the wrong gains are chosen the first time through the root locus, it can be redone. Typing a 5 will cause the root locus to be calculated using the last values of N1, N2, GAIN1, and GAIN2 shown. The root locus is calculated from these parameters by first calculating the feedback gains:

k1 = 0, GAIN1, 2*GAIN1, 3*GAIN1, . . . (N1-1)*GAIN1

k2 = 0, GAIN2, 2*GAIN2, 3*GAIN2, . . . (N2-1)*GAIN2

For N1 and N2 > 0; and

k1 = 0, GAIN1, 2*GAIN1, 4*GAIN1, . . . $2^{(|N1|-2)}$*GAIN1.

k2 = 0, GAIN2, 2*GAIN2, 4*GAIN2, . . . $2^{(|N2|-2)}$*GAIN2.

For N1 and N2 < 0. These gains are then fed back through gain matrices which are generated by ICAD using CONTROL subroutines. CONTROL subroutines calculate these matrices, K1 and K2, from block diagram information fed in through one of ICAD's data files. The format and usage of this information is discussed in reference 15, and will not be presented here. An example of the required data is given in section B.2. The resulting root locus is based on the feedback equation

$u = Fx$, where

$F = k1*K1 + k2*K2$.

Root loci are calculated in the s-plane for continuous systems, and in both the z-plane and the w'- plane for sampled data systems. After the root locus has been calculated, the following prompt appears:

TEKTRONIX TERMINAL GRAPHICS; TYPE 1 TO BYPASS [I1]

If the user is at a Tektronix 4010 compatible terminal, the s-plane or w'-plane root locus can be viewed on the screen by entering a <cr> here. A discussion of the resulting graphics prompts is given in section B.1.2.

DO YOU WANT ANOTHER ROOT LOCUS? <NO> [I1]

This allows the root locus to be redone any number of times, using different values of the variables mentioned above. When a "No" or <cr> is entered here, the user is prompted to enter the inner- and outer- loop gains to be used in the feedback control system:

TYPE IN THE SELECTED k1 [F12.6]

TYPE IN THE SELECTED k2 [F12.6]

The entered gains are then echoed back:

k1= 0.250000
k2= 1.300000

GAINS OK? <YES>

A "No" causes prompts for the gains to be reentered. After a "Yes" answer or <cr> in response to this question, the closed loop time history and PSD/frequency response are optionally performed, as before. Graphical analysis of the response is then available (described in section B.1.2), followed by this prompt to continue the design looping procedure:

Is this design satisfactory? <No> [A1]

This is the exit point for the program. Typing "Yes" completes the design process and stops execution, while typing "No" brings up the following options (these options are different if optimal techniques have been chosen; optimal techniques options will be discussed later):

CHOOSE FOR NEXT DESIGN:
SELECT NEW GAIN -- 1
NEW ROOT LOCUS -- 2
OPTIMAL DESIGN -- 3
END -- 4 [I1]

<1> sends the program back to the "SELECT k1" prompt.
<2> sends the program back to the set of 5-options for the root locus, where parameters for a new root locus may be entered.
<3> allows entry into the optimal design loop.
<4> ends the program.

If "3" is chosen here, for instance, the following prompts are given. These

prompts represent the top of the design looping procedure:

Do you want a Sampled Data System? <Yes>

FOR THE ACTIVE CONTROL SYSTEM
OPTIMAL DESIGN TECHNIQUES..... TYPE 1
CLASSICAL TECHNIQUES..... TYPE 2 [I1]

Here classical design techniques can be continued, or entry into optimal techniques (discussed in section B.1.1.2) can occur.

B.1.1.2 OPTIONS - OPTIMAL TECHNIQUES

Select Desired Optimal Control Structure:
Standard Optimal Regulator .....TYPE 1
Control Rate Weighting <CRW> .....TYPE 2
NONE of the Above .....TYPE 4 [I1]

Two types of optimal design may be chosen at this point. For a discussion of these methods, see Chapter 4. A choice of "NONE of the Above" causes an open loop analysis to be done.

EXTRA PRINTOUT THRU ASYMREG ?? <NO> [A1]

A "Yes" response here will cause some of the intermediate steps in the optimal design to be printed to the screen.

USE DISCREG ?? <NO> (DEFAULT IS RICTNWT) [A1]

This Question allows a choice of two methods for solving the Ricatti equation:

RICTNWT : A Newton-Rapson root finding method. This is the suggested method unless for some reason (a numerical or convergence problem) it does not find the solution.
DISCREG : A backward integration of the Ricatti equation in time, until a solution is reached-this is a much slower method, and is not recommended.

Do you want a Time Response? <Yes> [A1]

FOR THE TIME HISTORY
NO EXTRA PRINTOUT..... TYPE 1
EXTRA PRINTOUT..... TYPE 2 [A1]

The above two prompts are repeated here, to illustrate that they are

available after each design, and to add the following two prompts, which are given only if a digital design has been implemented.

WHAT FRACTION OF Ts IS THE Td (.01-1.0) <1.0> [F12.6]

Here any desired computational time delay can be entered as a fraction of sample time. This affects only the time history simulation. After the analysis has been performed, the following prompt allows another time history to be done with a different time delay. Thus, sensitivities on time delay can be performed.

DO YOU WANT A DIFFERENT TIME-DELAY (Y/N) <N> [A1]

Is this design satisfactory? <No> [A1]

Again, this allows the interactive run to be terminated.

A "No" answer to the above question during an optimal design loop brings up the following menu, which allows the weighting matrices to be changed.

WHICH MATRIX (MATRICES) DO YOU WISH TO CHANGE ?
THE "Q" MATRIX ..... TYPE 1
THE "R" MATRIX ..... TYPE 2
BOTH THE "Q" AND "R" MATRICES ..... TYPE 3
NEITHER "Q" OR "R" MATRIX ..... TYPE 4 [I1]

If a choice of 1-3 is made above, the proper matrix is echoed and the following prompt is given:

TYPE NUMBER OF PARAMETER TO BE CHANGED.(QUIT=0) [I3]

The number given in response to the above prompt represents the column-packed location of the matrix entry which the user wishes to change. The matrices are numbered down the columns, proceding from leftmost to rightmost column as the numbers increase. For example, a 4X4 matrix would be numbered as follows:

1	5	9	13
2	6	10	14
3	7	11	15
4	8	12	16

For example, if a 4 is entered in response to this prompt, the following prompt results:

Q or R(4)= 0.00000 NEW Q or R(4) = ?? [F10.5]

The user then enters the new value desired at that location. When all changes have been made, a zero or carriage return at the "TYPE NUMBER OF

PARAMETER TO BE CHANGED" prompt causes an echo of the changed matrices and one more chance to adjust them:

MORE CHANGES TO EITHER MATRIX ?? <NO> [A1]

A "No" or <cr> here takes the user to the top of the interactive design loop, from which either the optimal or classical design techniques can be executed:

Do you want a Sampled Data System? <Yes> [A1]

FOR THE ACTIVE CONTROL SYSTEM
OPTIMAL DESIGN TECHNIQUES..... TYPE 1
CLASSICAL TECHNIQUES ..... TYPE 2 [I1]

This completes the explanation of the optimal techniques design loop. If, during either classical or optimal design looping, the option to look at graphics is chosen, another set of prompts must be answered. These are explained in the next section.

B.1.2 INTERACTIVE GRAPHICS

Two interactive graphics subroutines exist. The first is GRAPHS, which allows any previously generated time histories, PSDs or frequency responses to be viewed. The second is LOCUS, which plots each root locus. Both are interactive, and require that the terminal being used is compatible with Tektronix 4010 graphics. GRAPHS is dicussed in section B.1.2.1, and LOCUS is discussed in section B.1.2.2.

B.1.2.1 GRAPHS

The following is a description of each of the interactive questions asked by graphs:

TEKTRONIX TERMINAL GRAPHICS; TYPE 1 TO BYPASS [I1]

This question must be answered by a <cr> or an I1 integer. It allows the plots to be bypassed completely.

Set terminal command character to |,then <CR>.

If the terminal being used is not a Tektronix 4025, This prompt should be ignored; simply enter a <cr> to continue. If the terminal is a TEK 4025, this message acts as a reminder for the following steps to be taken (if the command character is not already set):

A. On the TEK 4025, type SHIFT-STATUS (the status key is in the far upper right hand corner of the keyboard).

B. The command character will appear between two status numbers. If, for instance, the command character is %, something similar to the following sequence will be displayed:

23 %D345

C. If the command character is not |, then the following command to the TEK will change it (replace the % in the command below with whatever character comes up in step B):

%COM |<cr>

D. After entering the above command, another <cr> will allow the program to continue.

Note that a <cr> is all that is needed if the command character has been set; in other words, steps A-C are executed only once for any terminal session.

Do you want:

1. Time histories
2. Power spectras
3. Frequency responses?
(Type zero if done) [I1]

An I1 answer chooses one of the three options, and a <cr> exits the subroutine.

2 runs have been conducted.

Enter numbers of runs to be observed,
one at a time; append with zero: (2 DIGITS) [I2]

Each "run", or iteration through the design loop, has been numbered. This number has been recorded to the screen and the summary file, starting with 1 for the open loop case. These can now be viewed in any combination or order by entering the proper integers, followed by <cr>s and a terminating zero or <cr>.

Enter any note that you want to appear on the graphs
(A cursur will appear for the placement of this note) [A60]

LINE 1 **LINE 2**
THIS IS ANY MESSAGE OR LEGEND DESIRED ON THE GRAPHS

1. Time Histories. If a time history has been chosen, the following menu will allow any of the time history variables to be plotted:

The following variables are available in each time history:
1. **Az(ft/s2)**
2. **Alfa(deg)**
3. **Q(deg/s)**
4. **Thet(deg)**
5. **D-e(deg)**
6. **D-f(deg)**
7. **COMD-E**
8. **COMD-F**

Enter variable to be observed,zero when done: (2 DIGITS) [I2]

The variables available are those selected for inclusion in the output vector (not the state variables) and the control commands, which go to the servos. As mentioned earlier, the labels given above are only examples; actual labels must be supplied in a data file.

new note <no>? [A1]

This allows the note entered earlier to be changed.

default x scale? <yes> [A1]

A <cr> or "Yes" here will signal the subroutines to base the x scale on the minimum and maximum x values in the first time history to be plotted. If a "No" answer is entered here, the following prompts must be answered with real values:

enter minimum x value: [F10.4]

enter maximum x value: [F10.4]

default y scale <yes>? [A1]

Again, a <cr> indicates that the minimum and maximum y value in the first time history are to be used to set the scales. Note that if the second time history in the string of "numbers of runs to be observed" contains larger maximums or smaller minimums, its plot will go off the screen. The remedies for this are:

1. Use non-default y values based on the actual desired maximums and minimums.

2. Reorder the "runs to be observed" so that the time history with the largest values is plotted first. The maximum and minimum values which become the defaults are then based upon this plot.

After the scaling questions are answered, the desired time histories will be plotted. After the first time history, a cursor will appear for the placement of the label entered previously. The plots of the same variable for each of the other "time histories to be observed" will then be plotted after each entry of a <cr>.

2. or 3. PSD's or Frequency Responses. The following menu appears instead of the "variables available in each time history available" menu if PSD's or frequency responses have been chosen for plotting.

The following transfer functions are available:

1. Az(ft/s2)/ W-gust
2. Q(deg/s) / W-gust

Enter the transfer function to be observed, zero when done:(2 DIGITS) [I2]

All other prompts are similar to those discussed for the time history. When all desired plots have been made, a series of <cr> responses (or zeroes) to the subroutine prompts will send ICAD back to the main program.

B.1.2.2 LOCUS

LOCUS is called during classical design looping, after each root locus is executed. The screen graphics in this subroutine are only available to Tektronix 4010 compatible terminals. The prompts given by LOCUS are explained below.

TEKTRONIX TERMINAL GRAPHICS; TYPE 1 TO BYPASS [I1]

As in GRAPHS, a <cr> response to the above prompt indicates that plots are

desired, while a 1 bypasses the subroutine.

Set terminal command character to |, then <CR>.

This is the same reminder given by GRAPHS. Section B.1.2.1 details the responses needed to set the command character. If a Tektronix 4025 terminal is not being used, or if the command character has already been set, a <cr> is all that is required here.

PRESS ANY KEY TO CONTINUE.

This prompt signals that all the data is loaded and ready for plotting. Hitting any key allows LOCUS to proceed with the plot. This plot is of the 2nd quadrant of the s- or w'-plane, with a symbol at each of the pole locations from the most recent root locus. Double root loci are represented by changing the symbol type each time the outer loop gain (k2) changes. The symbol types are:

X - 1st outer loop gain
Δ - 2nd " " "
□ - 3rd " " "
☆ - 4th " " "
◇ - 5th " " "

A cross-hair cursor and menu line appear on the screen after the plot is completed. Cursor movement is accomplished using the keypad arrow keys. The menu line indicates the possible one-letter commands:

<CR>==>VIEWING AREA CORNERS; G==>GAINS; K==> KEY IN X LIMITS; Q==> QUIT

<CR>: This command allows any region on the screen to be expanded to full screen size. To define a viewing area for expansion:

1. Using the keypad arrow keys, move the cursor to the lower left hand corner of the desired area. Press <cr>.

2. Move the cursor to the upper right hand corner of the desired area. Press <cr>.

The root locus in the defined area will be plotted automatically after the second carriage return. The cursor and menu reappear after each new plot.

G: This command allows the gains of any pole to be displayed. To use the "G" command, simply center the cross-hair cursor over a pole, and press "G". A small box will be drawn around the cursor location to indicate the region inside which LOCUS searches for poles. The gains (k1 and k2) of the first pole found in this box will be displayed adjacent to the box. Only one pair of gains is given, so care should be taken to make sure that

only one pole is enclosed by the box. One way to do this is to define a small enough viewing area with the <cr> or K command to spread out the poles.

K: The K command, like the <cr> command, is used to define a new viewing area. After the letter K is pressed, LOCUS gives prompts to enter the X and Y limits of the desired viewing region:

KEY IN X LIMITS; FOLLOW EACH WITH A <CR> [F10.5]

Here the lower, followed by the upper bound of the desired x range must be entered, each followed by a carriage return.

NOW KEY IN Y LIMITS; FOLLOW EACH WITH A <CR> [F10.5]

The lower and upper limits, in that order, for the desired vertical axis range, are entered after this prompt. Each entry is followed by a <cr>. After the second Y limit has been entered, a new plot will be made based on the limits entered.

Q: This command causes exit from LOCUS and return to the main program to occur. First, however, the following prompt is given:

DO YOU WANT THE FULL ROOT LOCUS BACK? <YES>

This prompt is included for those times when a small viewing area has been defined, and the original viewing area is desired. Instead of keying in the limits of the larger region with the K command, the user can simply type Q, followed by a <cr> or "Y" response to the above prompt. The default scale root locus will then appear.

B.2 DATA FILES

The following are the logical unit number (LUN) assignments which are required to run ICAD:

LUN	Type	Usage
11	output	time history output file
12	output	PSD/frequency response output file
13	output	root locus output file
14	output	summary file
15	input	disturbance data file
18	input	aircraft data file
19	input	general information data file
20	inter-active	assigned to the Physical Device Number (PDN) of the terminal being used
21	inter-active	assigned to the PDN of the terminal being used
22	output	short summary data file

Section B.2.1 details the the requirements for the input files (LUN's 15, 18, and 19). The only other requirement for input/output is that each LUN above be assigned to either a data file or a physical device (CRT terminal or Teletype for user interface).

B.2.1 INPUT DATA FILES

The purpose of the input data files is to initialize both the aircraft data and the desired analysis procedures to minimize the interactive input required from the user. The data files required are:

1. Aircraft parameters data file (LUN 18).
2. General information data file (LUN 19).
3. Disturbance time history file (LUN 15).

These three input data files are required for any run. The first two include non-data or comment lines that are generally used as formatting and

data reminders. Although these lines do not contain any information explicitly read by ICAD, a line must exist corresponding to each line in the following examples, or data will be input improperly.

The aircraft data file contains all information that typically changes from one flight condition to the next. This includes the system matrices, flight condition parameters, labels and titles, and the output matrices.

The general information data file contains data that will not normally change from one flight condition to another. It will interface properly with any aircraft input file which contains matrices of similar dimensions, and will cause the same augmentation and feedback strategies to be applied on each.

The disturbance time history data file contains any sequence of desired inputs to the system. These will be implemented during the time history analysis at the specified chronological intervals. This data file, combined with the D matrix, allows the digital simulation of the open and closed loop response of the system to any disturbance or set of disturbances.

Refer to the example files in Figures B.2 through B.4 for the sequence and formatting of the data files. These figures indicate the lines which are prompt lines. The format of these lines is not critical, but they must be included. What follows is a detailed explanation of each input variable, ordered as in the data file itself.

B.2.1.1 AIRCRAFT DATA FILE

Refer to Figure B.2. The non-data lines in this example file give the format required on the data lines directly below them in brackets [ ]. The following is an explanation of what each data line contains:

Line 3: Title to be used by the ORACLS subroutines.

Line 5: Aircraft matrix dimensions before servo augmentation:

NN = number of aircraft states,

NC = number of controls,

NM = number of outputs,

NZ = not implemented, and

ND = number of disturbances.

line 7: Information for generation of power spectral densities:

ALTD = altitude above ground level,

TAS = true air speed, and

SIGMW1 = gust field rms (each input gust value is multiplied by this value).

line 10: Label for each of the augmented controls, plus a label for each disturbance (total # of labels should be NC + ND).

line 13: Label for each output (total # of labels here should be NM).

line 15-EOF: Aircraft matrices. These data lines should be formatted as in the example, i.e. each matrix must be preceded with an identification line. Also, two lines must be included for IDENT. IDENT is a flag which should be set when the H matrix is unity, to allow ORACLS to skip part of its analysis procedures. Matrix dimensions are given in the example file (i.e. matrix B is NN by NC).

```
1     5   10   15   20   25   30   35   40   45   50        60        70
2 ***** FILENAME:  402B    <26-JUL-83> **********************[20A4]
3 Cessna 402B, Flgt # 1 [ Output = Az, Alpha, Th-Dot, Theta ]
4 **NN, NC , NM , NZ , ND ************************************[5I5]
5     4    2    6    2    1
6 **** ALTD,      TAS,  SIGMW1 *********************************[3F10.4]
7 500.00    183.862   6.00
8 ***** CONTROL INPUT LABELS (FIT TO FOLLOWING 'FORMAT')******[6A10]
9 "....1...""....2..."  "..3..."  "..4..."  "..5..."  "..6..."  "..7..."
10      U-E       U-F      W-gust    Q-gust
11 ***** OUTPUT LABELS (FIT TO FOLLOWING 'FORMAT')************[6A10]
12 "....1...""....2...""....3...""....4...""....5...""....6...""....7..."
13  Az(ft/s2) Alfa(deg)  Q(deg/s) Thet(deg)  D-e(deg)  D-f(deg)
14 ***** A MATRIX (NN x NN) ***********************************[8F10.6]
15  -1.172860 -0.001734  0.913378 -0.024888
16   9.657603 -0.0278230 0.0     -31.780448
17  -5.498211  0.000676 -7.532734  0.078358
18   0.0       0.0       1.000     0.0
19 ***** B MATRIX (NN x NC) ***********************************[8F10.6]
20  -0.180128 -0.226209
21   0.0      -4.508151
22 -18.824925  1.116317
23   0.0       0.0
24 ***** G1 MATRIX (NM x NN) **********************************[8F10.6]
25  183.862   0.0       0.0       0.0
26  0.0       0.0       0.0       0.0
27  0.0       0.0       0.0       0.0
28  0.0       0.0       0.0       0.0
29  0.0       0.0       0.0       0.0
30  0.0       0.0       0.0       0.0
31 ***** IDENT = 1 FOR  H = IDENTITY MATRIX, ELSE IDENT=OTHER*[5I5]
32     0
33 ***** H1 MATRIX (NM x NN) **********************************[8F10.6]
34  0.0       0.0      -183.862   0.0
35 57.296     0.0       0.0       0.0
36  0.0       0.0      57.296     0.0
37  0.0       0.0       0.0      057.296
38  0.0       0.0       0.0       0.0
39  0.0       0.0       0.0       0.0
40 ***** FU1 MATRIX (NM x NC) *********************************[8F10.6]
41  0.0       0.0
42  0.0       0.0
43  0.0       0.0
44  0.0       0.0
45 57.296     0.0
46  0.0      57.296
47 ***** TZ MATRIX (NZ x NN) **********************************[8F10.6]
48  0.0       0.0       0.0       0.0
49  0.0       0.0       0.0       0.0
```

Figure B.2 Example Aircraft Data File

B.2.1.2 GENERAL INFORMATION FILE

Refer to Figure B.3:

line 2: Formatting variables for ORACLS subroutines. These are discussed in the ORACLS manual, and will effect primarily the format of the output matrices. For instance, the field FMT1 specifies the data file output format for matrices, and the field FMT2 specifies the format of matrices to be printed out to the screen.

line 4: Convergence criteria for use in ORACLS, plus one CONTROL variable, ISUBNAM, which causes a subroutine trace to occur. For most applications, the values in Figure B.3 will not change.

line 6: Frequency response and PSD controlling information:

IFREQ = initial PSD and frequency response frequency, and

FFREQ = final PSD and frequency response frequency.

NOTE: CONTROL calculates the w'-plane frequency response for digital systems, and assumes that the input IFREQ and FFREQ are s-plane values. The following conversion is done, which will yield erroneous results for values of IFREQ or FFREQ > Ts/2 :

w'-plane frequency = TAN(s-plane frequency*Ts/2) * 2/Ts

where Ts = Sample time of the digital control system.

DELFRQ = step multiplier in geometric progression from IFREQ to FFREQ.

DUMMY = not implemented.

ITCOND = 1 for Clear Air Turbulence gust field modeling;
2 for Thunderstorm gust field modeling.

IDCOND = 1 for longitudinal gust field modeling;
2 for lateral directional gust field modeling.

```
1      LIN,NLP ,NEPR,FMT1                *,FMT2 ***************[3I5,2(6A4)]
2     1 1000    7 (8F13.6)                (3X,8F13.6)
3 **EPSAM,EBSAM  ,SUMCV  ,RICTCV ,SERCV  ,IACH,MAXSUM,ISUBNAM*[5E8.1,3I5]
4  1.0E-10 1.0E-10 1.0E-10 1.0E-02 1.0E-08   12   50    1
5 ****IFREQ,    FFREQ,   DELFRQ,   DUMMY ,ITCOND,IDCOND*******[4F10.4,1I1]
6 0.10       10.0       1.1        00.000     1 1
7 **   T(1),     T(2),    ALPHA,     BETA,NTIMES,NPRINT*******[4F10.4,2I2]
8  .10        10.       .95       -.*        1010
9 ***** Q MATRIX (NM x NM) *****
10  0.01      0.0       0.0       0.0
11  0.0       1.0       0.0       0.0
12  0.0       0.0       1.0       0.0
13  0.0       0.0       0.0       4.0
14  0 0       0.0       0.0       0.0       0.5       0.0
15  0.0       0.0       0.0       0.0       0.0       0.5
16 ***** R MATRIX (NC x NC) *****
17  1.0       0.0
18  0.0       1.0
19 *******CONTROL COMMON BLOCK DATA FOR SERVO AUGMENTATION****[/,8I9]
20      READ,  SYSTEM,  OUTPUT,     NXC,     NUC,      N1,      N2,  DIGITL,
21         1         1         3         0         0         0         0         0
22    CONTUR,  NUMERS,    FRPS,   TRESP,   MODEL,  NSCALE,     SAV,    CMAT,
23         0         0         0         0         0         0         0         0
24       NK2,   IFLAG,     IGO,    FORM,     IPT,   READ3,   MIXED,  MULTRT,
25         0         0         0         0        -2         0         1         0
26    SCAPLT,     ZOH,   KOUNT,    ICON, ISUBNAM,
27         0         0         0         0      000
28 GAIN1     ,GAIN2     ,MN ***************************************[3F10.5]
29 0.0        0.00      0.000
30 ******* DATA FOR SERVO AUGMENT AS SINGLE BLOCK SERVOS
31      2    0
32      1    0    0    0    1
33      2    0    0    0    2
34      1    1    2
35      2    1    2
36 1.
37 1.
38 10.        1.
39 10.        1.
40 10.        10.
41      1    2    3    4    5    6
42      3    4
43      0    2    0
44      1    1
45      2    2
46 *******CONTROL COMMON BLOCK DATA FOR SUBOPTIMAL DESIGN TECHNIQUES
47      READ,  SYSTEM,  OUTPUT,     NXC,     NUC,      N1,      N2,  DIGITL,
```

Figure B.3 Example General Information File

```
48          1         3         1         6         2        01        01       001
49    CONTUR,   NUMERS,     FRPS,    TRESP,    MODEL,   NSCALE,     SAV,     CMAT,
50          0         0         0         0         0         0         0        0
51       NK2,    IFLAG,      IGO,     FORM,      IPT,    READ3,   MIXED,   MULTRT,
52         01         0         0         0        -1         0         1        0
53    SCAPLT,       ZOH,   KOUNT,     ICON, ISUBNAM,
54          0         2         0         1        01
55 GAIN1     ,GAIN2     ,MN **************************************[3F10.5]
56 1.0        01.0       0.000
57 ********TWO FEEDBACK LOOPS - TWO UNITY BLOCKS
58      2    0
59      1    0    0    0   -1
60      2    0    0    0    2
61      1    1    1
62      2    1    1
63 1.
64 1.
65 1.          1.
66 1.          1.
67 1.          1.          1.          1.
68      1    2    3    4    5    6
69      1    2
70      3    0   02
71      1    1
72      4    1
73      1    2
74      7    1
75      8    2
```

Figure B.3 Example General Information File (Continued)

line 8: Time history controlling information:

T(1) = sample time for modeling of digital systems
(program sets CONTROL's DELT=T(1)).

T(2) = final time. Initial time is automatically set to T=0.

ALPHA = not implemented.

BETA = not implemented.

NTIMES = number of continuous time history calculations between each sample time:

time history Δt = T(1)/NTIMES.

NPRINT = number of time history Δt's between each printout of the state variables. The state variables are updated each T(1)/NTIMES regardless of the value of NPRINT.

These variables are followed immediately by the Q and R weighting matrices for optimal control techniques. These are formatted similarly to the aircraft matrices, and must be included, in their proper dimensions, regardless of the control strategy (optimal or classical) to be used (blank lines for these matrices will make them zero matrices).

The Q and R matrices are followed by the CONTROL common block data for the servo augmentation procedure. The format consists of a label line followed by the corresponding variables (see example file) in 8I9 format. These variables are explained in Reference 15, except for the following variations:

IPT = -2 to suppress all CONTROL printout.
-1 to suppress all but eigenvalue printout (for root locus).
0 through 2 behave as with the original CONTROL.

ICON = 1 during root locus runs (causes printout to LUN 14). This is an imperitive root locus parameter.

ISUBNAM = 1 to cause a subroutine trace through control to occur.

The servo augmentation is accomplished by a MIXED option run through control. The required block data is input through the general information file, as shown in the example file. This file illustrates a 10/s+10 servo augment to each of two controls, delta-e and delta-f. This section is formatted exactly as specified in the CONTROL users manual.

The final section of the general information data file is the [illegible] MIXED option information for classical root locus [illegible]. This section is not required if optimal design techniques are to be employed exclusively during the interactive run. See Reference 15 for details on usage of this section.

B.2.3 DISTURBANCE INPUT DATA FILE:

The format of this file is simply (F6.2,10F10.5). Each new line represents the next time step at which the input disturbance changes, and contains the time, usually in seconds, and the disturbance input corresponding to that time. This requires that there be an F10.5 column for each column in the disturbance matrix. An F6.2 entry of 999.00 terminates the entry of disturbance changes.

Changes in the input disturbance can occur at any integer mulitiple of the time history Δt (T(1)/NTIMES), but are not required at every Δt. The last input disturbance will be considered constant over the intervals between actual inputs. Figure B.4 gives an example disturbance file.

```
  1     0.00    0.00000          0.00000
  2     0.04    0.00109          0.00402
  3     0.08    0.00111          0.00335
  4     0.12    0.00107          0.00279
  5     0.16    0.00286          0.00895
  6     0.20    0.00335          0.00925
  7     0.24    0.00279          0.00583
  8     0.28    0.00222          0.00291
  9     0.32    0.00181          0.00097
 10     0.36    0.00147         -0.00042
 11     0.40    0.00139         -0.00064
 12     0.44    0.00152         -0.00010
 13     0.48    0.00240          0.00323
 14     0.52    0.00087         -0.00279
 15     0.56    0.00077         -0.00268

                    .
                    .
                    .

246     9.80    0.00984         -0.00508
247     9.84    0.00905         -0.00731
248     9.88    0.00858         -0.00793
249     9.92    0.00825         -0.00799
250     9.96    0.00788         -0.00819
251    10.00    0.00772         -0.00746
252   999.00
253   ALT=5000.00000 UO= 198.26300 SIGMA=    1.25000
254   RMS =    1.23978
255   AVER=    0.09211
256   SEED= 176.87730
257   999.99
```

Figure B.4 Example Disturbance File

APPENDIX C. REAL-TIME ANALOG SIMULATION

C 1 THE ANALOG COMPUTER

All analog simulations were carried out on an EAI TR-48 analog computer obtained on loan from NASA. The TR-48 (figure C.1) is a general purpose analog computer consisting of 48 dual DC amplifiers that can be used with other computing devices to perform linear continuous computations such as integration, summation, and inversion. It also contains 60 manually set potentiometers and has an operating voltage range of ±10 volts.

C.2 APPROACH

Figure C.2 illustrates the schematic used for the real-time analog simulation.

The input to the Dryden filter is a psuedo-random white noise output from a FFT analyzer. The white noise output has a signal level of 0 to +1 volt peak-to-peak. It is, therefore, first biased to bring the signal level to a RMS value of 1 volt. The unity variance white noise signal is then passed through a Dryden filter to generate the random gust field required to excite the aircraft. The + or - 10 volt reference supply of the analog computer can also be used (after attenuation) to generate step or ramp gusts if desired.

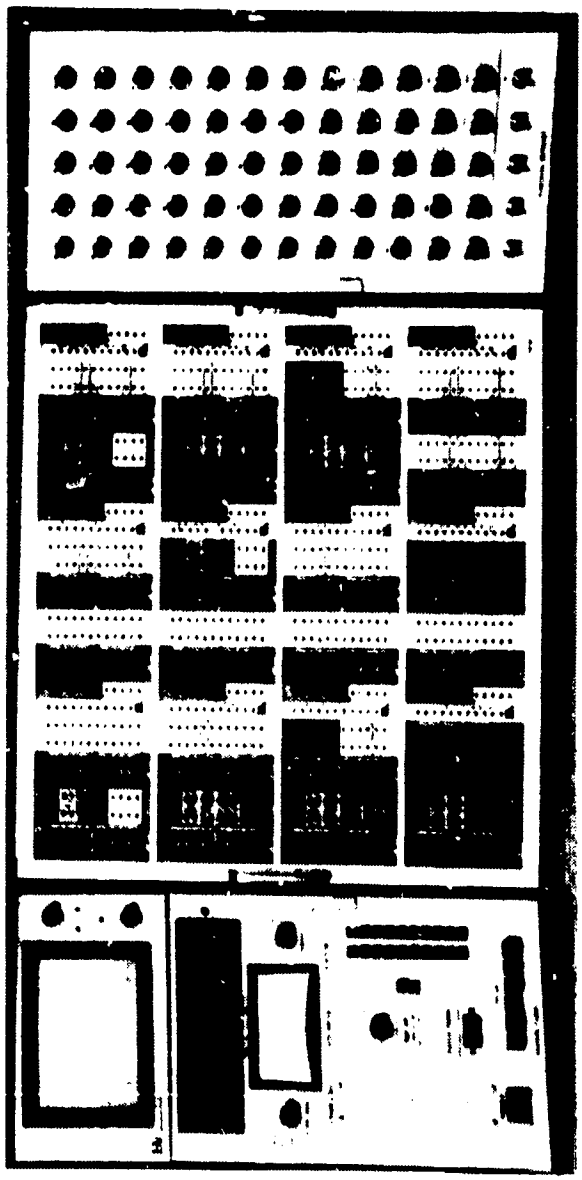

Figure C.1 The EAI TR-48 Analog Computer

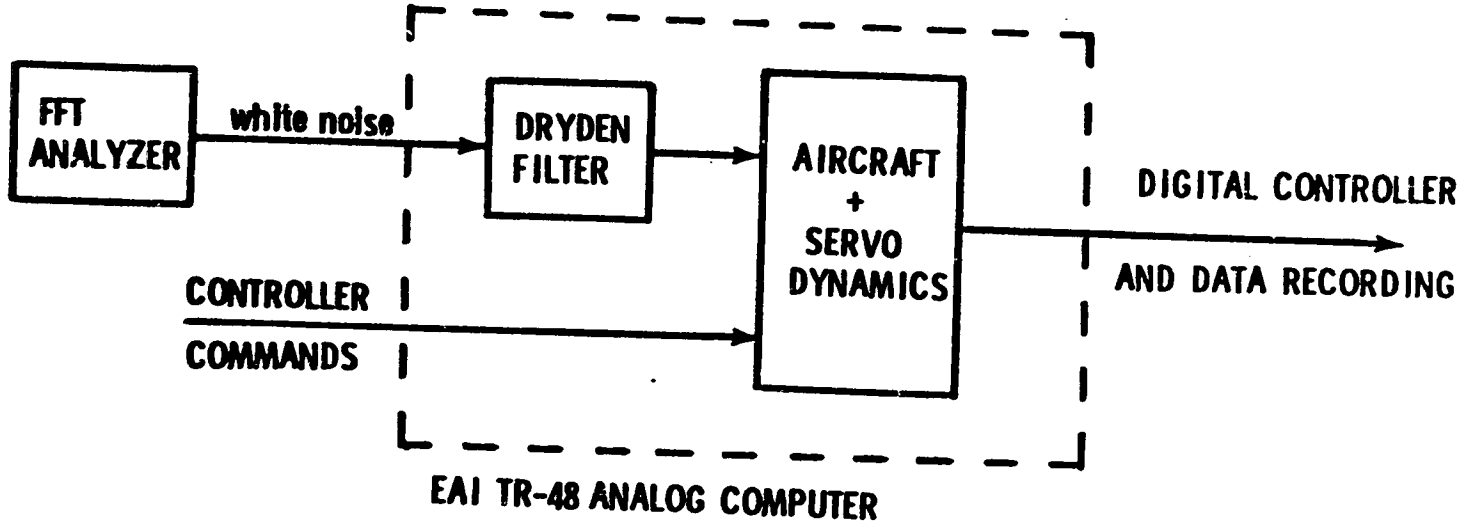

Figure C.2 Schematic for the Real-Time Analog Simulation

C.3 SIMULATION OF THE AIRCRAFT AND DISTURBANCES

The Cessna 402B in a takeoff configuration is represented in state space form as

$$\dot{x} = Ax + Bu \qquad (C.1)$$

$$y = Hx$$

where

$$x' = \{\alpha, u, q, \theta, \delta_e, \delta_f\}$$

$$u' = \{U_e, U_f\}$$

with the A matrix:

-1.1729	-0.0017	0.9134	-0.0249	-0.1801	-0.1131
9.6576	-0.0278	0.0000	-31.7805	0.0000	-4.5082
-5.4982	0.0007	-7.5327	0.0784	-18.8249	0.5581
0.0000	0.0000	1.0000	0.0000	0.0000	0.0000
0.0000	0.0000	0.0000	0.0000	-10.0000	0.0000
0.0000	0.0000	0.0000	0.0000	0.0000	-10.0000

the B matrix:

0.0000	0.0000
0.0000	0.0000
0.0000	0.0000
0.0000	0.0000
10.0000	0.0000
0.0000	10.0000

and the H matrix:

-215.6444	-0.3188	-15.9265	-4.5760	-33.1187	-20.7928

The two extra states are introduced in the mathematical model as a result of augmenting the two first order servos with the aircraft dynamics.

Note that the parameter values in the above set of equations cover the range from 0.0007 (smallest) to -215.6444 (largest). This system therefore has to be magnitude scaled for an accurate solution.

From reference 14, the Dryden filter in state space form is

$$\begin{bmatrix} \dot{a}_g \\ \dot{q}_g \\ \dot{\alpha}^a_g \end{bmatrix} = \begin{bmatrix} -\frac{V}{L_w} & 0 & \frac{\sigma_w}{L_w}(1-\sqrt{3})\sqrt{\frac{V}{L_w}} \\ -\frac{nV}{4b}\cdot\frac{V}{L_w} & -\frac{nV}{4b} & \frac{nV}{4b}\cdot\frac{\sigma_w}{L_w}(1-\sqrt{3})\sqrt{\frac{V}{L_w}} \\ 0 & 0 & -\frac{V}{L_w} \end{bmatrix} \begin{bmatrix} a_g \\ q_g \\ \alpha^a_g \end{bmatrix} + \begin{bmatrix} \frac{\sigma_w}{V}\sqrt{\frac{2V}{L_w}} \\ \frac{nV}{4b}\cdot\frac{\sigma_w}{V}\sqrt{\frac{V}{L_w}} \\ 1 \end{bmatrix} [\eta_a] \qquad \text{(C.2)}$$

For the Cessna 402B in a takeoff configuration and at an altitude of 500 ft.

L_w=100 ft., V=183.86 fps, and σ_w=6.00 fps.

The σ_w value of 6.00 fps corresponds to a 0.01 probability of exceedance as defined in MIL-F-8785C [25].

On substitution, (C.2) simplifies to

the disturbance A matrix:

$$\begin{matrix} -0.3677 & 0.0000 & -0.0053 \\ -1.3319 & -3.6220 & -0.0193 \\ 0.0000 & 0.0000 & -0.3677 \end{matrix} \qquad \text{(C.3)}$$

the disturbance B matrix:

$$\begin{matrix} 0.0343 \\ 0.1242 \\ 1.0000 \end{matrix}$$

To obtain an accurate simulation, magnitude scaling will again be required. A systematic approach to magnitude scale dynamic equations expressed in state space form is described in the next section [33].

C.4 SCALING IN STATE SPACE

The system to be simulated is represented in state space form as

$$\dot{x} = Ax + Bu$$
$$y = Hx \qquad \text{(C.4)}$$

The initial state of the system is taken to be zero, and the simulation will be performed over the time interval $t_0<t<t_f$. To complete the simulation, it is necessary to scale all of the computer variables so that they do not exceed the maximum allowable limits of the computer (10 volts for the TR-48).

For satisfactory scaling, one must be able to make a reasonable estimate of the maximum values of the physical variables; otherwise, rescaling will be required (explained later). Using the maximum-problem-unit/machine unit method for the scale factor selection, it is possible to define matrices which relate the magnitude scaled variables to the original problem vectors as

$$\begin{aligned} x &= S_x x_s & x_s &= S_x^{-1} x \\ u &= S_u u_s \quad \text{or} & u_s &= S_u^{-1} u \\ y &= S_y y_s & y_s &= S_y^{-1} y \end{aligned} \qquad \text{(C.5)}$$

where x_s, u_s, and y_s are the scaled state, control, and output vectors respectively and S_x, S_u, and S_y are the scale factor matrices defined as

$$
\begin{aligned}
&S_x = \text{diagonal } [S_{x_i}] \\
&\max x_i \leq S_{x_i} \leq 2\max x_i, \quad i=1,n \\
&S_u = \text{diagonal } [S_{u_i}] \\
&\max u_i \leq S_{u_i} \leq 2\max u_i, \quad i=1,m \\
&S_y = \text{diagonal } [S_{y_i}] \\
&\max y_i \leq S_{y_i} \leq 2\max y_i, \quad i=1 \text{ for 1 output (Az)}
\end{aligned}
\tag{C.6}
$$

It is clear that the scaled computer variables x_S, u_S, and y_S will have values less than 1 machine unit if their maximum values have been correctly estimated.

Rewriting the state space equations yields

$$
\begin{aligned}
S_x \dot{x}_S &= AS_x x_S + BS_u u_S \\
S_y y_S &= HS_x x_S
\end{aligned}
\tag{C.7}
$$

On using a simplified notation

$$
\begin{aligned}
\dot{x}_S &= A_S x_S + B_S u_S \\
y_S &= H_S x_S
\end{aligned}
\tag{C.8}
$$

where

$$
\begin{aligned}
&A_S = S_x^{-1} A S_x \,, \; B_S = S_x^{-1} B S_u \,, \\
&\text{and } H_S = S_y^{-1} H S_x
\end{aligned}
\tag{C.9}
$$

The above equations represent the properly magnitude scaled state space system to be simulated and may now be simulated successfully, if the eigenvalues of the system are reasonable for the bandwidth of the computer and the output devices which are to be used. Otherwise, time scaling of

the simulation will have to be implemented.

The maximum values of the computer variables are estimated using data from the digital simulation and applying the restrictions specified in equations (C.3).

Then, for the aircraft with servos

max α = 0.07 rad	S_{x_1}= 0.07 rad/m.u.
max u = 20.0 fps	S_{x_2}= 20.0 fps/m.u.
max q = 0.08 rad/sec	S_{x_3}= 0.08 rad/sec/m.u.
max θ = 0.12 rad	S_{x_4}= 0.12 rad/m.u.
max δ_e= 0.02 rad	S_{x_5}= 0.02 rad/m.u.
max δ_f= 0.30 rad	S_{x_6}= 0.30 rad/m.u.
max U_e= 0.02 rad	S_{u_1}= 0.02 rad/m.u.
max U_f= 0.30 rad	S_{u_2}= 0.30 rad/m.u.
max Az= 10.0 f/s**2	S_{y_1}= 10.0 f/s**2/m.u.

and for the Dryden filter

max α_g = 0.07 rad	S_{x_1}= 0.07 rad/m.u.
max q_g =0.08 rad/sec	S_{x_2}= 0.08 rad/sec/m.u.
max α_g^* =1.00 rad	S_{x_3}= 1.00 rad/m.u.

Using these estimated maximum values, the system can then be represented as:

1. aircraft with servos -

the scaled A matrix:

$$\begin{bmatrix} -1.1729 & -0.4955 & 1.0439 & -0.0427 & -0.0515 & -0.4847 \\ 0.0338 & -0.0278 & 0.0000 & -0.1907 & 0.0000 & -0.0676 \\ -4.8109 & 0.1690 & -7.5327 & 0.1175 & -4.7062 & 2.0929 \\ 0.0000 & 0.0000 & 0.6667 & 0.0000 & 0.0000 & 0.0000 \\ 0.0000 & 0.0000 & 0.0000 & 0.0000 & -10.0000 & 0.0000 \\ 0.0000 & 0.0000 & 0.0000 & 0.0000 & 0.0000 & -10.0000 \end{bmatrix}$$

the scaled B matrix:

$$\begin{bmatrix} 0.0000 & 0.0000 \\ 0.0000 & 0.0000 \\ 0.0000 & 0.0000 \\ 0.0000 & 0.0000 \\ 10.0000 & 0.0000 \\ 0.0000 & 10.0000 \end{bmatrix} \qquad \text{(C.10)}$$

the scaled H matrix:

$$\begin{bmatrix} -1.5095 & -0.6376 & -0.1274 & -0.0549 & -0.0663 & -0.6238 \end{bmatrix}$$

2. Dryden filter -

the scaled disturbance A matrix:

$$\begin{bmatrix} -0.3677 & 0.0000 & -0.0761 \\ -1.1654 & -3.6220 & -0.2412 \\ 0.0000 & 0.0000 & -0.3677 \end{bmatrix} \qquad \text{(C.11)}$$

the scaled disturbance B matrix:

$$\begin{bmatrix} 0.4897 \\ 1.5518 \\ 1.0000 \end{bmatrix}$$

The system will now be properly scaled and can be programmed on the analog computer.

Note that the analysis so far has been based on the assumption that the maximum values of the physical variables have been correctly estimated.

Therefore, it is not unreasonable to expect that most simulations will require changes in the original estimates.

Rescaling is relatively simple. If, for instance, the ith state variable x_i overloads, then double the ith column of A_s, half the ith row of A_s and B_s, and double the ith column of H_s (see C.9). All changes require either multiplication or division by a factor of two. The concept, therefore, is easily used as an iterative procedure for computerized automatic scaling.

C.5 COMPUTER PATCHING DIAGRAMS

Analog simulation of state space equations is relatively simple. Figure C.3 illustrates the only logical approach that can be taken to simulate a dynamical system described by equation C.1.

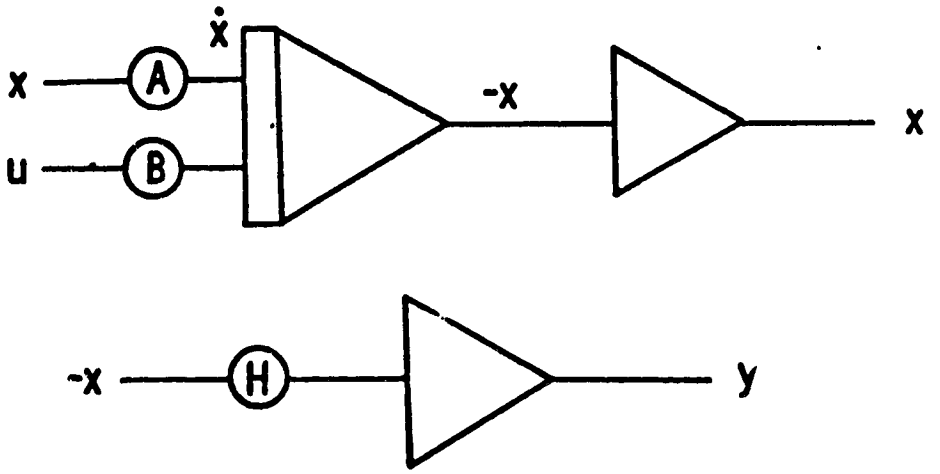

Figure C.3 State Space Simulation of a Dynamical System

Extending this approach to the set of scaled equations C.10 and C.11, it is possible to generate the computer programs required for the simulation (figures C.4 to C.7).

Note that for very low coefficient values, it may become necessary to patch the output of 1 potentiometer into the input of another to increase the effective value of the coefficient. In this way, increased accuracy can be obtained.

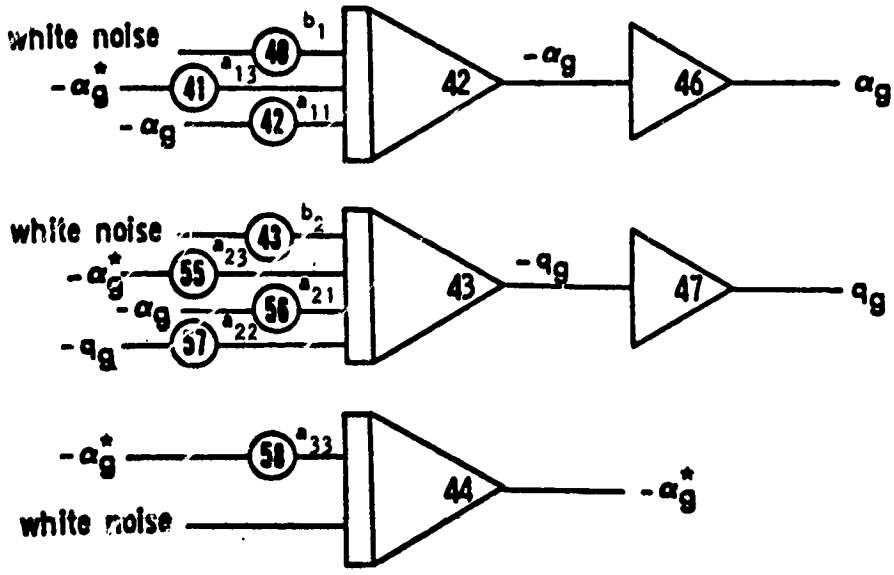

FIGURE C.4 Simulation of Disturbances

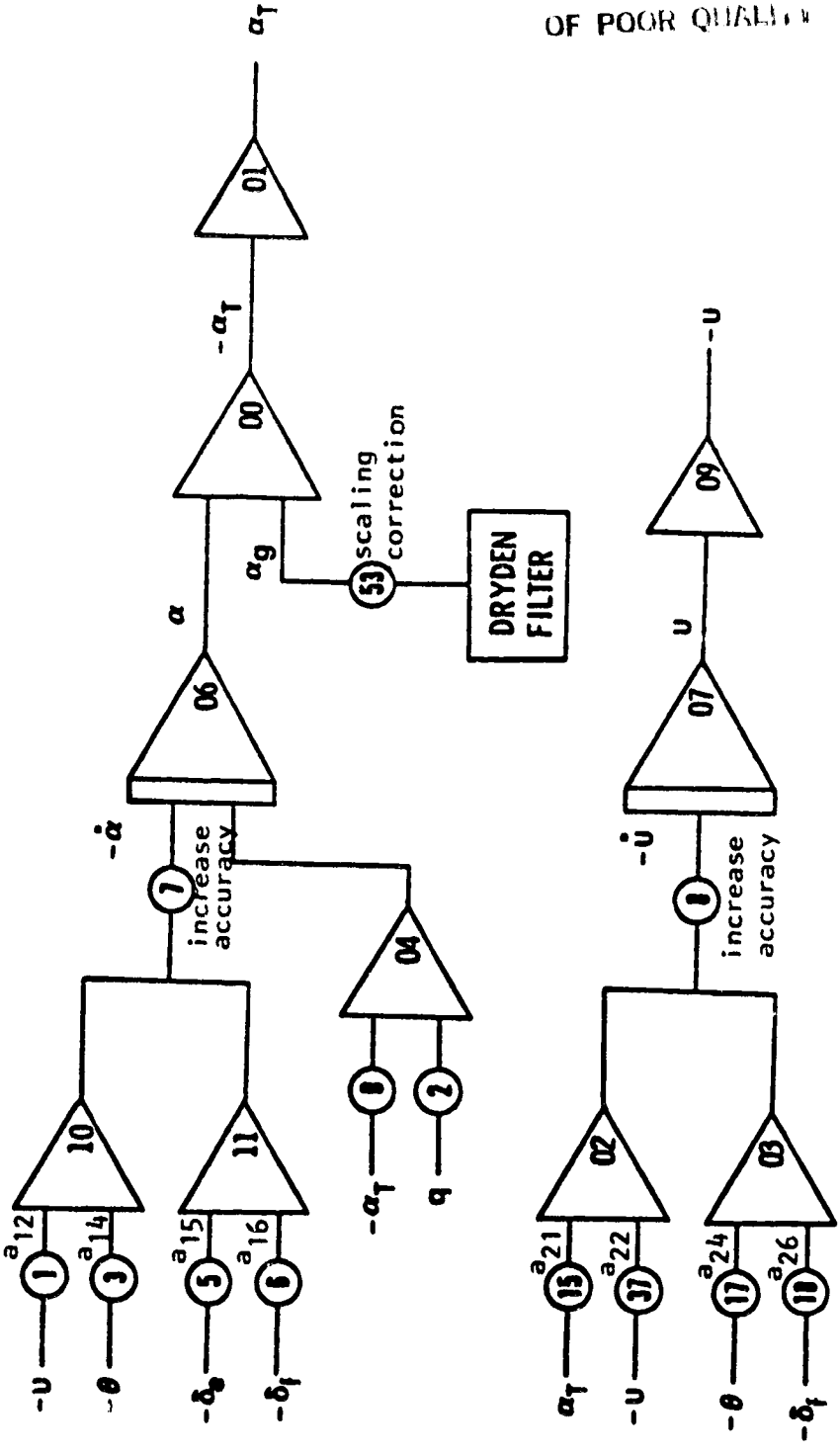

FIGURE C.5 Simulation of Angle of Attack and Forward Velocity

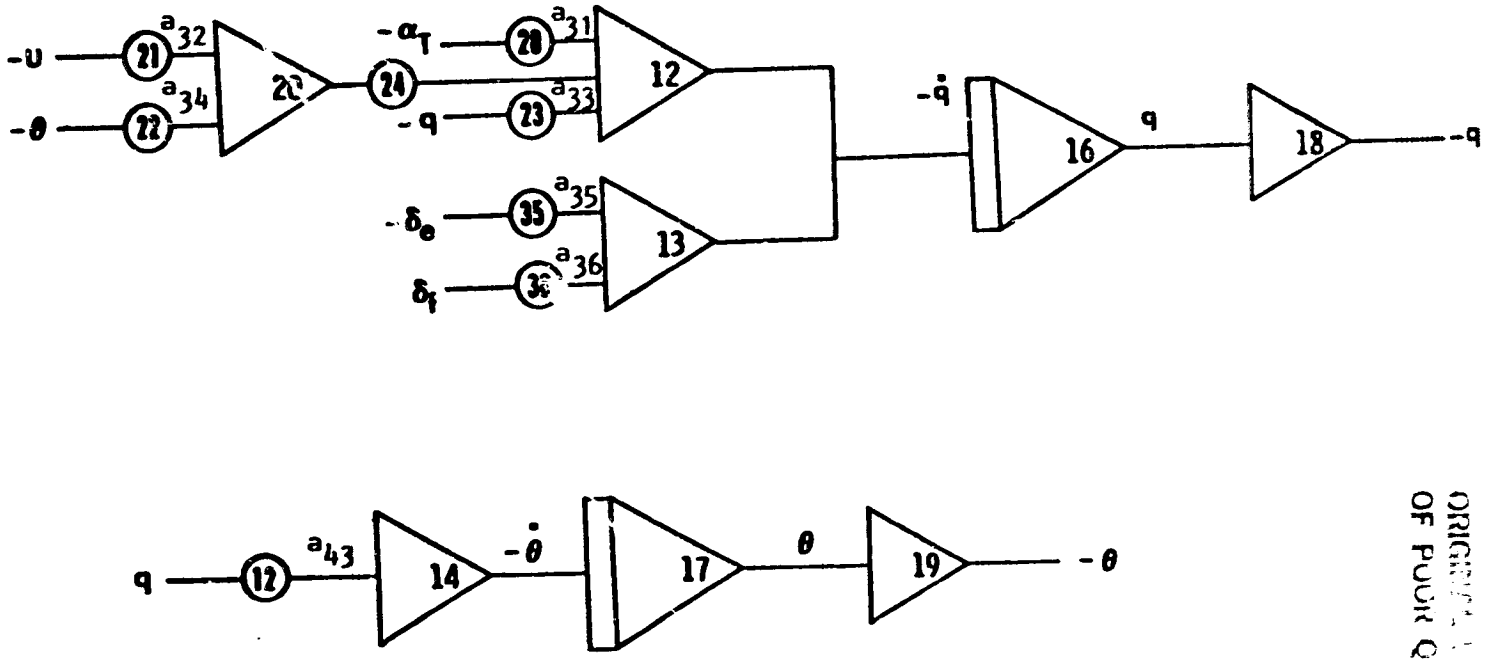

FIGURE C.6 Simulation of [illegible] Rate and Attitude Angle

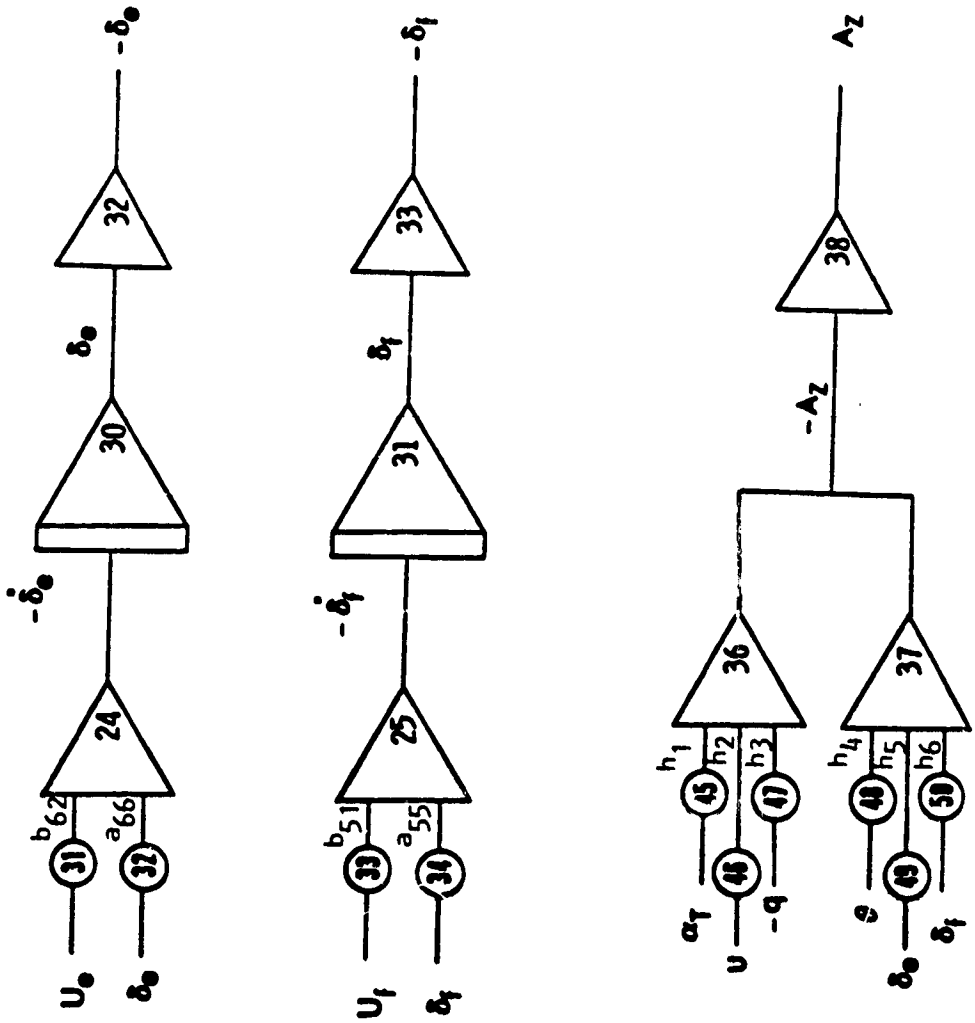

FIGURE C.7 Simulation of the Controls and Acceleration

APPENDIX D. SERVO REQUIREMENTS

In this appendix, the basic performance that a ROAS would require from an electromechanical actuator (EMA) are estimated. This is done to insure that the servo demands of the ROAS are realistic. The process of estimating these requirements will consist of an aerodynamic load analysis, a conversion of those loads into actuator loads, and finally an examination of the characteristics of current EMAs.

For the Cessna 402B, the following aerodynamic data will be used to calculate the aerodynamic torques acting on the direct lift flaps. This analysis is done only for the flaps, because any actuator that can meet the requirements imposed by the flap can easily meet the requirements for the elevator control.

Table D.1 Aerodynamic Data

Flap Lift Curve Slope ($C_{l.\delta f}$)			
0 deg trim		0.95 /rad	(0.0166/deg)
30 deg trim		0.34 /rad	(0.0059/deg)
Reference Area	195.7 ft^2		
Wing Chord at Flap	5.55 ft		
Flap Chord	1.66 ft		

Using the maximum flap deflections from the digital simulation, maximum lift values were calculated for each of the flight conditions by the standard lift equation shown below

$$L = q S C_{L\delta f} \delta_f . \qquad (D.1)$$

These lift values were first divided by 2 to account for the load per flap, and then were converted into torques by assuming that the flaps were symmetric airfoils, and that the center of pressure was at 25% flap chord. An estimate of the dimension for the torque lever arm for this calculation was taken from Figure D.1 [34]. The lever arm was taken to be approximately 4 inches, and the resultant torques (in in-lbf) are shown in Table D.2.

Table D.2 Maximum Torques for Each Flight Condition

Flight Condition	L(lbf)	L per flap	Torque(in-lbf)
Takeoff (SL)	956.4	478.2	1912.9
Climb (500 ft)	981.3	490.6	1962.5
Climb (5000 ft)	946.9	473.5	1893.8
Cruise (20,000 ft)	470.4	235.2	940.7
Approach (SL)	618.0	309.0	1236.0

From Table D.2, the climb at 500 ft demands the maximum torque per flap from all of the flight conditions. Therefore, the maximum torque requirement will be set at 2000 in-lbf. Figure D.2 shows a linear variation of the servo torque required as a function of the direct lift flap deflection for this flight condition (Model B design).

The control surface rate of deflection required is from 100 to 150 deg/sec. Again using Figure D.1 for a reference, a moment arm of 4 inches is estimated, and the rate requirement for a linear actuator can be

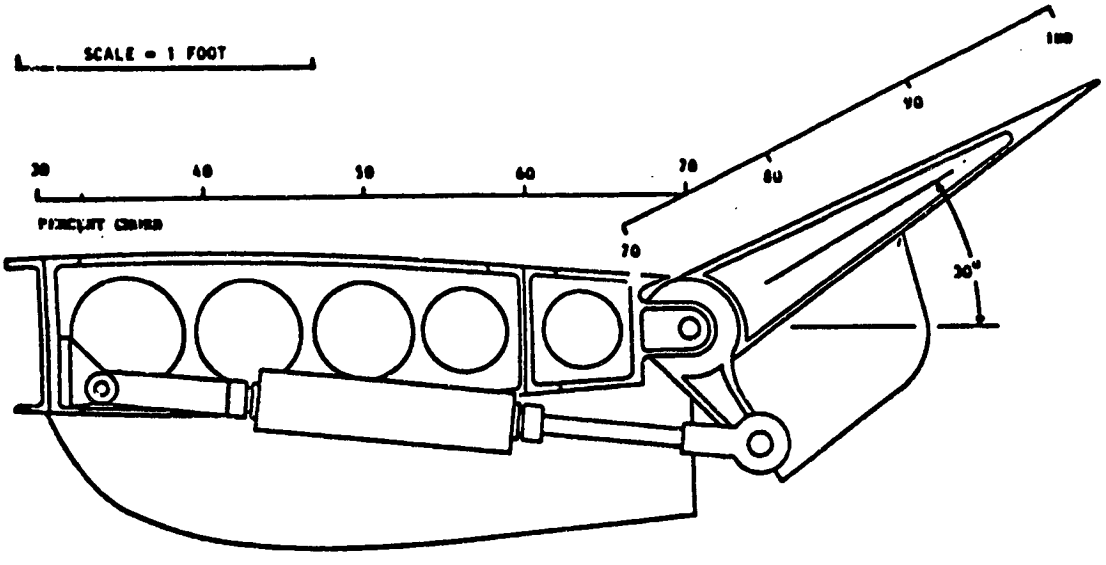

FIGURE D.1 Sample Servo and Flap Mechanism

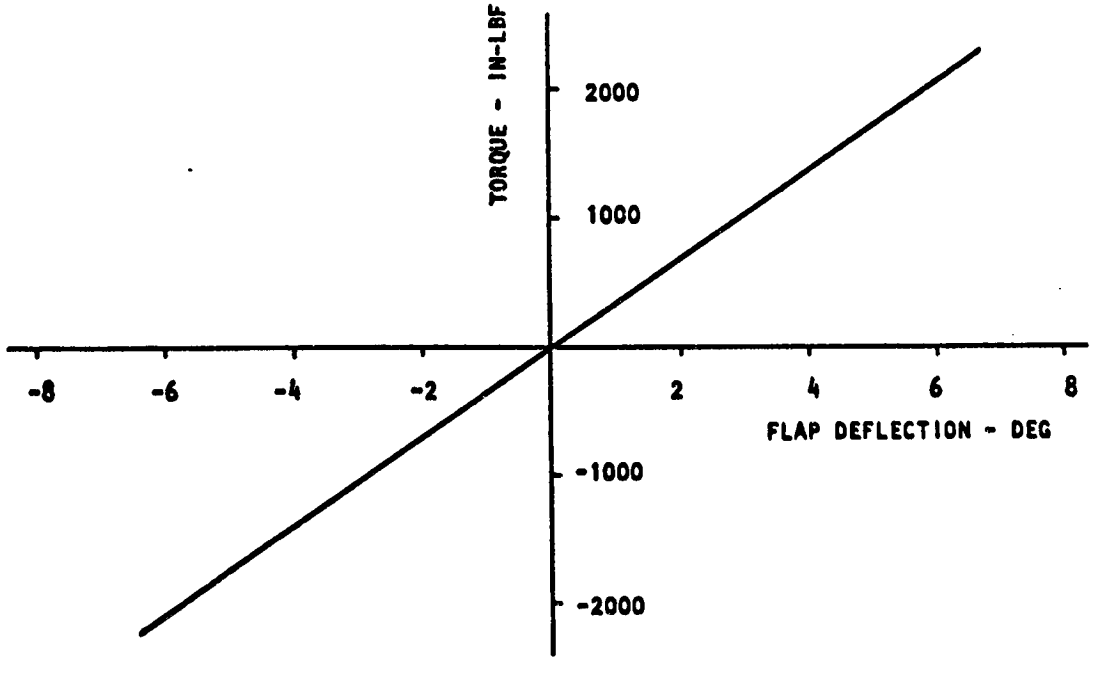

FIGURE D.2 Torque Requirements for the Climb Configuration [full flap control power (Model B)]

estimated from equation (D.2) below,

$$V_{act} = \delta_f \, dh \qquad (D.2)$$

where, V_{act} is the actuator rate in in/sec, δ_f is the control surface rate of deflection in rad/sec, and dh is the moment arm in inches. Based upon the lever arm estimated, the linear actuator rates required will be from 6.98 to 10.47 in/sec corresponding to control surface rates of deflection from 100-150 deg/sec, respectively. Actuator loads, which for a linear actuator are the torque divided by the lever arm, of up to 500 lbf would be required for this particular setup. Studies into an optimum moment arm would involve tradeoffs between the angular rates and torques required versus the actuator operating loads and linear rates available, and are beyond the scope of this analysis.

Rotary actuator characteristics can be compared directly with the aerodynamic torques, and the flap deflection rates. Based on a survey of current EMAs, torques of 2000 in-lbf and rates of over 100 deg/sec are well within the state-of-the-art. Cited below are some basic calculations based on equations taken from reference 34, which show that even in 1978 these actuator requirements were within the capability of EMAs.

With samarium cobalt actuators, the maximum theoretical efficiency is the ratio of the operating speed to the no-load speed. Therefore, it is important to operate these actuators at speeds near no-load. To achieve this, the design stall torque output must be much higher than what is normally needed. The applied current can then be limited to control torque output and the motor will operate at speeds near no-load. Selecting

the design stall torque as 2000 in-lbf, the peak power (P_{pk}) output occurring at this value is given by

$$P_{pk} = T_{max} * \delta_f/550 \text{ (hp)}, \tag{D.3}$$

where T_{max} is the maximum torque in ft-lbf, and δ_f (at T_{max}) is in rad/sec. The peak power output would be 0.50 hp using a δ_f value at the stall torque of 100 deg/sec, and 0.75 hp at 150 deg/sec. From reference 34, these peak power output values result in a motor length of between 3.8 to 4.2 inches.

The EMA design investigated in reference 34 was for an actuator with approximately the characteristics needed in our case. That actuator produced a torque of 2550 in-lbf at a no load rate of 100 deg/sec, and a full load rate of 75 deg/sec. That particular design example chose a BW of 50 rad/sec. The conclusion was reached that this EMA performed well in both the no-load and load conditions, and could be modeled as a simple first order lag system.

Based on this review, the use of EMA for RQAS applications appears well within the limits of the current technology.

APPENDIX E: SUPPORTING TABLES AND FIGURES

Appendix E includes the additional tables and figures referenced in the body of the report and in the Table of Contents. A brief summary of the tables and figures included is provided below.

Tables E.1 through E.5, and Figures E.1 through E.25 pertain to the digital simulation of the optimal RQAS designs. Tables E.1-E.5 are the time history summaries for the five flight conditions. Figures E.1-E.5 are the digital simulation PSDs for the Model A designs, and Figures E.6-E.10 are the PSDs for the Model B designs. Figures E.11-E.25 are plots from the optimal design parameter investigations: Figures E.11-E.15 show the effect of Ts on the five configurations; Figures E.16-E.20 show the effect of Td on the takeoff configuration; and Figures E.21-E.25 show the effect of servo bandwidth on the five flight configurations.

Tables E.6 through E.10, and Figures E.26 through E.40 pertain to the digital simulation of the classical RQAS designs. Tables E.6-E.10 provide the time history summaries for the classical designs. Figures E.26-E.40 provide data on the parametric investigations: Figures E.26-E.30 show the effect of Ts on the nominal designs; Figures E.31-E.35 show the effect Td on the takeoff configuration; and Figures E.36-E.40 show the effect of the servo bandwidth on the five flight configurations.

Figures E.41 through E.50 are PSD plots from the KU hybrid and the NASA moving base simulation. Figures E.41-E.45 are from the hybrid simulator for Model A for both optimal and classical designs, and Figures E.46-E.50 are PSD plots for Model C for only the optimal designs from the NASA simulation.

TABLE E.1 TAKEOFF CONFIGURATION SUMMARY
(MODEL A)

THE ALTITUDE IS:	Sea Level
THE AIRSPEED IS:	183.86 ft/sec
THE SAMPLE TIME IS:	0.100 sec
THE TURBULENCE INTENSITY IS:	6.00 ft/sec

OPEN LOOP RESPONSE:

	Az(ft/s2)	Alfa(deg)	Q(deg/s)	Thet(deg)	D-e(deg)	D-f(deg)
MAX	-8.939	2.394	-1.615	-1.123	0.000	0.000
RATE	-126.660	33.263	-23.191	1.580	0.000	0.000
RMS	3.095	0.877	0.614	0.583	0.000	0.000

Z-REAL	Z-IMAG	W'-REAL	W'-IMAG	FREQUENCY	DAMPING
0.515923	0.000000	-6.386562	0.000000	6.386562	1.000000
0.809889	0.000000	-2.100803	0.000000	2.100803	1.000000
0.999542	0.015149	-0.003431	0.151556	0.151594	0.022631
0.999542	-0.015149	-0.003431	-0.151556	0.151594	0.022631
0.367879	0.000000	-9.242343	0.000000	9.242343	1.000000
0.367879	0.000000	-9.242343	0.000000	9.242343	1.000000

3.50 ft/sec^2 IS THE RMS VALUE FROM THE DIGITAL PSD

NOMINAL DESIGN:

	Az(ft/s2)	Alfa(deg)	Q(deg/s)	Thet(deg)	D-e(deg)	D-f(deg)
MAX	-7.105	2.604	-1.700	-1.678	-0.341	-14.414
RATE	-129.025	32.802	-7.564	1.699	2.601	-102.658
RMS	2.403	0.949	0.697	0.916	0.144	5.263

PROTOTYPE DESIGN:

	Az(ft/s2)	Alfa(deg)	Q(deg/s)	Thet(deg)	D-e(deg)	D-f(deg)
MAX	-6.390	2.625	-1.781	-1.694	-0.351	-14.540
RATE	-119.873	32.802	8.248	1.780	2.654	-102.985
RMS	2.261	0.960	0.706	0.919	0.146	5.355

MINIMUM Td DESIGN:

	Az(ft/s2)	Alfa(deg)	Q(deg/s)	Thet(deg)	D-e(deg)	D-f(deg)
MAX	-5.848	2.657	-1.849	-1.712	-0.356	-14.719
RATE	-132.056	32.887	8.345	1.848	3.280	101.880
RMS	2.028	0.977	0.718	0.923	0.148	5.475

Z-REAL	Z-IMAG	W'-REAL	W'-IMAG	FREQUENCY	DAMPING
0.389104	0.332495	-7.235152	6.518994	9.738824	0.742918
0.389104	-0.332495	-7.235152	-6.518994	9.738824	0.742918
0.314105	0.000000	10.438976	0.000000	0.438976	1.000000
0.889470	0.000000	-1.169956	0.000000	1.169956	1.000000
0.995260	0.005682	-0.047349	0.057087	0.074167	0.638404
0.995260	-0.005682	-0.047349	-0.057087	0.074167	0.638404

2.76 ft/sec^2 IS THE RMS VALUE FROM THE DIGITAL PSD

TABLE E.2 CLIMB (Sea Level) CONFIGURATION SUMMARY
(MODEL A)

THE ALTITUDE IS:	Sea Level
THE AIRSPEED IS:	210.85 ft/sec
THE SAMPLE TIME IS:	0.100 sec
THE TURBULENCE INTENSITY IS:	6.00 ft/sec

OPEN LOOP RESPONSE:

	Az(ft/s2)	Alfa(deg)	Q(deg/s)	Thet(deg)	D-e(deg)	D-f(deg)
MAX	-9.659	2.029	-1.201	-1.292	0.000	0.000
RATE	222.913	-45.271	-7.607	1.201	0.000	0.000
RMS	3.718	0.784	0.540	0.577	0.000	0.000

Z-REAL	Z-IMAG	W'-REAL	W'-IMAG	FREQUENCY	DAMPING
0.490186	0.000000	-6.842280	0.000000	6.842280	1.000000
0.789424	0.000000	-2.353557	0.000000	2.353557	1.000000
0.999218	0.014891	-0.006713	0.149023	0.149174	0.045002
0.999218	-0.014891	-0.006713	-0.149023	0.149174	0.045002
0.367879	0.000000	-9.242343	0.000000	9.242343	1.000000
0.367879	0.000000	-9.242343	0.000000	9.242343	1.000000

3.98 ft/sec^2 IS THE RMS VALUE FROM THE DIGITAL PSD

NOMINAL DESIGN:

	Az(ft/s2)	Alfa(deg)	Q(deg/s)	Thet(deg)	D-e(deg)	D-f(deg)
MAX	-8.558	2.053	-2.272	-2.248	0.607	-9.212
RATE	245.930	-45.205	12.455	2.270	-11.795	123.910
RMS	2.911	0.799	1.030	1.015	0.150	4.170

PROTOTYPE DESIGN:

	Az(ft/s2)	Alfa(deg)	Q(deg/s)	Thet(deg)	D-e(deg)	D-f(deg)
MAX	-8.181	2.061	-2.277	-2.249	0.575	-9.271
RATE	239.071	-45.136	12.726	2.277	-11.335	122.204
RMS	2.738	0.801	1.034	1.017	0.143	4.177

MINIMUM Td DESIGN:

	Az(ft/s2)	Alfa(deg)	Q(deg/s)	Thet(deg)	D-e(deg)	D-f(deg)
MAX	-7.940	2.073	-2.221	-2.254	0.566	-9.255
RATE	227.128	-45.254	14.987	2.220	13.976	122.653
RMS	2.490	0.805	1.036	1.020	0.147	4.188

Z-REAL	Z-IMAG	W'-REAL	W'-IMAG	FREQUENCY	DAMPING
0.401931	0.329953	-7.034567	6.362747	9.485235	0.741633
0.401931	-0.329953	-7.034567	-6.362747	9.485235	0.741633
0.313690	0.000000	10.448573	0.000000	0.448573	1.000000
0.806157	0.000000	-2.146474	0.000000	2.146474	1.000000
0.995781	0.004833	-0.042161	0.048529	0.064285	0.655834
0.995781	-0.004833	-0.042161	-0.048529	0.064285	0.655834

3.05 ft/sec^2 IS THE RMS VALUE FROM THE DIGITAL PSD

TABLE E.3 CLIMB (5000 ft) CONFIGURATION SUMMARY
(MODEL A)

THE ALTITUDE IS:	5000.	ft
THE AIRSPEED IS:	227.34	ft/sec
THE SAMPLE TIME IS:	0.100	sec
THE TURBULENCE INTENSITY IS:	7.02	ft/sec

OPEN LOOP RESPONSE:

	Az(ft/s2)	Alfa(deg)	Q(deg/s)	Thet(deg)	D-e(deg)	D-f(deg)
MAX	8.693	-1.892	1.283	-1.021	0.000	0.000
RATE	-141.080	28.822	-7.653	-1.282	0.000	0.000
RMS	2.738	0.567	0.449	0.600	0.000	0.000

Z-REAL	Z-IMAG	W'-REAL	W'-IMAG	FREQUENCY	DAMPING
0.534976	0.000000	-6.059031	0.000000	6.059031	1.000000
0.773058	0.000000	-2.559899	0.000000	2.559899	1.000000
0.999319	0.014276	-0.005797	0.142849	0.142966	0.040546
0.999319	-0.014276	-0.005797	-0.142849	0.142966	0.040546
0.367879	0.000000	-9.242343	0.000000	9.242343	1.000000
0.367879	0.000000	-9.242343	0.000000	9.242343	1.000000

2.79 ft/sec^2 IS THE RMS VALUE FROM THE DIGITAL PSD

NOMINAL DESIGN:

	Az(ft/s2)	Alfa(deg)	Q(deg/s)	Thet(deg)	D-e(deg)	D-f(deg)
MAX	7.708	-1.915	1.347	-2.030	0.390	11.015
RATE	-124.741	29.099	-8.647	-1.345	-3.022	-117.537
RMS	2.161	0.614	0.546	1.101	0.121	4.318

PROTOTYPE DESIGN:

	Az(ft/s2)	Alfa(deg)	Q(deg/s)	Thet(deg)	D-e(deg)	D-f(deg)
MAX	7.339	-1.933	1.364	-2.049	0.391	11.121
RATE	-131.127	29.184	-8.449	-1.363	-3.131	-117.415
RMS	1.971	0.624	0.555	1.108	0.123	4.398

MINIMUM Td DESIGN:

	Az(ft/s2)	Alfa(deg)	Q(deg/s)	Thet(deg)	D-e(deg)	D-f(deg)
MAX	6.550	-1.960	1.422	-2.077	0.414	11.385
RATE	-122.343	29.295	-8.082	-1.421	-3.353	-117.130
RMS	1.712	0.639	0.565	1.118	0.127	4.515

Z-REAL	Z-IMAG	W'-REAL	W'-IMAG	FREQUENCY	DAMPING
0.381168	0.341437	-7.293053	6.747095	9.935387	0.734048
0.381168	-0.341437	-7.293053	-6.747095	9.935387	0.734048
0.304610	0.000000	10.660500	0.000000	0.660500	1.000000
0.896133	0.000000	-1.095568	0.000000	1.095568	1.000000
0.997721	0.002633	-0.022776	0.026390	0.034860	0.653370
0.997721	-0.002633	-0.022776	-0.026390	0.034860	0.653370

2.15 ft/sec^2 IS THE RMS VALUE FROM THE DIGITAL PSD

TABLE E.4 CRUISE CONFIGURATION SUMMARY
(MODEL A)

THE ALTITUDE IS:	20000.	ft
THE AIRSPEED IS:	357.91	ft/sec
THE SAMPLE TIME IS:	0.100	sec
THE TURBULENCE INTENSITY IS:	3.57	ft/sec

OPEN LOOP RESPONSE:

	Az(ft/s2)	Alfa(deg)	Q(deg/s)	Thet(deg)	D-e(deg)	D-f(deg)
MAX	4.330	-0.599	0.710	-0.629	0.000	0.000
RATE	70.670	-9.167	3.690	-0.710	0.000	0.000
RMS	1.496	0.199	0.262	0.291	0.000	0.000

Z-REAL	Z-IMAG	W'-REAL	W'-IMAG	FREQUENCY	DAMPING
0.648355	0.099974	-4.177678	1.466391	4.427561	0.943562
0.648355	-0.099974	-4.177678	-1.466391	4.427561	0.943562
0.999092	0.010273	-0.008556	0.102820	0.103176	0.082925
0.999092	-0.010273	-0.008556	-0.102820	0.103176	0.082925
0.367879	0.000000	-9.242343	0.000000	9.242343	1.000000
0.367879	0.000000	-9.242343	0.000000	9.242343	1.000000

1.50 ft/sec^2 IS THE RMS VALUE FROM THE DIGITAL PSD

NOMINAL DESIGN:

	Az(ft/s2)	Alfa(deg)	Q(deg/s)	Thet(deg)	D-e(deg)	D-f(deg)
MAX	3.469	-0.601	0.872	-0.828	0.048	3.172
RATE	74.955	-9.180	-4.282	-0.872	-0.990	38.296
RMS	1.271	0.202	0.358	0.371	0.015	1.106

PROTOTYPE DESIGN:

	Az(ft/s2)	Alfa(deg)	Q(deg/s)	Thet(deg)	D-e(deg)	D-f(deg)
MAX	3.345	-0.605	0.929	-0.828	0.049	3.178
RATE	91.878	-9.167	-4.500	-0.929	-1.038	38.596
RMS	1.185	0.203	0.362	0.372	0.015	1.110

MINIMUM Td DESIGN:

	Az(ft/s2)	Alfa(deg)	Q(deg/s)	Thet(deg)	D-e(deg)	D-f(deg)
MAX	-2.957	-0.610	0.976	-0.828	0.053	3.185
RATE	-84.876	-9.078	-4.386	-0.976	-1.115	39.003
RMS	1.058	0.205	0.366	0.373	0.015	1.114

Z-REAL	Z-IMAG	W'-REAL	W'-IMAG	FREQUENCY	DAMPING
0.473915	0.262046	-6.307067	4.677101	7.852030	0.803240
0.473915	-0.262046	-6.307067	-4.677101	7.852030	0.803240
0.312647	0.000000	10.472785	0.000000	0.472785	1.000000
0.725713	0.000000	-3.178820	0.000000	3.178820	1.000000
0.996989	0.003975	-0.030074	0.039873	0.049943	0.602162
0.996989	-0.003975	-0.030074	-0.039873	0.049943	0.602162

1.30 ft/sec^2 IS THE RMS VALUE FROM THE DIGITAL PSD

TABLE E.5 APPROACH CONFIGURATION SUMMARY
(MODEL A)

THE ALTITUDE IS:	Sea Level
THE AIRSPEED IS:	160.25 ft/sec
THE SAMPLE TIME IS:	0.100 sec
THE TURBULENCE INTENSITY IS:	6.00 ft/sec

OPEN LOOP RESPONSE:

	Az(ft/s2)	Alfa(deg)	Q(deg/s)	Thet(deg)	D-e(deg)	D-f(deg)
MAX	-8.915	2.984	-1.324	-1.207	0.000	0.000
RATE	-114.571	39.223	-5.342	1.324	0.000	0.000
RMS	3.033	1.092	0.577	0.604	0.000	0.000

Z-REAL	Z-IMAG	W'-REAL	W'-IMAG	FREQUENCY	DAMPING
0.580511	0.000000	-5.308267	0.000000	5.308267	1.000000
0.833621	0.000000	-1.814757	0.000000	1.814757	1.000000
0.996593	0.021108	-0.031892	0.211779	0.214167	0.148910
0.996593	-0.021108	-0.031892	-0.211779	0.214167	0.148910
0.367879	0.000000	-9.242343	0.000000	9.242343	1.000000
0.367879	0.000000	-9.242343	0.000000	9.242343	1.000000

3.10 ft/sec^2 IS THE RMS VALUE FROM THE DIGITAL PSD

NOMINAL DESIGN:

	Az(ft/s2)	Alfa(deg)	Q(deg/s)	Thet(deg)	D-e(deg)	D-f(deg)
MAX	-7.041	2.964	-2.252	-2.159	0.750	-17.534
RATE	-115.317	39.142	-7.784	2.251	-5.860	99.990
RMS	2.475	1.158	1.008	1.081	0.339	6.819

PROTOTYPE DESIGN:

	Az(ft/s2)	Alfa(deg)	Q(deg/s)	Thet(deg)	D-e(deg)	D-f(deg)
MAX	-6.906	2.970	-2.346	-2.172	0.757	-17.546
RATE	-114.416	39.160	8.484	2.345	-5.883	99.466
RMS	2.380	1.160	1.010	1.082	0.340	6.818

MINIMUM Td DESIGN:

	Az(ft/s2)	Alfa(deg)	Q(deg/s)	Thet(deg)	D-e(deg)	D-f(deg)
MAX	-6.781	2.979	-2.406	-2.183	0.791	-17.515
RATE	-114.326	39.186	8.917	2.406	-6.419	96.663
RMS	2.250	1.164	1.012	1.084	0.341	6.828

Z-REAL	Z-IMAG	W'-REAL	W'-IMAG	FREQUENCY	DAMPING
0.446426	0.312207	-6.423309	5.703391	8.589969	0.747769
0.446426	-0.312207	-6.423309	-5.703391	8.589969	0.747769
0.331634	0.000000	10.038295	0.000000	0.038295	1.000000
0.992731	0.008964	-0.072547	0.090290	0.115824	0.626352
0.992731	-0.008964	-0.072547	-0.090290	0.115824	0.626352
0.843143	0.000000	-1.702065	0.000000	1.702065	1.000000

2.28 ft/sec^2 IS THE RMS VALUE FROM THE DIGITAL PSD

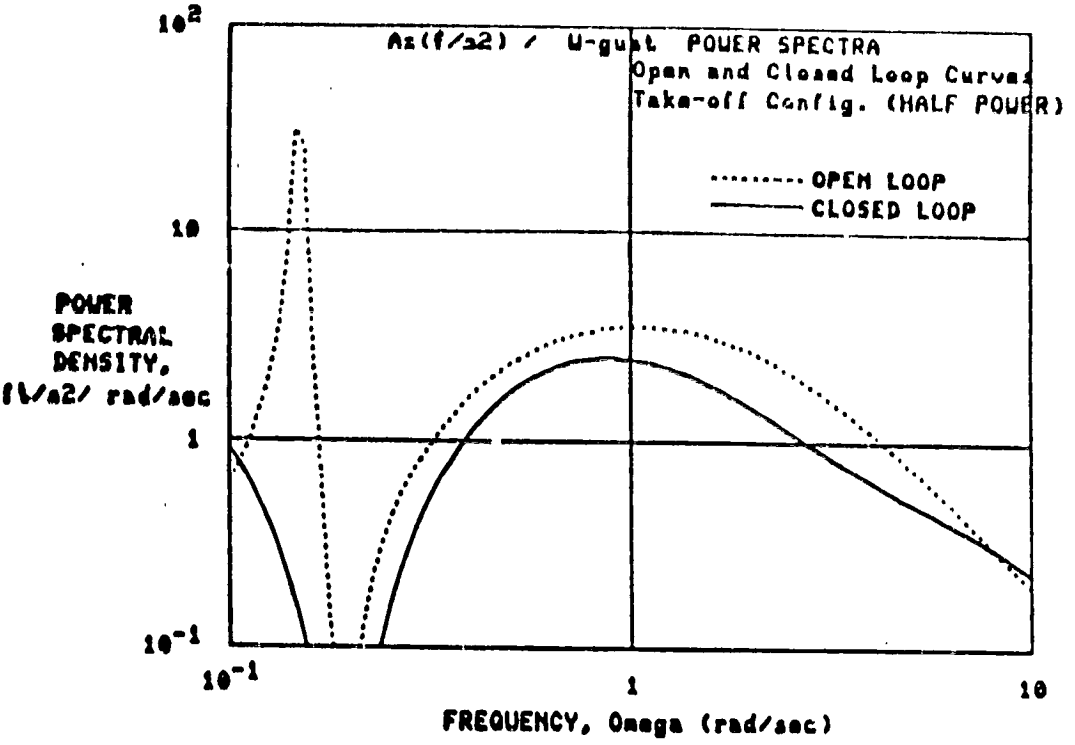

FIGURE E.1 Takeoff Configuration PSD (Model A)

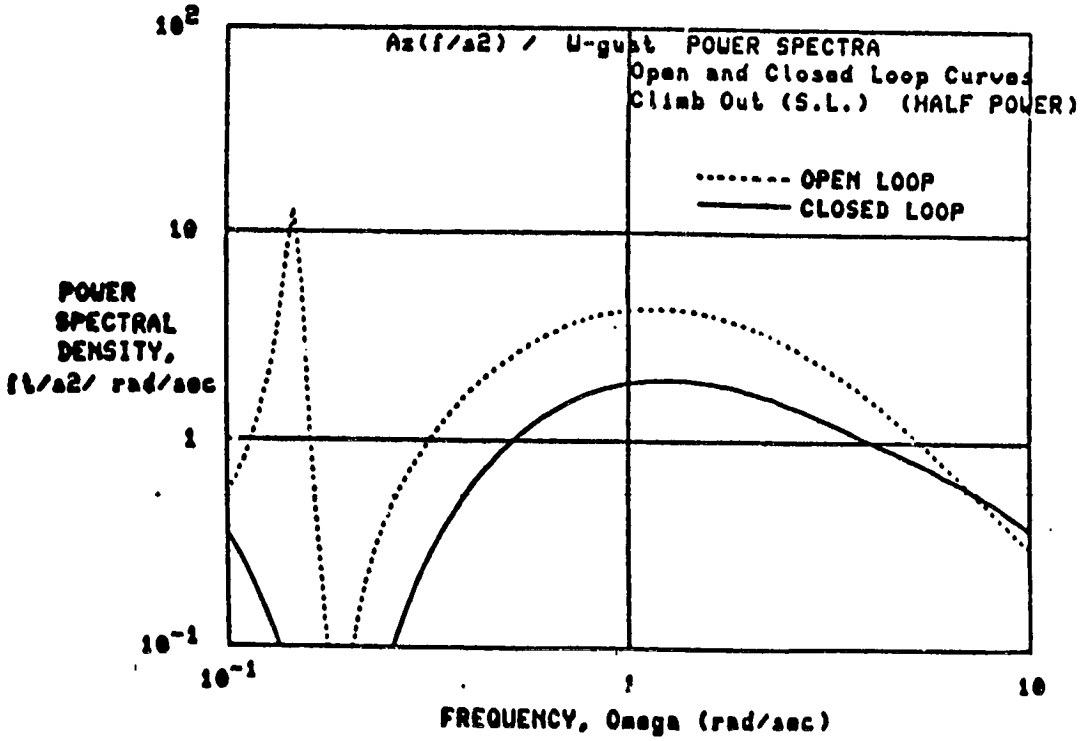

FIGURE E.2 Climb (SL) Configuration PSD (Model A)

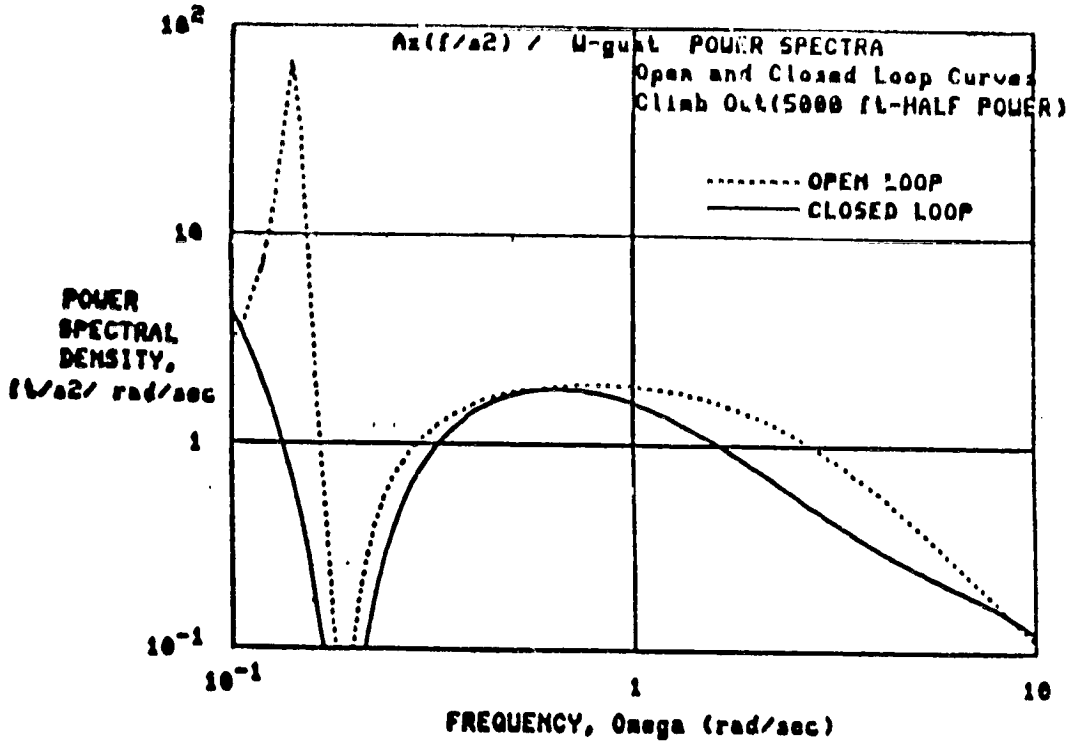

FIGURE E.3 Climb (5000 ft) Configuration PSD (Model A)

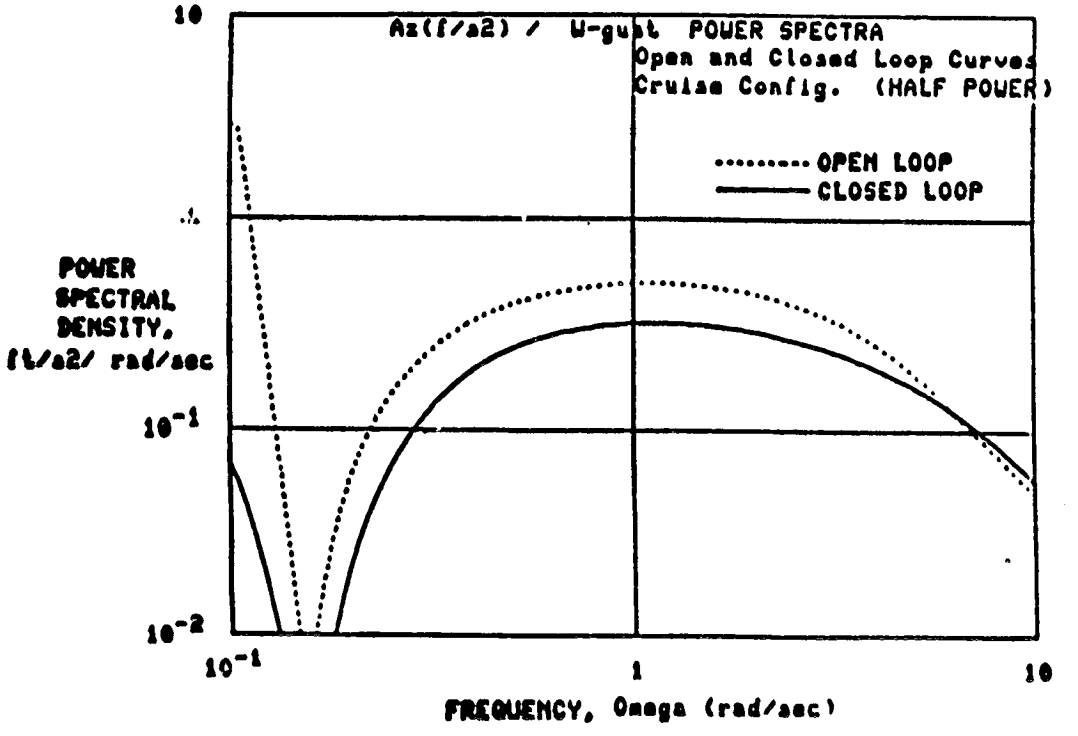

FIGURE E.4 Cruise Configuration PSD (Model A)

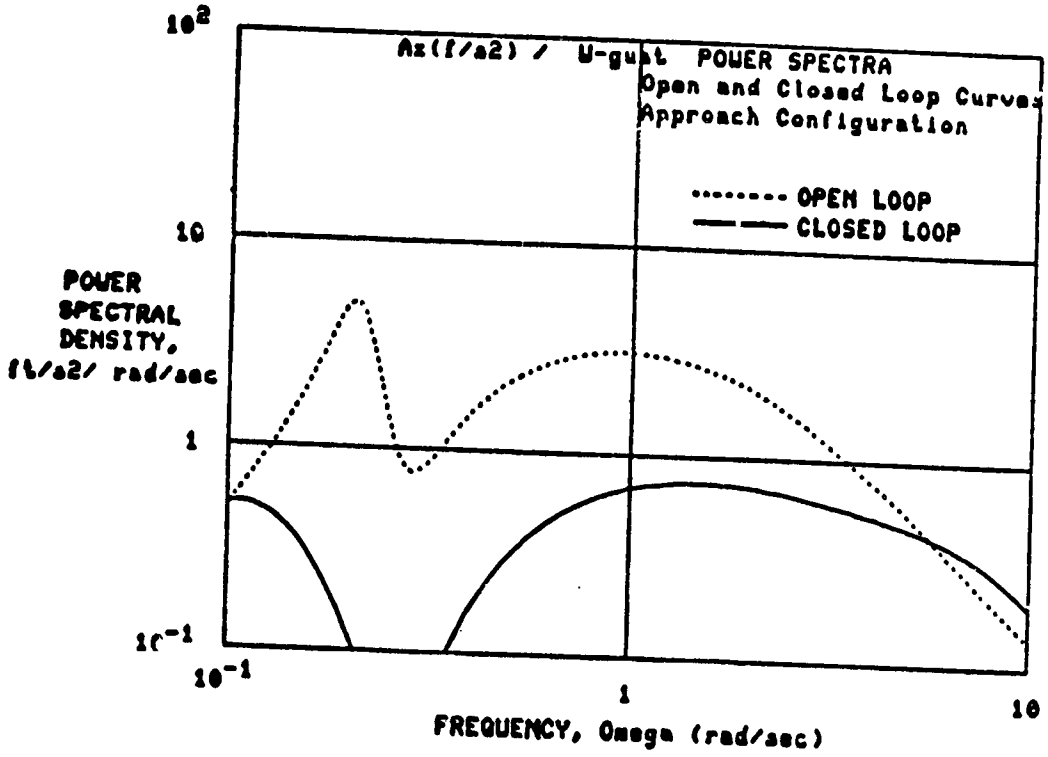

FIGURE E.5 Approach Configuration PSD (Model A)

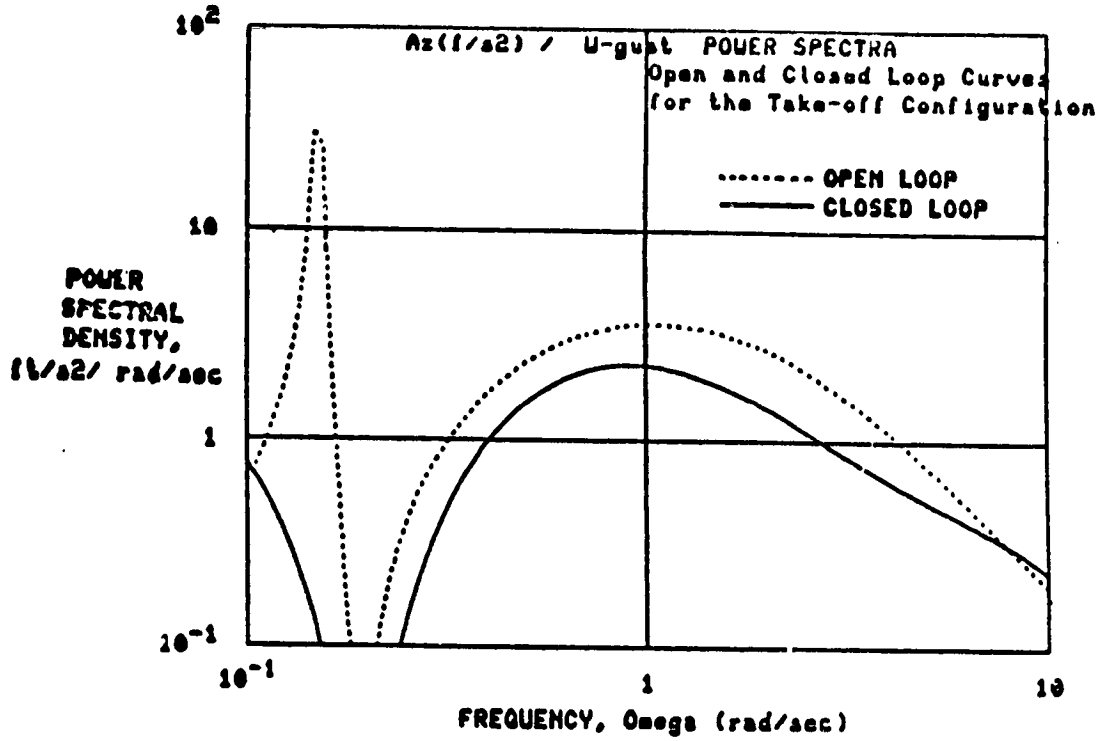

FIGURE E.6 Takeoff Configuration PSD (Model B)

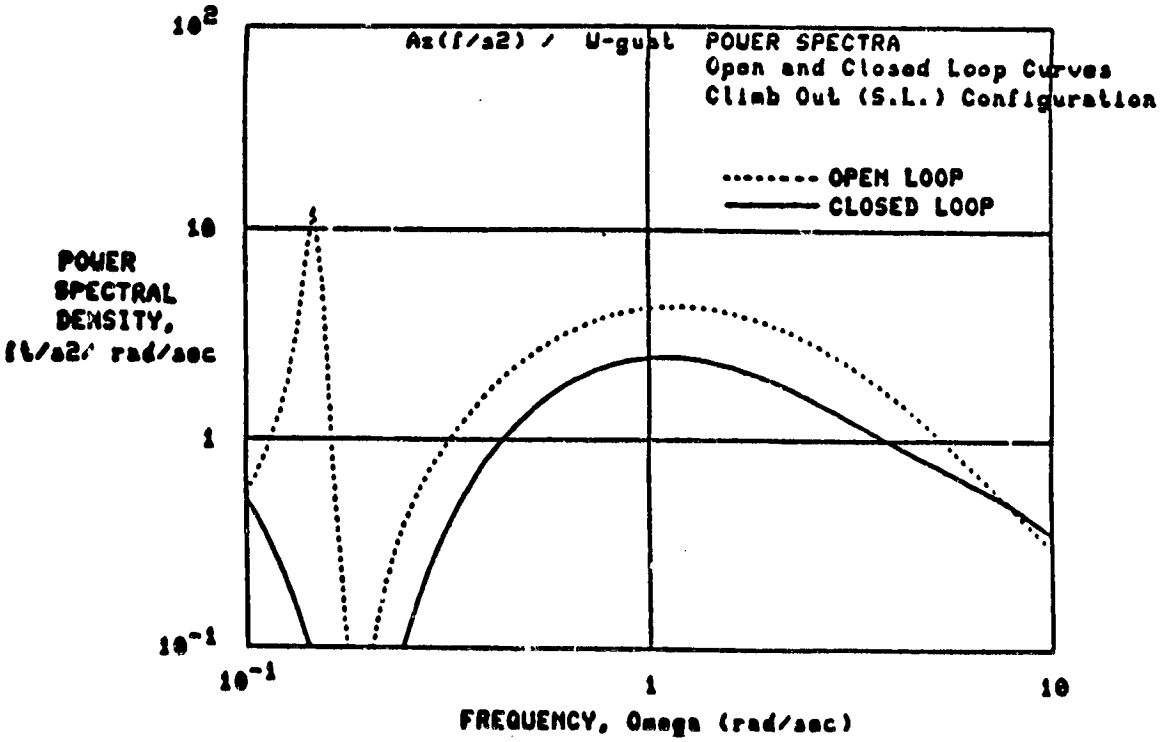

FIGURE E.7 Climb (SL) Configuration PSD (Model B)

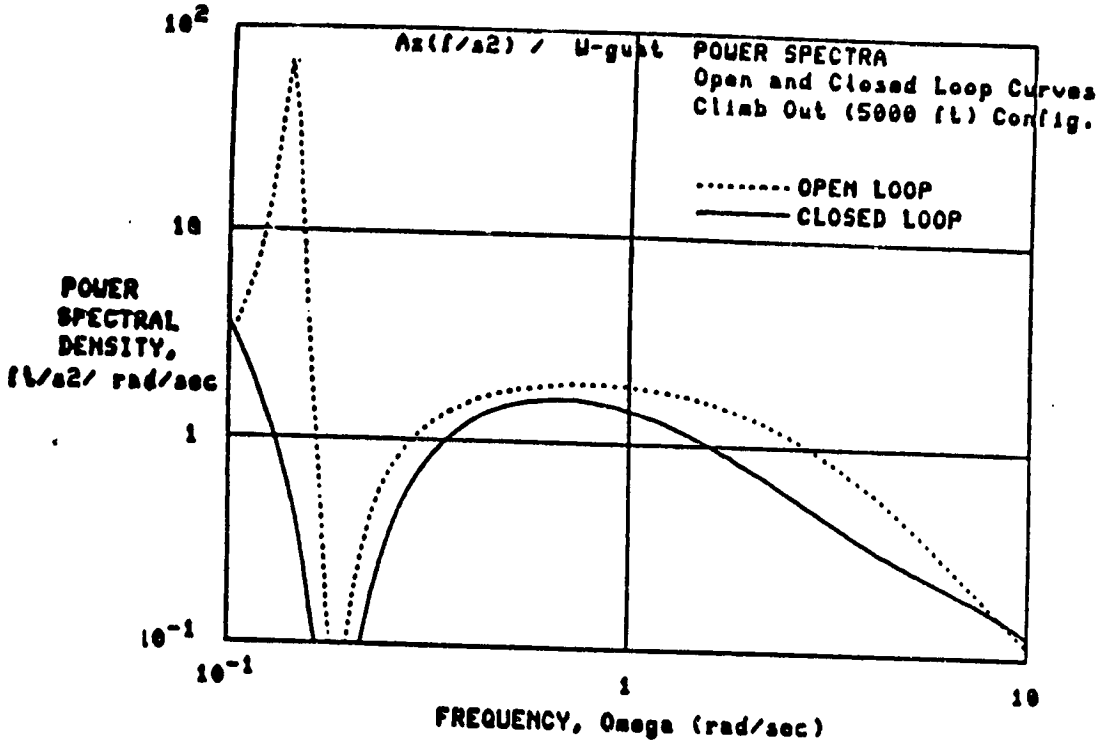

FIGURE E.8 Climb (5000 ft) Configuration PSD (Model B)

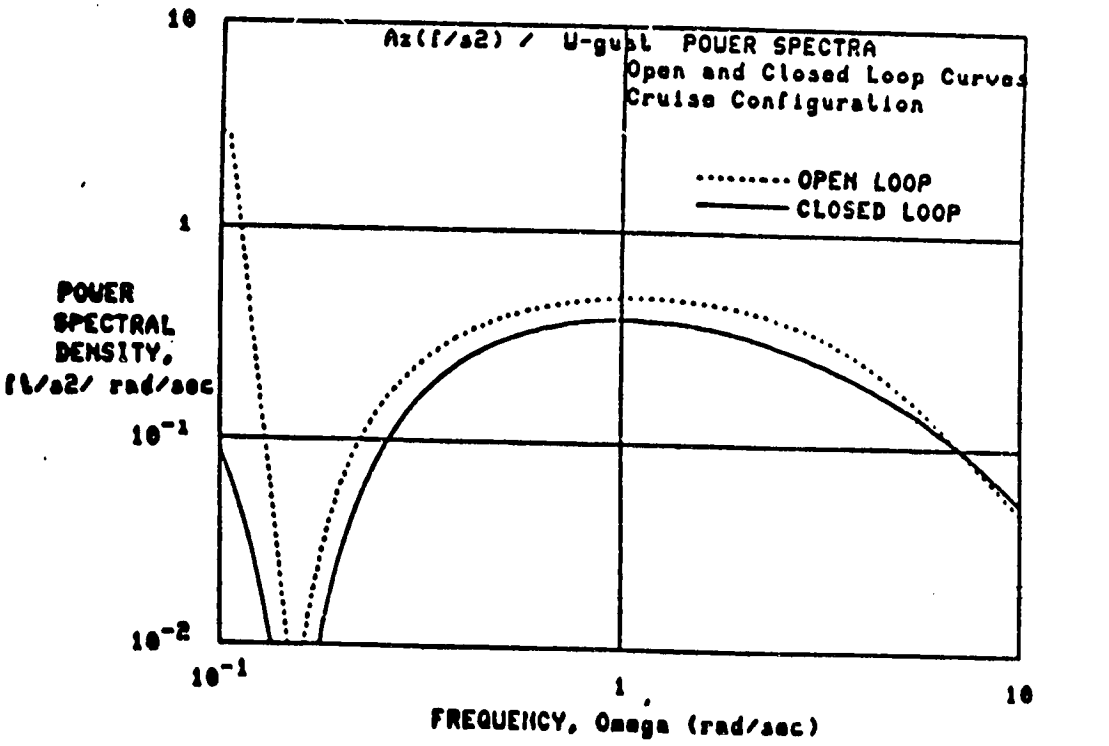

FIGURE E.9 Cruise Configuration PSD (Model B)

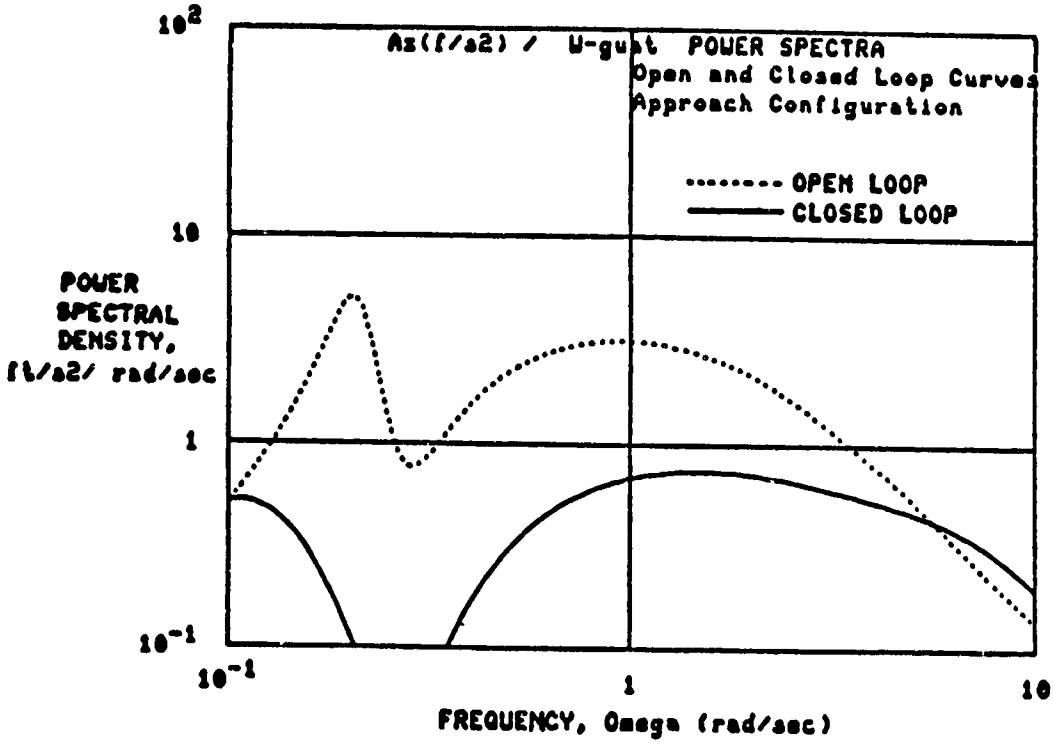

FIGURE E.10 Approach Configuration PSD (Model B)

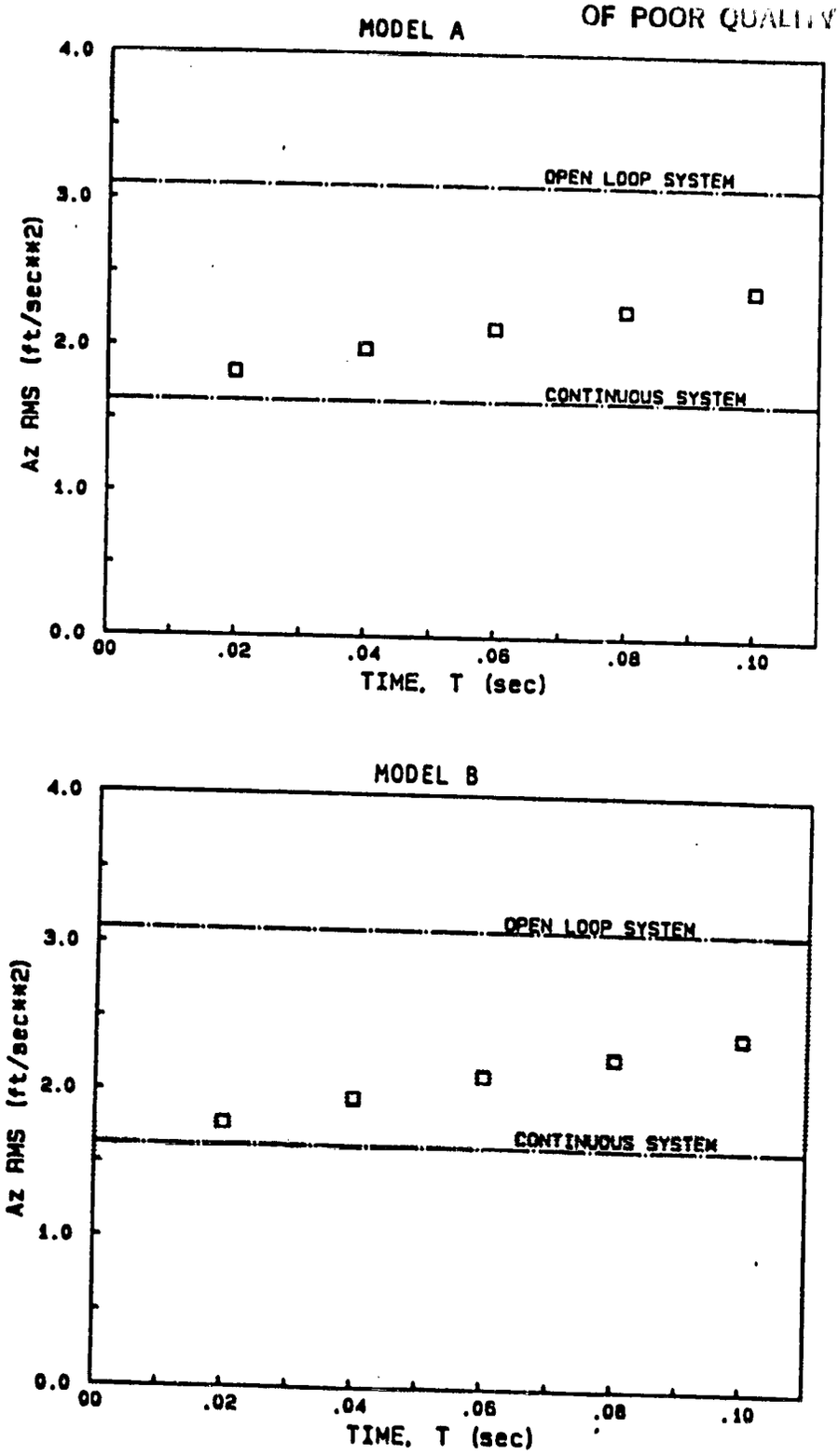

FIGURE E.11 Effect of Sample Time - Takeoff Configuration

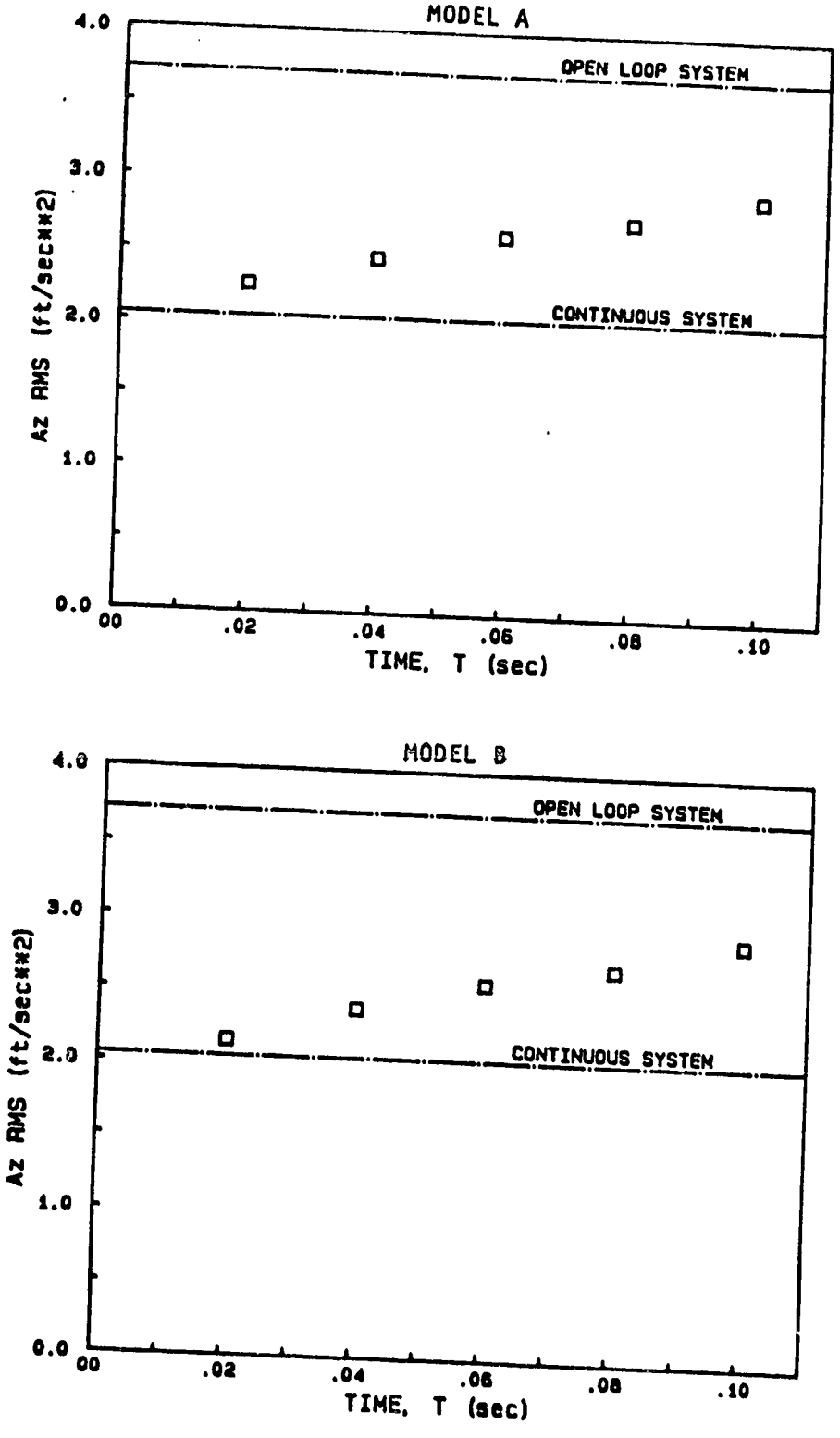

FIGURE E.12 Effect of Sample Time - Climb (SL) Configuration

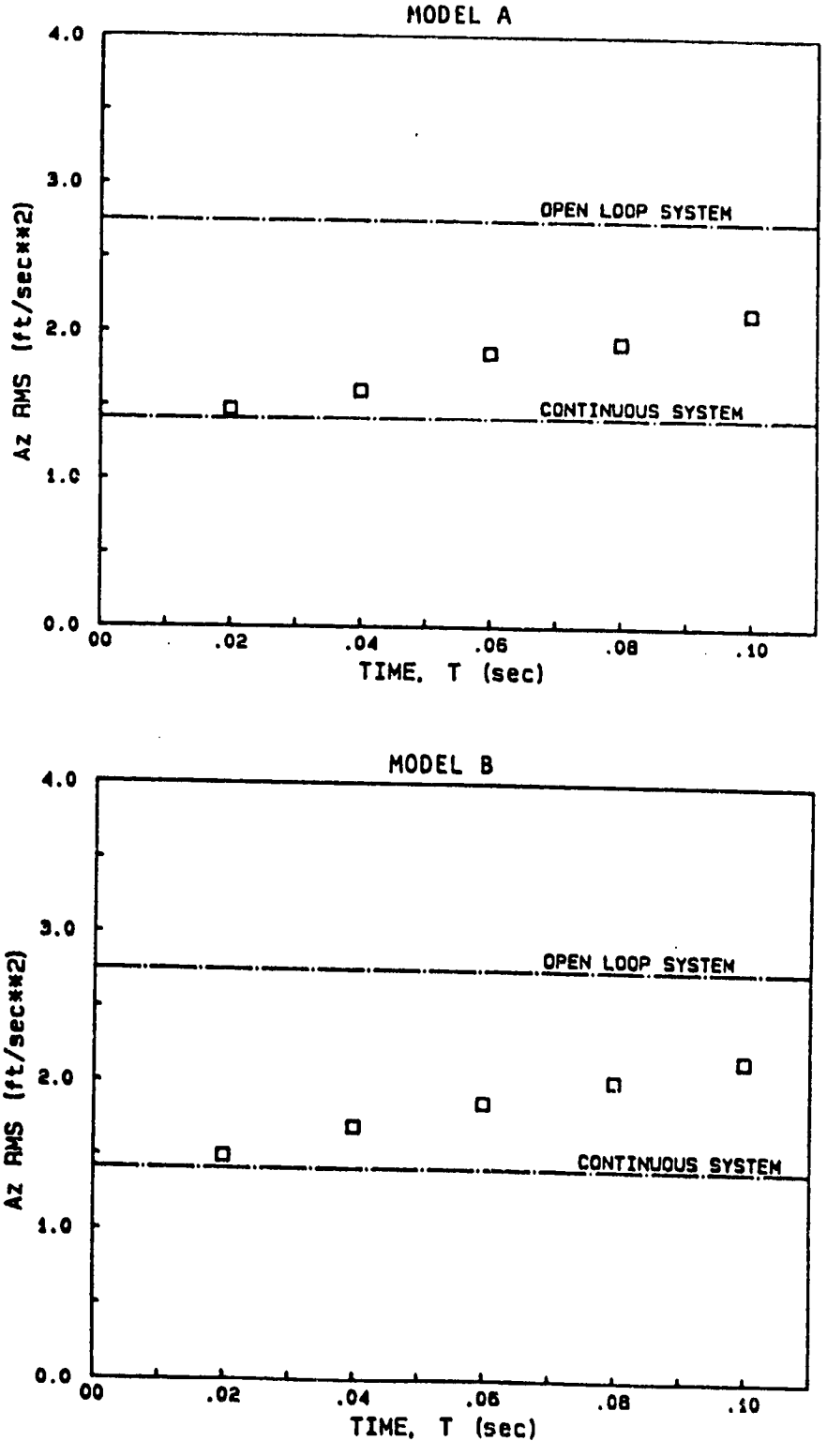

FIGURE E.13 Effect of Sample Time - Climb (5000 ft) Configuration

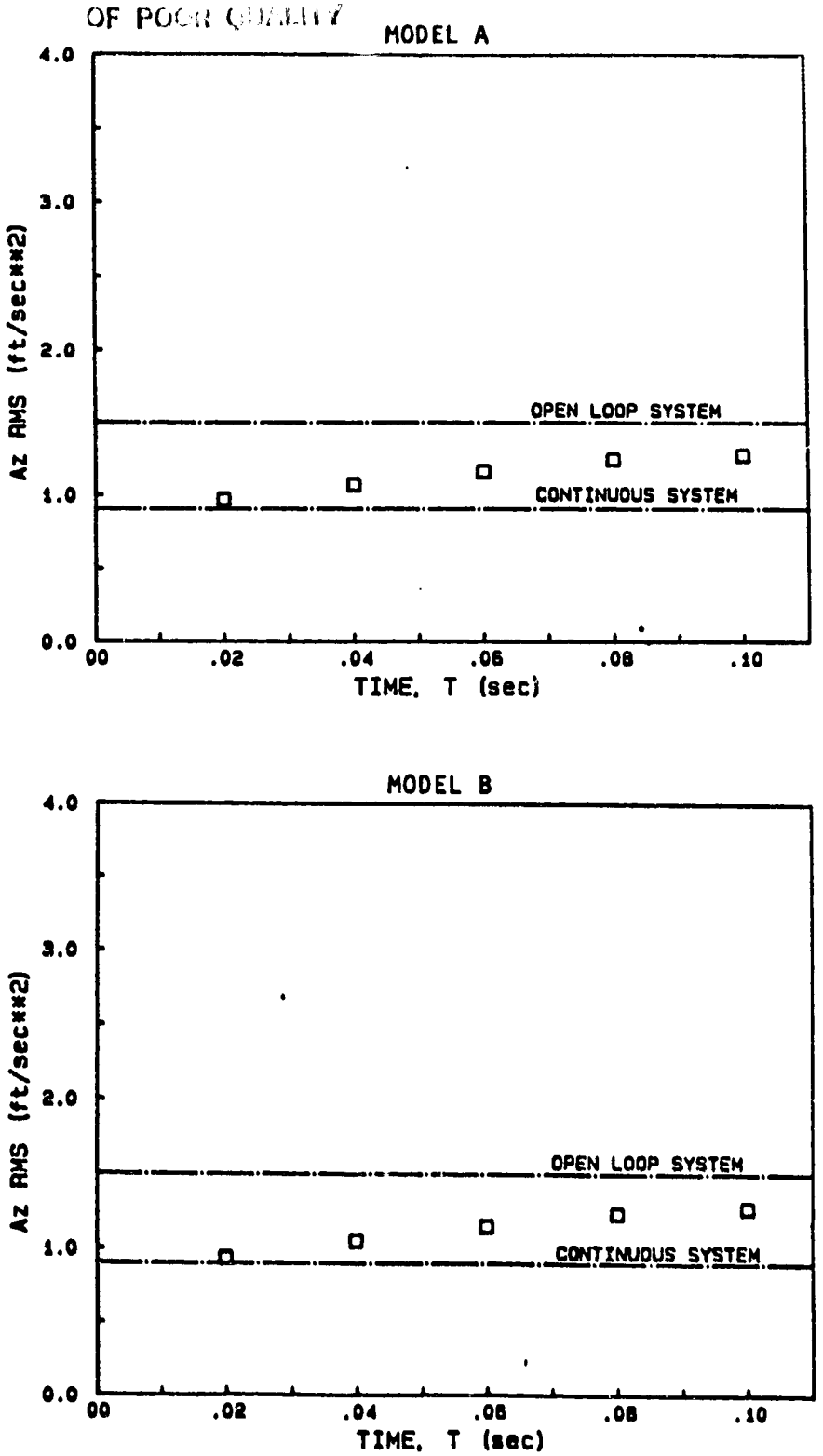

FIGURE E.14 Effect of Sample Time - Cruise Configuration

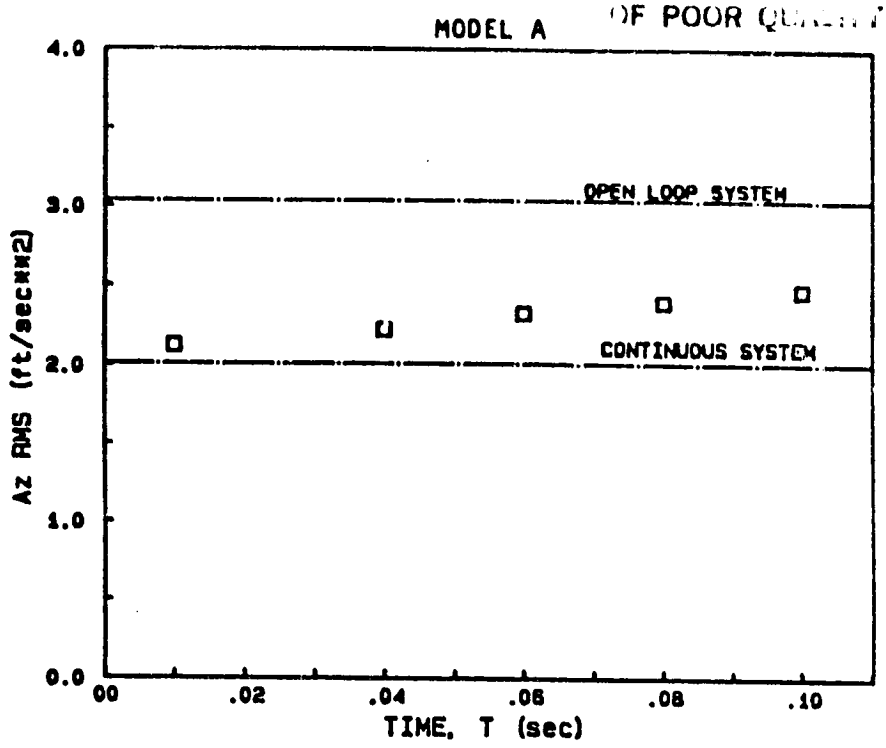

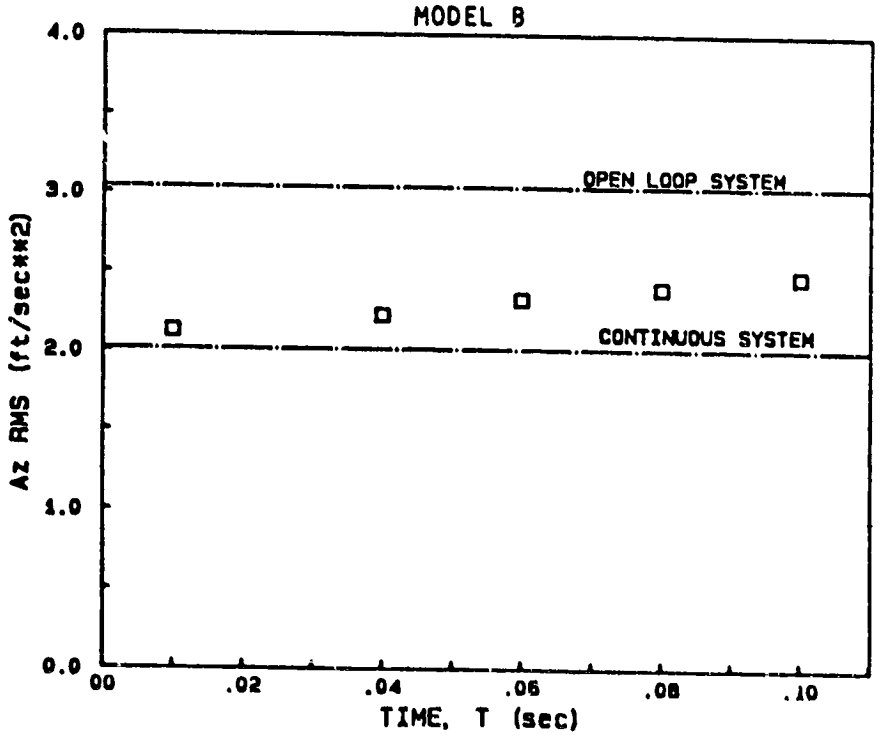

FIGURE E.15 Effect of Sample Time - Approach Configuration

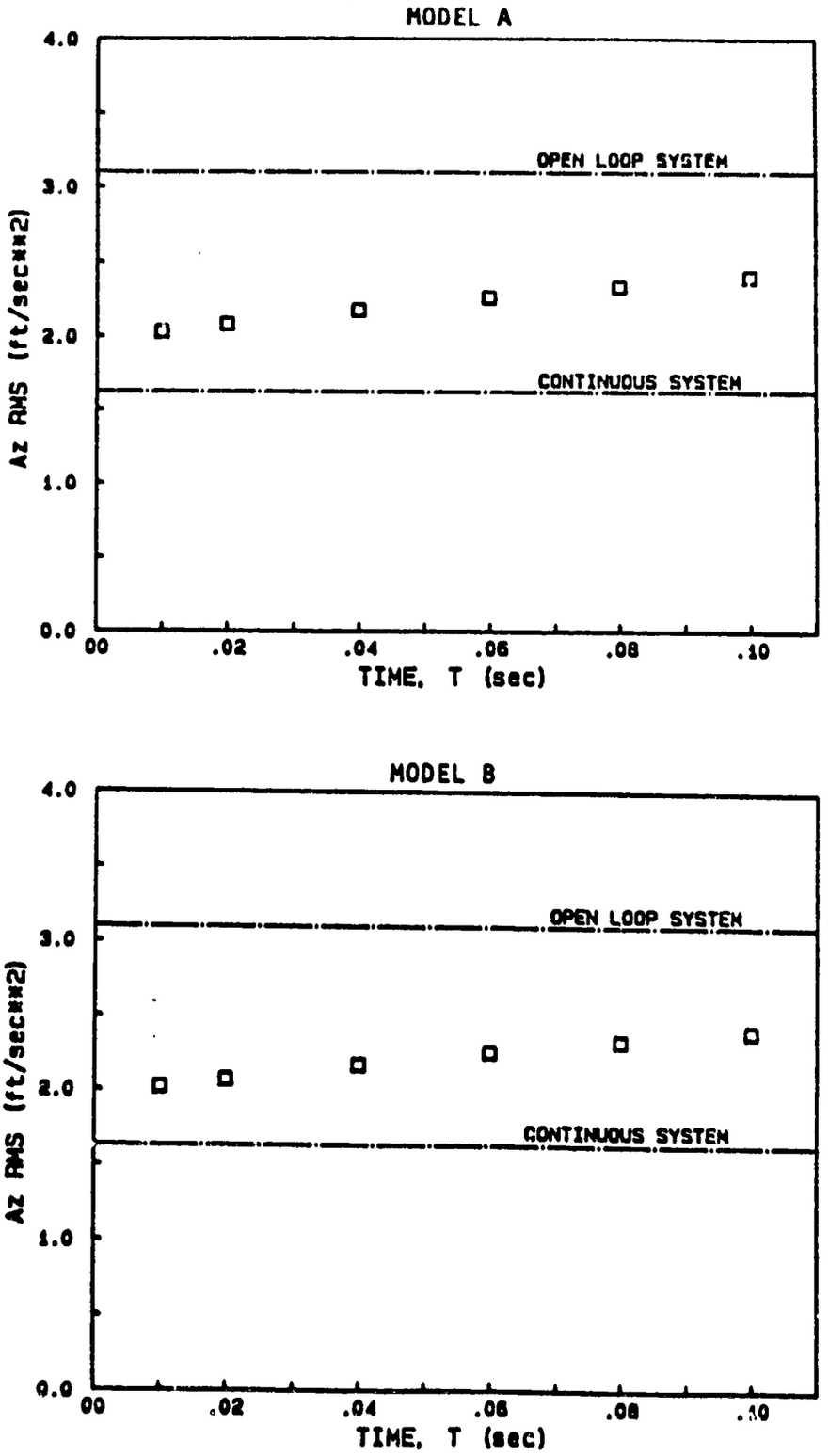

FIGURE E.16 Effect of Delay Time - Takeoff Configuration (Ts = 0.1 sec)

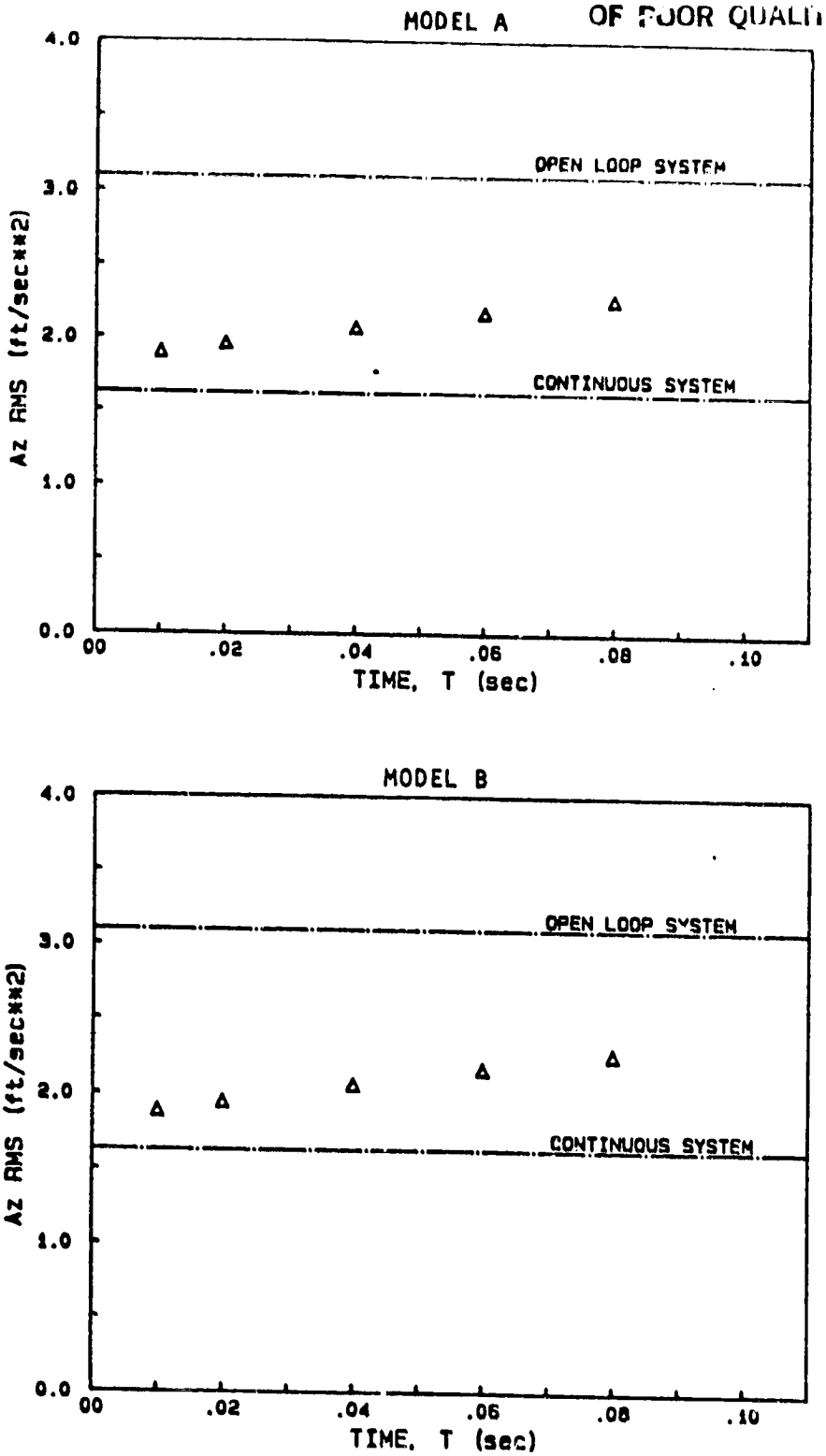

FIGURE E.17 Effect of Delay Time - Takeoff Configuration

(Ts = 0.08 sec)

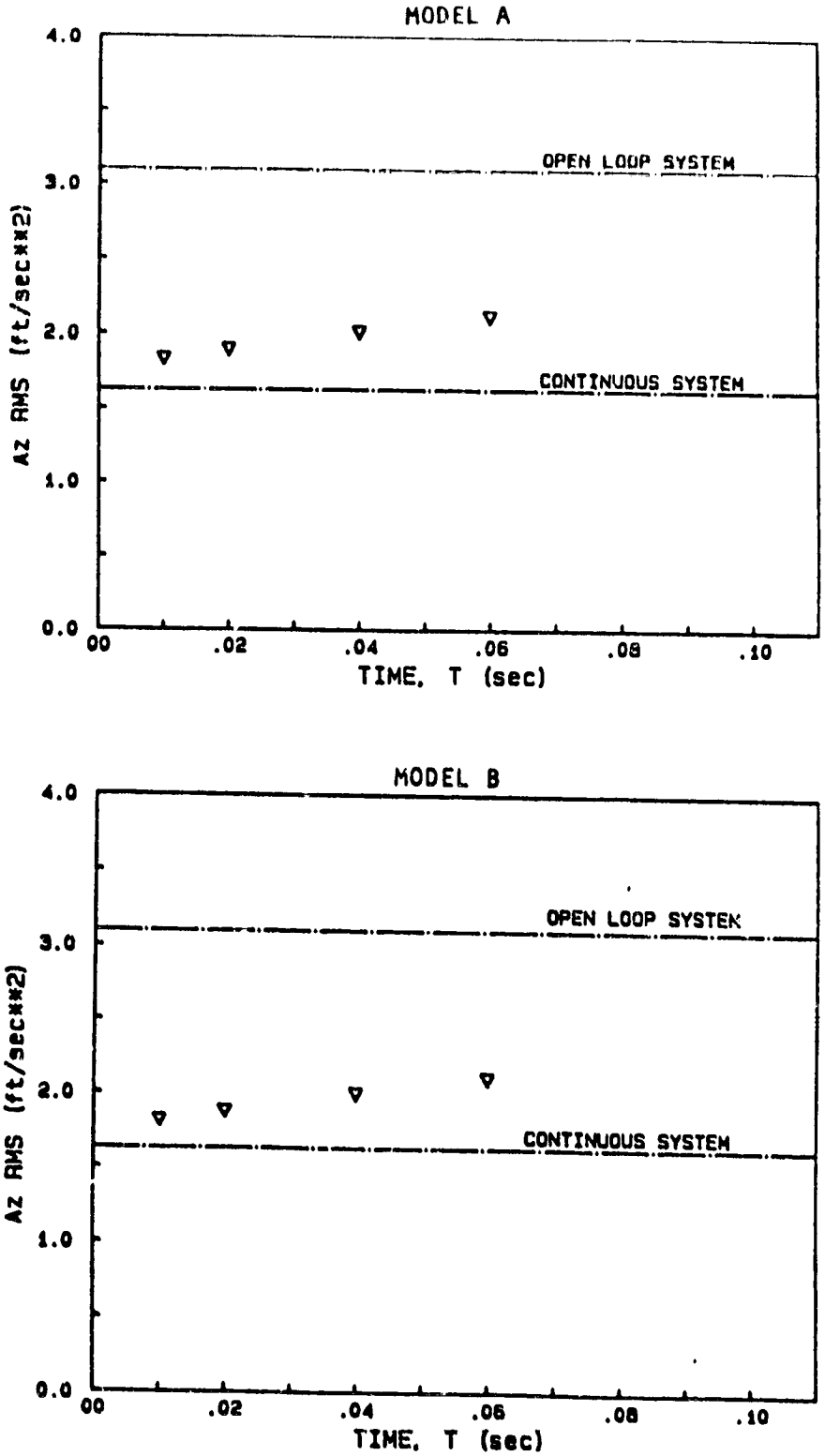

FIGURE E.18 Effect of Delay Time - Takeoff Configuration
(Ts = 0.06 sec)

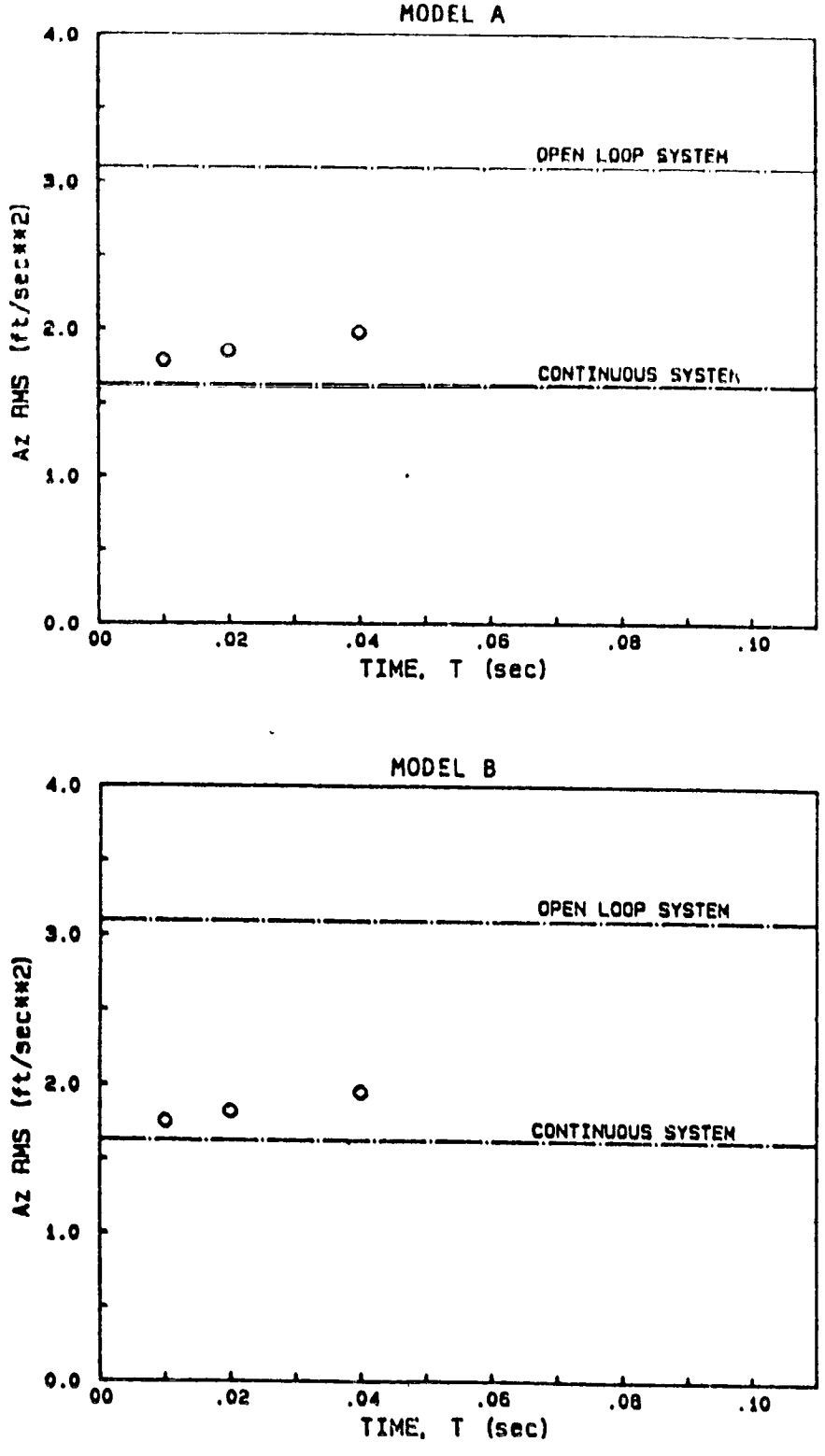

FIGURE E.19 Effect of Delay Time - Takeoff Configuration (T_s = 0.04 sec)

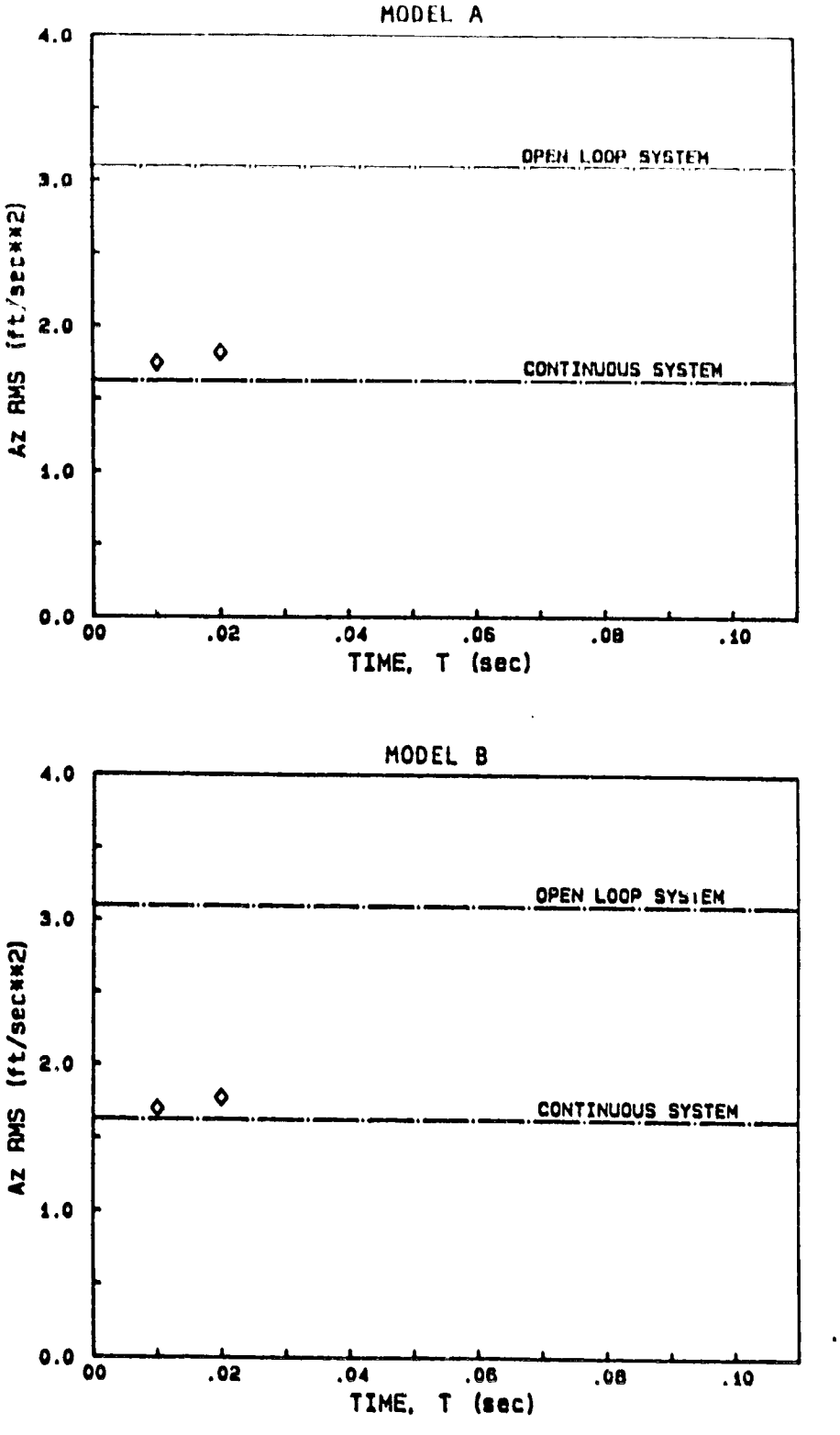

FIGURE E.20 Effect of Delay Time - Takeoff Configuration
(T_s = 0.02 sec)

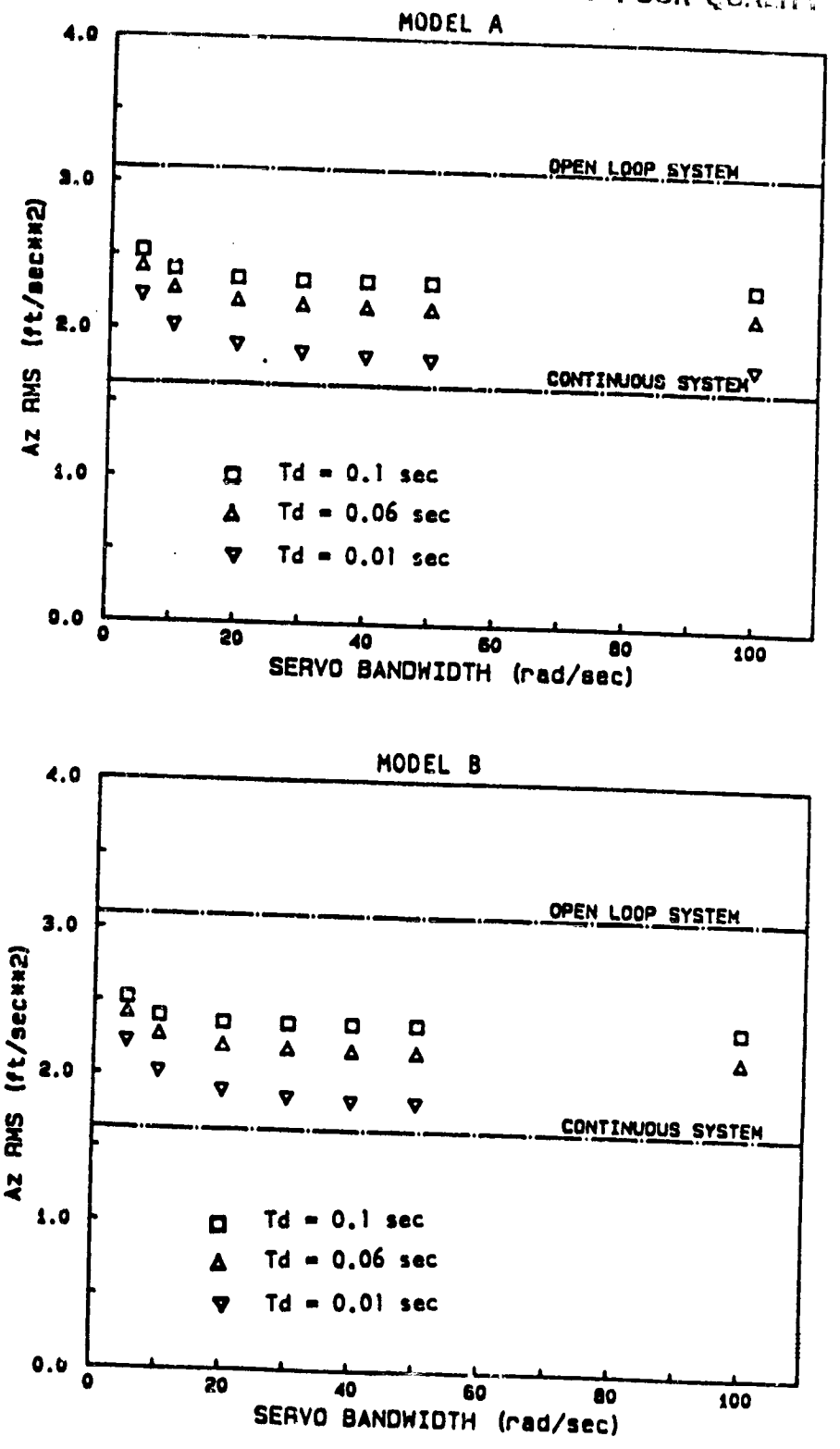

FIGURE E.21 Effect of Servo Bandwidth - Takeoff Configuration

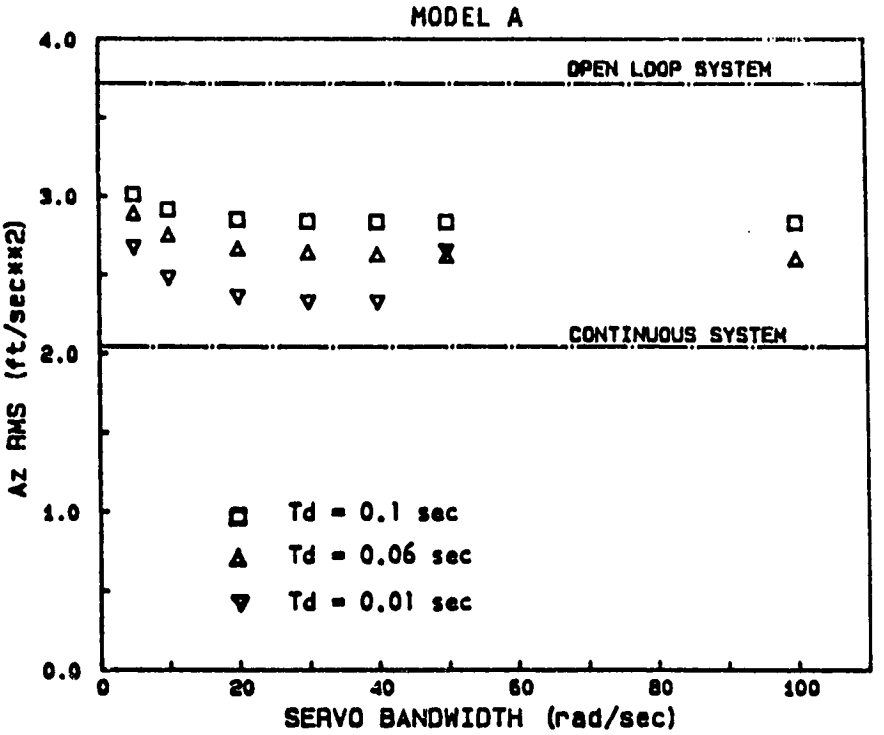

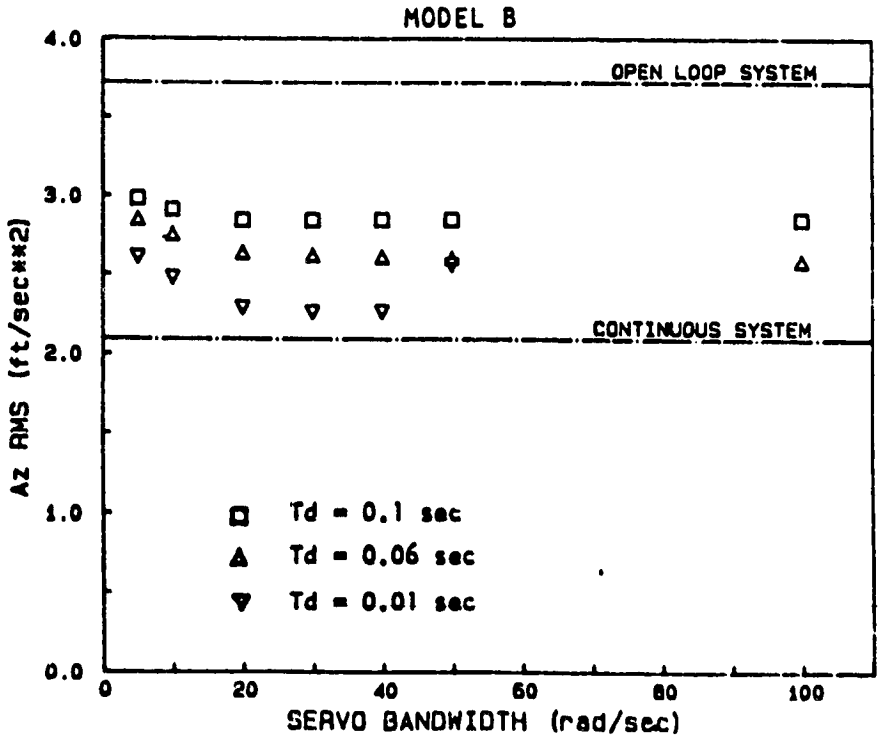

FIGURE E.22 Effect of Servo Bandwidth - Climb (SL) Configuration

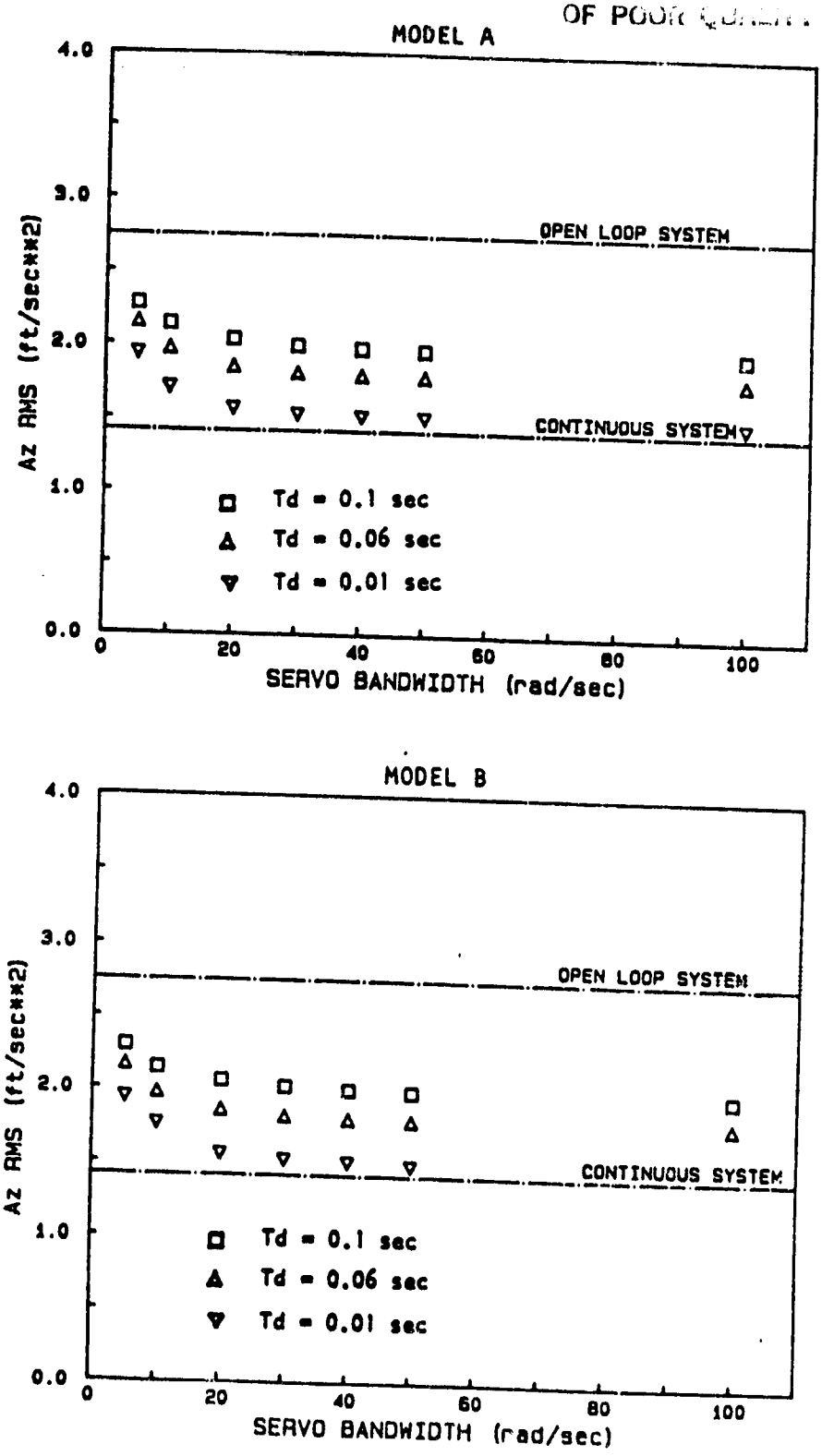

FIGURE E.23 Effect of Servo Bandwidth - Climb (5000 ft) Configuration

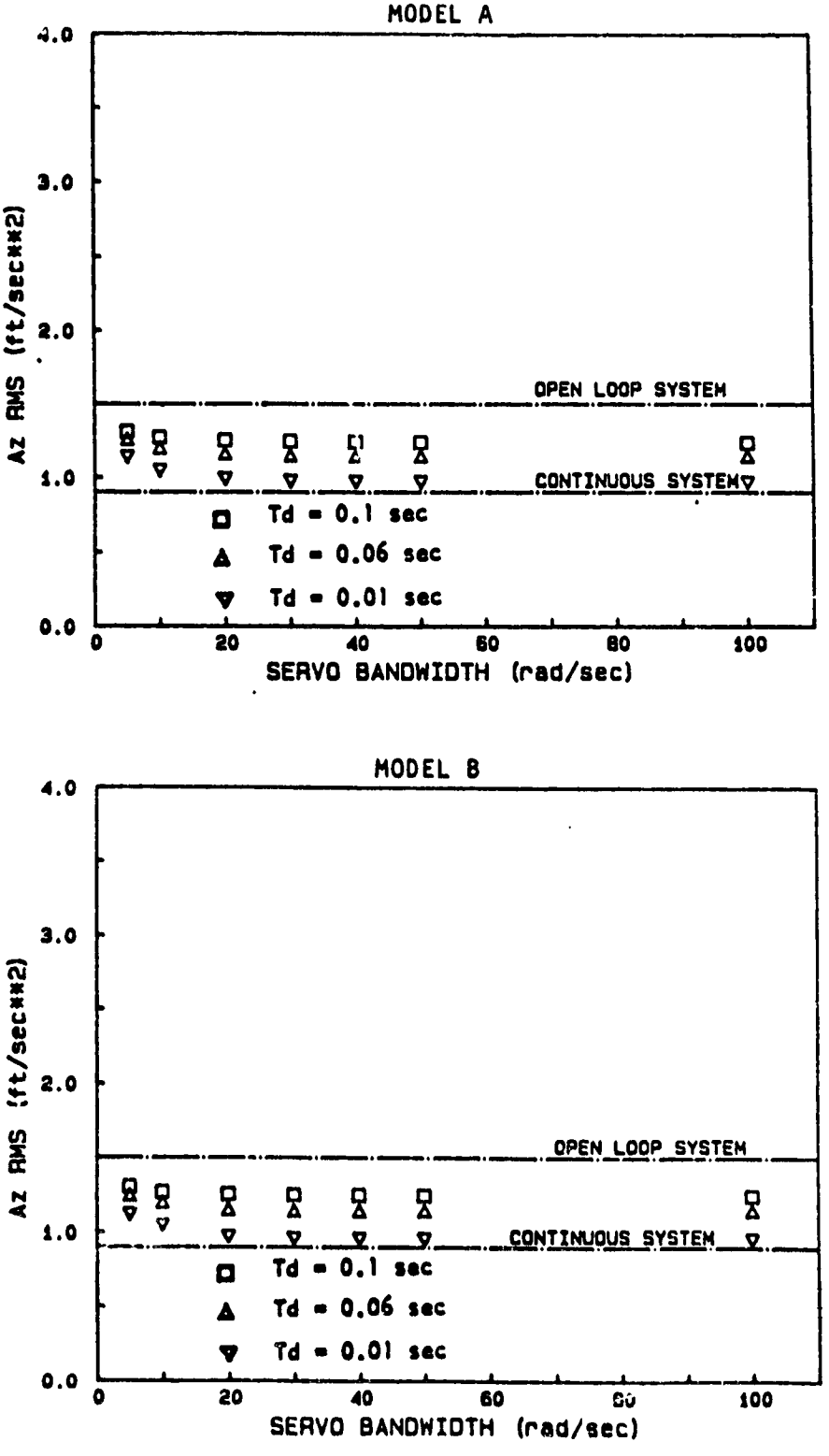

FIGURE E.24 Effect of Servo Bandwidth - Cruise Configuration

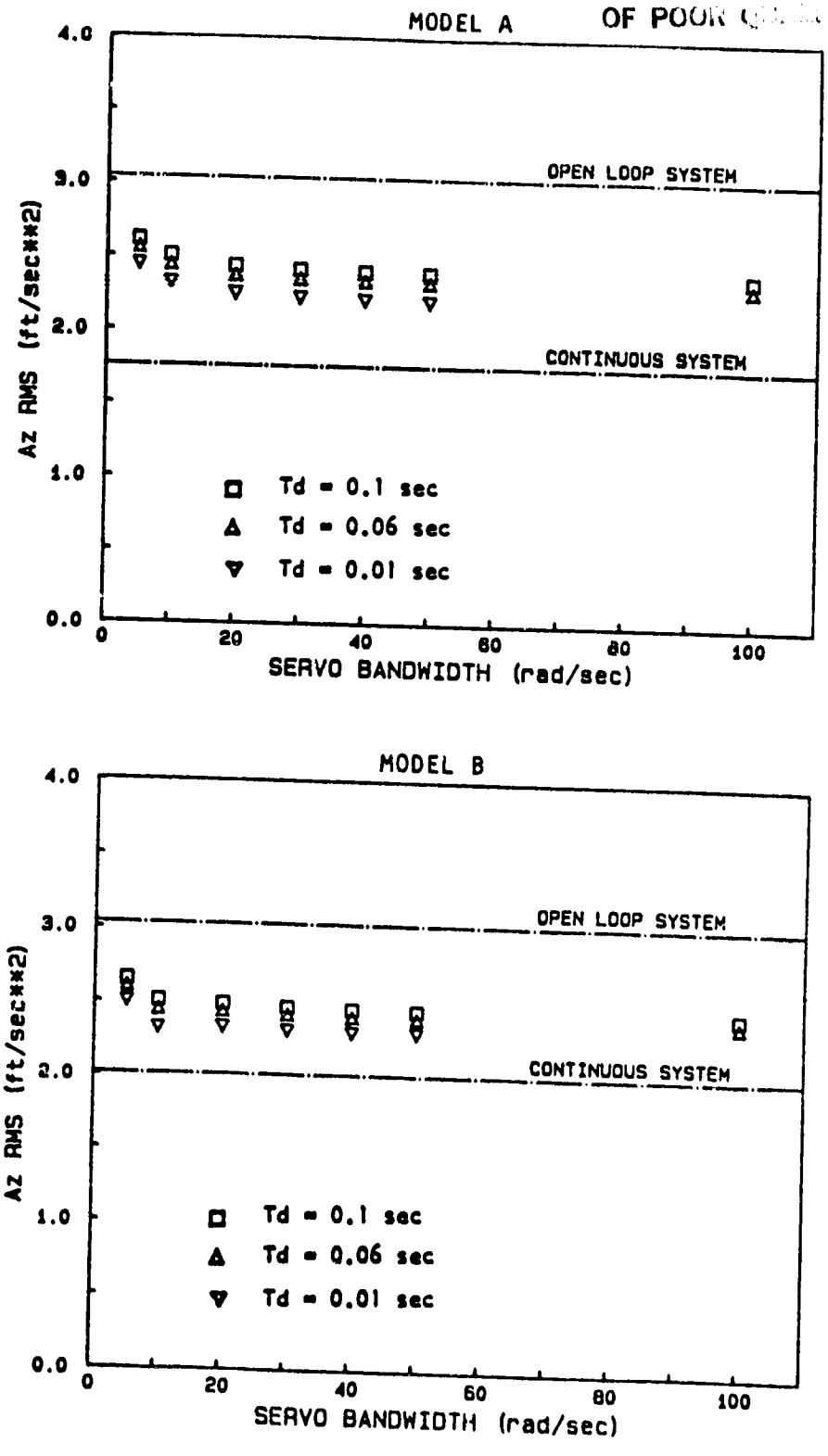

FIGURE E.25 Effect of Servo Bandwidth - Approach Configuration

TABLE E.6 TAKEOFF CONFIGURATION SUMMARY

THE ALTITUDE IS:	500.	ft
THE AIRSPEED IS:	183.86	ft/sec
THE SAMPLE TIME IS:	0.100	sec
THE TURBULENCE INTENSITY IS:	6.00	ft/sec

OPEN LOOP RESPONSE:

	Az(ft/s2)	Alfa(deg)	Q(deg/s)	Thet(deg)	D-e(deg)	D-f(deg)
MAX	-8.939	2.394	-1.615	1.123	0.000	0.000
RATE	-126.660	33.263	-23.191	-1.580	0.000	0.000
RMS	3.095	0.877	0.614	0.583	0.000	0.000

Z-REAL	Z-IMAG	W'-REAL	W'-IMAG	FREQUENCY	DAMPING
0.515923	0.000000	-6.386562	0.000000	6.386562	1.000000
0.809889	0.000000	-2.100803	0.000000	2.100803	1.000000
0.999542	0.015149	-0.003431	0.151556	0.151594	0.022631
0.999542	-0.015149	-0.003431	-0.151556	0.151594	0.022631
0.367879	0.000000	-9.242343	0.000000	9.242343	1.000000
0.367879	0.000000	-9.242343	0.000000	9.242343	1.000000

3.50 ft/sec^2 IS THE RMS VALUE FROM THE DIGITAL PSD

THIS IS A DIGITAL DESIGN.

COMPUTATIONAL DELAY TIME = 0.010

	Az(ft/s2)	Alfa(deg)	Q(deg/s)	Thet(deg)	D-e(deg)	D-f(deg)
MAX	-5.502	2.211	3.446	2.192	-1.093	-10.995
RATE	-137.826	33.262	21.496	3.445	-13.294	147.385
RMS	2.023	0.811	1.399	0.982	0.368	3.851

Z-REAL	Z-IMAG	W'-REAL	W'-IMAG	FREQUENCY	DAMPING
-0.169644	0.000000	-28.172128	0.000000	28.172128	1.000000
0.673837	0.226194	-3.468613	3.171428	4.699918	0.738016
0.673837	-0.226194	-3.468613	-3.171428	4.699918	0.738016
0.310056	0.000000	-10.533041	0.000000	10.533041	1.000000
0.995214	0.009296	-0.047544	0.093406	0.104810	0.453617
0.995214	-0.009296	-0.047544	-0.093406	0.104810	0.453617

TABLE E.7 CLIMB (Sea Level) CONFIGURATION SUMMARY

THE ALTITUDE IS:	500.	ft
THE AIRSPEED IS:	210.85	ft/sec
THE SAMPLE TIME IS:	0.100	sec
THE TURBULENCE INTENSITY IS:	6.00	ft/sec

OPEN LOOP RESPONSE:

	Az(ft/s2)	Alfa(deg)	Q(deg/s)	Thet(deg)	D-e(deg)	D-f(deg)
MAX	-9.659	2.029	-1.201	1.292	0.000	0.000
RATE	222.913	-45.271	-7.607	-1.201	0.000	0.000
RMS	3.718	0.784	0.540	0.577	0.000	0.000

Z-REAL	Z-IMAG	W'-REAL	W'-IMAG	FREQUENCY	DAMPING
0.490186	0.000000	-6.842280	0.000000	6.842280	1.000000
0.789424	0.000000	-2.353557	0.000000	2.353557	1.000000
0.999218	0.014891	-0.006713	0.149023	0.149174	0.045002
0.999218	-0.014891	-0.006713	-0.149023	0.149174	0.045002
0.367879	0.000000	-9.242343	0.000000	9.242343	1.000000
0.367879	0.000000	-9.242343	0.000000	9.242343	1.000000

3.98 ft/sec^2 IS THE RMS VALUE FROM THE DIGITAL PSD

THIS IS A DIGITAL DESIGN.

COMPUTATIONAL DELAY TIME = 0.010

	Az(ft/s2)	Alfa(deg)	Q(deg/s)	Thet(deg)	D-e(deg)	D-f(deg)
MAX	-7.799	1.957	-2.705	2.267	0.595	-10.710
RATE	219.784	-45.172	18.140	-2.704	-8.709	150.153
RMS	2.407	0.724	1.266	1.012	0.241	3.838

Z-REAL	Z-IMAG	W'-REAL	W'-IMAG	FREQUENCY	DAMPING
-0.238321	0.000000	-32.515527	0.000000	32.515527	1.000000
0.655797	0.182980	-3.866089	2.637414	4.680021	0.826084
0.655797	-0.182980	-3.866089	-2.637414	4.680021	0.826084
0.324094	0.000000	-10.209328	0.000000	10.209328	1.000000
0.996272	0.009409	-0.036907	0.094444	0.101399	0.363979
0.996272	-0.009409	-0.036907	-0.094444	0.101399	0.363979

TABLE E.8 CLIMB (5000 ft) CONFIGURATION SUMMARY

THE ALTITUDE IS:	5000.	ft
THE AIRSPEED IS:	227.34	ft/sec
THE SAMPLE TIME IS:	0.100	sec
THE TURBULENCE INTENSITY IS:	7.02	ft/sec

OPEN LOOP RESPONSE:

	Az(ft/s2)	Alfa(deg)	Q(deg/s)	Thet(deg)	D-e(deg)	D-f(deg)
MAX	8.693	-1.892	1.283	1.021	0.000	0.000
RATE	-141.080	28.822	-7.653	1.282	0.000	0.000
RMS	2.738	0.567	0.449	0.600	0.000	0.000

Z-REAL	Z-IMAG	W'-REAL	W'-IMAG	FREQUENCY	DAMPING
0.534976	0.000000	-6.059031	0.000000	6.059031	1.000000
0.773058	0.000000	-2.559899	0.000000	2.559899	1.000000
0.999319	0.014276	-0.005797	0.142849	0.142966	0.040546
0.999319	-0.014276	-0.005797	-0.142849	0.142966	0.040546
0.367879	0.000000	-9.242343	0.000000	9.242343	1.000000
0.367879	0.000000	-9.242343	0.000000	9.242343	1.000000

2.79 ft/sec^2 IS THE RMS VALUE FROM THE DIGITAL PSD

COMPUTATIONAL DELAY TIME = 0.01

	Az(ft/s2)	Alfa(deg)	Q(deg/s)	Thet(deg)	D-e(deg)	D-f(deg)
MAX	5.779	-1.777	3.232	1.819	-0.685	10.882
RATE	-124.860	28.882	-16.789	3.232	-7.619	-151.542
RMS	1.696	0.558	1.055	0.964	0.185	3.472

Z-REAL	Z-IMAG	W'-REAL	W'-IMAG	FREQUENCY	DAMPING
-0.432816	0.000000	-50.523805	0.000000	50.523805	1.000000
0.669657	0.211332	-3.579260	2.984481	4.660282	0.768035
0.669657	-0.211332	-3.579260	-2.984481	4.660282	0.768035
0.326207	0.000000	-10.161213	0.000000	10.161213	1.000000
0.996814	0.008397	-0.031560	0.084234	0.089952	0.350857
0.996814	-0.008397	-0.031560	-0.084234	0.089952	0.350857

TABLE E.9 CRUISE CONFIGURATION SUMMARY

THE ALTITUDE IS:	20000.	ft
THE AIRSPEED IS:	357.91	ft/sec
THE SAMPLE TIME IS:	0.100	sec
THE TURBULENCE INTENSITY IS:	3.57	ft/sec

OPEN LOOP RESPONSE:

	Az(ft/s2)	Alfa(deg)	Q(deg/s)	Thet(deg)	D-e(deg)	D-f(deg)
MAX	4.330	-0.599	0.710	0.629	0.000	0.000
RATE	70.670	-9.167	3.690	0.710	0.000	0.000
RMS	1.496	0.199	0.262	0.291	0.000	0.000

Z-REAL	Z-IMAG	W'-REAL	W'-IMAG	FREQUENCY	DAMPING
0.648355	0.099974	-4.177678	1.466391	4.427561	0.943562
0.648355	-0.099974	-4.177678	-1.466391	4.427561	0.943562
0.999092	0.010273	-0.008556	0.102820	0.103176	0.082925
0.999092	-0.010273	-0.008556	-0.102820	0.103176	0.082925
0.367879	0.000000	-9.242343	0.000000	9.242343	1.000000
0.367879	0.000000	-9.242343	0.000000	9.242343	1.000000

1.50 ft/sec^2 IS THE RMS VALUE FROM THE DIGITAL PSD

THIS IS A DIGITAL DESIGN.

COMPUTATIONAL DELAY TIME = 0.010

	Az(ft/s2)	Alfa(deg)	Q(deg/s)	Thet(deg)	D-e(deg)	D-f(deg)
MAX	-4.152	0.491	1.432	0.912	-0.211	-3.829
RATE	-121.047	-8.582	-7.840	1.431	-4.600	94.950
RMS	1.006	0.187	0.536	0.390	0.068	1.305

Z-REAL	Z-IMAG	W'-REAL	W'-IMAG	FREQUENCY	DAMPING
-0.513123	0.000000	-62.156293	0.000000	62.156293	1.000000
0.652283	0.310363	-3.383870	4.392395	5.544701	0.610289
0.652283	-0.310363	-3.383870	-4.392395	5.544701	0.610289
0.333887	0.000000	-9.987553	0.000000	9.987553	1.000000
0.997348	0.005588	-0.026398	0.056025	0.061933	0.426235
0.997348	-0.005588	-0.026398	-0.056025	0.061933	0.426235

TABLE E.10 APPROACH CONFIGURATION SUMMARY

THE ALTITUDE IS:	500.	ft
THE AIRSPEED IS:	160.25	ft/sec
THE SAMPLE TIME IS:	0.100	sec
THE TURBULENCE INTENSITY IS:	6.00	ft/sec

OPEN LOOP RESPONSE:

	Az(ft/s2)	Alfa(deg)	Q(deg/s)	Thet(deg)	D-e(deg)	D-f(deg)
MAX	-8.915	2.984	-1.324	1.207	0.000	0.000
RATE	-114.571	39.223	-5.342	-1.324	0.000	0.000
RMS	3.033	1.092	0.577	0.604	0.000	0.000

Z-REAL	Z-IMAG	W'-REAL	W'-IMAG	FREQUENCY	DAMPING
0.580511	0.000000	-5.308267	0.000000	5.308267	1.000000
0.833621	0.000000	-1.814757	0.000000	1.814757	1.000000
0.996593	0.021108	-0.031892	0.211779	0.214167	0.148910
0.996593	-0.021108	-0.031892	-0.211779	0.214167	0.148910
0.367879	0.000000	-9.242343	0.000000	9.242343	1.000000
0.367879	0.000000	-9.242343	0.000000	9.242343	1.000000

3.10 ft/sec^2 IS THE RMS VALUE FROM THE DIGITAL PSD

THIS IS A DIGITAL DESIGN.

COMPUTATIONAL DELAY TIME = 0.010

	Az(ft/s2)	Alfa(deg)	Q(deg/s)	Thet(deg)	D-e(deg)	D-f(deg)
MAX	-6.321	-2.772	-3.797	2.781	-0.679	-15.110
RATE	-114.567	39.558	18.309	-3.795	-5.436	143.947
RMS	2.173	1.062	1.617	1.301	0.237	5.611

Z-REAL	Z-IMAG	W'-REAL	W'-IMAG	FREQUENCY	DAMPING
0.065686	0.000000	-17.534502	0.000000	17.534502	1.000000
0.702691	0.198492	-3.177245	2.701898	4.170748	0.761793
0.702691	-0.198492	-3.177245	-2.701898	4.170748	0.761793
0.995540	0.014177	-0.043683	0.142395	0.148945	0.293285
0.995540	-0.014177	-0.043683	-0.142395	0.148945	0.293285
0.344616	0.000000	-9.748261	0.000000	9.748261	1.000000

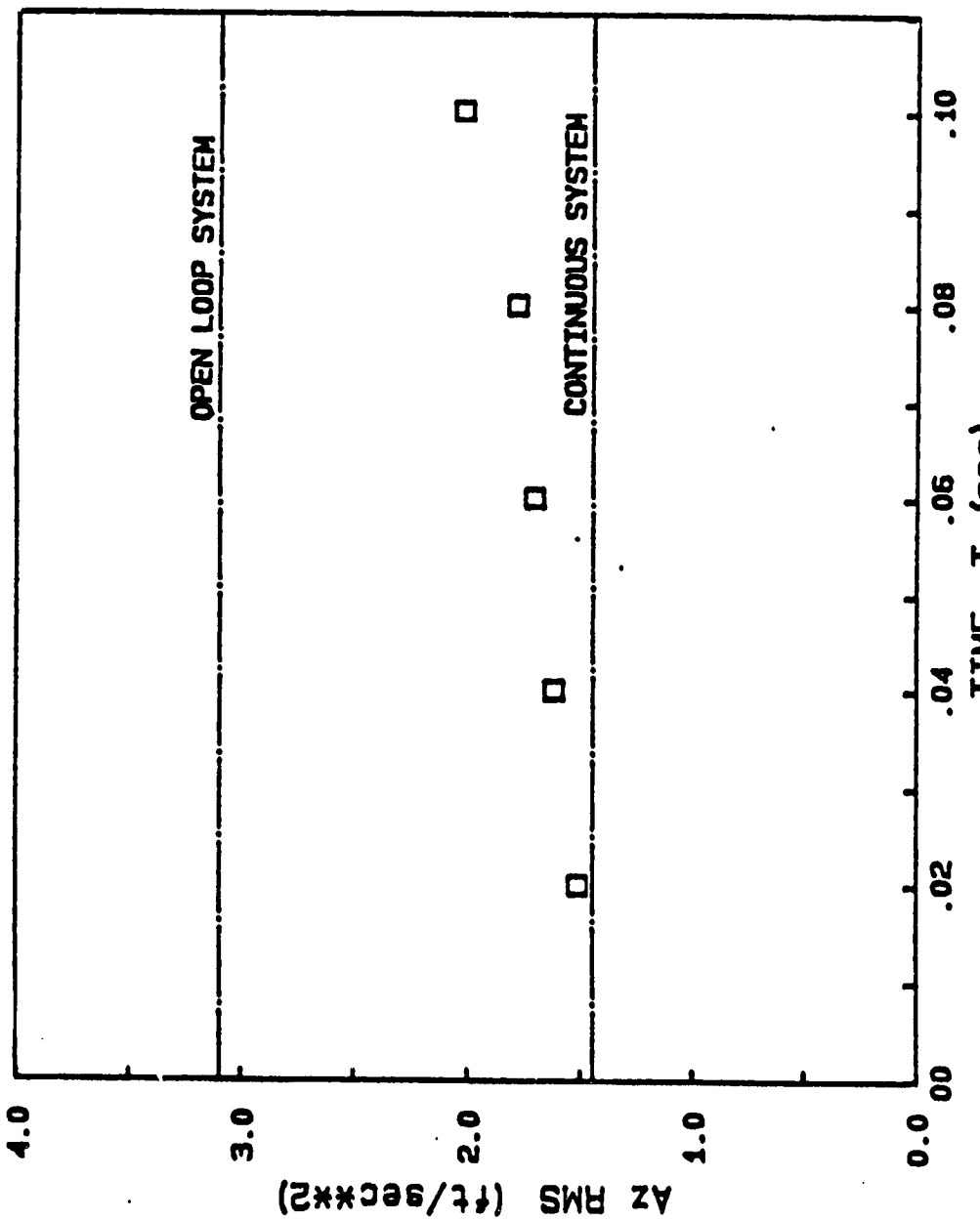

FIGURE E.26 Effect of Sample Time - Takeoff Configuration

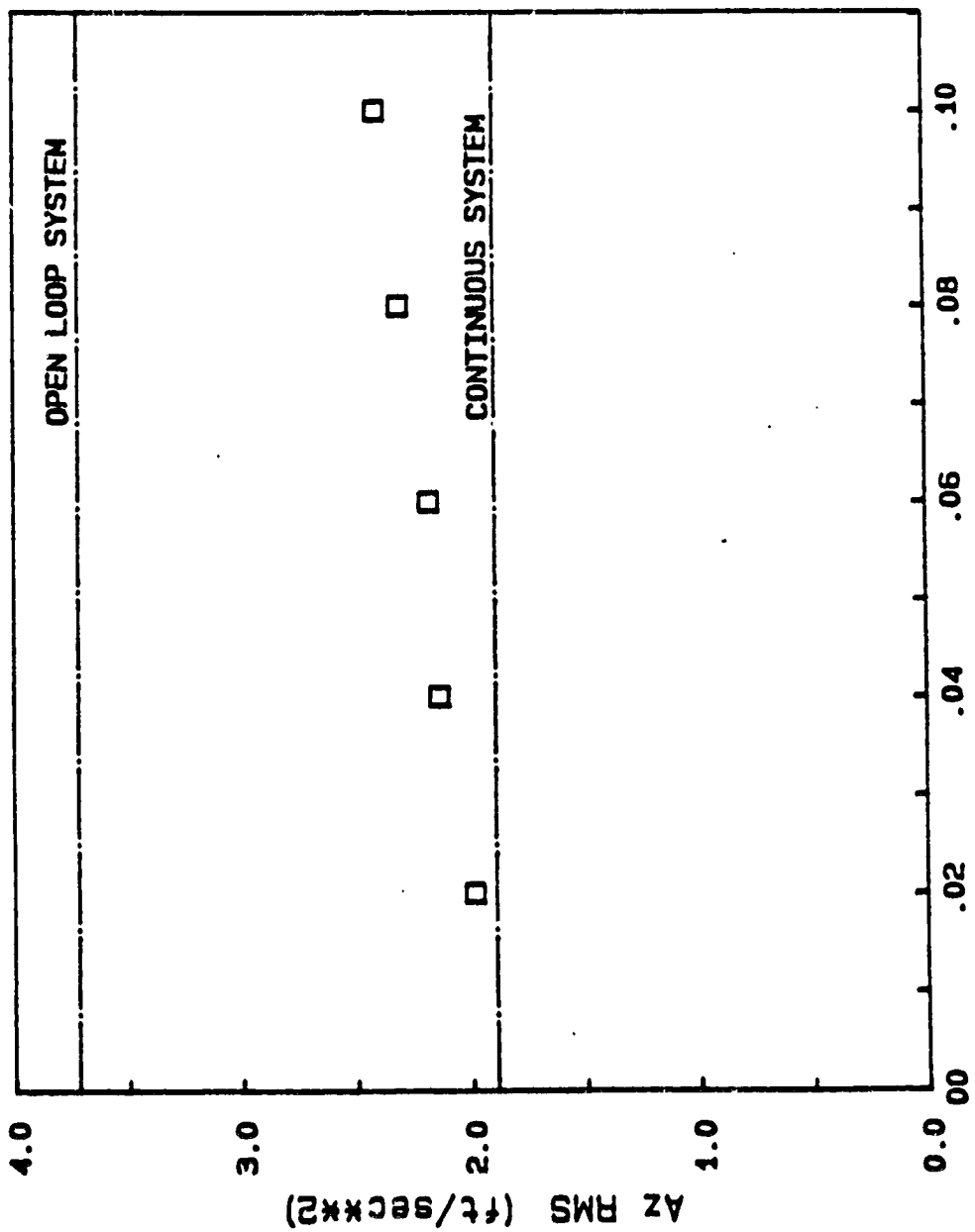

FIGURE E.27 Effect of Sample Time - Climb (SL) Configuration

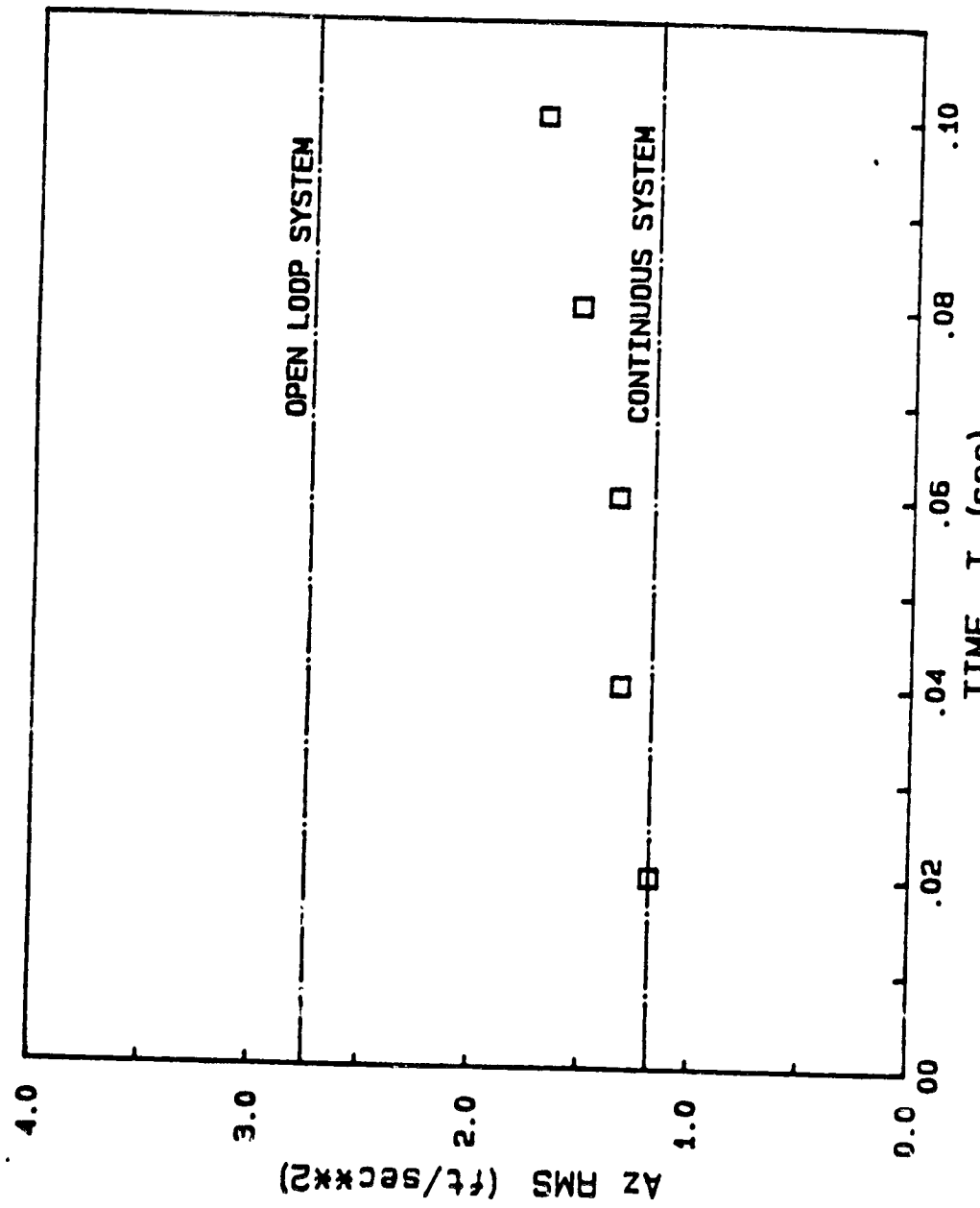

FIGURE E.28 Effect of Sample Time - Climb (5000 ft) Configuration

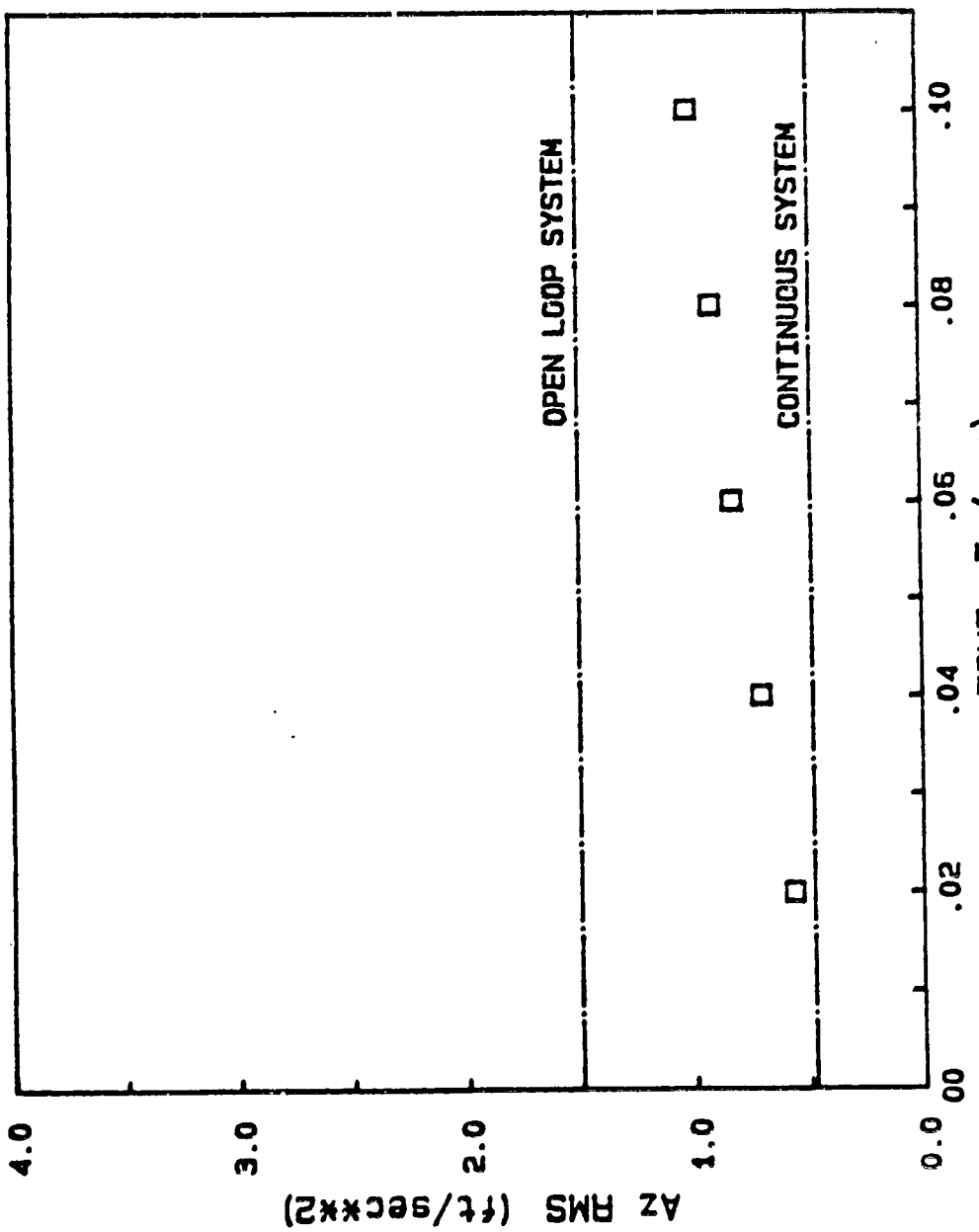

FIGURE E.29 Effect of Sample Time - Cruise Configuration

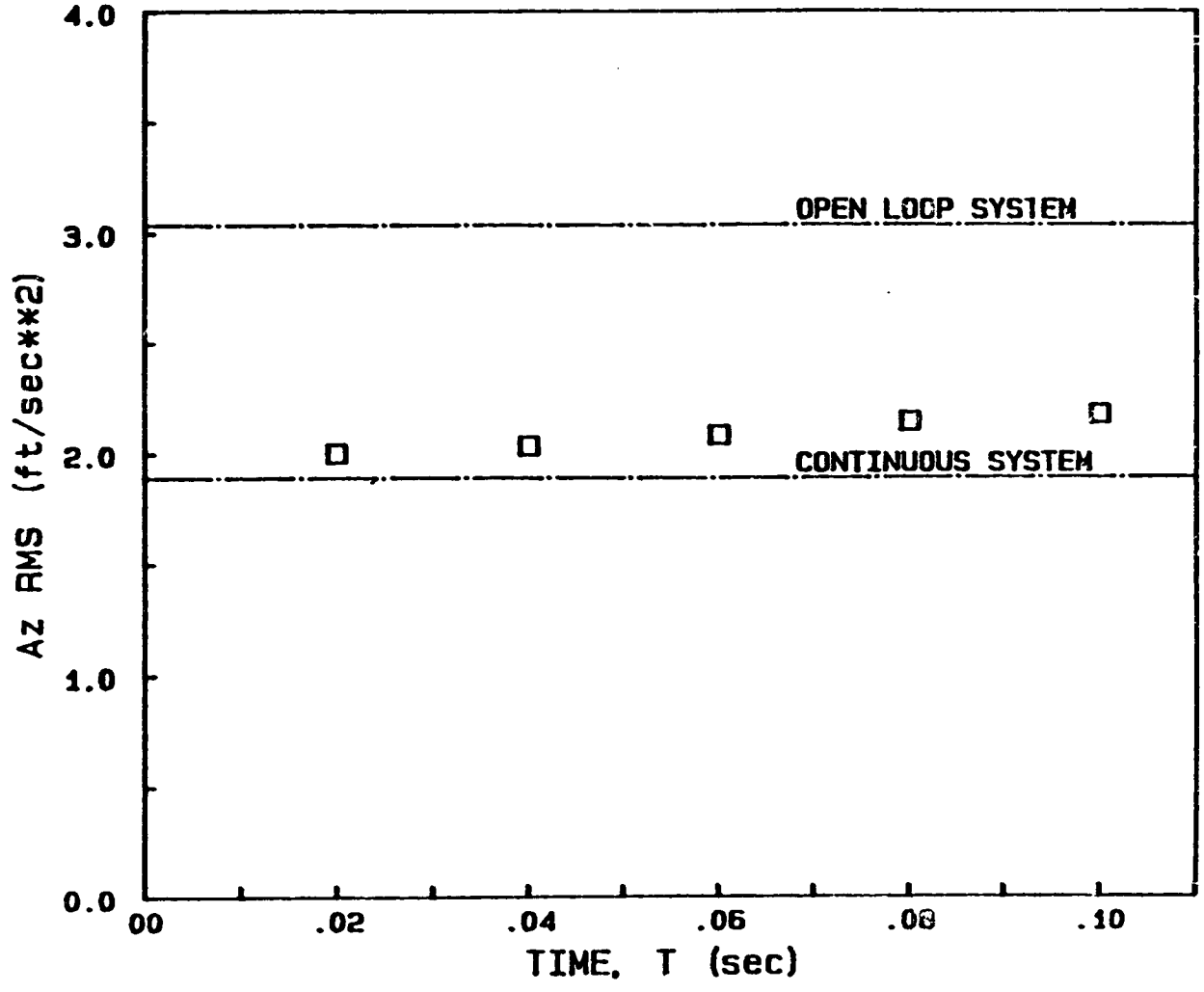

FIGURE E.30 Effect of Sample Time – Approach Configuration

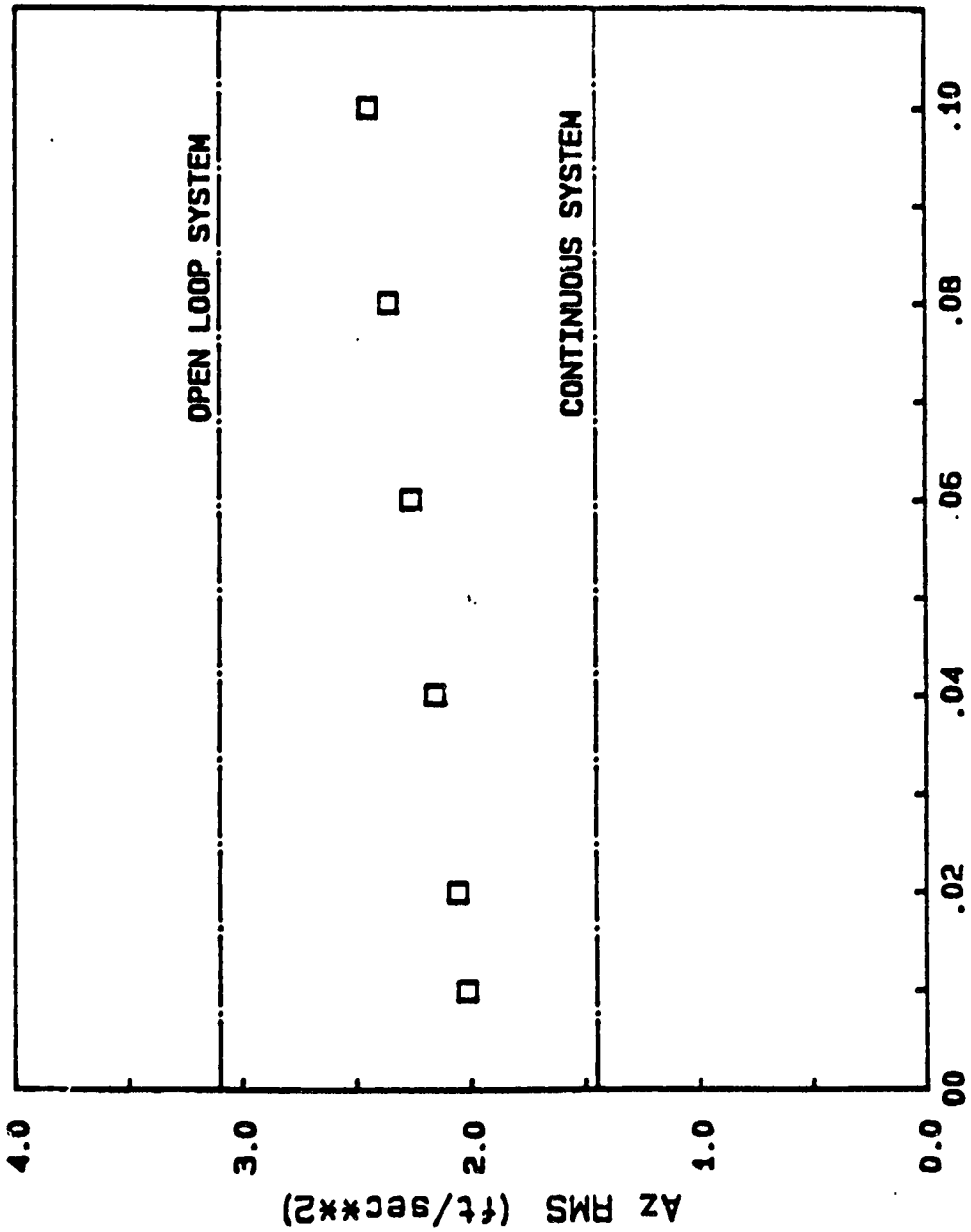

FIGURE E.31 Effect of Delay Time – Takeoff Configuration

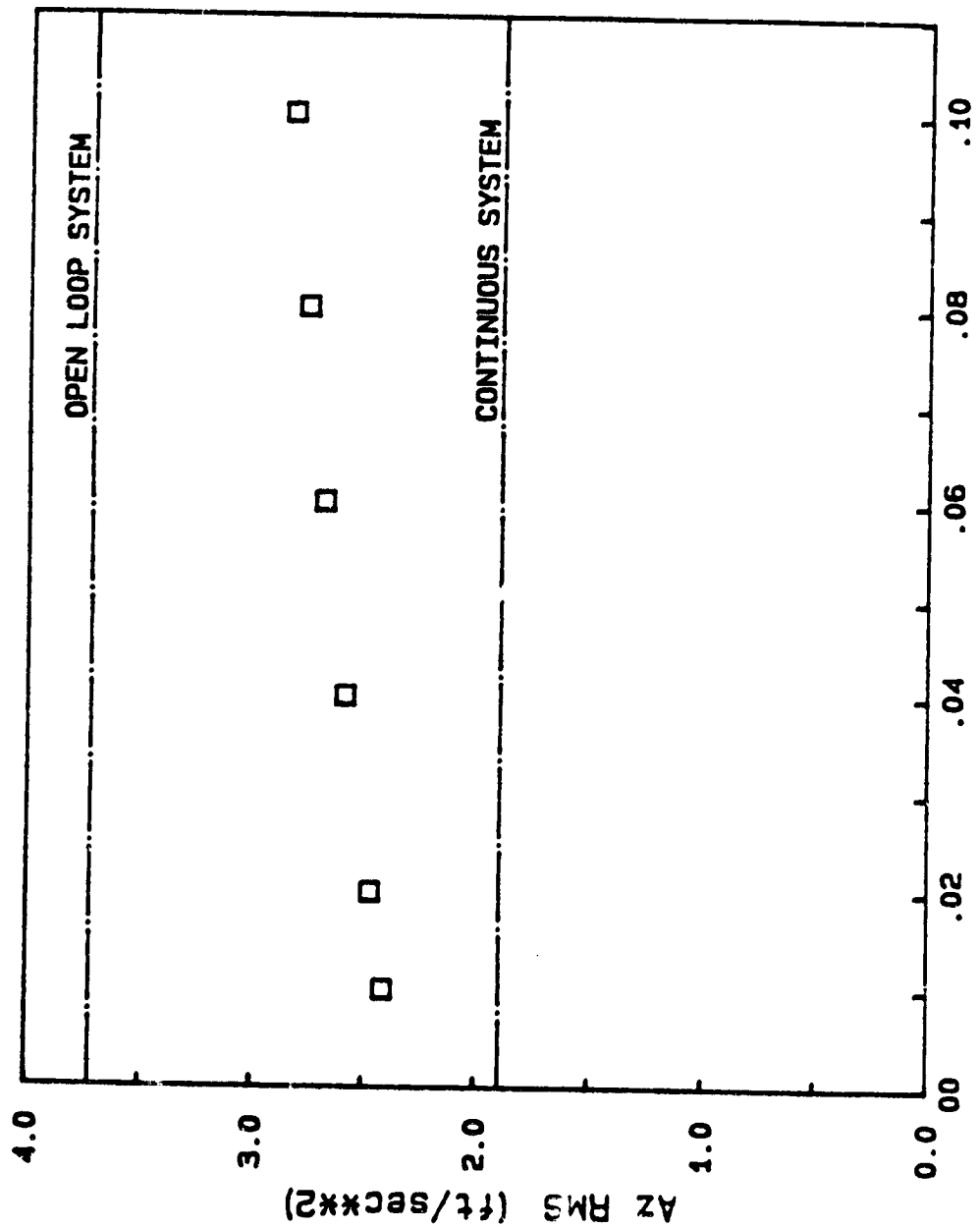

FIGURE E.32 Effect of Delay Time - Climb (SL) Configuration

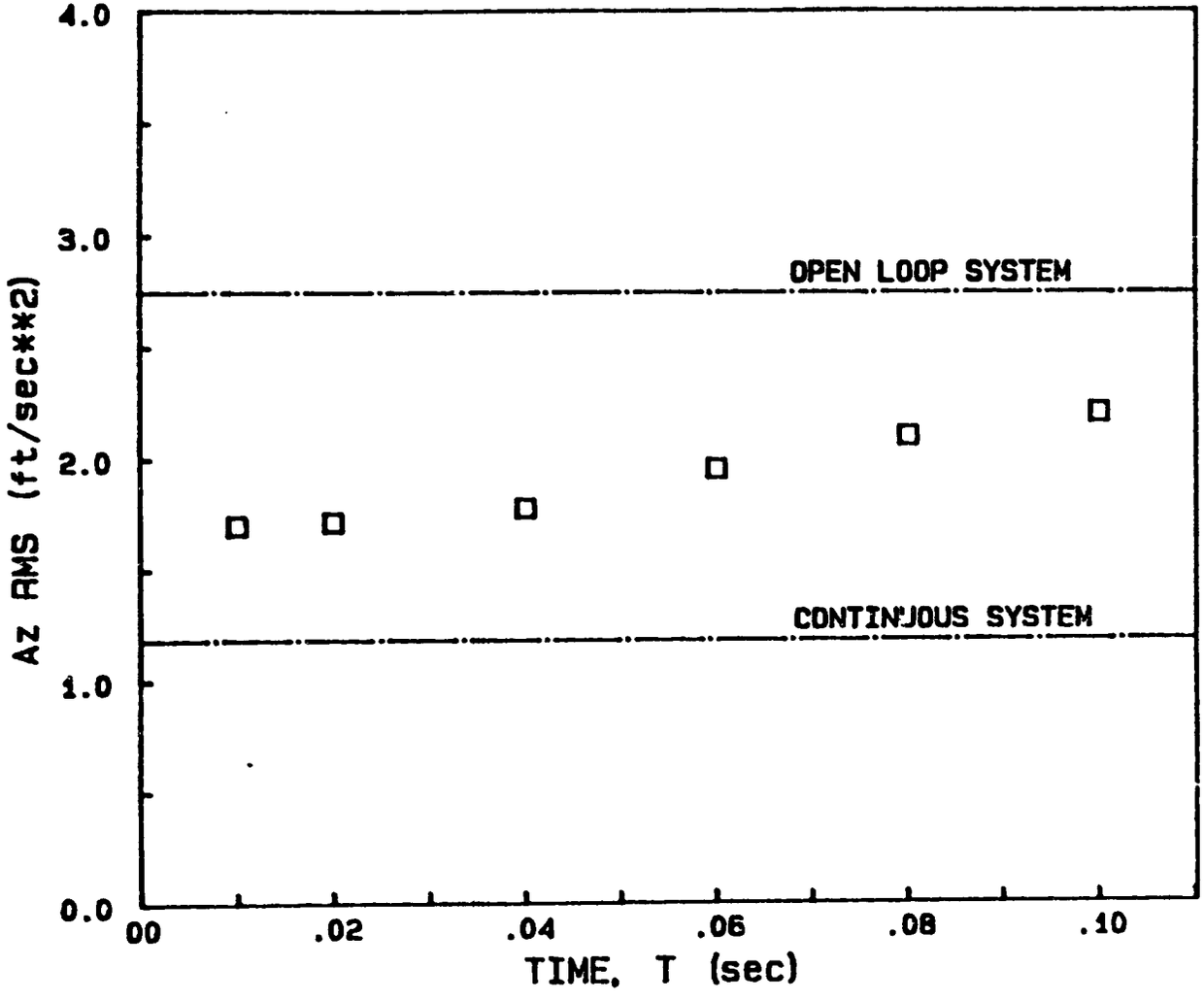

FIGURE E.33 Effect of Delay Time – Climb (5000 ft) Configuration

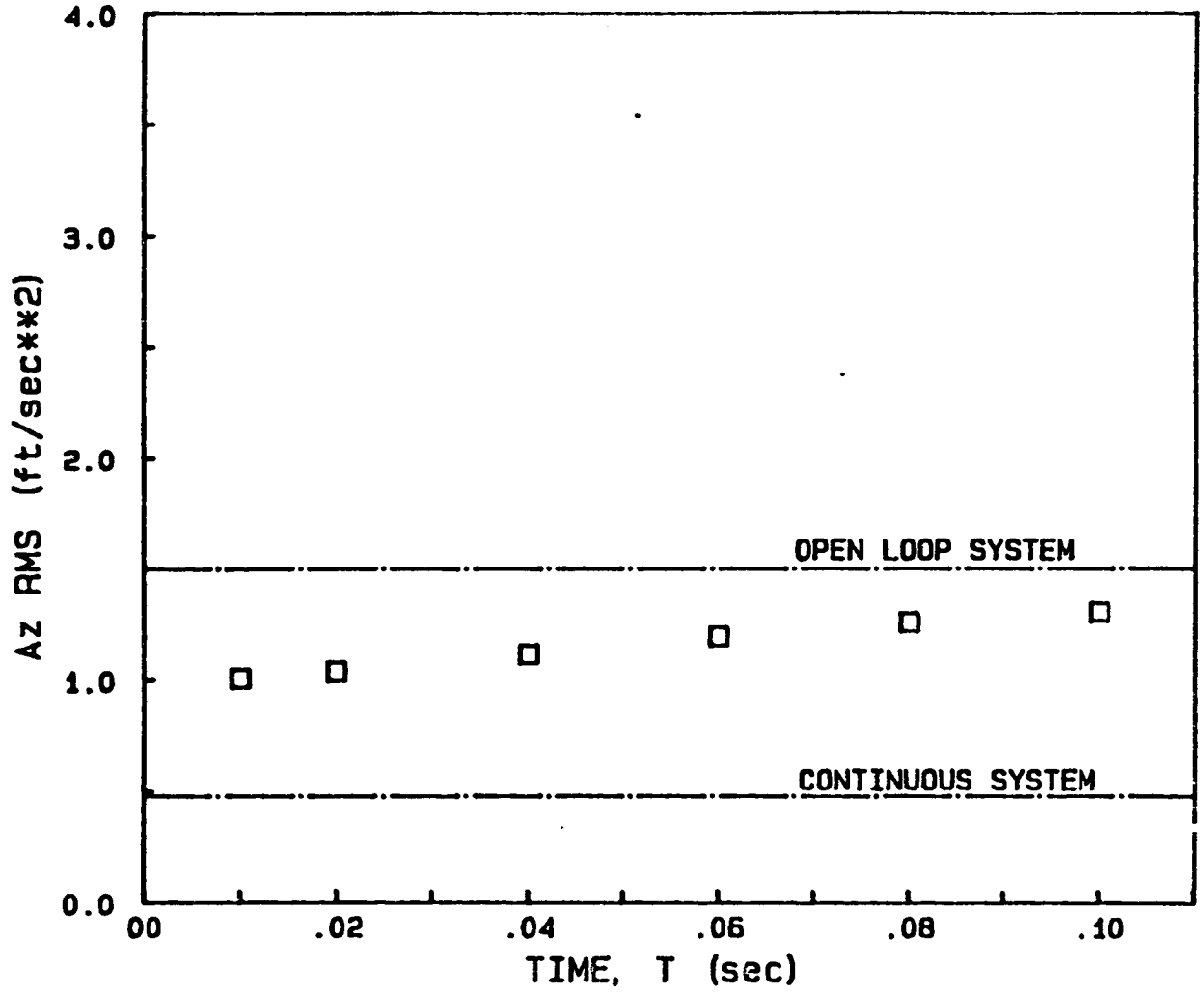

FIGURE E.34 Effect of Delay Time - Cruise Configuraion

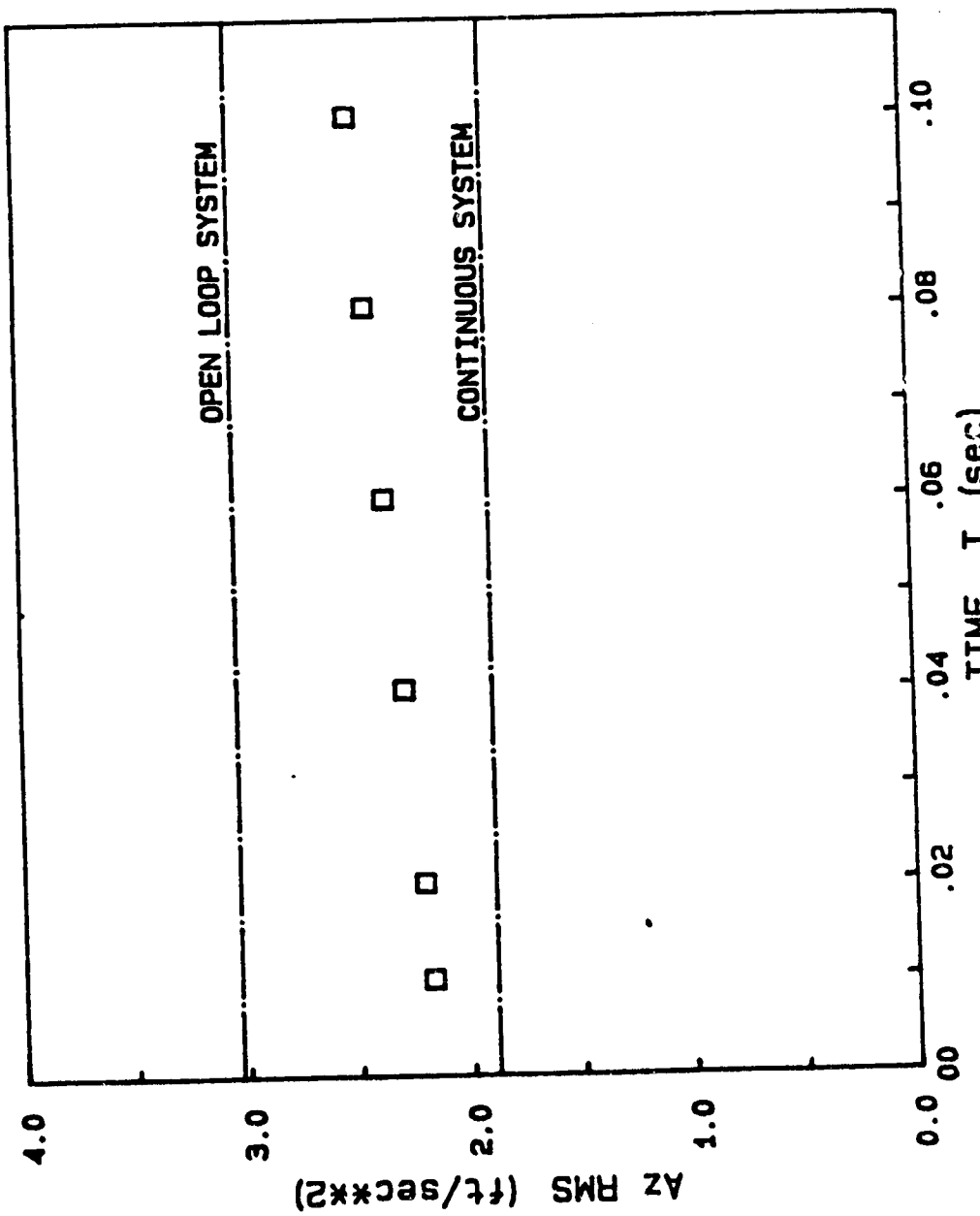

FIGURE E.35 Effect of Delay Time - Approach Configuration

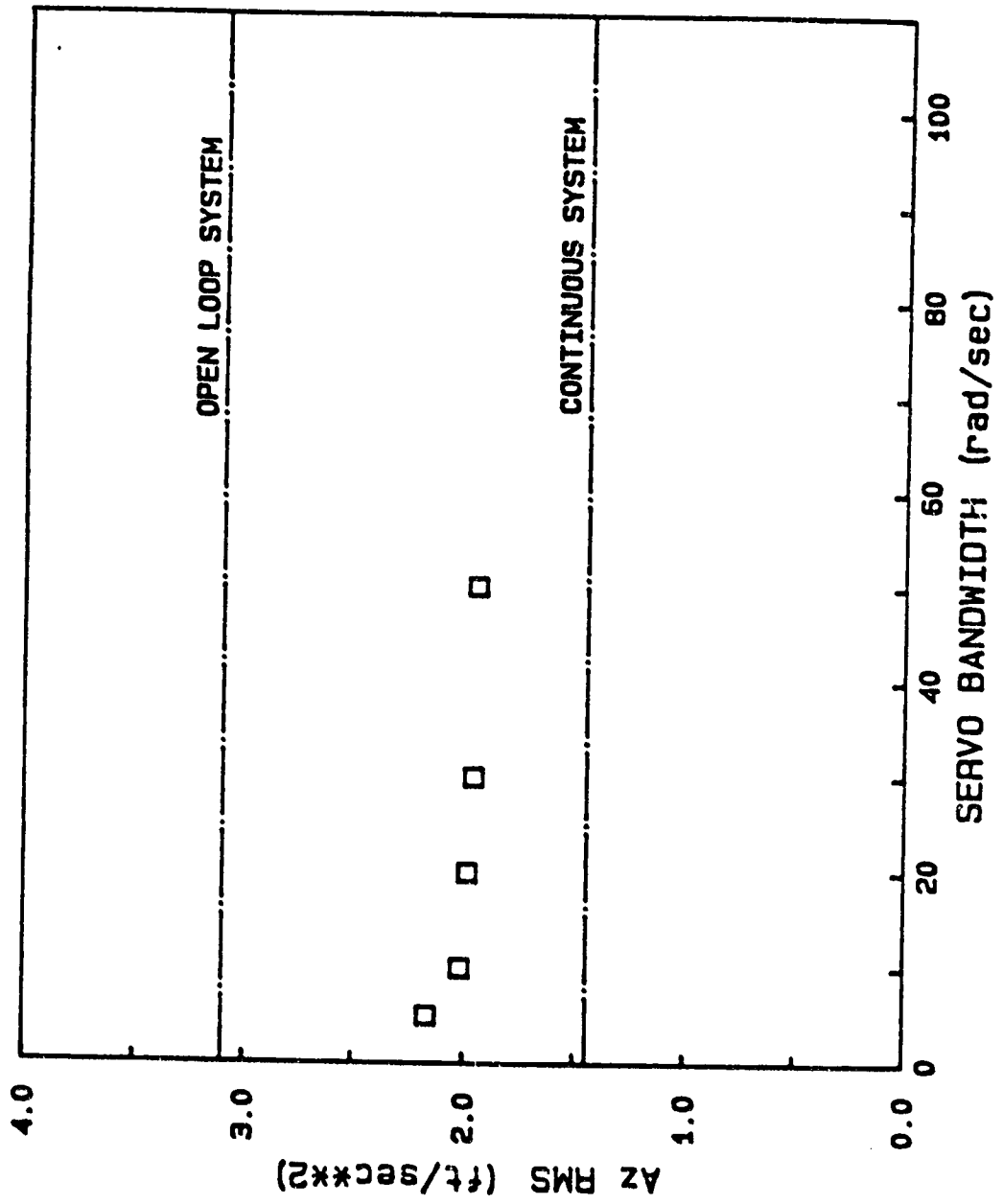

FIGURE E.36 Effect of Servo Bandwidth - Takeoff Configuration

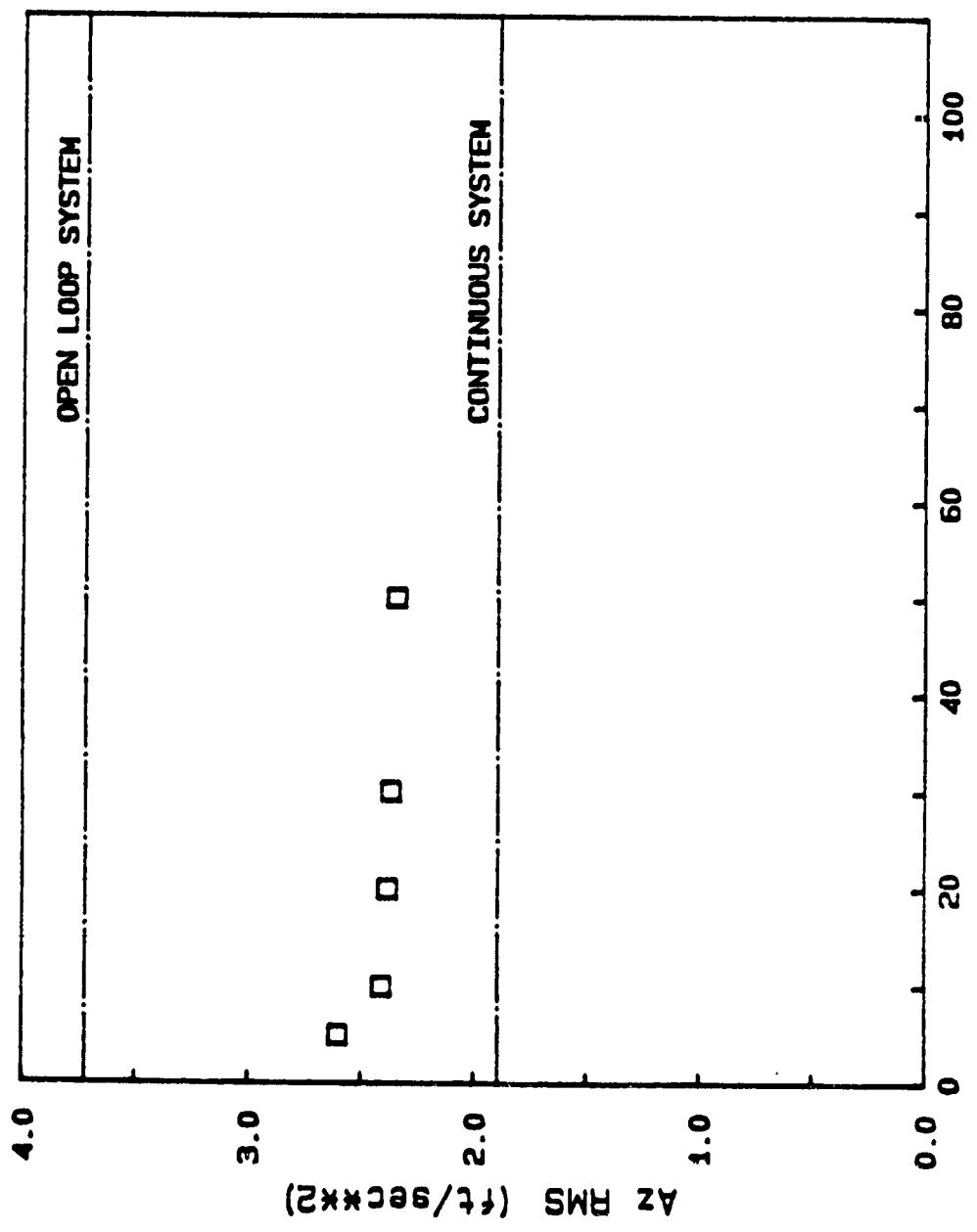

FIGURE E 37 Effect of Servo Bandwidth - Climb (SL) Configuration

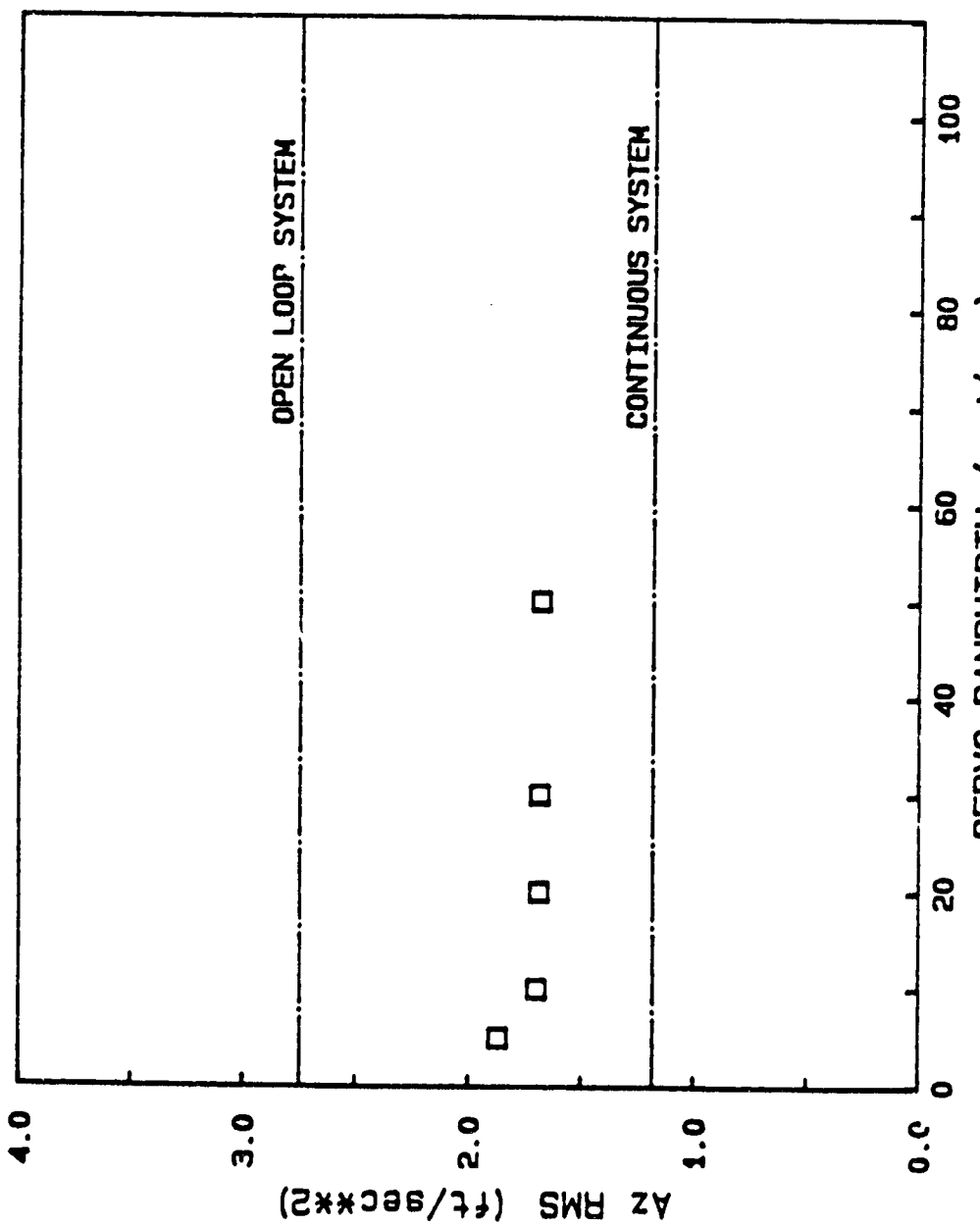

FIGURE E.38 Effect of Servo Bandwidth - Climb (5000 ft) Configuration

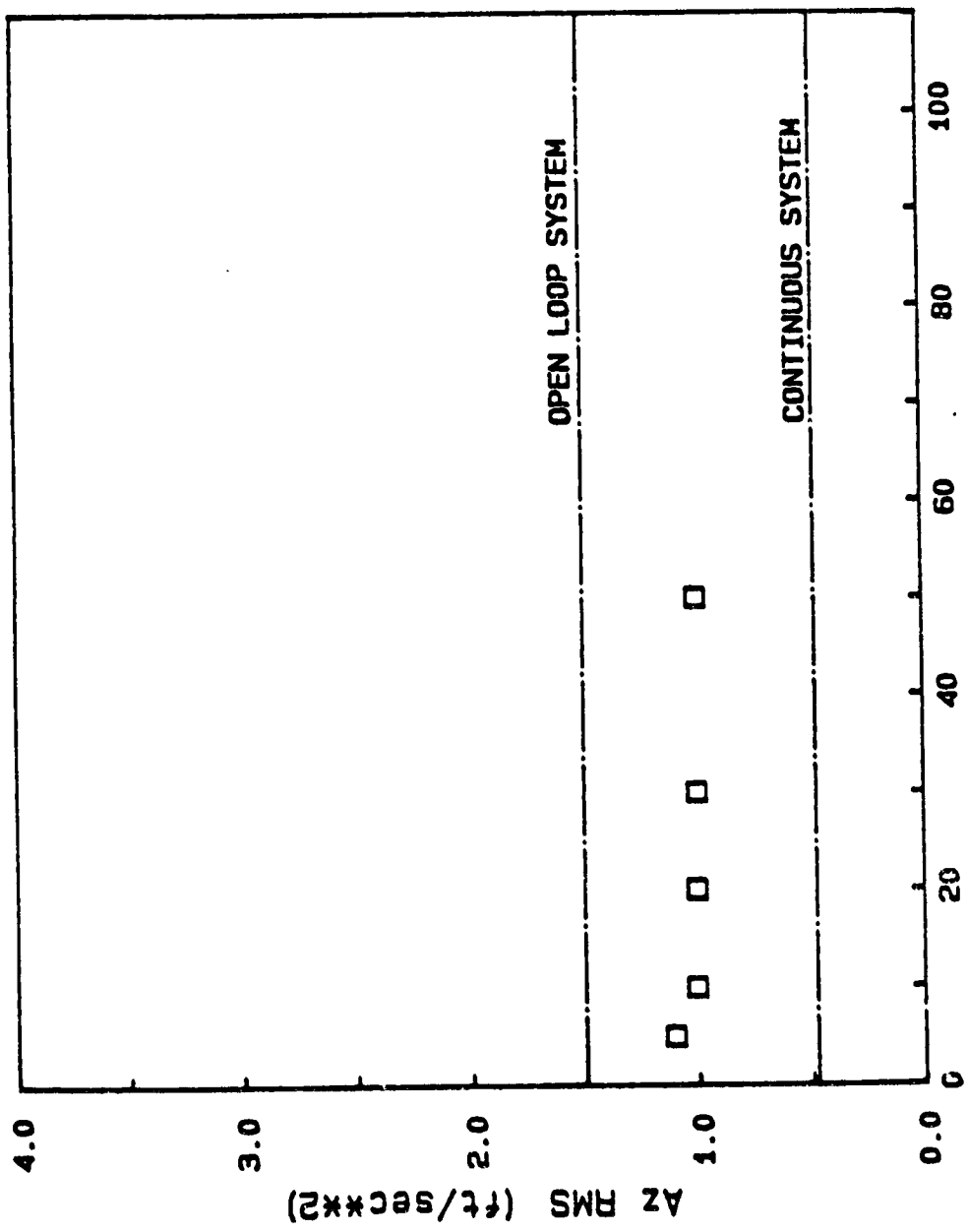

FIGURE E.39 Effect of Servo Bandwidth - Cruise Configuration

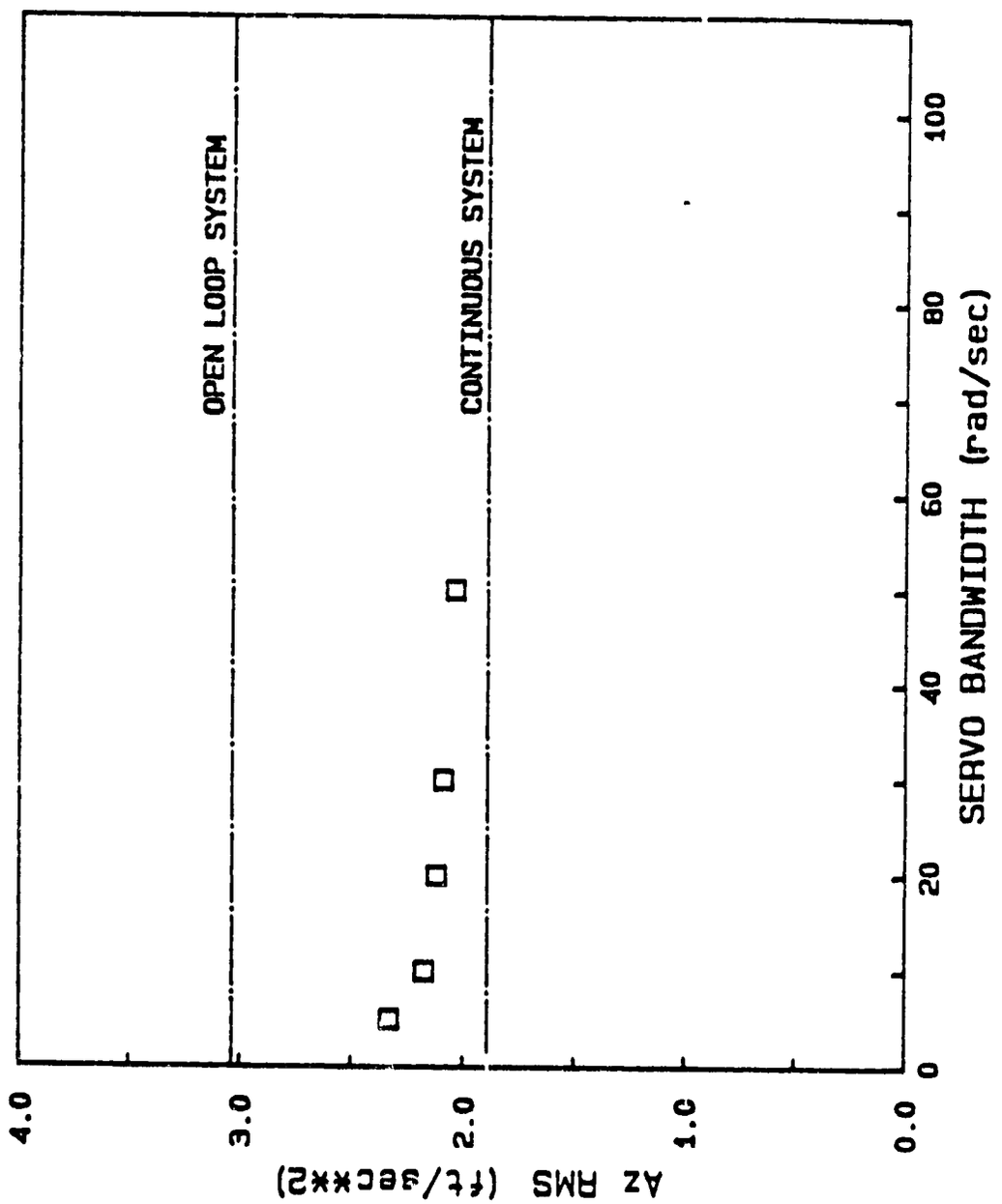

FIGURE E.40 Effect of Servo Bandwidth - Approach Configuration

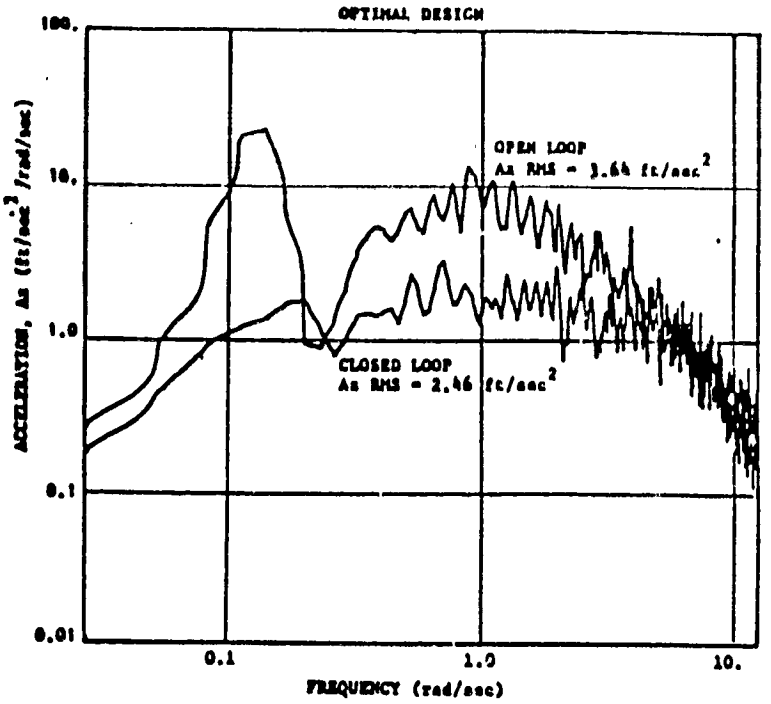

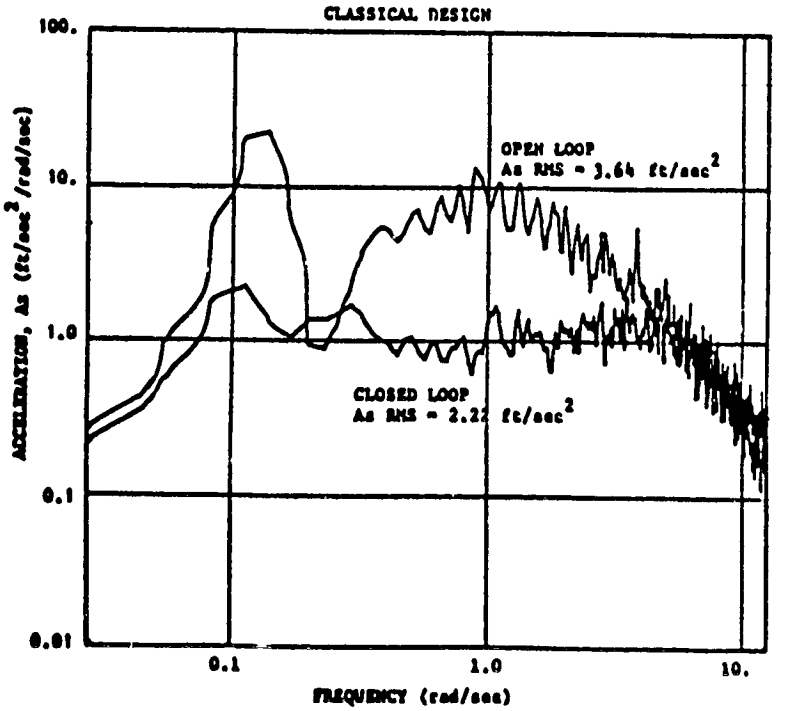

FIGURE E.41 Hybrid Simulation PSD - Takeoff Configuration (Model A)

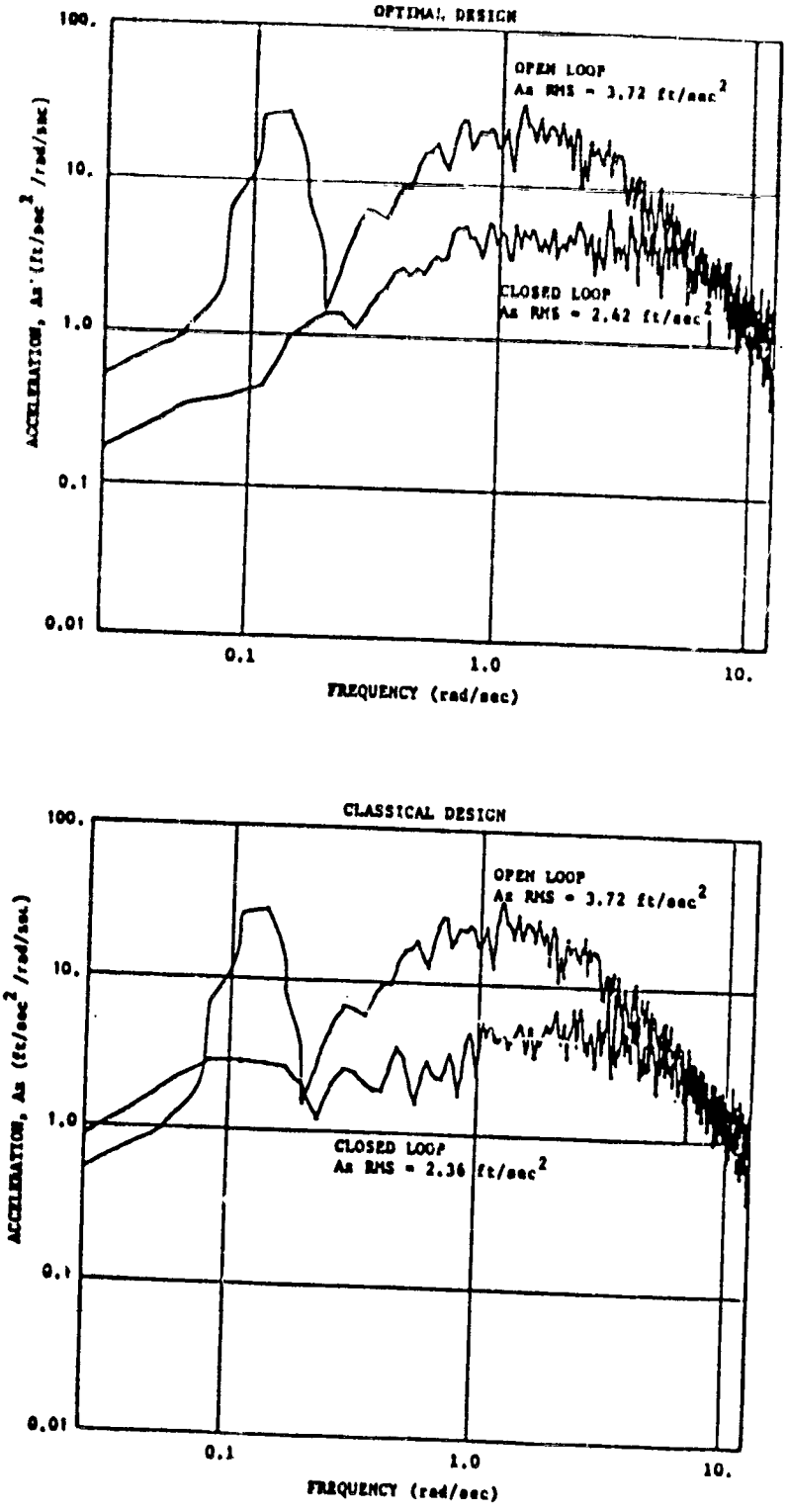

FIGURE E.42 Hybrid Simulation PSD - Climb (SL) Configuration (Model A)

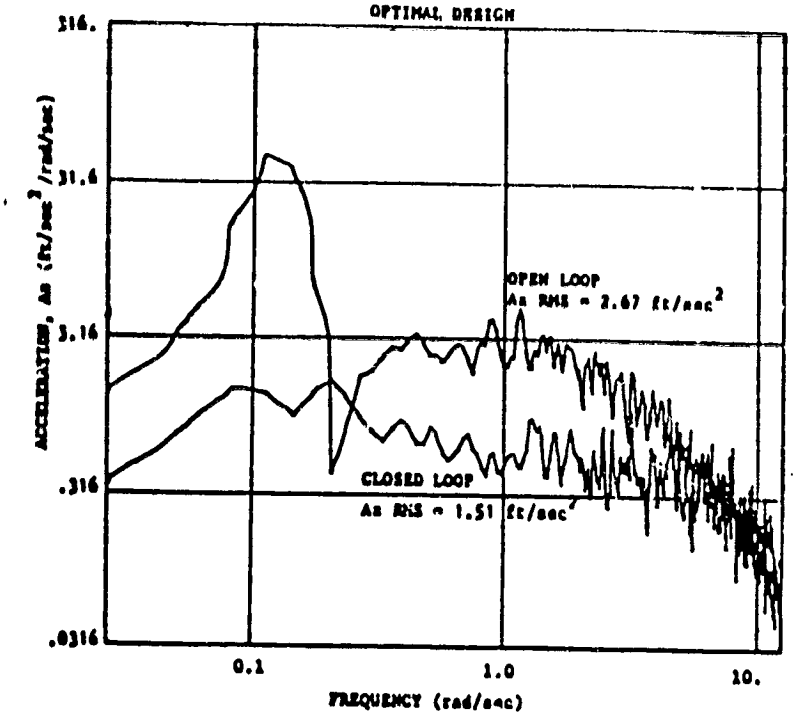

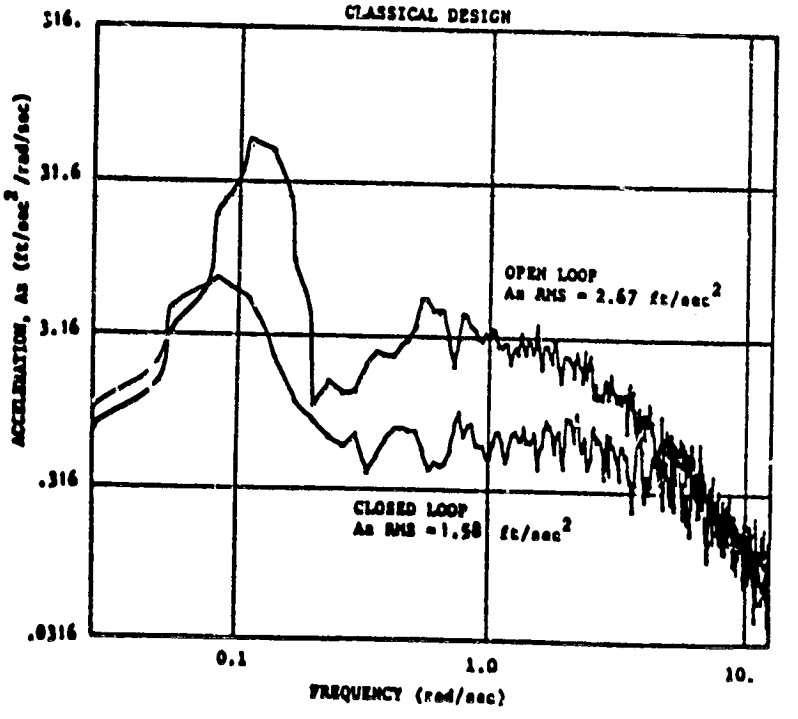

FIGURE E.43 Hybrid Simulation PSD - Climb (5000 ft) Configuration (Model A)

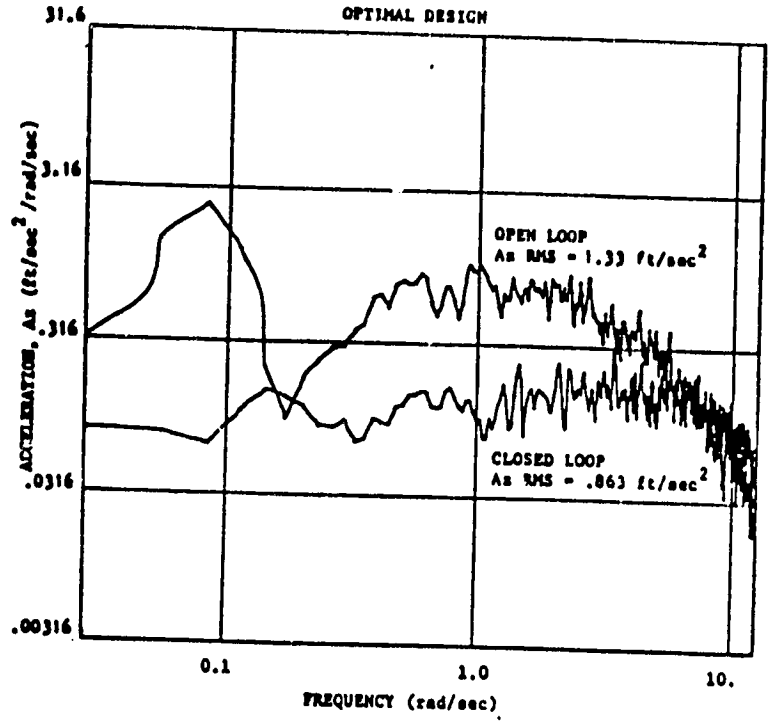

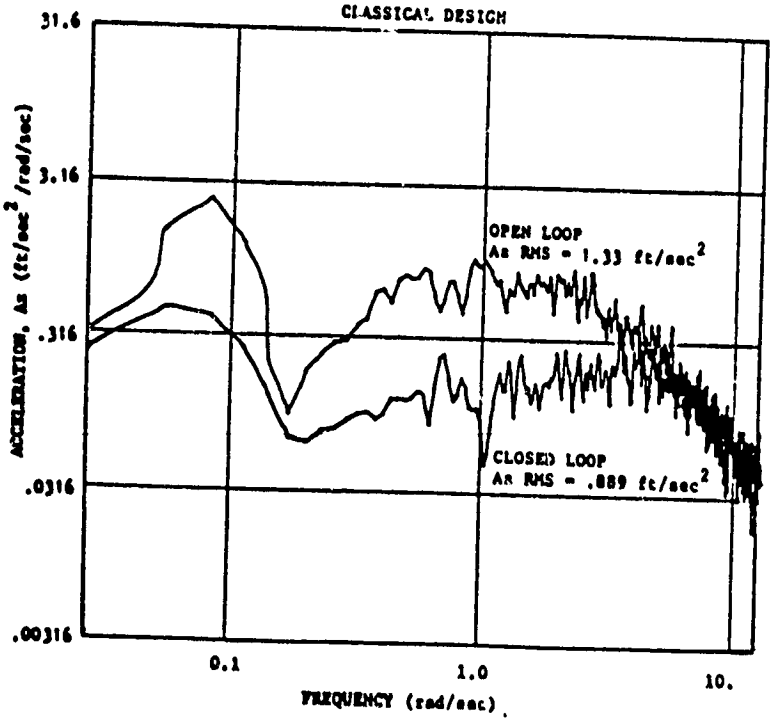

FIGURE E.44 Hybrid Simulation PSD - C[illegible]e Configuration (Model A)

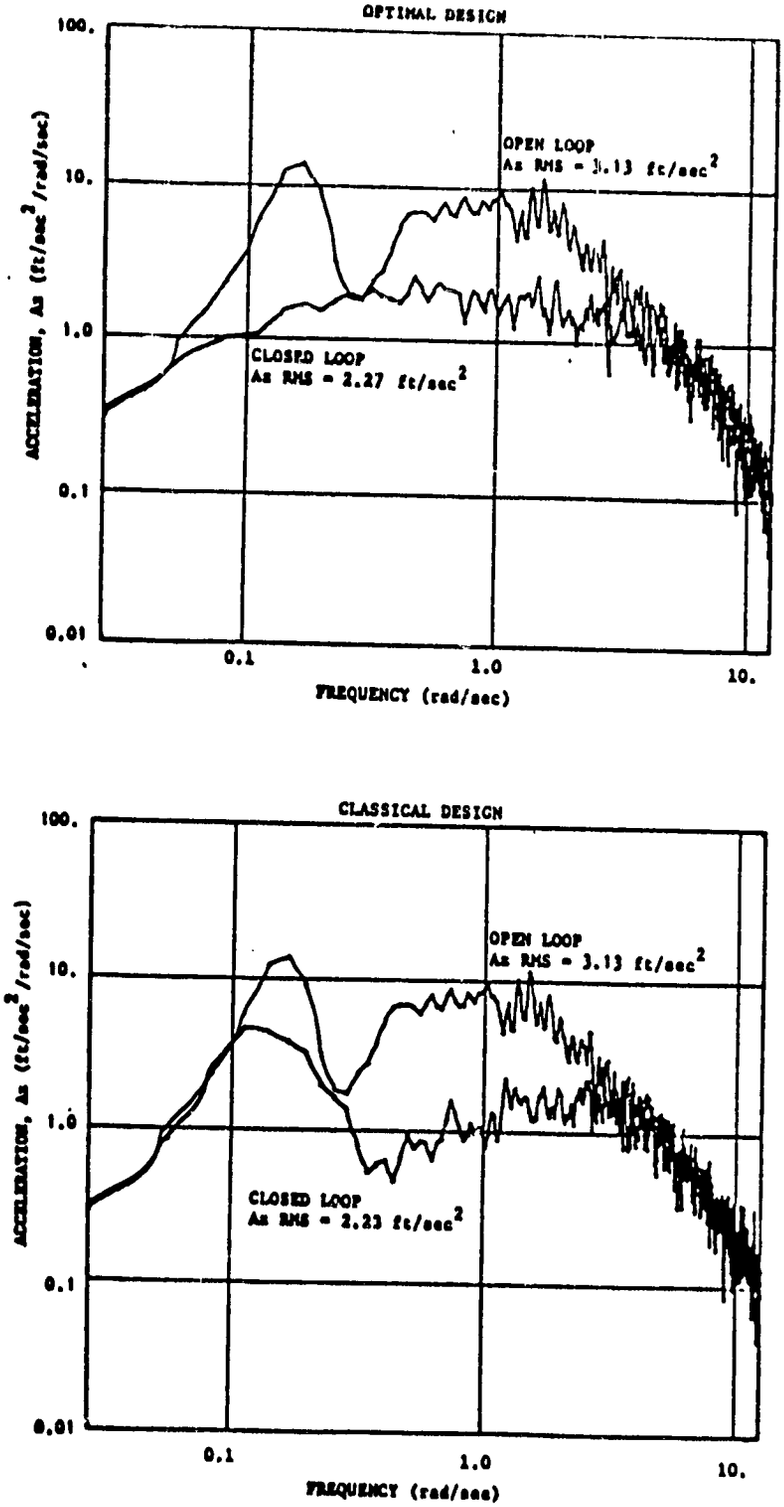

FIGURE E.45 Hybrid Simulation PSD - Approach Configuration (Model A)

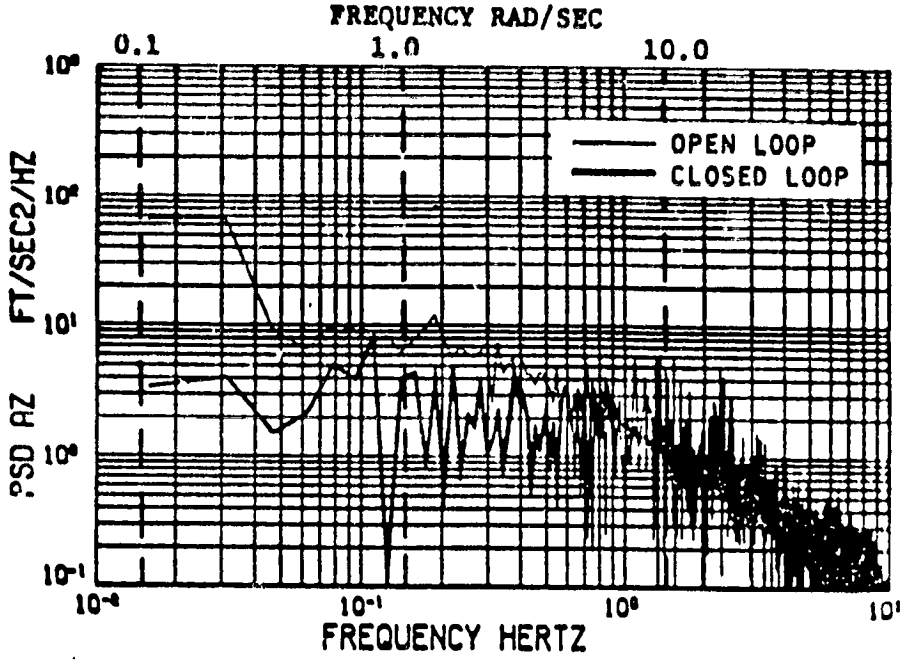

Figure E.46a

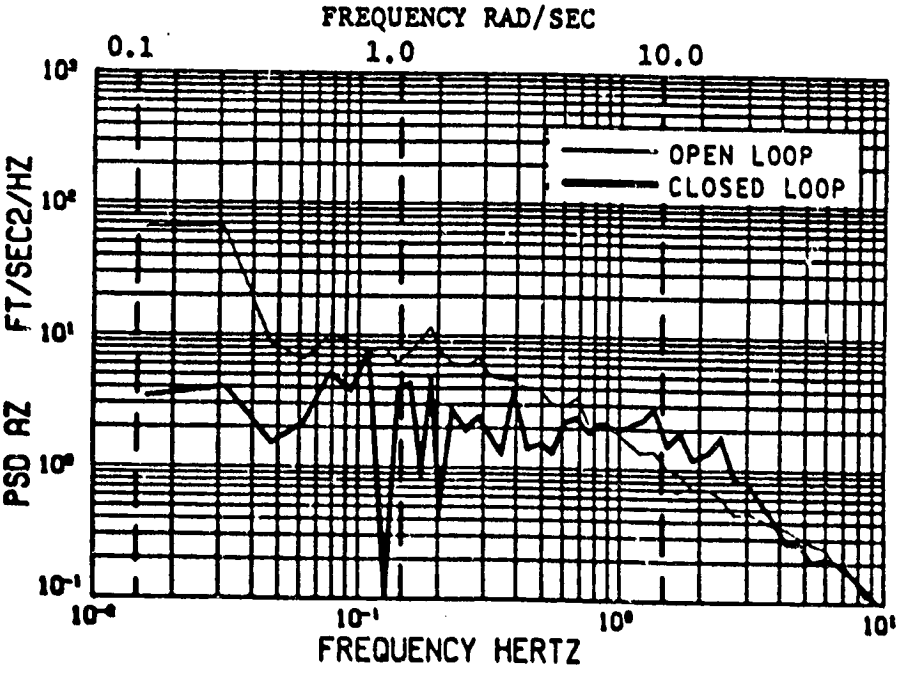

Figure E.46b

Figure E.46 NASA Simulation PSD - Takeoff Configuration (Approximate Full Power)

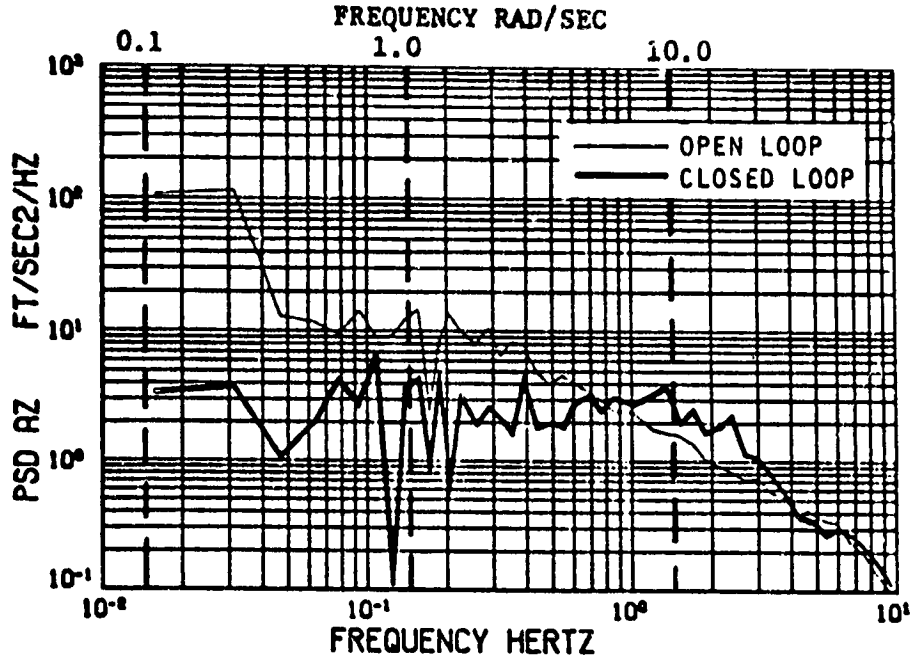

Figure E.47 NASA Simulation PSD - Climb (SL) Configuration (Approximate Full Power)

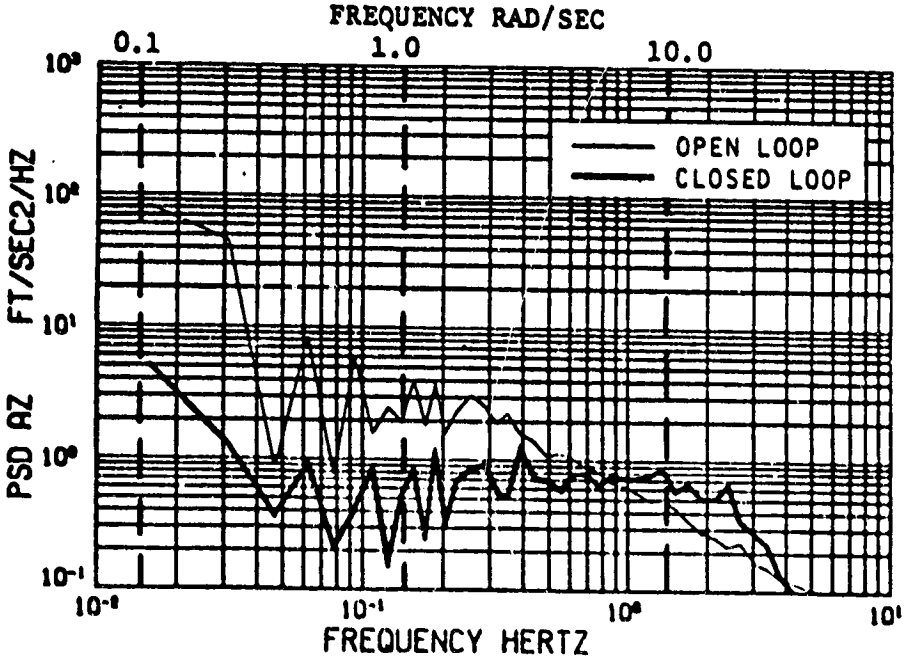

Figure E.48 NASA Simulation PSD - Climb (5000 ft.) Configuration (Approximate Full Power)

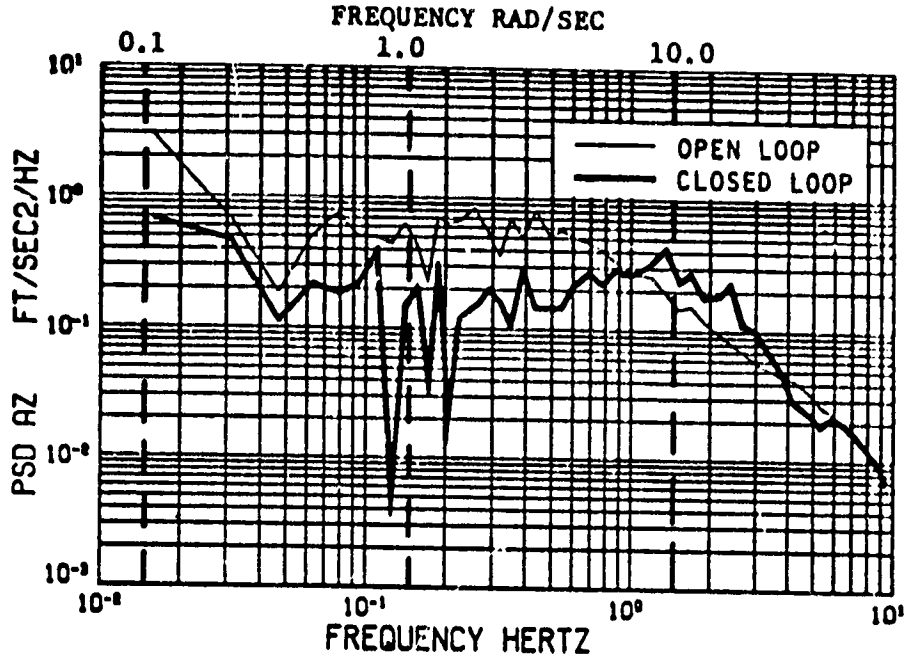

Figure E.49 NASA Simulation PSD - Cruise Configuration (Approximate Full Power)

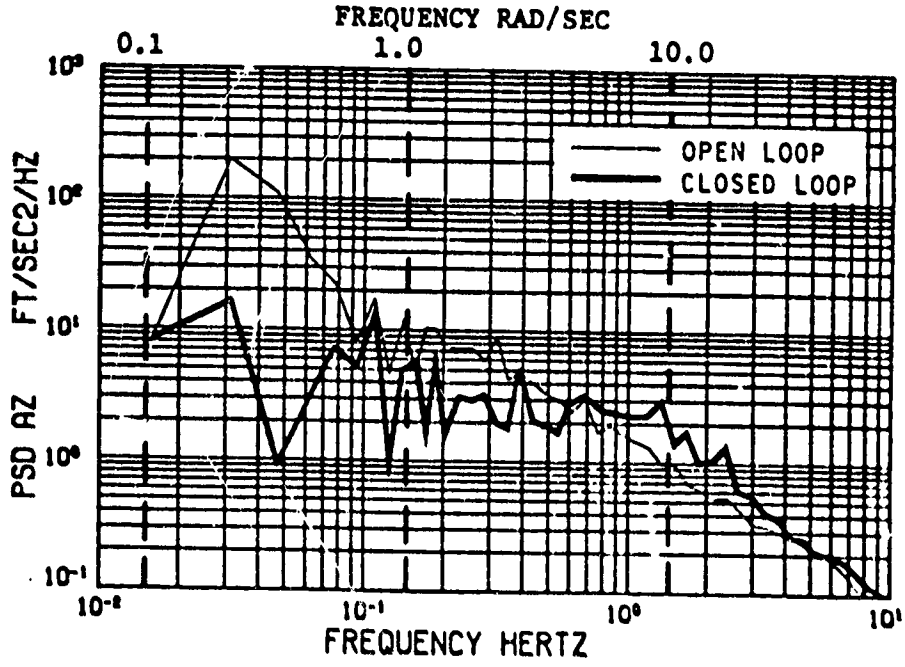

Figure E.50 NASA Simulation PSD - Approach Configuration (Approximate Full Power)